State and Learning Dependent Changes in Olfactory Granule Cells

A dissertation presented by

Brittany CAZAKOFF

to the

Watson School of Biological Sciences

in partial fulfillment of the requirements for the degree of

Doctor of Philosophy

in

Biological Sciences

at

Cold Spring Harbor Laboratory

November 16, 2016

Declaration of Authorship

I, Brittany CAZAKOFF, declare that this thesis titled, "State and Learning Dependent Changes in Olfactory Granule Cells" and the work presented in it are my own. I confirm that:

- This work was done wholly or mainly while in candidature for a research degree at Cold Spring Harbor Laboratory.
- Where any part of this thesis has previously been submitted for a degree or any other qualification at Cold Spring Harbor Laboratory or any other institution, this has been clearly stated.
- Where I have consulted the published work of others, this is always clearly attributed.
- Where I have quoted from the work of others, the source is always given. With the exception of such quotations, this thesis is entirely my own work.
- I have acknowledged all main sources of help.
- Where the thesis is based on work done by myself jointly with others, I have made clear exactly what was done by others and what I have contributed myself.

Signed:

_____

Date:

_____

"I have no idea what I'm doing, but I know I'm doing it really, really well"

Andy Dwyer, Parks and Recreation

Abstract

Olfactory granule cells (GCs) act as a central hub between incoming sensory inputs and top-down, centrifugal inputs to the main olfactory bulb (MOB). This makes them a primary candidate for updating olfactory sensory information in accordance with an animal's state and in accordance with an animal's previous memories for stimuli and their associated outcomes. However, due to their small size and inactivity in anesthetized animals, *in vivo* recordings from these cells have been difficult to collect. We thus still lack an understanding of how contextual cues update GC activity. In this thesis, I outline methods that, for the first time, allow us to record from GCs in awake animals. I further exploit these methods to demonstrate significant state and learning dependent activity in GCs.

The thesis is divided into five chapters. In Chapter 1, I outline our current understanding of GCs and why, based on existing studies, we believe GCs should display state and olfactory learning dependent activity. In Chapter 2, I describe the head-fixed, loose patch recording set-up used to record from GCs in awake animals and demonstrate that, using this set-up, we can record for long enough periods in which to assay odor evoked GC activity. Then, in Chapters 3 and 4, I describe how I used this method to explore the dynamics of GC activity in awake mice. In particular, I report that GCs display dramatically different activity in awake animals, passively experiencing odors compared to the activity displayed by GCs in anesthetized animals. I then report that subsets of GCs show activity consistent not just with odor responses but with animal's an animal's ability to associate odors with different behavioural outcomes and with the animal's engagement in a discrimination task. These results demonstrate, for the first time, that GC activity is dynamically regulated by the context in which animals experience odors and that this dynamic updating of activity can dramatically alter representations of odor stimuli in the MOB. In Chapter 5, I consider these implications and postulate what we still have left to examine concerning how GCs modulate olfactory networks.

Acknowledgements

Countless individuals provided both technical and personal support throughout the completion of this work. I am forever indebted to these people for their advice, assistance, and votes of confidence.

First, I want to thank my thesis advisor, Steve Shea. I could not have asked for a more generous supervisor or a better advocate. He gave me freedom to explore my ideas, and he provided invaluable direction when I was not sure how to bring these ideas to fruition. I'm grateful that his door was always open whether I wanted to discuss my data, my aspirations, or the latest in American political follies. He continuously demonstrated what it means to be a rigorous scientist, a gracious colleague, and an expert tweeter. While I may not have picked up that last skill over the course of my PhD, I'd be honored to show even one tenth of his capacity for critical thought and consideration of others as I continue on in my career.

To my thesis committee members, Anne Churchland, Chris Hammell, Glenn Turner, and Tony Zador. Your encouragement was integral to any success I achieved, and your input undoubtedly made my thesis better. To my external advisor, Leslie Kay, thank you for your helpful comments and your willingness to donate your time and expertise.

To the past, present, and interim staff of the Watson School of Biological Sciences - Adrian, Alex, Alyson, Carrie, Dawn, Keisha, Kim C. Kim G., Linda, and Leemor. You welcomed me into the Watson School family and made moving away from my Saskatchewan one that much easier. Thank-you for your advice and for putting up with all of my indecisiveness. Thank you also to the Farish-Gerry family for the fellowship that supported my studies.

To the staff at CSHL – thank you for taking care of my animals, building me equipment on a moment's notice, updating all of my software, and just generally keeping the whole place running. Without the work you do, none of this science stuff would ever get done.

Thank you to all of the creators/staff of both Parks and Recreation and 30 Rock (and to Netflix for streaming this content). Sometimes, a PhD can leave one feeling a bit downtrodden, and I thank you for giving me an easy outlet through which to find laughter.

To all those other folks in the Shea lab, at CSHL, and beyond; thank you for being my friends and mentors. You challenged my ideas and made me a more thoughtful, interesting person. I'll cherish those summers we spent tossing around the disc, the late nights we spent swimming at the YMCA, the weekend Skype sessions, the endless Youtube clickbait marathons, and all that is in between. I'm lucky to have spent so much time getting to know you all and even luckier that you still want to hang around with me.

Finally, thank you to my family. You've provided unflinching support throughout all of my endeavours (even when I was a pain to be around), and you never ceased to remind me that what I was doing was important and that my joy, and your pride in me, lie not in my success but in my being a kind, attentive person. To Justus, thank you for your love and for acting as my sounding board (even if that board was a bit argumentative). Numerous times, you picked me up and reminded me I was capable even though I just felt like giving up. I look forward to completing our next journey together as long as we don't have to complete that journey in your old Saturn go-cart.

Contents

List of Figures

List of Tables

List of Abbreviations

2AFC	Two-alternative forced choice
AL	Antennal lobe
AP	Action potential
AUROC	Area under the ROC Curve
cAMP	Cyclic adenosine monophosphate
ChR2	Channelrhodopsin-2
CR	Correct rejection
dSAC	Deep short-axon cell
EPL	External plexiform layer
EPSP	Excitatory post-synaptic potential
FA	False alarm
GL	Glomerular layer
GPCR	G-protein coupled receptor
GC	Granule cell
GCL	Granule cell layer
GCid	Granule cell identified
HDB	Horizontal diagonal band of Broca
IEG	Immediate early gene
ISI	Interstimulus interval
LC	Locus coeruleus

LFP Local field potential

MC Mitral cell

MCL Mitral cell layer

MOB Main olfactory bulb

MT Mitral/Tufted cell

NA Noradrenaline

NB Neurobiotin

OFC Orbitofrontal cortex

OR Olfactory receptor

OSN Olfactory sensory neuron

PC Piriform cortex

PFA Paraformaldehyde

PG Periglomerular cell

PSTH Peri-stimulus time histogram

QHCl Quinine hydrochloride

ROC Receiver operating characteristic

RMI Response modulation index

SAC Short-axon cell

TC Tufted cell

TTX Tetrodotoxin

Chapter 1

Introduction

1.1 Overview

The world is a messy place. Each day, vast and varying amounts of stimuli bombard our senses, and we must decide what to do with them. We must extract the identity of stimuli among a backdrop of other distractions, recognize the relevance of these stimuli, and then direct an appropriate response. To complicate matters, the relevance and response can change depending on the context in which we experience the stimuli [1].

For example, imagine yourself as a tourist in New York City. Like any good NYC tourist, you know you should try at least one slice of pizza[2] while you visit. So, you decide on a restaurant close to your hotel, head to that location, and order a slice. However, just as you are about to eat, you look down and notice a mouse escape into a hole in the wall all the while jauntily carrying a piece of mozzarella in its mouth. You look down at your slice of pizza — it still looks like pizza, smells like pizza, and probably tastes like pizza — but, all of a sudden, you are unsure about its safety for consumption. Correspondingly, some activity pattern in your brain must change to reflect this contextual information. In the extreme, a failure to do so might result in a severe disruption to the the rest of your vacation.

[1] Context as it is used here is a catchall term. It describes both the internal state of the animal, including its level of arousal, expectation, and its attention to the stimulus. It can also describe the external environment of the animal, including the reward/punishment outcomes associated with a stimulus and the influence of background stimuli that surround a target of interest.

[2] The author in no way wishes to imply that NYC pizza is better than any other pizza particularly not Chicago pizza.

Environmental complexity complicates this extraction of meaningful information. Unlike the simple stimuli often presented to laboratory subjects, stimuli in real life rarely appear in isolation. If you actually find a suitable pizza spot, you may only enjoy the smell of the freshly baked pizza once you suppress the putrid food smells lingering from yesterday's garbage out on the sidewalk. Again, activity in the brain must not only reflect these different smells even when you experience them in temporal and spatial proximity but must also signal that, if eaten, one of these stimuli will assuage your hunger while the other will likely give you an upset stomach.

How the brain recognizes stimuli and extracts meaning from them is as a fundamental question in neuroscience. While it is impossible to answer this question in a single thesis, my work here serves as an attempt to address at least a small part of it. In particular, I focused on how activity in the main olfactory bulb (MOB), a primary sensory structure for sensing odours, and, in particular, how activity in the MOB granule cell (GC) interneurons change in response to complex stimuli and behaviourally relevant variables. Camillo Golgi first described GCs in 1873. Since then, a significant amount of research has suggested that GCs shape olfactory bulb output according to the context in which organisms experience odours. This includes modulating MOB activity when organisms experience odours among other irrelevant stimuli and modulating MOB activity in accordance with learned odour associations. However, despite their discovery close to 150 years ago, the activity of GCs has never been described in a behaviourally relevant context. In fact, when I first started this work, the activity of GCs had never even been described in an awake animal. The work here describes the first attempts to rectify this.

I divided the thesis into five chapters. In Chapter 1, I review the literature concerning GCs and how they may subserve flexibility in olfactory processing. In Chapters 2, I detail how we recorded, for the first time, from GCs in awake animals using a head-fixed, loose patch electrophysiology method Then in Chapter 3, I detail how we used this paradigm to demonstrate remarkable differences in GC activity across anesthetized and awake states. I further describe in Chapter 4 how we exploited the methods outlined in Chapter 2 to assay

GC activity in animals learning meaningful and flexible odour associations. Finally, in Chapter 5, I discuss how the aforementioned studies have advanced our knowledge concerning the influence that an organism's internal state and learning history have on the MOB activity and postulate what we still have left to learn. I hope it becomes apparent that state and contextual cues highly modulate brain activity, and that contrary to a widely held view, this modulation occurs even at the level of early sensory circuits.

1.2 A Brief Overview on Context and Learning

Classical views of contextual experience and learning focus on limbic and cortical structures in the brain. In these models, cues in the environment act on peripheral receptors to evoke or suppress activity in peripheral sensory neurons. These peripheral neurons communicate (often through one or two synapses) with neurons in downstream primary sensory areas that reliably represent basic features of the stimulus including its identity and strength. Sensory areas then form connections with "more complex", higher order centres that increasingly represent more abstract features of the stimulus. For example, typical models of the visual system (Fig.1-1) posit a hierarchy where higher order cortical regions like V4 progressively pool information from simpler areas starting at the sensory retina. In this model, neurons in early visual areas like the retina and primary visual cortex (V1) detect basic stimulus features like object edges while higher areas pool this information in order to represent more complex objects like faces.

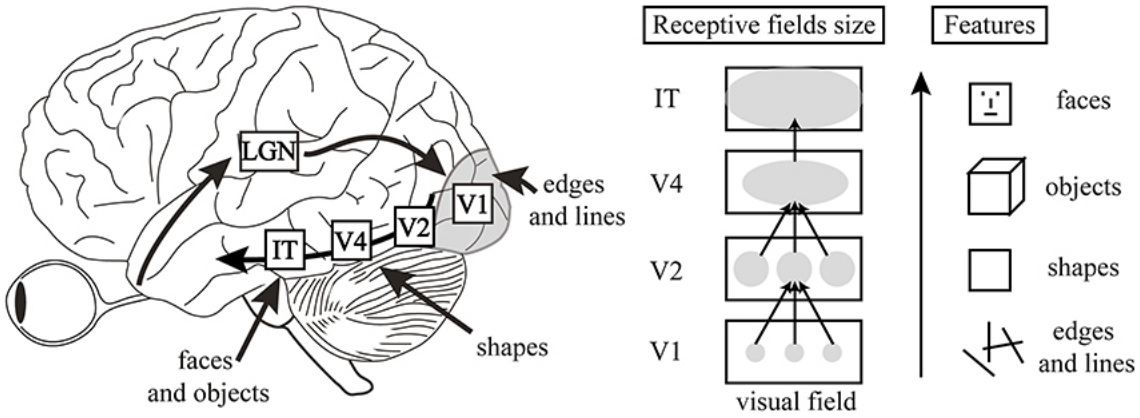

FIGURE 1.1: **Hierarchal and feedforward structure in neural circuits.** In classical models of visual processing, information flows from the retina, through the LGN, and then to progressively "higher" cortical areas. The receptive fields of these areas get larger as more information is pooled from the previous areas. While this sort of information flow certainly exists in the brain, it can underestimate the influence of feedback from the higher areas back onto earlier areas of processing. Figure adapted from Manassi et al 2013.

However, hierarchal models, while not explicitly wrong, can be incomplete and can fail to capture the connectivity among the different areas of the brain. Many of these "early' sensory areas receive massive and diverse feed-back from the higher-order cortical centres. Further, they also receive input from neuromodulatory nuclei whose activity is thought to represent non-sensory related variables like stimulus value. As a result, sensory circuits may be updated in accordance with more complex, contextual cues including information concerning the environment in which the animal experiences the sensory stimulus of interest, the animal's previous experiences with the stimulus (memory), and the animal's arousal or attentional state (Gilbert & Sigman, 2007; Niell & Stryker, 2008; Otazu et al., 2009; Poort et al., 2015). Recent evidence demonstrates that even primary sensory areas in the visual circuit like V1 are heavily modulated by the movement state and learning history of the animal (Poort et al., 2015; Niell & Stryker, 2010; Vinck et al., 2015). Such factors may modulate the activity of sensory circuits to improve an animal's detection of relevant stimuli and assist the animal in more quickly and accurately meeting environmental demands (Gilbert & Sigman, 2007).

In the cortex, several groups have highlighted the role that interneurons — defined by their use of GABA as their primary neurotransmitter — may play in patterning neuronal circuits in accordance with neuromodulation and an organism's behavioural state (Gentet et al., 2012; Haider, Häusser, & Carandini, 2013; Kepecs & Fishell, 2014). Interneurons likely play a similar role in early sensory areas, but we are only just now beginning to understand their role in context-dependent updating of neuronal circuits. Ideally, to explore this role, we would perform these studies in sensory areas in which we can easily and cleanly manipulate both the cell populations and top-down feedback.

1.2.1 The Olfactory Bulb: A Good Model for Sensation in Context

For several reasons, the main olfactory bulb (MOB), the primary olfactory sensory area, makes for an excellent study in contextual modulation of sensory circuits. First, olfactory cues serve as a primary source of information for mice and rats, dominant mammalian experimental models. Rodents possess a formidable capacity to identify odours, even among a

varying background (Rokni et al., 2014), and they further readily adapt their odour-guided behaviour in response to changing outcomes (Kay & Laurent, 1999; Doucette & Restrepo, 2008). Several invertebrates including flies, locusts, and honeybees, also rely on olfactory cues to navigate much of their environment. While these organisms lack an MOB, neurons in the analagous antennal lobe (AL) display many of the same features as those of the MOB. As a result, olfactory principles gleaned from invertebrates greatly inform studies in the MOB and vice versa. Second, the laminar structure of the MOB permits relatively easy interrogation of the different, gross cell types in the olfactory bulb circuit even without genetic markers. These layers receive dense feedback from many higher order cortical and neuromodulatory centres, and often, this feedback preferentially terminates in specific layers. As a result, one can, with moderate precision, assay and influence the cells and feedback in the distinct regions of the MOB. The MOB consists of both excitatory output neurons as well as dense networks of interneurons that are often separated among these layers. As a result, the flexible influence of these inhibitory networks can, in principle, be easily examined. Finally, many behavioural experiments along with accompanying measures of neuronal activity suggest that both MOB excitatory neurons and the feedback to the MOB display or confer context related activity. However, to date, a mismatch exists between our understanding of feedback anatomy and the influence of contextual cues on the MOB. While the the majority of our information concerning olfactory processing comes from MOB excitatory neurons, most centrifugal input to the MOB targets inhibitory neurons. In particular, many of these inputs target inhibitory GCs. As described below, converging evidence from both experimental and modelling studies suggest GCs act as powerful regulators of MOB activity in light of contextual cues, yet few studies have actually assayed GC activity in situations where context influences olfactory sensory activity.

1.3 Anatomical Organization of the Main Olfactory System

How might GCs reflect or modulate MOB circuits in accordance with meaningful odour information? To understand this, it is first useful to examine how odours themselves are

represented in the olfactory system and what MOB circuits – and in particular GC circuits – look like.

In mammals, odours first bind to receptors located on the dendrites of olfactory sensory neurons (OSNs) found in the animal's nose (Fig.1-2A). These olfactory receptors (ORs) constitute a large and distinct class of G-protein coupled receptors (GPCRs) encoded by over 1000 different genes in rats and mice (around 350 in humans and 60 in flies; Buck & Axel, 1991; Mombaerts, 2004; Wilson & Mainen, 2006). Individual sensory neurons express only one OR gene out of the class, and axons of OSNs expressing the same receptor type converge at the same location in the MOB (Belluscio et al., 2002; Mombaerts, 2004; Wang et al., 1998). While the number of OR genes is large, this number is still vastly outpaced by the number of unique odours in the environment, limiting the ability of the system to recognize odours based on a one-to-one match between the odour and receptor. Instead, the receptive fields of ORs (often referred to as the molecular receptive range or MRR) substantially overlap. Different odour molecules activate a distinct subset of receptors resulting in a combinatorial coding scheme (Wachowiak & Cohen, 2001; Wilson & Mainen, 2006). Sufficient activation of ORs by odours results in the generation of action potentials (APs) in the OSNs. These APs propagate down the OSN axons to the MOB where neurons in the MOB read out this combinatorial code (Fig.1-2A).

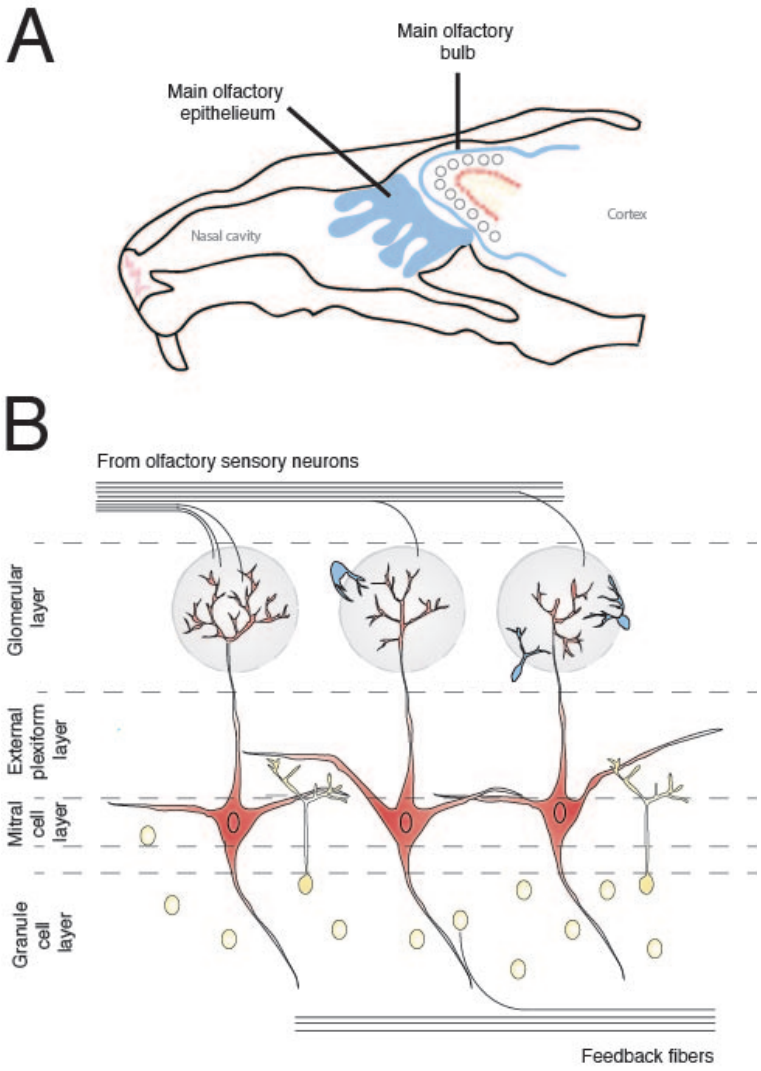

FIGURE 1.2: **Organization of the main olfactory bulb.** (A) Schematic of the mouse nasal cavity and olfactory bulb. Odour information flows from the main olfactory epithelium to the main olfactory bulb via olfactory sensory neuron axons. (B) The olfactory bulb is comprised of 5 distinct layers. The glomerular layer (GL) consists of the neuropil of OSNs, MTs, and several interneurons including periglomerular cells. This neuropil collectively forms glomeruli. The external plexiform layer (EPL) is populated by many interneurons as well as the dendrites of both MTs and GCs. Mitral cells, principle excitatory neurons of the MOB, are found in the MCL. Below the MCL are the internal plexiform layer (IPL, not labelled) and the granule cell layer (GCL) where one finds the GC cell bodies. Centrifugal fibres coursing from other structures in the brain predominately target the GL and GCL.

Five different layers, defined by the cell types and neuropil found within the layers, make up the MOB (Fig.1-2B). Olfactory sensory neuron axons terminate in the glomerular layer (GL) in discrete, roughly 50 μm structures called glomeruli. Neuropil belonging to both OSNs and various olfactory bulb neurons comprise these glomeruli. Individual OSNs usually project to two ipsilateral glomeruli while individual glomeruli receive projections from OSNs expressing the same OR. In a single glomerulus, OSN axons synapse both with local interneurons, including short-axon (SAs) and periglomerular cells (PGs), and with the main excitatory neurons of the bulb: the mitral cells (MCs) and the tufted cells (TCs, collectively MTs). The cell bodies of MCs are found in the mitral cell layer (MCL) while the cell bodies of TCs are found throughout the external plexiform layer (EPL), a layer deep to the GL containing both cell bodies and dendrites of various neurons. Mitral/tufted cells extend a primary apical dendrite into the GL as well as several secondary dendrites into the EPL. In mammals, MTs extend only one apical dendrite into one glomerulus and thus they only receive information from one OSN type. Unlike other sensory systems, olfactory evoked activity does not pass from the initial sensory region to the thalamus. Instead, MTs directly send their axons to a number of different structures including the piriform cortex (PC), the anterior olfactory nucleus (AON), the olfactory tubercle (OT), and a subset of amygdaloid nuclei. Information in the olfactory system thus takes a short path from periphery to cortex.

These higher centres to which MTs project do not receive information that simply reflects the information from OSNs. MT activity is heavily modulated by the interneurons of the bulb, including GCs. In fact, GCs comprise the largest class of interneurons found in the MOB. These small cells (7-10 μm in diameter) populate the GCL along with a less numerous class of interneurons known as deep, short-axon cells (dSACs). Granule cells lack axons, but their spiny dendrites extend locally (100-200 μm spread) into both the IPL and the EPL. Here, GC dendrites form synapses with the secondary dendrites of MTs. These synapses form the key connection through which GCs can modulate MOB activity.

1.3.1 Modulation of MOB Output through Dendrodendritic Synapse

Any effect of odour context on GCs must ultimately manifest in MTs as MTs are, to date, the only known output target of GCs. Unlike traditional synapses which communicate through a presynaptic axon terminal and postsynaptic dendritic spine or process, GCs communicate with MTs through dendrodendritic synapses (Price & Powell, 1970; Rall et al., 1966). Secondary MT dendrites in the EPL synapse on spines located along the GC dendritic tree. Early *in vitro* studies noted that a long-lasting afterhyperpolarization (AHP) followed the depolarization of a single MT (Jahr & Nicoll, 1980; Jahr & Nicoll, 1982a). This effect was blocked by the application of the $GABA_A$ receptor antagonist bicuculline (Isaacson & Strowbridge, 1998; Wellis & Kauer, 1993) but not blocked by the application of TTX, suggesting the hyperpolarization depends on local GABAergic connections with MTs. Due to their density in the bulb, GCs were proposed to be the source of this inhibition, and subsequent studies have demonstrated corresponding excitatory post-synaptic potentials (EPSPs) in GCs upon MT stimulation (Chen, Xiong, & Shepherd, 2000; Isaacson & Strowbridge, 1998). The basic circuit is thus organized as follows: APs initiated at the MT cell body back-propagate along MT secondary dendrites, and in turn, the presynaptic dendrite releases glutamate onto GC dendritic spines (Fig.1-3). Depolarization of the spine then stimulates GABA release back on to the MT dendrite. (Isaacson & Strowbridge, 1998; Jahr & Nicoll, 1980; Jahr & Nicoll, 1982a). Interestingly, this interaction appears to depend on Ca^{2+} entry through NMDA and voltage gated Ca^{2+} channels (VGCCs) found on GC dendrites. Bath application of the NMDA receptor blocker, APV, largely abolishes both the MT hyperpolarization and GC EPSP (Chen, Xiong, & Shepherd, 2000; Schoppa et al., 1998; Halabisky et al., 2000) while blockade of AMPA receptors has less of an effect (Chen, Xiong, & Shepherd, 2000; Schoppa et al., 1998). Similarly, bath application of the P/Q type Ca^{2+} channel blocker also abolishes the IPSP in MTs. GC depolarization thus shows a primary dependence on Ca^{2+}. Subsequent spine imaging studies have shown that signaling through ligand and voltage gated Na^{+} channels can augment the entry of Ca^{2+} into the GC spine and boost Ca^{2+} mediated depolarization (Egger, 2008).

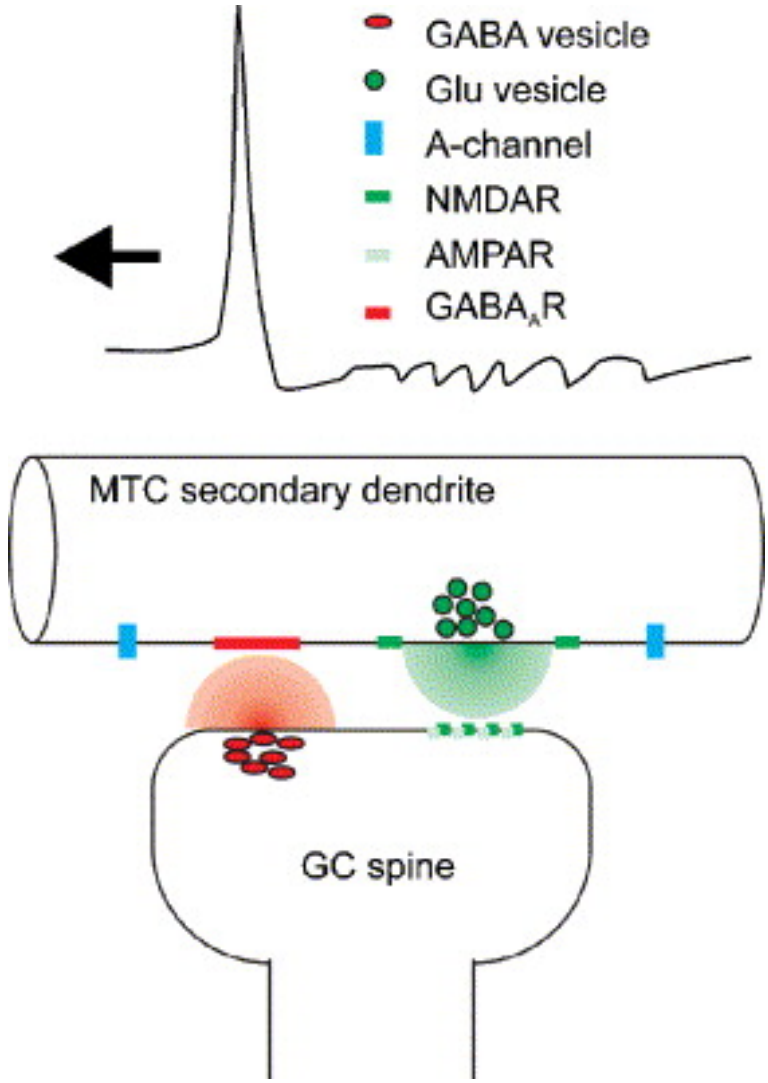

FIGURE 1.3: **The Dendrodendritic synapse.** Granule cells influence MOB output neurons, MTs, through signaling at the MT secondary dendrites. Action potentials (top) propagate in secondary MT dendrites and stimulate glutamate release. This glutamate release (green) and sufficient excitation stimulates reciprocal GABA release (red) from the GC. Excitation of the GC is both AMPA and NMDA dependent. GABA inhibition of MTs depends on $GABA_A$ receptors. Figure adapted from Egger and Urban, 2006.

Calcium signaling in the GC spine confers dendrodendritic synapses with several unique properties. First, GABA release from the GC dendritic spine can occur both in the presence and absence of GC somatic APs. As already noted, early reports demonstrated that reciprocal inhibition of MTs occurs in the presence of TTX+, suggesting APs are not required for GC release of GABA (Isaacson & Strowbridge, 1998). Thus, at least at in their local vicinity, GCs can inhibit activity at MTs through subthreshold — defined by changes in membrane voltage that are too small to evoke spikes — synaptic signaling alone. However, *in vivo* and *in vitro*, GCs also fire APs and low-threshold spikes (LTS; Egger, Svoboda, & Mainen, 2003; Egger, Svoboda, & Mainen, 2005). These LTSs are characterized by widespread Ca^{2+} entry throughout the GC spines and dendritic tree as well as dependence on T-type Ca^2+ channels (Egger, Svoboda, & Mainen, 2003; Egger, Svoboda, & Mainen, 2005). Why might these APs and LTSs be necessary? One possibility is that APs are simply an inevitable consequence of summing GC EPSPs. However, a more interesting scenario is that this higher voltage activity can spread further through the dendritic tree and depolarize additional spines on the GC beyond those sufficiently depolarized by MT input. Such distributed activity may be important for lateral inhibition and coincident activity dependent plasticity, two mechanisms proposed to be crucial for olfactory learning and memory.

Activity at dendrodendritic synapses is not static. Rather, GC activity, in particular, is sensitive to inputs from cortical (PC and AON) and neuromodulatory centres (ex: cholinergic HDB and noradrenergic LC). Because the inputs originate in centres that traditionally receive information from the MOB (a feedforward circuit), they are often referred to as feedback or centrifugal projections. Importantly, these centres are thought to process information concerning an animal's internal state and stimulus meaning. The information they provide to GCs can thus dynamically update GC activity in accordance with contextual cues. This can have powerful effects on the MOB circuit. For example, increased feedback activity to GCs could augment the excitability of GCs such that when GCs receive odour evoked activity from MTs, the GCs reach spike threshold more quickly and provide more inhibition to the MT network. If we consider that MTs carry odour information to the rest of the brain, such changes in inhibition can ultimately have a large effect on how an organism detects,

recognizes, and responds to odours.

1.3.2 Mapping Odour Identity in the MOB

The discrete projection patterns of OSNs and MTs suggest the MOB may be organized as a sensory map and that organisms may recognize odours based on this map. That is, the spatial position of MOB neurons (i.e. glomeruli and MTs) may be functionally relevant for the identification of some odourant feature such that (1) neurons that respond to a particular stimulus tend to be clustered in space and (2) the tuning profile of the neuron shows a systematic relationship with the neuron's location or positioning in relation to other neurons (Knudsen, Lac, & Esterly, 1987; Wilson & Mainen, 2006). Clustering of information in maps can aid "read-out" of information in downstream structures as, in addition to the spiking activity, the pattern of connectivity carries relevance (i.e. the structure reading out activity knows the activity derives from one area of the bulb vs. another). Further, clustering may aid interactions among neurons and subsequently sharpen sensory responses.

Both anatomical and physiological evidence indicate MOB neurons cluster in a functionally relevant way. Depending on their position in the epithelium, OSNs project to distinct areas along the MOB dorsal-ventral axis (Miyamichi et al., 2005; Murthy, 2011; Schoenfeld & Cleland, 2005), and across animals, the positioning of individual glomeruli is conserved (Soucy et al., 2009; Royet et al., 1987; Rubin & Katz, 1999; Wachowiak & Cohen, 2001). Early 2-deoxyglucose studies as well as subsequent fluorescent imaging studies have further demonstrated that individual odours often activate specific combinations of glomeruli (Soucy et al., 2009; Belluscio & Katz, 2001; Spors & Grinvald, 2002) and that these responsive glomeruli tend to be grossly clustered in space. For example, ketones tend to activate the lateral MOB while carboxylic acids tend to activate the anteromedial MOB.

At a finer scale, however, there is no obvious relationship between odour identity and MOB layout. That is, at least to our knowledge, the chemical features of odours do not map in an organized way with glomerular positioning. Early reports posited that similar odours (typically straight-chain alchohols or aldehydes) that differed systematically in carbon chain

length would activate adjacent glomeruli. For example, an odourant composed of 6 carbons would activate one glomerulus while an odourant in the same molecular class but composed of seven carbons would activate a nearby glomerulus. This patterning of glomeruli would provide downstream structures with information about stimuli based on glomerular positioning, and through lateral inhibition of nearby neurons, enhance constrast among similar stimuli. Consistently, however, groups have failed to demonstrate such a layout in the mammalian MOB. Putatively similar odours (i.e. $\pm$ 1 carbon, ring structures, etc. . .) can activate distant areas of the MOB (Bozza et al., 2004; Soucy et al., 2009), and nearby glomeruli can have dramatically different tuning (Bozza et al., 2004). Within a cluster, several inactive glomeruli can be situated between those glomeruli that are activated by similar odours (Soucy et al., 2009), and these inactive glomeruli often respond to chemically distinct molecules. Thus, the MOB does not appear to be organized as a chemotopic map. Instead, spatial patterns are grossly distributed (Murthy, 2011).

1.4 Flexibility in MOB Responses

This distributed map may reflect the high-dimensionality of odour feature space. Currently, we lack an understanding of what features in odour space are important and what features of odour space may have been relevant in the development/evolution of the olfactory system. One intriguing hypothesis is that MOB activity not only carries information about the pure molecular identity of an odour but also represents what that odour might mean behaviourally for the organism (Kermen et al., 2016; Nunez-Parra, Li, & Restrepo, 2014). In this scenario, MOB output would reflect sensory and non-sensory information including any contingencies associated with the odour, the animal's previous experiences with the odour, and the animal's current motivational state. The MOB, in other words, might reflect both sensory and behavioural context. In the sections below, I detail the evidence for this idea and outline how MOB circuit mechanisms may support such representation. In particular, I focus on two major contexts: (1) an animal's internal state and (2) olfactory learning/discrimination. The central positioning of GCs between MTs and centrifugal feedback

suggest they are poised to play a role in reformatting MOB circuits in accordance with both of these scenarios, and as further reviewed below, converging evidence suggests that GCs play a crucial role in reformatting MOB circuits to meet the demands of these contexts.

In review of this literature, I focus on several methods employed by researchers to assay olfactory bulb activity. Most of these assays fall into one of two categories: (1) molecular profiling through examinations of immediate early gene (IEG) expression and (2) functional profiling using electrophysiology or imaging. Enhanced expression of IEGs, as assayed post-mortem following a behaviour, is thought to indicate significant activation/plasticity of the brain area or neuronal population in which the increased IEG expression is observed. While many IEGs exist in the brain, researchers typically profile *cfos* and *arc* which have proven useful for pinpointing which brain areas and which cells in the brain may mediate a behavioural response. However, because IEG studies must be completed post-mortem, this technique lacks temporal specificity.

In contrast, neurons in behaving animals can be assayed in real-time either with imaging or electrophysiology. Imaging studies typically employ GCaMP, a Ca^{2+} chelator engineered to fluoresce upon Ca^{2+} binding. Increases in fluorescence reflect increased Ca^{2+} entry into the cell, a typical result of neuronal depolarization/excitation. Electrophysiology involves using electrodes to measure current and voltage changes in neurons both at the single neuron level (patch-clamp or array recordings) and at the population level through local field potential (LFP) recordings and measurement of brain rhythms. When recording from single neurons, researchers typically assay AP firing or subthreshold activity. In contrast, when recording from populations, researchers examine field potentials, defined by the coordinated activity of neural ensembles or rhythmic fluctuations in the activity of many neurons. In the MOB, these fluctuations can occur at distinct frequencies, perhaps the most intuitive of which, is the theta (breathing) rhythm. Animals sample their olfactory environment through breathing/sniffing, and in the MOB, many cells in the bulb fire in relation to this 3-10 Hz rhythm. The MOB also displays higher frequency rhythms including those in the gamma range (60-90 Hz in awake rats), which arise at the dendrodendritic synapse between MTs and

GCs (Lagier, Carleton, & Lledo, 2004; Osinski & Kay, 2016) and those in the beta range (15-30 Hz), thought to reflect more distributed activity in the MT-GC-cortical (PC) loop (David et al., 2015; Osinski & Kay, 2016). These two rhythms are of particular note because of their dependence on GC activity and because they can arise or increase in power when animals learn odour associations and discriminate among odours.

1.4.1 An Animal's Internal State Shapes MOB Responses

Perhaps not surprising to anyone who has ever skipped a meal, olfactory perception can be influenced by an organism's internal state, including its level of wakefulness and hunger. In humans, rodents, and flies, even short periods of fasting increase sensitivity to odours. Subjects can better detect odours at low concentrations, better discriminate between odours, and better locate food sources using olfactory cues (Cameron, Goldfield, & Doucet, 2012; Ko et al., 2015). Early studies in rats demonstrated that this altered perception may derive, at least in part, from altered responses in the MOB. Just prior to a meal, MT multi-unit activity increases in rats trained to expect food during only a two h period of day (Pager et al., 1972). Similarly, in flies, starvation increases the responsiveness of projection neurons (PNs), the AL output neurons, known to respond to food odours and suppresses the responses of distinct PNs known to evoke aversion responses (Root et al., 2011; Ko et al., 2015). In both flies and rodents, differences of MOB responses between fed and hunger states likely reflect altered neuromodulatory activity. In flies, knockout of the NPY receptor in ORNs that specifically synapse with food responsive PNs blocks the sensitization of these receptors following starvation. In mice, cannabinoid type-1 receptor blockade on cortical inputs to the MOB reduces food seeking/eating in hungry mice (Soria-Gómez et al., 2014). This effect is likely mediated through a decrease of excitatory transmission onto inhibitory GCs as blockade of NMDA receptors in the GCL restores eating in hungry mice lacking the cannabinoid type-1 receptor.

More recently, several groups have demonstrated a profound effect of wakefulness on both spontaneous and odour-evoked activity in the MOB. Under anesthesia, MTs display low spontaneous firing and strong, odour evoked responses (sometimes greater than 40 Hz change; Cang & Isaacson, 2003; Davison & Katz, 2007; Rinberg, Koulakov, & Gelperin, 2006).

In many cases, the tuning of MTs is broad where MTs respond to at least one odour out of a set of three and, in some case, respond to several odours (60 % of cells responded to two out of three odours; Bathellier et al., 2008; Rinberg, Koulakov, & Gelperin, 2006). Mitral/tufted cells in awake animals, however, display high spontaneous activity and sparse odour responsiveness. In one study, Rinberg et al (2006) recorded from the same neurons in an animal while it was awake or following ketamine/xylazine anesthesia. Neurons that showed no response to an odour in the awake animal subsequently displayed responses to many of these same odours while the animal was under anesthesia. One possibility for this stark difference is that, in the awake animal, inhibitory neurons become more responsive to odours and enforce MT response sparseness.

Evidence for the Role of Granule Cells in State Dependent MOB Processing

Few studies have explored the role of state on GC activity despite the fact that we know other MOB cells are heavily influenced by factors like hunger and wakefulness (see above). In 2014, Soria-Gomez et al. reported that different fed states of an animal modulate GC activity as demonstrated by cFOS staining. Fasted animals show less *cfos* expression in GCs compared to satiated animals, a decrease that may reflect endocannabinoid inhibition of GC spiking in fasted animals. This hypothesis is consistent both with Soria-Gomez et al's own report that endocannabinoid signalling in the MOB is required for food-seeking in fasted animals as well as *in vitro* demonstrations that endocannabinoids suppress GC activity (Heinbockel & Wang, 2016).

When I began this thesis work, no study had examined the activity of GCs across wakefulness states. The differences in MT tuning across state, however, suggested GCs might play a role. As part of this thesis, I set out to explore this possibility by recording from GCs in awake animals and contrasting their activity with that of GCs in anesthetized animals, an effort I detail in Chapters 2 and 3. I expected GCs would be more active and more broadly tuned in awake animals. This would drive the sparsening of MT tuning. In the course of completing my work, Kato et al. demonstrated through Ca^{2+} imaging that GCs displayed significant differences in the level of spontaneous and odour evoked activity in anesthetized

vs. awake animals. The work I described in Chapter 3 builds upon this result from Kato et al. and extends the examination of state modulation to consider how changes in breathing influence GC activity and how tuning at the level of single GCs may change across state.

1.4.2 Olfactory Learning and Discrimination Shapes MOB Responses

Key results pertaining to MOB excitatory neurons further provide evidence for the dependence of MOB activity on learning and the animal's past history with odour cues. These results bolster the hypothesis that the MOB reflects the contextual as well as basic sensory variables of a stimulus. Before I consider these results, it is useful to first review the typical methods for examining odour learning/discrimination in experimental animals. Researchers generally examine olfactory learning through the use of nonassociative/perceptual paradigms and associative – classical and operant conditioning – tasks. For the sake of brevity, I will focus on associative paradigms as the importance of inhibitory activity is well established in these tasks (but see Appendices B and C for more information on perceptual habituation paradigms).

Associative paradigms for studying olfactory learning and memory

In associative odour learning paradigms, subjects learn to associate odours with either a rewarding or punishing outcome. Typically, these odours are behaviourally irrelevant at first, but through association with another stimulus or particular outcome, the odours elicit behavioural responses from the animal that are consistent with that outcome. In classical conditioning paradigms, a previously neutral stimulus evokes a behavioural response from an organism as a result of pairing the stimulus with another factor that usually evokes that response. For example, in fear conditioning, the most commonly used classical conditioning paradigm, researchers pair a sensory stimulus with a footshock. Animals then learn to freeze their movement upon exposure to the odour as they would normally freeze to the footshock. In operant conditioning paradigms, an organism's responses to stimuli are shaped according to the pairing of the stimulus with either reward or punishment. Researchers reward

behavioural responses to increase their occurrence and punish responses to decrease their occurrence. These behavioural tasks are summarized in Fig.1-4.

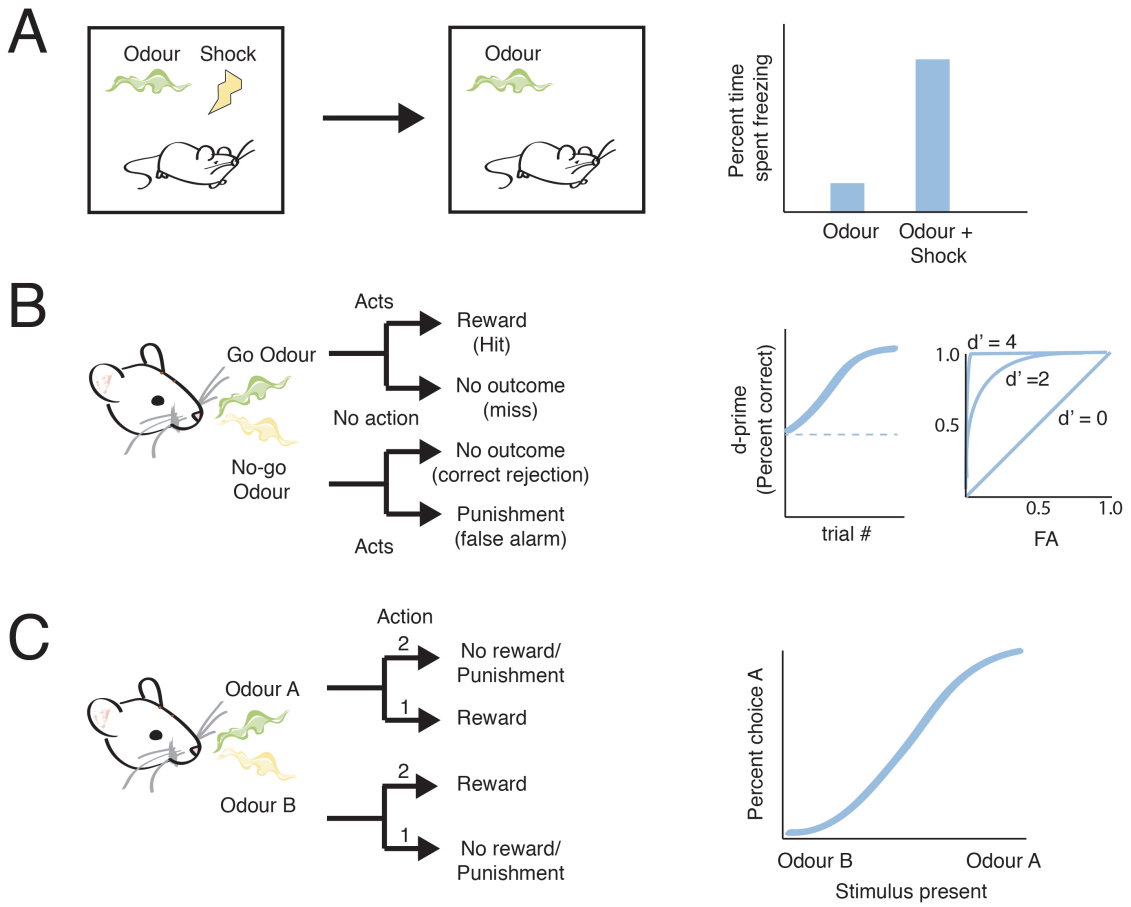

FIGURE 1.4: **Olfactory learning and discrimination paradigms** (A) Olfactory fear conditioning. In the acquisition phase, an odour is paired with a shock, and then, at some time point after this pairing, the animal is re-exposed to the same odour during the retrieval phase. Percent of time spent freezing to the odour during retrieval is quantified and compared to control animals exposed to the odour alone during acquisition. Variations of the task include exposing the animal to odours besides those paired with footshock to test the animal's discrimination and generalization capacity. (B) Operant olfactory go/no-go. In this paradigm, animals typically sample two odours: a go odour and a no-go odour. If the animal senses the go odour, it must perform the required response (often licking at a water spout) in order to receive reward (often water). Stealing from the signal detection literature, these trials are termed hits. In contrast, the animal must refrain from performing this action to no-go odours (correct rejection). Mistakes include misses (failing to lick to go odour) and false alarms (licking for no-go odour). Behavioural sensitivity is quantified on a ROC curve (not shown) from which one can read-out d-prime values over a set number of trials (higher d-prime = better performance). Many groups also quantify percent correct although this is not explicitly correct for many go/no-go paradigms. (C) Operant olfactory two-alternative forced choice. Like the go/no-go, the animal samples different odours. Each odour is associated with a different behavioural contingency. Often these are left vs. right choices. For example, odour A might be associated with licking towards a right spout or entering a right chamber while odour B might be associated with licking towards a left spout or entering a left chamber. Incorrect choices may be punished (air puffs to face, delayed periods in which the animal can start a new trials). Behavioural performance is quantified as a psychometric curve. Variations of go/no-go and 2AFC paradigms include changes in the reward/punishment type and amount as well as the presentation of morph odours (i.e. mixtures made of odour A and odour B in various ratios).

Olfactory fear conditioning

Much of what we know about the involvement of the MOB in olfactory learning comes from olfactory fear conditioning paradigms (Fig.1-4A). Researchers expose animals to an odour in the presence of a footshock, an aversive stimulus known to elicit both avoidance and freezing responses from flies, mice, and rats. Upon re-exposure to the odour in the absence of the footshock, animals freeze to the odour (or avoid it when given the option such as in inhibitory avoidance assays) indicating they associate the odour with the footshock. Animals typically learn these associations quickly (on the order of one to ten trials of odour-footshock pairings). Further, they specifically associate the footshock paired odour, as opposed to non-paired odours, with impending punishment.

Appetitive/Aversive odour paradigms

In appetitive/aversive paradigms (Fig:1-4B,C), animals learn to associate odours with a rewarding stimulus (often water or sucrose for mildly water deprived animals) and other odours with a punishing stimulus (aversive tastants or absence of water in water deprived animals). In contrast to fear-conditioning, the tasks often require many trials (on the order of hundreds to thousands) for the animal to learn. Researchers can then track cumulative changes over time as animals gradually learn the task. They also gain power for correlations between neural activity and behavioural responses. Appetive/aversive paradigms typically take the form of go/no-go or two-alternative forced choice tasks (2AFC). In go/no-go tasks, animals learn to associate one odour with reward (go odour) and another odour with either no reward or punishment (no-go odour). In response to the go odour, animals perform a specific behaviour (licking at a water spout, digging in a bowl) to receive the reward while they refrain from performing this behaviour upon detecting the no-go odour. In 2AFC tasks, animals learn to associate both odours with reward but must perform a different action for each odour; typically, this involves moving or licking to the right for one odour and moving/licking to the left for the other odour. While these two paradigms are often used to examine an animal's ability to discriminate odours, it is important to remember that they

are not necessarily equal in terms of task demands or behavioural outcome. In go/no-go tasks, animals must act for one stimulus and refrain from acting for the other. Further, even for perfect performance, only a subset of the trials are rewarded. In contrast, in 2AFC tasks, animals must commit actions in response to both stimuli, and contingent on correct performance, they can be rewarded on every trial. These task structure differences may result in different physiological responses in the olfactory system (Frederick et al., 2016).

Fear conditioning, go/no-go, and 2AFC paradigms involve both a learning component (i.e. learning to associate an odour with an outcome) and a discrimination component (distinguishing the go or right odour from the no-go or left odour). For ease of explanation, I treat these two phenomena as separable categories whereby learning refers to the acquirement of an association while discrimination refers to the animal's ability to distinguish among different odours once the animal has reached some high level of task performance. Discrimination thus relies on an organism's memory and ability to distinguish among odours rather than some ability to aquire a new skill or association. In practice, however, the two are not always easily separated. Learning in go/no-go as well as 2AFC paradigms necessarily requires some amount of discrimination. Further, evidence of learning in fear conditioning as well as simple odour-reward association paradigms is often assayed long after the learning has occurred. For example, researchers often measure neural activity and behaviour in olfactory fear conditioned mice upon re-exposure to the conditioned odour.

1.4.3 The Role of the Olfactory Bulb in Associative Learning

The behavioural paradigms described above allow researchers to manipulate the context in which animals experience olfactory stimuli. With learning, previously pleasing odours can take on new, repellent qualities (think about the pizza, the mozzarella, and the mouse) or neutral odours can become informative of reward. This new meaning likely reflects changes in several areas across the brain, but many groups have shown that some of these changes occur in the MOB. This evidence suggests that MOB activity may be profoundly different

depending on whether an odour is associated with a learned outcome and whether it is experienced alone or in the presence of other odours that may complicate its identification.

In fear conditioning paradigms, OSNs display enhanced responses to conditioned, but not unconditioned, odours (Kass et al., 2013). This increase is accompanied by a corresponding increase in MTs, particularly those that are only weakly activated by the odour before conditioning. The effects are specific to the conditioned odour. Similarly, enhanced responsiveness of glomeruli can be seen with appetitive paradigms. These studies demonstrate the MOB's remarkable plasticity and suggest the bulb is responsive to more than those features typically associated with odours (i.e. not only odour identity and concentration). Rather, the value of an odour also influences its representation at early stages in olfactory processing. In support of this, seminal work from from Kay and Laurent (Kay & Laurent, 1999) demonstrated that MTs display remarkably lability in responsiveness depending on whether an odour is associated with a rewarding (sucrose) or punishing (quinine) stimulus. In some cases, the responses tracked odour contingency: for example, odours that evoked responses from MTs when the odour was paired with sucrose failed to evoke a response from the MT when the odour was paired with quinine (QHCl). Thus, contrary to what might be expected with a clear chemotopic map, one could not predict the responses of MTs from glomerular input alone (Kay & Laurent, 1999; Doucette & Restrepo, 2008). Similar results have since been observed in mice (Doucette & Restrepo, 2008).

Recording LFPs in animals that have learned a go/no-go task for two different odours (gerianol and eugenol), researchers have demonstrated increases in beta frequency power in the MOB (Ravel et al., 2003; Martin et al., 2004). These same animals show a decrease in gamma power compared to naive animals. Enhancements in beta appear to track an animal's recognition of an odour and its accompanying stimulus value indicating at least some part of the MOB is responsive to odour meaning (Martin & Ravel, 2014). In support of this idea, differences in beta power can be observed depending on behavioural outcome in a 2AFC task. On trials which the animal performs correct, odours evoke an enhancement of beta power compared to incorrect trials (Kay & Beshel, 2010). At least some of this rhythmic activity is driven by centrifugal input to the bulb. Disruption of the centrifugal input to the

MOB blocks the increase in beta power on go/no-go tasks (Martin et al., 2006).

Evidence for the role of granule cells in associative learning

GCs are a prime target for this centrifugal feedback and a primary cell population implicated in the generation of beta rhythms (David et al., 2015; Osinski & Kay, 2016). This suggests that MOB dependent processing of odour associations likely depends on changes in GC activity. However, only a few studies have examined GCs in such associative tasks.

Early microdialysis studies first suggested that olfactory associative learning might alter GC activity. Animals that learn to associate odours with rewarding stimuli show an enhanced amount of GABA release in the MOB. This enhancement is specific to the associated odour as no such increase is observed with unassociated odours or to the reward stimulus alone (Brennan et al., 1998). Although microdialysis can not distinguish between GABA release from GCs vs. other interneurons, the placement of the microdialysis probe in the EPL suggests at least some contribution from GCs in associative tasks. Immediate early gene analysis supports this notion as GCs display both increased *cfos* and *arc* expression following odour-footshock pairing (Fletcher & Chen, 2010; Funk & Amir, 2000). This *cfos* expression likely represents increased activity in GCs, but nuances of such enhancement, including the temporal and spatial specificity of the GC response, cannot be explored using c-FOS. One possibility is that GC activity indiscriminately increases. This may serve to add some overall level of inhibition to MTs, dampening weakly activated MTs and enhancing signal to noise. Another possibility is that GC enhancement is specific to those GCs stimuled by the odour and its learned association. Recordings from GCs in animals that are forming or have formed an odour-punishment association could help to bring clarity to such results since responses to both associated and non-associated odours can be assayed with finer temporal and spatial resolution.

The fear conditioning experiments stand in contrast to results observed with manipulations of GCs during the learning of associative tasks. Manipulation of GCs using either

genetic or chemogenetic strategies often produce little to no effects on the learning of odour-reward associations (Abraham et al., 2010; Lepousez & Lledo, 2013). Why this difference exists is not clear although it may reflect differences in the representation of punishment vs. reward in GCs. Many of the manipulation studies do not use punishment for incorrect responses while in fear conditioning studies, footshock is inherently punishing. It may also reflect technical limitations in the number of GCs that are affected using manipulative strategies (on the order of less than 30 %) or the use of alternative task-solving strategies employed by the animal (Frederick et al., 2016) such as differences in odour sampling. Artificial inhibition and excitation of GCs quickly becomes complicated as adding and subtracting inhibition to the circuit can alter MT activity to the point where simple odour detection becomes difficult. Again, recording from GCs as animals form associations should bring clarity to these confusing results. Unlike manipulation studies which effectively treat all GCs as the same, recordings provide more nuanced information concerning the heterogeneity of responses that GCs may display when animals form odour associations.

1.4.4 The Role of the Olfactory Bulb in Olfactory Discrimination

In the MOB, patterns of MT activity evolve over time such that even perceptually similar odours that activate overlapping subsets of GCs tend to become decorrelated in their representation at the level of the MTs (Gschwend et al., 2015; Friedrich & Laurent, 2001). This can occur on even on a short time scale, such as that of a single breath, and indicates that MOB circuits can be reformatted in a manner that may support odour discrimination.

In behaving animals, changes in gamma emerge with this change in MT activity. Gamma oscillations increase in amplitude when animals discriminate among perceptually similar, but not distinct, odours in 2AFC tasks (Beshel, Kopell, & Kay, 2007; Stopfer et al., 1997). This enhancement in gamma is only observed in animals that efficiently perform the task. Interestingly, opposite effects in gamma oscillatory power are observed in animals trained in a go/no-go task (vs. 2AFC). Compared to naive animals, trained animals display decreased gamma power, with the decrease often stronger for rewarded odours vs. punished ones (Lepousez & Lledo, 2013). These differences may reflect differences in the demands of the

two tasks, differences in electrical activity, or both. The latter is most likely. Increases in gamma power are observed in a higher frequency (60-80 Hz) than the decreases in gamma power (50-60 Hz) suggesting two mechanisms are at play. Together, these studies suggest gamma oscillations help to decorrelate stimuli with overlapping input activity and are particularly important for difficult discriminations.

Evidence for the role of granule cells in the discrimination of odour mixtures

To date, no direct recordings from GCs upon passive exposure to complex mixture stimuli or during a discrimination task have been completed. However, excitation of multiple glomeruli (as might be seen with mixture stimuli) evokes stronger responses in single GCs than excitation of a single glomerulus, suggesting GCs receive input from multiple glomeruli. Further, the aforementioned oscillation measurements strongly suggest GC activity may change, particularly when an animal discriminates between perceptually similar stimuli (Beshel, Kopell, & Kay, 2007). Gamma power in the MOB increases when rats, in a 2AFC task, must discriminate among similar (molecules differing by only one carbon) but not different odours. This increase in power (particularly in the 65-80 Hz range) is restricted to the odour sampling window, occurs in the MOB but not the PC, and is only observed in animals that perform the task with high accuracy. Gamma is thought to reflect activity in the dendrodendritic synapses between MTs and GCs, and disruptions of GC activity can decrease gamma power (Fukunaga et al., 2014). This suggests changes in GC activity are involved, or at least reflect, the discrimination of odours in 2AFC tasks.

In go/no-go tasks, disruption of GABA signalling through blockade of the $GABA_3A$ receptor disrupts both the gamma power decrease observed in trained animals and the animals' ability to discriminate among perceptually similar odours (Lepousez & Lledo, 2013). These results mirror those observed in honeybees where picrotoxin mediated disruptions of oscillations at 20 Hz (a rhythm in invertebrates analgous to gamma) disrupt discrimination for complex stimuli (Stopfer et al., 1997). From these experiments, we might expect altered GC activity when animals experience perceptually similar odours. This activity will likely

become particularly apparent when animals have some motivation to discriminate among the odours (such as in a 2AFC task).

Behaviourally, GCs improve discrimination capacity, particularly for complex stimuli. Deletion of the GluA2 subunit in GCs — a manipulation that increases Ca^{2+} entry and subsequent GABA release in GCs — improves discrimination performance (Abraham et al., 2010). Mice more quickly discriminate difficult odour pairs (60:40 vs. 40:60 binary mixtures), while the manipulation has no effect on simple discriminations (two different monomolecular odours). Similarly, activation of GCs through stimulation of ChR2 – a cation channel that increases cell excitability upon stimulation with blue light — also speeds discrimination time for perceptually similar odour mixtures (Nunes & Kuner, 2015). Fittingly, inhibition of GCs impairs discrimination. Both knockout manipulations (NMDA GLuN1 subunit knockout to decrease Ca^{2+} entry and GABA release) and the activation of inhibitory DREADDs (receptors that hyperpolarize neurons upon activation) increases the time animals require to discriminate among two odours (Abraham et al., 2010; Gschwend et al., 2015). Together, these results suggest GCs play an important role in enhancing the differences among stimuli that likely activate the same glomeruli or glomeruli with similar receptive fields.

1.5 How Might Changes in GC Activity Support Learning and Discrimination?

Changes in GC activity will ultimately manifest as changes in the inhibition of MTs, the exclusive target of GC dendrites. The connectivity pattern between these cells supports both local and long-range inhibition of MTs by GCs. Granule cell dendritic projections are often spatial restricted (100-200 μm), but MT lateral dendrites can extend up to one mm. Several lateral dendrites from multiple MTs can thus converge onto a single GC. Activation of a GC by a MT can then lead to reciprocal inhibition of that MT or to lateral inhibition of the other MTs synapsing with the activated GC. In particular, lateral inhibition has long been speculated to play a role in sensory sharpening, pattern decorrelation, and improved detection of stimuli upon learning.

Early hypotheses concerning MOB dendrodendritic synapses suggested lateral inhibition might serve to enhance contrast among odour evoked responses in MTs. Among other functions, enhanced contrast may help an animal to more readily identify meaningful odours by enhancing the responsiveness of neurons that help to identify that odour (over the responses that do not identify that odour) or help an animal to discriminate among perceptually similar odours by decorrelating the representative population activity of these odours. Classic models of lateral inhibition and contrast enhancement consider closely apposed neurons with overlapping receptive fields. However, as I have already highlighted, the MOB displays no obvious mapping of similar MTs in space (see chemotopic mapping above). Mitral/tufted cells with non-overlapping receptive fields can often be found adjacent to each other while MTs with overlapping receptive fields can be found mm apart. This suggests that if GC lateral inhibition functions to enhance contrast among MTs, a more complex relationship exists between MTs and GCs. One proposal is that the secondary dendrites of MTs with overlapping receptive fields might converge on distinct GCs. MT dendrites may then traverse long distances through the MOB to synapse with GCs. Another suggestion is that GCs show activity dependent inhibition. Arevian and Urban (2008) suggest that GCs lateral inhibition is recruited by MTs firing with distinct activity patterns, an effect they successfully demonstrated *in vitro*. For example, consider a two MT cell circuit — MT1 and MT2 — connected by a GC. If both cells fire at very low activity, GCs are not recruited by MTs and thus do not inhibit surrounding MTs. If one MT1 sufficiently activates the GC but MT2 is still not active, GC inhibition will have little effect on MT2, Similarly, MT2 is maximally activated, it will maximally recruit GC inhibition. Thus, there can be no more recruitment from MT1, and MT1 will have little effect on MT2. The best regime, then, for lateral inhibition is one in which MTs have similar, moderate levels of input and can cooperatively activate a GC.

How might learning or discrimination alter dendrodendritic inhibition to enforce contrast enhancement? Granule cell-MT synapses are highly plastic and display both long-term potentiation and long-term depression (Gao & Strowbridge, 2009), characterized respectively by a strengthening and weakening of synapses between coincidentally active neurons. This plasticity has long been proposed to be significant for learning and memory (Nabavi

et al., 2014; Sweatt, 2016). Coincident activation of GCs by both odours and learning related centrifugal input could selectively strengthen some dendrodendritic synapses. Upon re-exposure to that same input, GCs then might be more active and inhibit several more MTs, such that few MTs now represent that odour (presumably the ones activated strongly enough to overcome GC inhibition). Similarly, centrifugal input could bring subsets of GCs closer to spike threshold such that they provide, to selective MTs, more inhibition upon odour input. Provided different odours activate different subsets of MTs with stronger and weaker activation (Koulakov, Gelperin, & Rinberg, 2007; Arevian, Kapoor, & Urban, 2008), this could act to decrease overlapping activity at the level of the MTs. Such a model is consistent with the observed activity of MTs in animals engaged in discrimination tasks. Mitral/tufted cells are often suppressed more in animals that must discriminate among odours vs. those that passively experience the same odours (Fuentes et al., 2008). From this, we might predict that GC activity increases, at least in a subset of GCs, during discrimination, and that learning might act to enhance GC activity.

The GC-MT synapse has also been proposed to shape the temporal output of MTs. Based on the aforementioned studies concerning MOB/AL oscillatory activity across species, many have suggested that action potential timing and population oscillatory activity are integral for odour coding. Here, the idea is that downstream structures (ex: PC , AON) are receptive to when an action potential fires in relation to an oscillatory rhythm and/or are receptive to MT inputs that are coordinated in time. For example, coordinated inputs from MTs may result in closely timed EPSPs in downstream neurons. These EPSPs can be summated and produce action potentials, but only in downstream neurons that receive EPSPs within a time window favorable for summation (Schoppa, 2006). Different rhythms and patterns of inhibition may bind together alternative subsets of MTs in time and thus change the information that is available/meaningful to downstream neurons. Consistent with this idea of temporal synchrony, MT firing tends to occur at distinct phases of the breathing cycle — MCs at inspiration and TCs at expiration (Fukunaga et al., 2012; Shusterman et al., 2011). Further, behaving animals can detect where during the breathing cycle MT spikes occurs (Smear et al., 2011).

GCs are thought to enforce some of this temporal synchrony in MT circuits at multiple time scales. Alterations of GC activity shift both gamma oscillations and the preferred firing phase of MTs, suggesting their activity works to modulate distinct temporal features of MT activity (Fukunaga et al., 2012; Lepousez & Lledo, 2013). Interestingly, changes in GC activity are also proposed to underlie shifts between gamma and beta oscillations in the MOB, and by extension, may shift MOB oscillations to support different processing states such as those underlying odour discrimination and olfactory learning. The MOB shows sharp shifts between gamma and beta. Gamma is thought to rely on local activity at the dendrodendritic synapse whereby the oscillations reflect MT recovery from inhibition (Brea, Kay, & Kopell, 2009; Lagier, Carleton, & Lledo, 2004; Isaacson & Strowbridge, 1998). In contrast, beta relies on feedback to the MOB from centrifugal inputs, as disruption of this feedback precludes beta. Computational studies suggest that this centrifugal feedback increases GC depolarization in at least some subset of GCs, causing them to spike (David et al., 2015). This spiking prolongs inhibition in MTs and resets the MOB from gamma into beta (David et al., 2015). In support of this, disruption of NMDA signaling, an manipulation that effects local signaling at the synapse, disrupts gamma, but not beta oscillations. Conversely, blocking GABA transmission, a manipulation that is expected to decrease the effect of spike dependent release of GABA, decreases beta oscillations (Lepousez & Lledo, 2013). Given the enhanced MOB beta power observed in go/no-go learning tasks, we might expect then that at least a subset of GCs will show enhanced spiking activity when animals learn odour associations.

1.6 Summary: GCs as Targets of Centrifugal Inputs and Key Hubs in MOB Flexibility

As I have highlighted throughout the above sections, the GC population is a key hub for the integration of odour related and context related activity in the MOB (Fig1-5). Granule cells receive input from centrifugal fibres and, in light of centrifugal input activity, modulate MTs through dendrodendritic synapses. They can thus have a powerful effect on the information that leaves the MOB and a powerful effect on how animals identify and respond to odours

in context. The evidence above also predicts that GCs will show dynamic activity *in vivo* and that this activity will change/update with learning.

To date, these predictions have not been explicitly tested. In fact, very few studies have examined the dynamics of GC activity *in vivo* at all, and those that have, examined GCs under anesthesia. These studies report low spontaneous firing rates (1-2 Hz) in GCs and breathing-locked activity that readily adapts with the first respiration cycle (Wellis & Kauer, 1993; Cang & Isaacson, 2003). Responses are generally sparse and excitatory (but see (Tan et al., 2010)). Such activity, while consistent with studies of MTs in anesthetized states, does not capture the activity we might expect for GCs in more complex contexts.

1.6.1 Goals of This Thesis

During the course of my thesis work, I endeavoured to better describe GC activity and its reflection of olfactory context. I specifically focused on two goals: (1) examining GC spiking activity across different states of the animal, particularly across anesthesia and wakefulness and (2) examining GC spiking activity during odour reward and punishment learning. I had two specific predictions concerning these experiments:

- Both modeling studies as well as observed sparseness of MTs in awake animals suggest GC activity is increased during wakefulness compared to anesthesia. Broader odour tuning of GCs might enforce sparseness in MTs.
- Previous studies on olfactory learning and memory suggest at least some subset of GCs will show enhanced activity during learning and that this activity, like beta oscillations, may depend on the association of an odour with some behavioural outcome (i.e. reward or punishment).

To address these predictions, I first had to establish a paradigm in which I could assay GC activity in these relevant contexts. Previous results have all examined GCs in *in vitro* or anesthetized contexts as GCs are small and particularly difficult to record from *in vivo*. In Chapter 2, I detail how I solved this problem using a head-fixed paradigm. I, along with collaborators in the lab, specifically chose to develop a paradigm that would allow us to

observe activity on a fast time scale and thus allow us to measure activity that might correlate with interesting behavioural rhythms. Importantly, this paradigm allowed us to examine differences in awake vs. anesthetized animal (Chapter 3). Having established an awake paradigm for recording GC activity, I then used this paradigm to examine how GCs reflect learned odour outcomes (Chapter 4). Specifically, I developed a paradigm that might allow us to see rapid changes in GC activity as animals learn to flexibly associate odours with punishing outcomes.

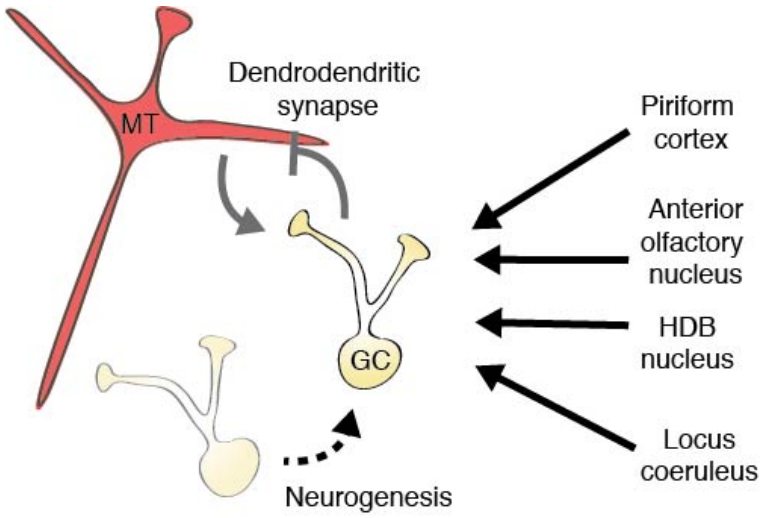

FIGURE 1.5: **GCs are a key hub for context related processing in the olfactory bulb.** Granule cells receive odour input from mitral cells and are thus privy to sensory information. They are also a primary target of centrifugal input to the bulb. These centrifugal signals carry information about the animal's state and odour meaning. Granule cells also undergo regular turnover, even in the adult animal. This neurogenesis has been implicated in several forms of learning. These key features make GCs an excellent cell population through which to modulate MOB activity in accordance with the animal's state and previous learning history.

Chapter 2

Recording from Granule Cells in Awake Animals

The work in this chapter was completed with help from Kerensa Crump and Billy Lau. Parts of this chapter were published in the book ***Neural Tracing Methods: Tracing Neurons and Their Connections*** *(ed. Ben Arenkiel) under the Chapter title "Simultaneous Collection of In Vivo Functional and Anatomical Data from Individual Neurons in Awake Mice." See Appendix A.*

2.1 Introduction

Main olfactory bulb excitatory neurons show considerable differences in activity dependent on the internal state of the animal and the animal's association of odors with rewarding and punishing outcomes (Rinberg & Gelperin, 2006; Kay & Laurent, 1999). As I have highlighted in Chapter 1, GCs are poised to play a fundamental role in this context-dependent processing of olfactory information. They are the primary targets of much of the centrifugal input that carries information about non-sensory variables, and importantly, through their dendritic processes, they can influence MOB excitatory neurons in accordance with this non-sensory information.

In the past, all *in vivo* studies of GCs were conducted in anesthetized animals (Cang & Isaacson, 2003; Tan et al., 2010; Wellis & Kauer, 1993). Anethestics limit the movement of animals and thus eased whole cell patch data collection from GCs that, due to their small

size and small amplitude APs, proved particularly difficult from which to record using more traditional techniques like metal electrode recordings (Doucette et al., 2011; Kay & Laurent, 1999; Rinberg, Koulakov, & Gelperin, 2006; all groups report no spikes detected when passing electrodes through GCL). Using patch techniques in anesthetized animals, researchers were able to observe, for the first time, the activity of GCs *in vivo* and provide powerful information concerning how GCs integrate subthreshold activity. However, this technique was not without caveats. Anesthetics can disrupt a neuron's intrinsic excitability as well as the activity of inputs to neuronal circuits of interest. This can ultimately change how GCs respond to odors. Further, awake animals, as opposed to anesthetized animals, can both actively sample their environment (through sniffing) and form odor associations that may alter how odors are coded in neuronal circuits. Thus, while we know GCs respond to odors *in vivo*, we still lack a clear understanding of the dynamics of this activity.

Recently, some groups have explored GC activity in awake animals using Ca^{2+} imaging (Kato et al., 2012; Wienisch & Murthy, 2016). These studies have demonstrated much more complex activity of GCs than previously expected from anesthetized recordings. Due to the relatively slow time course of GCaMP indicators, however, several interesting aspects of GC activity could not be explored. For example, GC spiking could not be observed in relation to an animal's breathing/sniffing as this rhythm is often faster than the full onset and decay time of GCaMP. Similarly, GC spiking in relation to faster MOB rhythms (gamma and beta) could not be examined. These fast rhythms, in particular, have been linked to activity in GCs, but the relationship of single neuron GC firing to this synchronized activity has never been assayed *in vivo*. Again, this largely relates to the fact that most techniques used to record from GCs lack temporal resolution or do not permit the examination of GCs in relevant contexts. Increased power in gamma and beta rhythms often arise in animals as they form odor associations or discriminate among odors (Beshel, Kopell, & Kay, 2007; Kay & Beshel, 2010; Kay et al., 2009), a state largely contingent on the animal's wakefulness.

Our lack of understanding concerning GC activity dynamics necessitates the development of methods to better record GCs in relevant contexts. From the anesthetized recordings previously conducted by others, we knew that patch recordings worked well to record the

fast (single APs) of GCs. We thus sought to develop a paradigm in which we could use similar techniques to reliably record from GCs but do so in awake animals. For several reasons, we chose to perform loose-patch recordings in head-fixed mice as we reasoned such a set-up would provide us with several advantages over other existing procedures. First, the use of head-fixed procedures would limit excessive or abrupt movement of the animals, providing a stable set-up in which to record from small GCs. Second, through the use of an electrophysiological technique (vs. an imaging technique), we could probe the fast activity of GCs, and in the future, examine how GC activity correlates with MOB rhythms. Third, using high impedance electrodes (as opposed to the lower impedance tetrodes), we would have an advantage in isolating single GC units and could thus easily identify even the small amplitude extracellular spikes exhibited by GCs. Finally, through use of dye fills following recording, we could unequivocably distiguish GCs from all other cells in the MOB.

Below, I describe our success in implementing this head-fixed loose patch paradigm to record from GCs in awake animals. Using this technique, we, for the first time, successfully recorded the fast activity of GCs in awake mice and recorded GC activity for long enough periods to assess odor evoked and contextual responses (further described in Chapters 3 and 4).

2.2 Methods

2.2.1 Animals

We performed experiments on adult (typically aged 6–12 weeks) male C57Bl/6 mice (Jackson Laboratory) and on adult CD-1 mice. We observed no differences in the success of the procedure across different strains. We maintained mice on a 12/12 h light dark cycle (lights on 0700 h) and provided the mice with food ad libitum. While, in principle, singly-housing mice could improve the stability of the head-bar (as other mice cannot groom the mouse or otherwise disrupt the head-bar), we did not notice significant differences in head-bar stability between singly house and group housed mice. Stability of our recordings instead depended

on the length of time between head-bar surgery and recording. We, thus, chose to group house mice in cages of up to five animals.

2.2.2 Surgery

We affixed custom-made titanium head-bars to the skull of mice using dental acrylic (Fig.2-1A). We anesthetized animals with an 80:20 mixture (1.25 ml/kg) of ketamine (100 mg/ml) and xylazine (20 mg/ml) and stabilized animals in a stereotaxic frame. We affixed a head-bar to the skull immediately posterior to the coronal suture using either adhesive luting cement (Parkell, Inc) or adhesive resin cement (RelyX Ultimate) followed by methyl methacrylate-based dental cement (TEETS). When we first set up these recordings, we secured four machine screws (Amazon Supply) to the skull prior to application of the luting/resin cement with the expectation that these screws would provide an additional anchor for the acrylic. However, as we have discovered over time, these screws are not absolutely necessary; and in cases where animals are used for long periods (> one week), the screws may actually degrade the stability of the head-cap as they can introduce fractures in the skull that worsen over time. Instead, we found head-cap stability was highest when we thoroughly dried the skull prior to applying the cement. Typically, we prepared and dried the skull through use of an etching solution (weak HF acid) and the application of pressurized air.

2.2.3 Electrophysiology

We conducted *in vivo*, blind loose-patch recordings using borosilicate micropipettes tip-filled with intracellular solution (125 mM potassium gluconate, 10 mM potassium chloride, 2 mM magnesium chloride, 10 mM HEPES, pH 7.2) and further filled with 1.5 % neurobiotin (NB). Neuronal spiking was recorded using a BA-03X bridge amplifier (npi Electronic Instruments), low pass filtered at 3 kHz, and digitized at 10 kHz. We acquired data using Spike2 software.

2.2.4 Immunohistochemistry

Following recording, we sacrificed animals using an overdose of sodium pentobarbital (Euthasol), and we transcardially perfused animals with PBS followed by 4 % paraformaldehyde (PFA). We extracted brains in the skull and stored them in PFA for 12–16h followed by 30 % sucrose for 24 h. To stain olfactory bulb sections (100 μm), we treated tissue according to standard immunohistochemistry procedures using 1:667 streptavidin:Alexa Fluor 594 or Alexa Fluor 488 (Invitrogen) in 0.3 % Triton-X in PBS. We first viewed sections under epifluorescence (Olympus BX43) and further examined images using a LSM 710 laser scanning confocal microscope (Carl Zeiss). Here, we only report cells identified as GCs or as being in the GCL as there was no difference in the activity between these two populations (See Chapter 3 Fig.3-2 for further detail).

A detailed description of the parts and construction of our recording set-up is included in Appendix A.

2.3 Results

2.3.1 Head-fixation of Mice Running on a Rotating Cylinder

Traditionally, researchers have conducted patch-clamp recordings either *in vitro* or in anesthetized animals largely because patch-clamp techniques require considerable stability. In traditional freely moving paradigms, researchers implant electrodes in mice and cement the holders for these electrodes to the head of the animal. Some groups have since adopted this latter strategy for intracellular recordings *in vivo* in both birds and mice (Fee & Long, 2011; Vallentin & Long, 2015; Schneider, Nelson, & Mooney, 2014). This method, a remarkable feat in single unit recording, provides the best measure of neuronal activity in context. Single units and subthreshold activity can be unequivocably distinguished while a mouse engages

with its environment in a manner closest to its natural state (i.e. free exploration). Unfortunately, the method is extremely low-throughput as once an electrode is implanted, the researcher cannot re-position the electrode in the medial/lateral or rostral/caudal dimensions nor can she implant a new electrode in the same spot.

We instead chose to use a head-fixed preparation in which we head-fixed an animal over a suspended, rotating cylinder. Prior to recording, we made acute craniotomies in the skull of the animals, and then after a waiting period (from 30 min to one day), we fixed the animal in place over the ball. We reasoned this regime would provide us with two advantages:

- the acute craniotomy would allow us to pass an electrode multiple times into the brain of the animal and maximize our chance at recording a GC (or several GCs) in a single session.
- the use of a rotating cylinder (wheel) would approximate some of the experience of the freely moving animal — the animal need not sit in place but can walk/run as desired. This would give us richer information concerning the dynamics of activity across state (i.e. differences between quiet and active states). Further, any forceful movements of the animal that might normally result in thrusts against the head-cap instead would be translated into rotational movement on the wheel, thus improving the stability of our recordings.

For head-fixation, we constructed custom-made, titanium head-bars (Fig.2-1A top). Over the course of our experiments, we designed several different bars to suit our recording and stability needs. For example, in some of our experiments, we recorded from GCs in animals passively experiencing odors (see Chapter 3). For these animals, straight head-bars with fixation points at either end of the bar sufficed (Fig.2-1A top left). We fixed this head-bar in place on an area of the skull directly posterior to the olfactory sulcus. In our experience, positioning the head-bar any further back decreased the stability of the recording. In other experiments, we first trained animals to associate odors with some stimulus outcome (see Chapter 4). Due to the extended period of time these animals spent head-fixed (often two to three weeks), we required head-bars with more fixation points (Fig.2-1A right). As such, we

designed a head-bar that could we could fix directly over the MOB and that we could hold at three different attachment points.

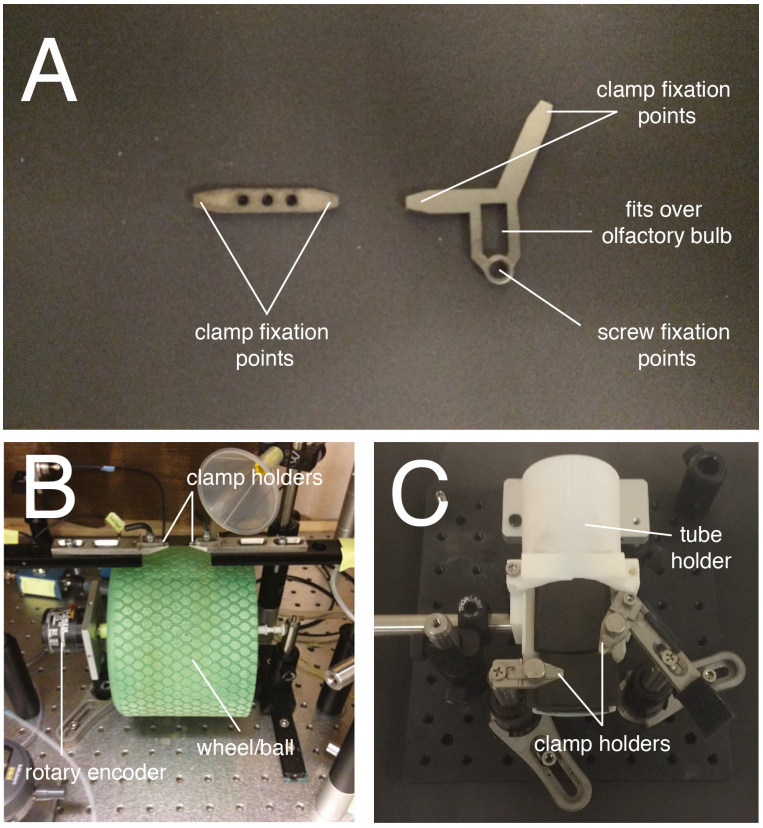

FIGURE 2.1: **Head-fixation set-up.** (A) Head-bars. Dependent on the experiment, we attached one of two head-bars to the skull. For recordings from passive animals, the head-bar on the left sufficed. For recordings in animals learning an olfactory task, we used the head-bar on the right. This head-bar had more attachment points including two clamp attachment points (one at 90 degrees to the nose and one at 45 degrees) and one attachment point on the front of the bar in which we could attach another holder with a screw. We passed recording electrodes through the empty rectangle in the middle of the head-bar. (B) Mouse wheel. We head-fixed mice in place over the a foam roller. We recorded running on the ball using a rotary encoder. (C) Mouse tube holder. In our experience, this type of holder did not work well for naive mice but was effective for mice trained in go-no go tasks.

We fixed mice in place over a wheel constructed from an exercise foam roller (Exervo TeraNova EVA) cut into a six inch section. We clamped the head-bar in place using custom made head-bar holders (Fig.2-1B). The ends of the bar fit snugly into a metal holder. We then clamped the top of the head-bar with custom clamps to further hold the head-bar and mouse's head in place. For mounting of the wheel, we hollowed out a section in the middle of the roller through which we placed a metal rod (ThorLabs mini series posts). We then mounted the wheel on one end using a fixed post and on the other end using a rotary encoder. This rotary encoder (see Appendix A) allowed us to track the walking/running of the animal during a recording session (Fig.2-2B top). In subsequent experiments, we have also used more traditional mouse holders including those in which we head-fixed the mouse in place in a custom 3-D printed, stationary tube (Fig.2-1C). In our experience, this holder worked well for trained mice, who over the course of several days, became more habituated to the holder. Further, the motivation to work for water rewards kept them much more calm than naive, untrained mice. We can thus recommend the use of a head-fixed wheel apparatus for both naive and trained mice but we can recommend the tube holder only for trained mice.

Overall, using a head-fixed set-up, we could stably place a mouse's head (and by extension brain) in a fixed position. This stable positioning in turn allowed us to record from the mouse using loose-patch electrophysiological recording methods.

2.3.2 Recording from and Identifying Granule Cells in Head-fixed Mice

To conduct single unit recordings from GCs, we made craniotomies in the skull over the MOB of mice with head-bars. To obtain stable recordings from GCs, it was critical that we made these craniotomies as small and as a clean (no blood) as possible. To do so, we thinned down the skull over the MOB and then cut out small areas (<200 μm by 200 μm) using a blade breaker. We did not need to clear away the dura as our patch electrodes were sharp enough to pierce it, and in fact, explicit attempts to clear the dura often resulted in more bleeding and damage that precluded recordings. We kept the craniotomy moist using saline

soaked gel-foam placed over the exposed brain. During recording, we further kept the areas moist and stable using 1 % agarose.

We conducted our recordings using borosillicate pipettes pulled on a Flaming/Brown type micropipette puller. Researchers who conduct loose patch and whole cell recordings in other settings typically use pipette resistances of 1-10 MΩ. We found it necessary to use higher resistances with our pipettes (20-25 MΩ). This greatly improved our ability to isolate single GCs that often had small extracellular spikes (1-2 mV).

We performed blind patch recordings from GCs. Similar to other groups (DeWeese, 2007), we searched for cells using small, regular current pulses (200 pA, 2.5 Hz, Fig.2-2A). In accordance with Ohm's law, changes in resistance are accompanied by changes in voltage (with stable current pulses). Because cell membranes have an associated resistance, we could thus recognize that we had encountered cells when we observed increases in the size of the current generated voltage steps. We typically searched for cells in the GCL between 600 and 1000 μm below the surface of the brain, but in some cases, we recorded cells in even deeper layers of the bulb (2000 μm). As shown in Fig.2-2B, would could reliably detect the spiking activity of GCs even when the animal ran on the wheel. We found that GC spike amplitudes ranged in size from 0.5 mV to 10 mV.

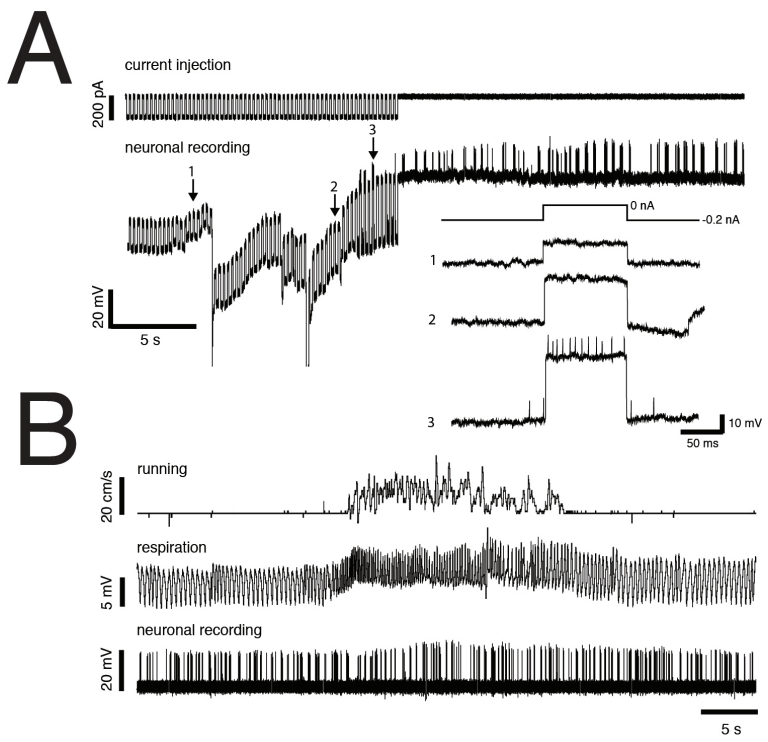

FIGURE 2.2: **Blind, loose patch recordings from mice running on a wheel.** Example data gathered during isolation and recording of a mouse main olfactory bulb GC in an awake, running mouse. (A) Raw physiology traces of current (top) and voltage (bottom) during acquisition and isolation of a GC. For the first half of this recording, we used 200 pA negative current pulses to monitor pipette resistance while searching for a cell. The numbered traces show the voltage response at the labeled time points. Note the increase in the voltage deflection. Near the halfway point, we turned off the pulses, in order to isolated spiking from a single unit. The numbered traces show the voltage response at the labeled time points. (B) In our setup, unit recordings are stable during free running. The top trace shows the signal output of our wheel velocity sensor, reflecting a 20–25 s episode of running. The middle trace depicts the signal from a nasally implanted thermistor to sense respiration. The bottom trace is the voltage trace from the same neuron depicted in (A).

In the absence of more involved opsin based identification or microscope guided recording techniques, researchers who use traditional metal electrode recording techniques, do not typically know from what type of cells they record. Fortunately, patch recordings not only allow researchers to assay the electrical activity of neurons but to also identify these same neurons using dyes. One can place these dyes in the micropipette used for recording and dye fill the neurons using electrical pulses. In our case, we injected a 1.5 % NB solution into GCs using large positive current injections (700-900 pA, 500 ms pulse duration) and identified the cells post-mortem using a streptavidin conjugated Alexa Fluor. In most cases, we only injected cells for 5-10 min as we often lost the seal/ability to record the cell following this time. Nevertheless, this was often enough time to inject an appreciable amount of NB in order to label the GC soma (Fig.2-3A). From this alone, we could characterize the recorded cells because GC soma are smaller in size than other cell types in the GCL (Pressler & Strowbridge, 2006; Schneider & Macrides, 1978). With longer fills, we also labelled GC dendritic trees (Fig.2-3B). We used both Alexa Fluor 488 and Alexa Fluor 594 to label NB filled neurons, but in practice, green neurons were often easier to identify. This likely relates to the fact that Alexa Fluor 488 has a higher quantum yield.

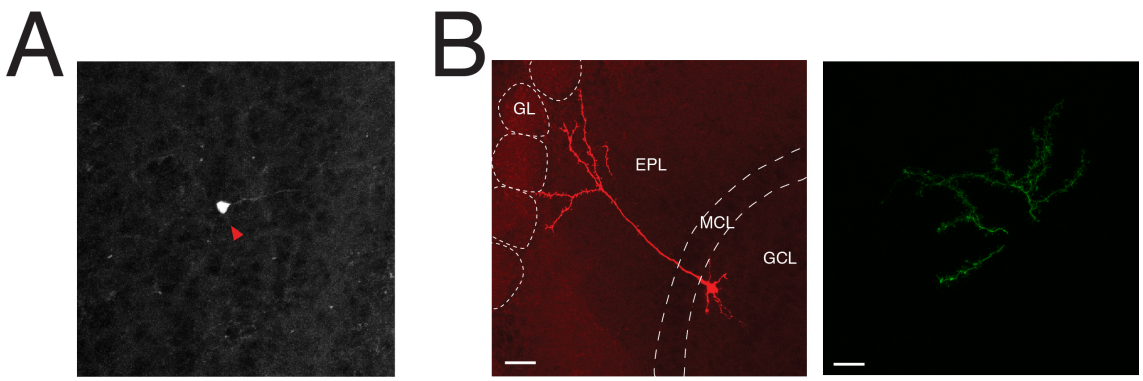

FIGURE 2.3: **Neurobiotin-streptavidin staining of granule cells.** Following GC loose patch recordings, we filled cells with a 1.5 % NB solution and stained post-mortem with streptavidin Alexafluor 488 or 594. (A) Shorter fills (on the order of 10 min) resulted in cell body labelling (red arrow labels cell body) while longer fills (B) also resulted in labeling of the GC dendrites. scale bar (A) = 20 μm and scale bar (B) 40 μm.

2.3.3 Granule Cells Can Be Reliably Recorded and Labeled in Awake Mice

Using our head-fixed paradigm, we could reliably find, record from, and fill GCs in awake animals. The loose patch techniques we describe here are inherently limited to recording from a single neuron in only one session (i.e. the same neuron cannot be recorded in another session). We thus asked whether the amount of time we were able to record from these neurons would be enough time during which we could collect any meaningful data concerning GC activity. We recorded from 118 neurons in awake mice. The mean recording time for this population of cells was 10.4 $\pm$ 5.7 minutes while the median recording time was 8.7 $\pm$ (Fig.2-4A). In principle, this is enough time to present several trials of a panel of odours to an animal (10 trials of five odours with a 10 s interstimulus interval = 8.6 min). This mean recording time was influenced by several factors including cell loss due to movement of the mouse's head as well as purposeful termination of the recording by the experimenter in order to begin filling the cell with NB. If we consider a median fill time of 10 min across all cells and then add the amount of time lost from recording due to purposeful terminations, we could increase the median recording time to 18 min and double the number of odour trials we might present (Fig.2-4A,C).

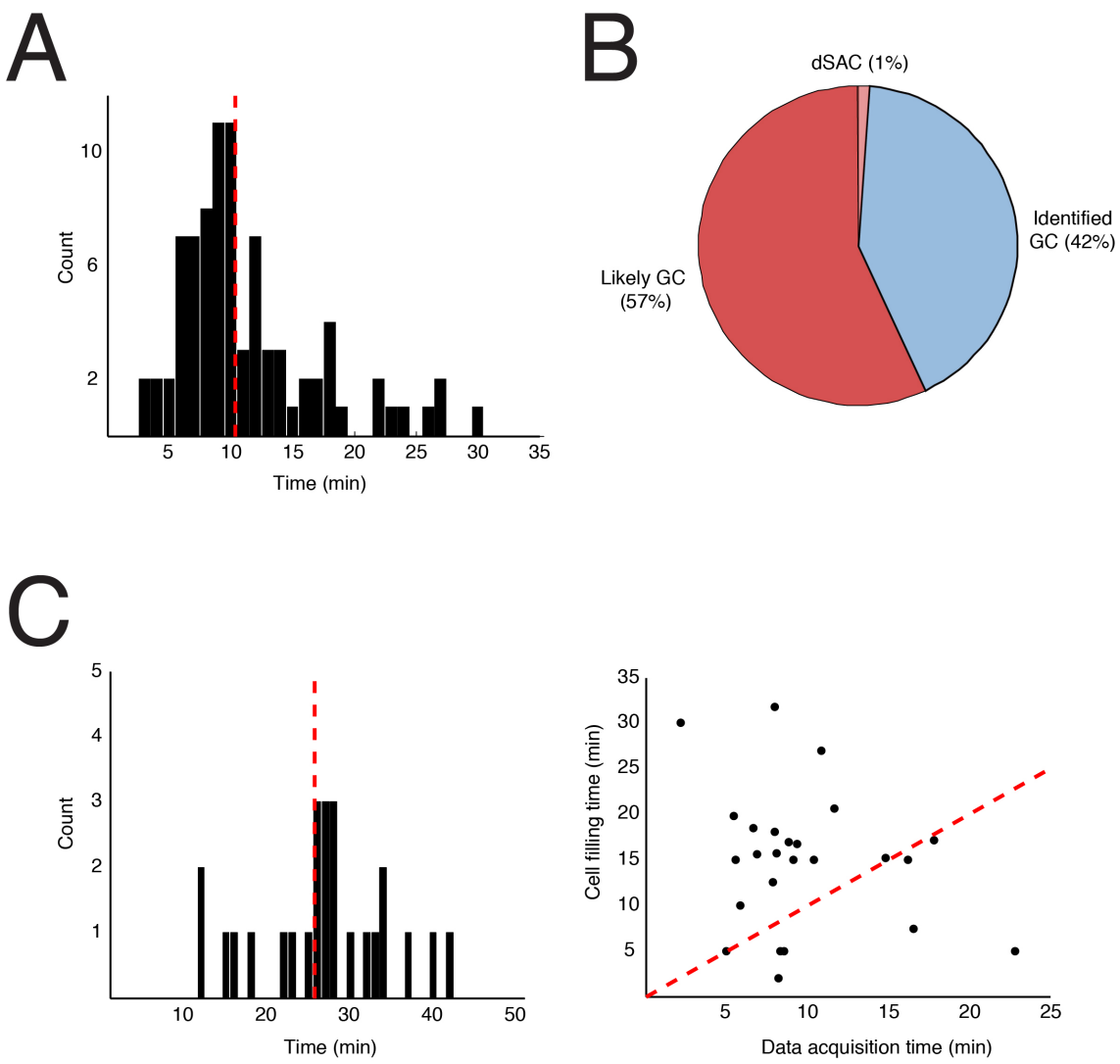

FIGURE 2.4: **Recording lengths in GC loose patch recordings.** (A) Histogram of recording lengths across all cells recorded (n=118 separate recordings). The length of recordings varied from a few minutes to half an hour with a mean of 10.4 $\pm$ 5.7 min. n = 118 (B) A subset of neurons could be unequivocably identified using NB fills and post-mortem streptavidin-fluorphore staining. While most of these cells we recorded are either identified GCs or likely GCs, a small percentage of the cells are deep short-axon cells. (C) Histogram of total recording time when cell fill time is also considered. Recording lengths dramatically increase if we consider the neuron filling time. The mean sum of data acquisition (i.e. time spent recording from a GC and presenting odours) and the cell fill time was 24.7 $\pm$ 7.9 min. There was no correlation between data acquisition time and cell filling time (r = -0.24).

This increase in median time, is likely an overestimate for many cells. We found that the quality of postmortem staining depended on the health of the cell and maintenance of a tight seal throughout the filling duration. We achieved this for a subset of the cells we recorded (38 %, Fig.2-4). In this subset of cells which we term GC identified (GCid), we could identify a cell body in the GCL. In the other subset of cells, we could not unequivocably identify the cell body of the recorded cell, but we could see either an electrode tract in the GCL or diffuse streptavidin staining in multiple cells. This indicated either a cell lost or a seal that degraded in quality during the filling. In our experience, we rarely recorded other cell types in the GCL (only 2 out of 45 identified neurons were dSACs; Fig.2-4B). Because of this, we defined the population of cells in which we did not see definitive staining as GC likely (see Chapter 3 for further characterization of the similarities between these two populations).

In order to gain a better representation of the recording time length, we calculated the fill time for those neurons which we could definitely identify as GCs and for which we had data concerning the fill time length (25 cells). Ideally, we would have filled all neurons for at least 20 min. However, in many cases, we could not do so because we either lost the cell or we abandoned the fill when the cell started to look unhealthy (i.e. excessive firing or loss of spike amplitude). Across the 45 neurons, fill times ranged from 2 min to 32 min. Adding the fill times to the data acquisition times increased the mean overall recording length to 24.7 ± 7.9 min (median 25.3 min, Fig.2-4C). For this subset of cells, there was no significant correlation between the recording time and the fill-time time (r = -0.24, Pearson correlation) indicating that the fill procedure itself can disrupt even excellent quality patch recordings. Overall, our data suggest that one can record from GCs for several min. We regularly recorded neurons for 10-30 min which is a long enough period to present several odour trials and even assess learning.

2.3.4 Spike Shape Does not Define Granule Cells

Researchers studying cortical neurons often use spike shape to distinguish between regular spiking (putative excitatory) and fast spiking neurons (putative parvalbumin positive interneurons, Niell & Stryker, 2008). We wondered whether we could use similar methods to

distinguish between inhibitory GCs and excitatory MTs. To examine this, we compared the spikes from population of 12 MTs to 17 GCs (Fig.2-5A). All of the cells we compared were positively identified post-mortem with streptavidin staining and had enough spikes to accurately described spike shape. For each cell, we determined the peak and trough height of each spike and computed a mean peak height to trough height ratio. We further determined the time between the peak and the subsequent trough for each spike (Fig.2-5B). In Fig.2-5C, we plot the mean ratio vs. time for each cell (mean across all spikes for an individual cell). Unfortunately, we do not observe any clear clustering of cells using this analysis. Many of the GCs overlap with MTs, indicating that, at least for a subset of our cells, we cannot use spike shape to reliably distinguish among GCs and MTs.

Unfortunately, due to lack of dSAC data, we could not reliably compare dSAC and GC data. The data for the two definitively identified dSACs (Fig.2-5C yellow) we did record, however, fell within the cloud of MTs and GCs. This suggests, that even if we had more data, we would not be able to reliably distinguish between dSACs and GCs based on spike shape. Overall, these results indicate that spike shape cannot be used to reliably distinguish among the MOB cell types we assayed. Instead, with single cell data, one must rely on other methods (ex: NB-streptavidin staining, optical tagging) to identify different cells.

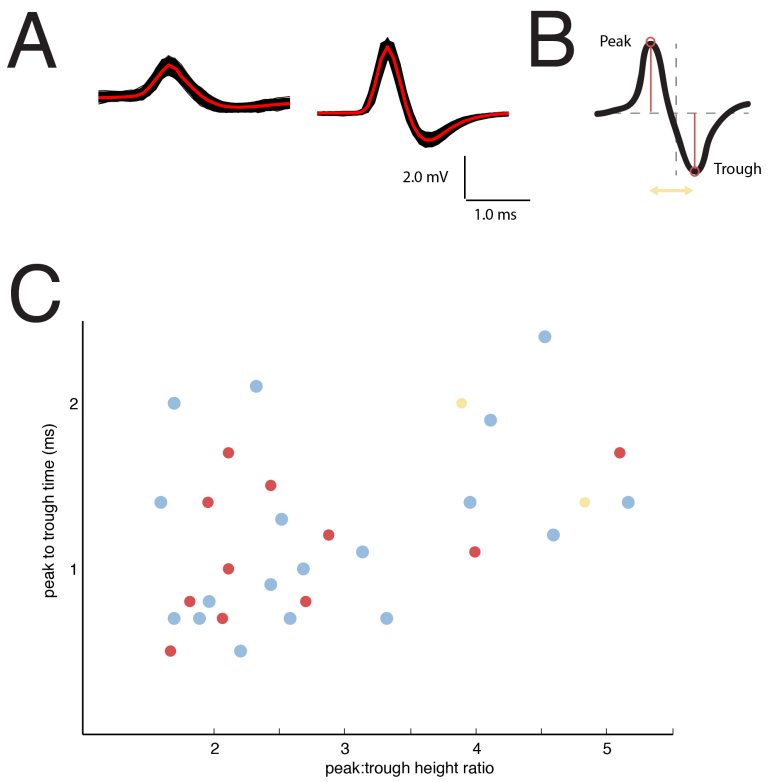

FIGURE 2.5: **GCs cannot be identified by spike shape.** We examined data from MTs, GCs, and dSACs as based on our recording depths (600-2000 μm), these are the cells we are most likely to record. (A) Example GC (left) and MT (right) waveforms. Red line displays the mean trace computed from all single, black traces. (B) For each spike of a given cell, we determined the waveform peak and trough. From this we computed a peak height to trough height ratio as well as the time (ms) from peak to trough (yellow arrow). (C) Scatter plot of height ratios to peak:trough time. Data from GCs (blue), MTs (red), and dSACs (yellow) showed significant overlap. n = 17, 12, and 2 respectively.

2.4 Discussion

Here, I described the method we used to record from GCs in awake animals. Using this method, we could reliably record many GCs for a period of time, that is, in principle, long enough to acquire meaningful data from GCs concerning their odour tuning.

Several methods for recording from single units *in vivo* exist including patch-clamp techniques, multi-unit recording with either single unit or tetrode arrays, and GCaMP imaging. Each of these methods has their own set of advantages and disadvantages, and largely, choice of technique depends on experimental question and, simply, what works. In our case, we chose to use blind-patch recordings for their ease of set-up, their superiority for recording single-units at fast time scales, and for the fact that using them, we could obtain reliable recordings from GCs. Other groups have also used GCaMP imaging to assay GC population activity in awake mice (Kato et al., 2012; Wienisch & Murthy, 2016). This, along with the methods described here, has provided unprecedented insight into the dynamic activity of GCs.

Importantly, the methods we describe in this chapter provide us with an advantage in studying the fast dynamics of GC activity. Extensive research now supports the idea that rhythmic activity in the MOB is important for odour coding and olfactory learning (for review see Kay et al., 2009). In particular, this rhythmic activity manifests at frequencies much faster than the onset and delay time-course of calcium imaging. In Chapter 3 and Chapter4, we exploit this fact to explore how GC activity correlates with breathing rhythms and evolves over the course of an odour presentation. Such explorations are not possible with current imaging techniques.

In the cortex, spike shape has been used to differentiate inhibitory neurons from excitatory neurons. In our case, spike shape was not a good predictor of cell type —- many GC spikes looked identical to MT spikes. In our experience, the best predictor of GC identity was spike amplitude as GCs often fire low amplitude spikes (1-5 mV). Unfortunately, at least with extracellular methods, this is not a good metric for identifying cell types as, in these type of recordings, spike amplitude can vary as a function of the distance of the

patch electrode from the cell or as a function of the tightness of the seal. In our recordings, we instead used distance from the pial surface as a rough indicator that we had placed our patch electrodes in the GCL (around 600-2000 μm in depth). Following recording, we filled neurons with a NB tracer that we detected post-mortem. We then identified GCs based on their morphology and placement in the GCL. Alternatively, one could use photo-stimulation methods to identify different cell-types during the recording. These methods exploit the CRE-dependent expression of ChR2 in genetically specified cell types (Lima et al., 2009). In theory, this should help in distinguishing GCs from MTs as one can express ChR2 in either transgenic mice that express *cre* in GABAergic or glutamatergic cells respectively. However, a broad *cre* line will not be useful for distinguishing among GCs and dSACs as both of these cell types express classic GABAergic markers (GAD, VGAT). While a single genetic marker that labels all GC cells and no dSACs has not been identified, dSACs as opposed to GCs may exclusively express somatostatin and neuropeptide Y (Scott, McDonald, & Pemberton, 1987).

Overall, the methods described here allowed us, for the first time, to record from GCs in awake animals *in vivo*. We exploited these methods to examine how GCs might differ in awake vs. anesthetized states (Chapter 3), a useful endeavour given to date, GC activity had only been explored *in vivo* in anesthetized animals. We further exploited these methods to explore GC activity dynamics across learning (Chapter 4).

Chapter 3

Granule Cells Display Profound State-dependent Activity

This chapter was previously published in Nature Neuroscience (2014) under the title "Broadly tuned and respiration-independent inhibition in the olfactory bulb of awake mice." I am indebted to Billy Lau, Kerensa Krump, and Heike Demmer for help with the experiments described. The text has been adapted in some places to reflect the overall tone of the thesis.

3.1 Introduction

Sensory representations are highly dynamic and can be reformatted to match shifting behavioural objectives (Gilbert & Sigman, 2007). Pervasive inhibitory networks intrinsic to sensory brain regions are well-positioned to broadly regulate temporal patterning and receptive fields, and they are therefore proposed to be critical for state-dependent activity (Cardin et al., 2009; Gentet et al., 2012; Haider, Häusser, & Carandini, 2013; Polack, Friedman, & Golshani, 2013; Sohal et al., 2009). As an example, neural activity in the MOB is state-dependent (Cury & Uchida, 2010; Davison & Katz, 2007; Doucette, Milder, & Restrepo, 2007; Doucette & Restrepo, 2008; Kato et al., 2012; Kay & Laurent, 1999; Rinberg, Koulakov, & Gelperin, 2006; Shusterman et al., 2011). It has long been suspected that this property is achieved through cortical and neuromodulatory feedback projections accessing the local network of inhibitory interneurons in the MOB (Boyd et al., 2012; Markopoulos et al., 2012; Mouret, Murray, &

Lledo, 2009). Nevertheless, the temporal activity patterns and stimulus selectivity exhibited by these interneurons during wakefulness are not known.

As highlighted in Chapter 1, MTs form the major class of excitatory neurons in the MOB that send sensory information to the olfactory cortex. Temporal patterning and receptive fields in MTs depend heavily on behavioural state (Cury & Uchida, 2010; Davison & Katz, 2007; Fuentes et al., 2008; Rinberg, Koulakov, & Gelperin, 2006; Shusterman et al., 2011). For example, odour representations in awake animals are sparser and more selective than those seen under anesthesia (Davison & Katz, 2007; Rinberg, Koulakov, & Gelperin, 2006), and MTs exhibit precise bursts of activity that are tightly synchronized to sniffing (Cury & Uchida, 2010; Shusterman et al., 2011). Thus, during wakefulness, MT activity is characterized by smaller, odour-specific neuronal ensembles and strongly respiration-locked output.

The inhibitory actions of GCs are well positioned to dynamically sculpt these state-dependent features of MT activity. It is well-established that GCs provide feedback inhibition to MTs through a reciprocal dendrodendritic synapse (Abraham et al., 2010; Isaacson & Strowbridge, 1998; Jahr & Nicoll, 1980). Based on this observation, it has been widely proposed that feedback inhibition from GCs contributes to temporally patterned activity and stimulus selectivity of MTs (Giridhar & Urban, 2012; Kay et al., 2009; Koulakov & Rinberg, 2011; Shepherd et al., 2007). While this is consistent with a number of studies (Tsuno, Kashiwadani, & Mori, 2008; Vucinić, Cohen, & Kosmidis, 2006; Yokoi, Mori, & Nakanishi, 1995), *in vivo* recordings from GCs have largely been limited to anesthetized animals (Cang & Isaacson, 2003; Kato et al., 2012; Tan et al., 2010; Wellis & Scott, 1990). Two-photon imaging and field potential measurements imply that state-dependent dynamics extend to the GC-MT circuit (Kato et al., 2012; Tsuno & Mori, 2009), but these studies did not resolve the temporal activity and selectivity of individual GCs. Thus, the role of GCs in shaping these features of MT firing is unclear.

Using the techniques described in Chapter 2, we made extracellular recordings from GCs in both anesthetized animals and awake, head-fixed mice. The data reveal that, under anesthesia, odours are represented in GCs by a temporally sparse code dominated by the respiratory rhythm. In contrast, during wakefulness GCs expand their dynamic range and

uncouple from the peak of inspiration to fire throughout the respiratory cycle. The increased activity of GCs during wakefulness suggests they have a stronger influence on the sparseness and selectivity of MT receptive fields through broadened lateral interactions. In contrast, the temporal structure of GC firing during wakefulness suggests they have a limited role in respiratory synchronization.

3.2 Methods

3.2.1 Animals

We performed experiments on adult (aged 6–12 weeks) male C57Bl/6 mice (Jackson Laboratory). Mice were maintained on a 12/12 h light dark cycle (lights on 0700 h) and received food ad libitum. We performed all experiments during the light cycle. Prior to surgery, we housed mice with up to five animals per cage, and after surgery, we singly housed animals. For awake recording, we removed water bottles from the cage 24 h prior to each session, and animals only had access to water through the recording apparatus lick port. All procedures were conducted in accordance with the National Institutes of Health's Guide for the Care and Use of Laboratory Animals and approved by the Cold Spring Harbor Laboratory Institutional Animal Care and Use Committee.

3.2.2 Surgery and Measurement of Respiration

For awake recordings, we affixed head-bars to the skull of the animal using adhesive luting cement (Parkell, Inc) and methyl methacrylate-based dental cement (TEETS) as described in Chapter 2. To assist in the measurement of breathing, we unilaterally implanted a cannula made from polyimide tubing (ID 0.0319, Amazon Supply) in the nasal cavity rostral to the olfactory epithelium using dental cement. When not recording, we plugged this cannula with a stainless steel dummy insert. In awake animals, we measured breathing using Teflon insulated thermocouples (0.13 mm OMEGA, part no. 5TC-TT-J-36-36) placed acutely in the

cannula. Data were amplified (Brownlee 410), digitally filtered, and acquired at 1 kHz using Spike2 (CED).

We conducted some recordings in animals that remained continually anesthetized. For these recordings, we anesthetized animals using either ketamine/xylazine (KX) or isoflurane (1 % in pure 0_2). We found no significant difference between KX or isoflurane animals (Fig.3-1), so we pooled these results for comparison with awake animals. We measured breathing using a foil strain gauge (Omega Engineering) placed on the animal's trunk.

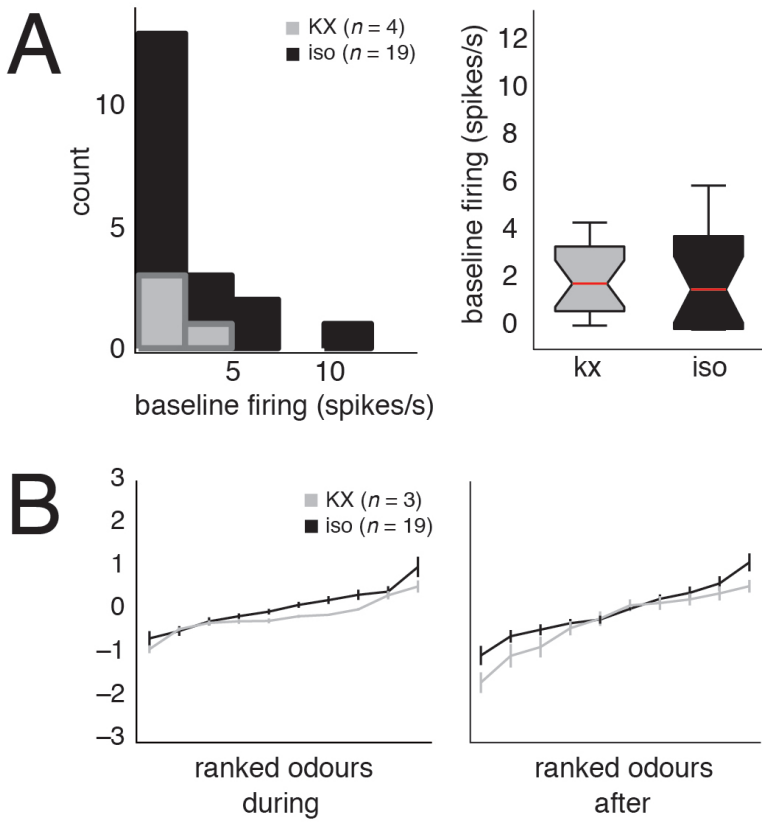

FIGURE 3.1: **GCs exhibit similar activity under two anesthetic regimes.**(A) Histogram of mean spontaneous firing rates from ketamine-xylazine (grey, n = 4 cells from 4 animals) and isoflurane (black, n = 19 cells from 18 animals) anesthetized animals. Mean ± s.e.m. results are summarized in boxplots (KX = 2.13 ± 0.92, iso = 2.42 ± 0.71). Rates between these two groups did not significantly differ (U(21) = 54, P = 0.65, Mann-Whitney U). KX = ketamine-xylazine, Iso = isoflurane. (B) Ranked tuning curves for both during odour presentation and after odour offset are plotted. Data are represented as the mean ± s.e.m. for each odour and plotted in order from the odour eliciting the most inhibitory response to the odour eliciting the most excitatory response. Curve slope was calculated for both the kx and isoflurane conditions and did not differ across the two anesthetics used (KX during = 0.18, iso during = 0.1611; KX after = 0.24, iso during = 0.25). Number of cells (n) is denoted for each of the anesthesia conditions.

3.2.3 Odour Stimuli

Odour stimuli were delivered as described (Shea, Katz, & Mooney, 2008). Stimuli consisted of a number of different monomolecular odours as well as natural food odourants (Table 1) diluted to 1 % V/V in mineral oil. An additional 1:10 flow dilution in our olfactometer resulted in a final concentration at the nose of 0.1 % saturated vapor. Typical odour presentations in the awake state consisted of 3–4 repetitions of 7–11 different odours. In anesthetized animals, the stability of recording permitted the presentation of many more odours (20–40). We presented all odours for a 2 s duration followed by a 13 s interstimulus interval (ISI). In order to keep awake animals engaged and comfortable, at the end of each odour presentation, we delivered water (20 μl) through a water port positioned at the animal's mouth. For assessment of cell firing between awake and anesthetized conditions in the same animal, we delivered isoflurane anesthetic (1 %) to the animal through the odour port in addition to the odours.

TABLE 3.1: List of Odourants

Monomolecular odours			Natural odours
acetophenone*	ethyl benzoylacetate	3-methyl-2-buten-1-ol	anise oil
4-allylanisole	ethyl butyrate	octanal*	cedarwood
2-butenol	ethyl propionate	1-pentanol*	cinnamon oil
butyl formate*	eucalyptol	pentylacetate	cloves
butyl propionate*	eugenol*	2-phenylethanol	cumin
butyaldehyde	heptanal	propionicaldehyde	nutmeg
camphor	2-heptanone	propyl acetae	peanut butter
cineole*	4-heptanone	pyrrolldine	peppermint
citral	hexanal	valeraldehyde	vanilla extract
cyclohexylacetate*	2-hexanone	valeric acid	
decanolactone	limonene*		

* denotes those odours used to construct odour tuning curves

3.2.4 Electrophysiology

We anesthetized mice (1 % isoflurane) and exposed the MOB with a small craniotomy. As described in detail in Chapter 2 and Appendix A, we head-fixed awake mice via the attached head-bar over a wheel that permitted them to walk and run in one dimension (backwards/forwards). In this case, we used a styofoam ball although in subsequent studies of awake animals, we used the roller wheel. Following each recording, we labeled cells using positive current injection (+700 pA; 1 Hz) of NB for 15–25 min. Here, we only report cells identified as GCs or as being in the GCL as there was no difference in the activity or odour tuning between these two populations (Fig.3-2).

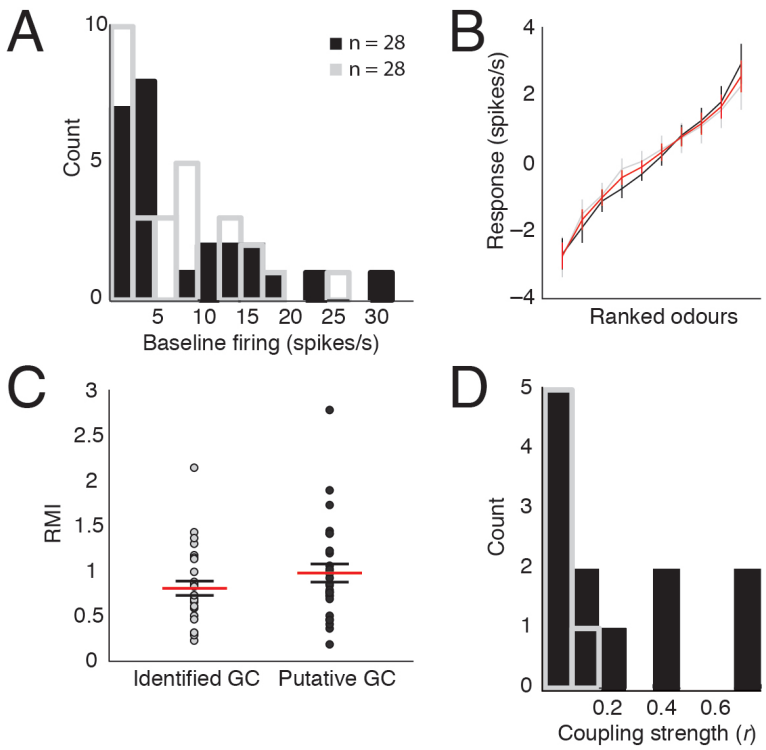

FIGURE 3.2: **Putative vs. identified granule cells.** Granule cell layer neurons (putative GCs) and identified GCs do not differ in their properties (A) Histogram of identified GCs (grey) and putative GCs (black) shows no difference in spontaneous activity between the two cell populations U(54) = 784, P = 0.8249, Mann-Whitney U. Identified GCs had a mean ± s.d. baseline rate of 7.30 ± 6.55 spikes/s (n = 28 cells from 19 animals) while putative GCs had a baseline rate of 7.99 ± 7.76 (n = 28 cells from 17 animals). (B) Ranked tuning curves for identified and putative GCs are similar. Identified GC curve is plotted in grey, putative GCs are plotted in black, and the combined curve is plotted in red. Only spike rates during the odour presentation are shown. (C) Response modulation index (RMI, see Methods) does not differ between the two groups. Each data point represents the RMI value for one cell. Mean ± s.d. RMI identified GC = 0.81 ± 0.42, n = 28 cells from 19 animals; RMI putative GC = 0.98 ± 0.54, n = 28 cells from 17 animals; U(54) = 706, P = 0.1890, Mann-Whitney U. (D) Coupling of spiking to breathing is not significantly different in the two groups (U(16) = 43, P = 0.2129, Mann-Whitney U). In both the identified GC (grey outline, n = 6 cells from 5 animals) and putative GC (black, n = 12 cells from 6 animals) groups, most cells show little coupling with breathing.

3.2.5 Data Analysis

Recordings sometimes included contamination from other spikes or artifacts, so we manually spike sorted data with Spike2 (CED) to isolate single unit spike trains. We performed all subsequent analyses in Matlab (Mathworks). We calculated mean ongoing firing rate from the 6 s period just prior to each stimulus. We then subtracted this baseline from the spike rates measured during the 2 s stimulus and during the 1 s after the stimulus offset to compute response strength by firing rate and tuning curves.

To assess statistical significance of responses to individual odours, we used a bootstrap procedure as follows. If n trials were collected with the response window length t, then a distribution was created by sampling n length t windows from the full spike record 100000 times and taking the mean deviation of each window from the spike rate measured in the prior 6 s. Responses that were in the top or bottom 2.5 % of this distribution were deemed significantly excitatory or inhibitory respectively. We computed our response modulation index (RMI, Hegdé & Van Essen, 2005) with the exception that in our data, responses could be negative, and thus no correction for non-normally distributed data was required. Briefly, RMI for each cell was calculated as the ratio of the variance across stimuli over the variance across all trials:

$$RMI = \frac{(\sum(\bar{x_s} - \bar{x_N})^2 * n)/s - 1}{(\sum(x - \bar{x_s})^2)/N - s} \tag{3.1}$$

where x is the response on one trial of an odour, n is the number of trials for one odour, N is the total number of trials across all odours, s is the number of stimuli, x_s is the mean response to an individual stimulus, and x_N is the mean response for all trials across all odours. We computed the strength and phase of coupling between spiking and respiration using the publicly available Matlab library Circstat (Berens, 2009). Further, we determined statistical significance of coupling for a given stretch of data with a Rayleigh test (Berens, 2009).

We analyzed breath synchronized odour responses as follows. First, we identified the time of each inspiratory peak (maximum inspiration) in the entire record for a given cell as the peak of strain gauge signal or the peak of the first derivative of the thermocouple signal (Fig.3-3). This time served as zero phase and occurred shortly after sniff initiation in

awake (median: 83 ms/1.54 radians; n = 26172 sniffs from 18 cells) and anesthetized mice (median:135 ms/1.36 radians; n = 54392 sniffs from 16 cells). Then, we computed spike rate for each breath in a window between the halfway point to the prior breath and the halfway point to the subsequent breath. We designated the first inspiration to peak after the onset of the odour as breath one, and we designated baseline per breath firing as the mean per breath firing rate for the 20 breaths immediately prior to the odour trial. We subtracted this baseline value from the mean per breath firing rate for the breaths that occurred during the stimulus to compute breath synchronized response strength. We constructed "whole breath" tuning curves and histograms in this way while we constructed "partial breath" tuning curves and histograms in the same manner but considered only a specific window of 25 % of the breath cycle. To assess cycle-dependent structure in the tuning curves and histograms, we considered a sliding window over a range of positions on the breath cycle.

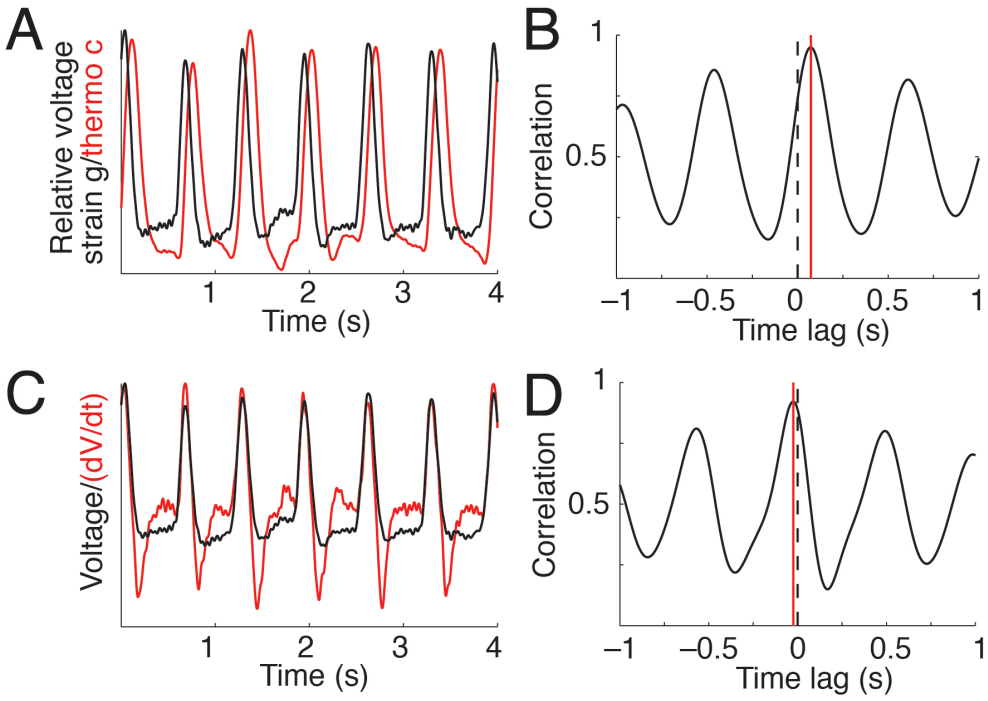

FIGURE 3.3: **Comparison of two methods for measuring respiration.** (A) Example raw traces from simultaneous respiratory recordings using a nasally implanted thermocouple (red) and a foil strain gauge (black). We observed that the peak of the strain gauge signal closely matched the point of maximum rate of change for the thermocouple signal. (B) Cross correlation of the two signals shows a lag of 68 ms for the thermocouple relative to the strain gauge. Mean and s.d. time between peaks was 67 ± 5 ms (C) Comparison of the strain gauge with the differentiated thermocouple signal shows a good match of the signal peaks. (D) Cross correlation of the two signals in (d) shows a greatly reduced lag of 15 ms for the strain gauge relative to the thermocouple. Mean and s.d. time between peaks was 0 ± 7 ms.

For statistical comparison, we qualitatively assessed data for normality by plotting individual data points. When possible, we used parametric tests of significance. All t-tests were two-sided, and in Fig.3-7F, we employed an unpaired t-test (unequal variances). In several cases, we assessed data to be non-normally distributed, so we used nonparametric tests (Mann-Whitney U, Kolmogorov Smirnov; indicated throughout).

In Fig. 3-14, we excluded one cell from each group from the analysis because these cells had values > 6 s.d. above the mean for their condition.

3.3 Results

3.3.1 Ongoing Firing Characteristics of Granule Cells are State-dependent

To measure the state-dependent spiking activity of GCs, we used juxtacellular 'loose-patch' methods to achieve extracellular recordings in anesthetized (isoflurane or ketamine-xylazine) and awake, head-fixed male mice (see Appendix A). Because we were interested in temporal firing patterns with respect to breathing, respiration was also monitored during many experiments.

Figure 3-4A shows data from an example recording in an anesthetized mouse and the subsequently recovered dye fill of the recorded GC. Of the 80 neurons reported here, 50 were definitively identified as GCs by their small soma size and dendritic morphology. The remaining 30 cells were confirmed to be in the GCL but no other morphological data were available. Although there are other cell types like dSACs found in the GCL, they were very infrequently labeled (2/75 labeled neurons). Moreover, the two data sets were statistically indistinguishable with respect to their basic properties (Fig.3-2). Therefore, we pooled them for all subsequent analyses.

Qualitatively, GCs recorded under anesthesia exhibited low firing rates, robustly rhythmic ongoing activity, and odour responses that consisted of modulation of the amplitude of the rhythmic bursts (Fig.3-4A). In contrast, GCs recorded during wakefulness exhibited

higher levels of aperiodic firing and responded to stimuli with a mix of increases and decreases in firing rate with variable onset and offset times (Fig.3-4B). Mean ongoing firing rates were significantly higher in the awake condition as compared with those seen under anesthesia (awake: mean $\pm$ s.d. = 7.41 $\pm$ 7.1 spikes/s, n = 58 cells from 26 animals; anesthesia: 1.90 $\pm$ 1.9 spikes/s, n = 22 cells from 21 animals; U(78) = 533, p = 0.00012,) (Fig.3-4C). These differences appear to reflect state-dependent properties in the same population of neurons rather than properties of distinct populations of neurons. A subset of cells recorded across behavioural state transitions exhibited the same differences between anesthesia and wakefulness (Fig.3-5).

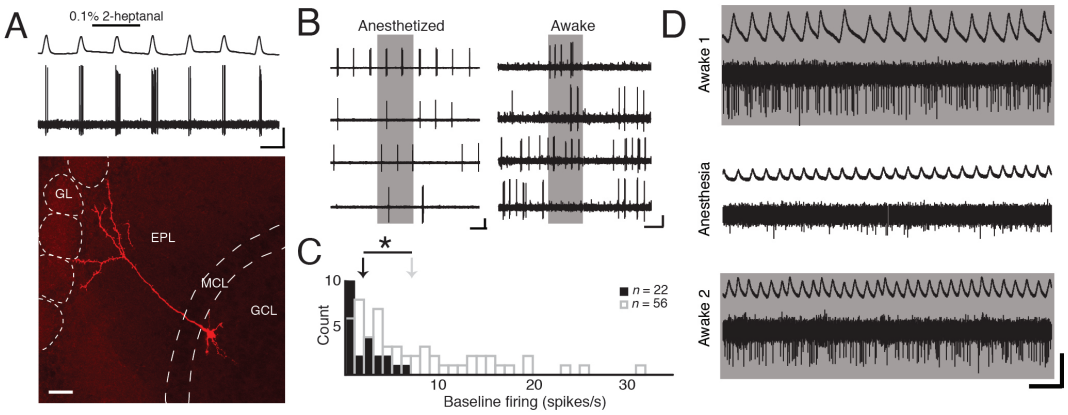

FIGURE 3.4: **Recording from identified MOB GCs in the awake and anesthetized mouse** (A) Representative recording from a GC in an anesthetized mouse showing a neuronal spiking trace and respiratory signal above. Scale bar = 2.5 mV / 1 s. The lower panel is a photomicrograph of the corresponding NB filled cell exhibiting hallmark GC features including the apical dendrite extending into the EPL and numerous dendritic spines. Scale bar = 40 μm, GCL = granule cell layer, MCL = mitral cell layer, EPL = external plexiform layer, GL = glomerular layer. (B) Representative traces showing the heterogeneity of odour responses in the awake state. In contrast to anesthetized state GCs, cells in the awake animals variably responded with activation (awake trace 1), delayed onset activation (awake trace 2) and inhibition (awake trace 4) in response to different odours. Scale bar anesthetized = 5 mV /1 s. Scale bar awake = 2 mV / 1 s. (C) Distribution of spontaneous firing rates during anesthetized (black bars, mean $\pm$ s.d. = 1.90 $\pm$ 1.9 spikes/s) and awake states (gray bars, mean = 7.41 $\pm$ 7.1 spikes/s). Spontaneous activity of GCs is significantly increased in awake animals (Mann-Whitney U test, p = 0.00012). (D) In select cases, individual cells were recorded during both anesthesia and wakefulness. Spontaneous firing decreases when isoflurane is administered (unshaded trace) and returns to pre-anesthesia level when anesthesia is turned off . Scale bar = 1 mV / 1 s.

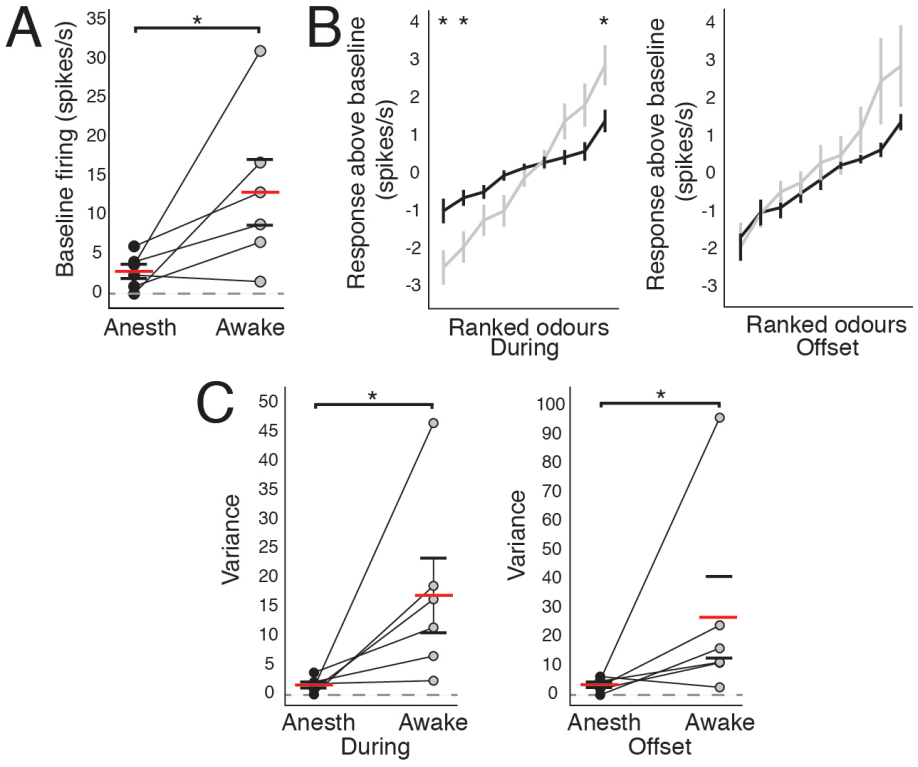

FIGURE 3.5: **Recordings from GCs across wakefulness state show state-dependent activity changes within individual GCs.** In a subpopulation of cells (n=6 cells from 6 animals), recordings were made from the same cell in both the awake and isoflurane anesthetized animal. (A) Spontaneous activity significantly increased in GCs across the anesthetized (black) to awake (grey) transition (U(5) = 25, p = 0.026, Mann-Whitney U). Mean firing rate ± s.e.m (red line and black lines respectively) are plotted. Anesthetized state mean ± s.d. = 2.86 ± 0.91; mean firing rate in the awake state = 13.00 ± 4.21. Paired data are plotted for each cell with the connecting line linking mean firing rate for an individual cell in each state. (B) Ranked tuning curves during 2 s odour presentation and 1 s after odour offset are plotted for transitional cells in both the anesthetized (black line) and awake (grey line) state. * denotes odours that elicited responses significantly different from baseline. (C) Tuning curve variance during both the 2 s odour presentation and 1 s following odour offset was greater in the awake state (during mean ± s.e.m = 17.04 ± 6.42; after = 26.94 ± 14.13) than in the anesthetized state (during = 1.64 ± 0.53; after = 3.53 ± 0.95, during U(5) = 22, p = 0.043; after U(5) = 25, p = 0.026, Mann-Whitney U). Individual data points represent one cell and mean ± s.e.m. are plotted as horizontal red and black lines respectively.

Typically, mice intermittently ran on the freely rotating ball, and we measured running velocity during most recording sessions. Although neurophysiological changes to sensory gain and stimulus selectivity have been observed during locomotion (Polack, Friedman, & Golshani, 2013; Niell & Stryker, 2010), our analysis suggests that the locomotion related firing changes we observed were likely explained by elevated breathing during running (Fig.3-6). For individual cells the relationship of GC firing rate to respiratory rate could be either positive or negative, so there was no systematic pattern (Fig.3-6).

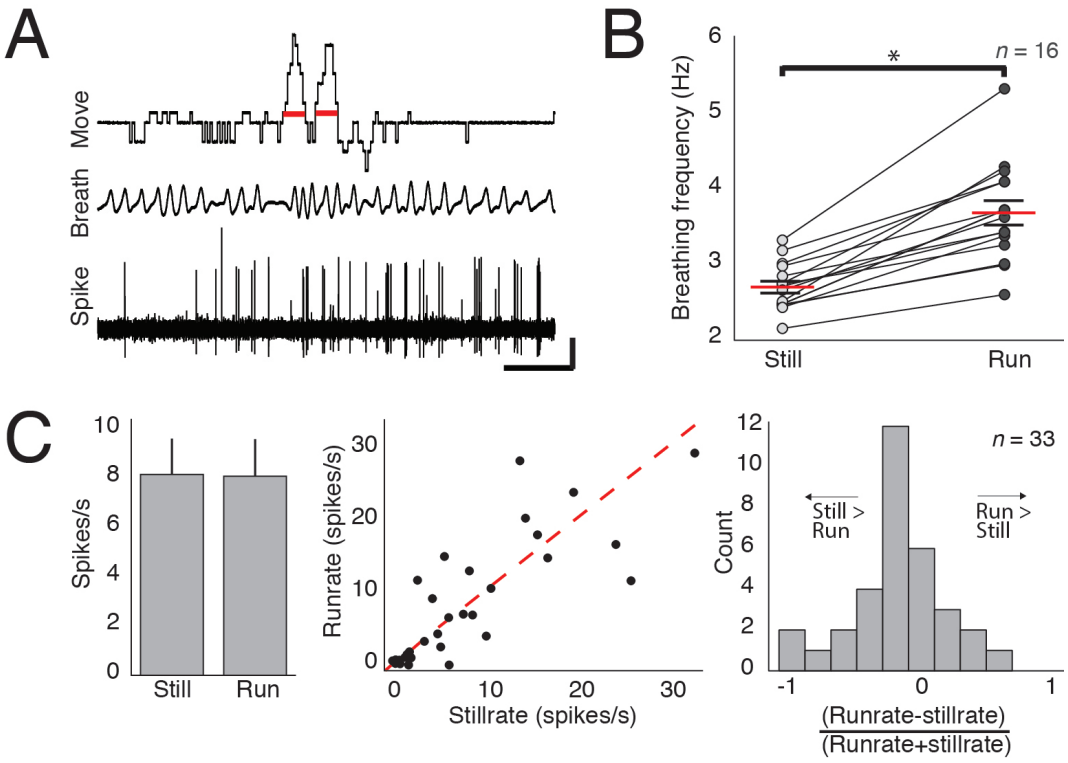

FIGURE 3.6: **Changes in breathing and GC firing with changes in locomotion.** (A) Example trace of GC activity (bottom), respiration (middle), and running velocity (top). Running was measured on an axially rotating Styrofoam ball via a rotary encoder. Locomotor activity was divided into 2 s bins, and running bins with RMS > 2 (red lines; Scale bar is 1 s and 4 cm/s for locomotion, 1 mV for breathing and 1.5 mV for GC spiking. (B) Breathing frequency increases with running. Breathing during the entire recording session was binned into 2 s intervals, and a mean rate during periods of rest or during periods of running was calculated. For all animals (n = 16 cells from 8 animals), breathing significantly increased during running (Mean breathing rate $\pm$ s.e.m. rest = 2.69 $\pm$ 0.08; running 3.68 $\pm$ 0.16; U(15) = 157, p = 0.000026, Mann-Whitney U). (C) GC activity is largely invariant with activity. Mean spike rate $\pm$ s.e.m. between periods of rest (8.15 $\pm$ 1.46 spikes/s) and periods of increased locomotion (8.08 $\pm$ 1.50 spikes/s) was not significantly different (U(32) = 1077, p = 0.71, Mann-Whitney U, left). Plotting individual data points (middle, left histogram, n = 33 cells from 19 animals) indicates a sub-population of cells is modulated with activity. Dotted red line runrate = stillrate.

3.3.2 During Wakefulness, Granule Cells Exhibit Stronger Firing Rate Changes in Response to Odours

Odour responses in MTs of awake animals are sparser and more selective than those seen under anesthesia (Cury & Uchida, 2010; Davison & Katz, 2007; Fuentes et al., 2008; Rinberg, Koulakov, & Gelperin, 2006; Shusterman et al., 2011). One possible mechanism for this change is greater activity in the GC network facilitating more extensive lateral interactions among MTs. We tested this possibility by comparing the strength and selectivity of odour responses during anesthesia and wakefulness.

We found that GC odour responses in wakefulness were more robust, broadly tuned and variable in their temporal dynamics than those seen under anesthesia (Cang & Isaacson, 2003; Wellis & Scott, 1990; Tan et al., 2010). Figure 3-7A shows a typical example response histogram for a GC recorded from an anesthetized mouse. Note that tuning curves quantified as mean baseline-subtracted firing rate during (black) and after (grey) the stimulus are very flat.

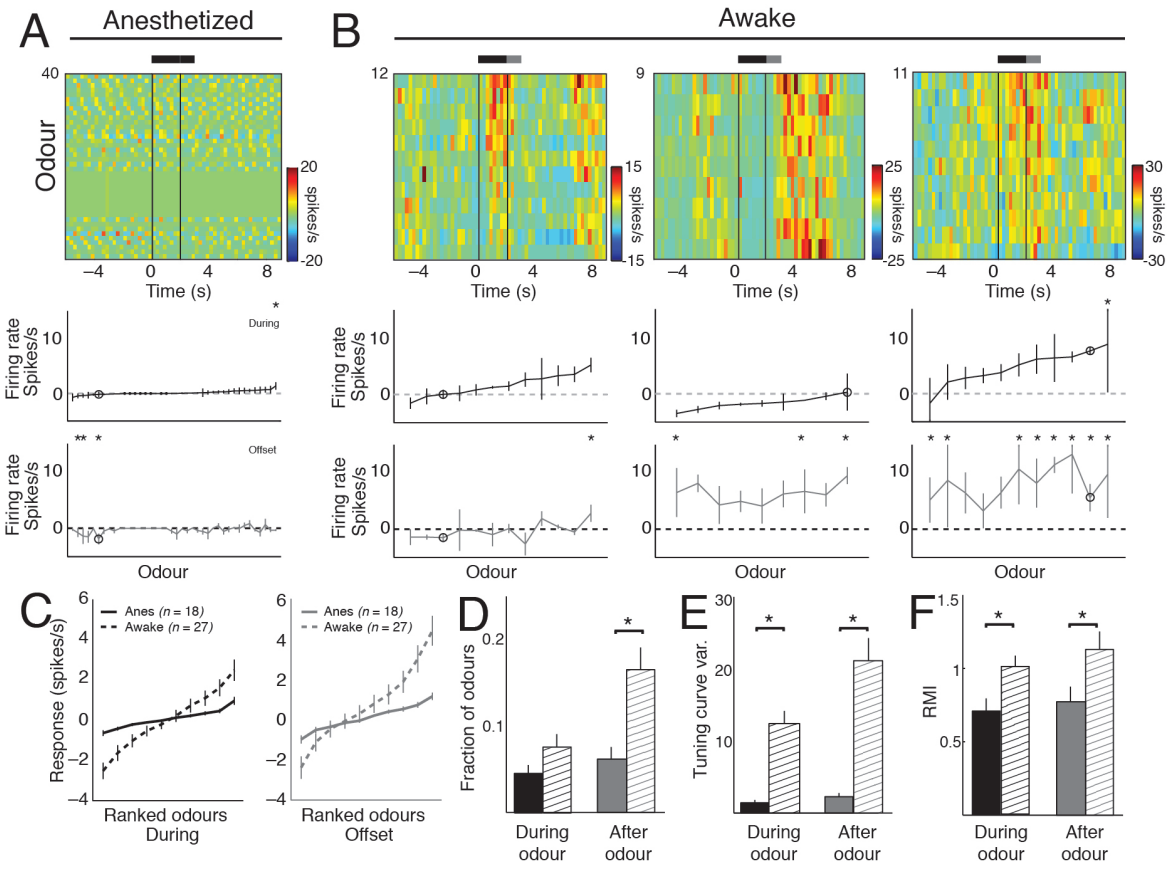

FIGURE 3.7: **Measures of GC firing rates show stronger and more dynamic odour responses during wakefulness.** (A) The top panel is a 2-D peristimulus time histogram (PSTH) with a different odour on every row. Data are from a cell recorded under isoflurane anesthesia. Responses are mean responses computed from at least two trials of each odour. Most odours were presented three times each. Color represents baseline subtracted firing rate binned at 250 ms, and rows are sorted with the most excitatory odour response at the top. The vertical black lines denote odour onset at 0 s and odour offset at 2 s. Baseline subtracted tuning curves computed from the 2 s during the odour (black) and the 1 s following odour offset (grey) are plotted below. Tuning curves are ranked according to strength of the response during the odour as in the histogram. The black circle denotes the response to the blank odour. (B) Representative histograms and tuning curves from three different cells during wakefulness. (C) Baseline subtracted ranked mean tuning curves (mean $\pm$ s.e.m.) for all cells across 10 standard odours in anesthesia (bold) and awake (light) experiments. Tuning curves during the 2 s odour presentation (black) and for 1 s (grey) following odour offset are shown. (D–F) Odour-evoked firing rates were significantly different between anesthesia (bold) and wakefulness (dashed) using three different measures of robustness. The two states showed significant differences (denoted by *, $p < 0.05$, see text for values) before and after odour onset in fraction of odours evoking a response, in tuning curve variance across odours, and in response modulation index (RMI). Mean $\pm$ s.e.m. are shown sub-population of cells is modulated with activity.

A bootstrap procedure testing the significance of individual odour responses (see Methods) revealed only a few weak responses. In contrast, we commonly observed robust firing rate changes in GCs of awake mice during the odour. Qualitative assessment of histograms revealed these robust responses also frequently outlasted the stimulus (Fig.3-7B). GC responses in awake mice commonly consisted of a mixture of some excitatory and some suppressive responses to different odours (Fig.3-7B). The sign and magnitude of responses during and after the odour were typically not mutually predictive. For awake-state GCs, rank correlation values between baseline subtracted tuning curves computed from activity during the stimulus and baseline subtracted tuning curves computed from data just after the stimulus were variable but generally low (r = 0.36 $\pm$ 0.04, Spearman's rank correlation coefficient). For most cells (36/49), there was no significant relationship (p > 0.05). We therefore considered them as independent response phases.

Mean ranked tuning curves collected for a standard set of 10 odourants were steeper for GCs in awake mice (Fig.3-7C) both during the stimulus (anesthesia slope: mean $\pm$ s.d. = 0.18 $\pm$ 0.1 [spikes/s]/odour, n = 18 cells; awake slope: 0.56 $\pm$ 0.3 1 [spikes/s]/odour, n = 27 cells; U(43) = 250, p = 0.00015) and after the stimulus (anesthesia slope: 0.24 $\pm$ 0.2 [spikes/s]/odour, n = 18 cells; awake slope: 0.76 $\pm$ 0.4 [spikes/s]/odour, n = 27 cells; U(43) = 231, p = 0.000024). The increase in the overall slope of the tuning curves resulted nearly equally from increased excitation to some odours and increased firing suppression to others (Fig.3-7C). Considering all odours presented to all cells, GCs in awake mice responded to a significantly greater fraction of stimuli after odour offset (Fig.3-7D; anesthesia: mean $\pm$ s.d. = 6.3 $\pm$ 7 %, n = 22 cells from 21 animals; awake: 16.8 $\pm$ 1.5 %, n = 49 cells from 24 animals; U(68) = 592.5, p = 0.0117,) and tuning curves collected during both analysis epochs had significantly higher variance (Fig.3-7E; anesthesia variance during: mean $\pm$ s.d. = 1.42 $\pm$ 1.8 spikes/s, n = 22 cells from 21 animals; awake variance during: 12.2 $\pm$ 12 spikes/s, n = 49 cells from 24 animals; U(375) = $\breve{}$5.18, p = 2.2×10^7,) (anesthesia variance after: 2.26 $\pm$ 2.4 spikes/s, n = 22; awake variance after: 21.1 $\pm$ 22 spikes/s, n = 49; U(374) = -5.19, p = 2.1×10^7). This latter analysis does not account for differences in firing statistics between behavioural states. Therefore, we further computed a response modulation index (RMI; see Methods)

that normalizes the variability across stimuli to the variability across trials separately for each state. Even when correcting for the different levels of noise in this way, the significantly enhanced modulation of firing rate across stimuli in the awake state persisted both during (anesthesia RMI: mean $\pm$ s.d. = 0.70 $\pm$ 0.4, n = 22 cells from 21 animals; awake RMI: 1.01 $\pm$ 0.52, n = 49 cells from 24 animals; t(51.5) = -2.64, p = 0.011) and after the stimulus (anesthesia RMI: 0.77 $\pm$ 0.5, n = 22; awake RMI: 1.13 $\pm$ 0.85, n = 49; t(65) = -2.24, p = 0.028).

These data show that GCs respond more strongly and to a broader range of odours in the awake state as compared to the anesthetized state. Even after correcting for different firing statistics, our analysis reveals that GC spiking in response to odours has a greater dynamic range across stimuli. This expanded dynamic range did not result from elevated breathing rates during wakefulness. Among the awake data, tuning curve variance was unrelated to breathing rate (Pearson correlation: r = 0.23; p = 0.36) or variability (Pearson correlation: r = 0.04; p = 0.86). These data reveal that GCs exhibit stronger, more broadly-tuned responses in the awake as opposed to the anesthetized state. This may result in amplified lateral interactions between MTs via GCs. Further, our finding that GC responses frequently continue beyond the end of the stimulus raises the possibility that during wakefulness GCs reflect non-sensory events or cortical influence. Dissociation of these factors from prolonged influence of bottom-up sensory processes awaits further study.

3.3.3 Respiratory Coupling of Granule Cells is State-dependent

Under anesthesia, activity in MTs and GCs is strongly coupled to respiration (Cang & Isaacson, 2003; Chaput & Holley, 1980; Fukunaga et al., 2012; Macrides & Chorover, 1972; Meredith, 1986). During wakefulness, MT spikes are also locked to breathing and sniffing (Cury & Uchida, 2010; Shusterman et al., 2011); however, the temporal structure of GC firing in this state is unknown. Inhibition from the GC network during wakefulness may play an important role in enforcing respiratory locking of spikes in MTs. We therefore examined whether GC firing is coupled to breathing, whether it is coupled to a characteristic phase of breathing, and whether this coupling changes with behavioural state.

We quantified the strength of coupling between GC firing and the respiratory cycle using a metric r that ranges from zero to one, with zero corresponding to a uniform distribution of spikes throughout the breath cycle and one corresponding to all spikes occurring at the same point in the breath cycle (Berens, 2009). To our surprise, during wakefulness GCs were much more weakly coupled to respiration than they were under anesthesia. Figure 3-8A (left panel) shows respiratory phase histograms for representative (near mean) GCs recorded during anesthesia (black) and during wakefulness (gray).

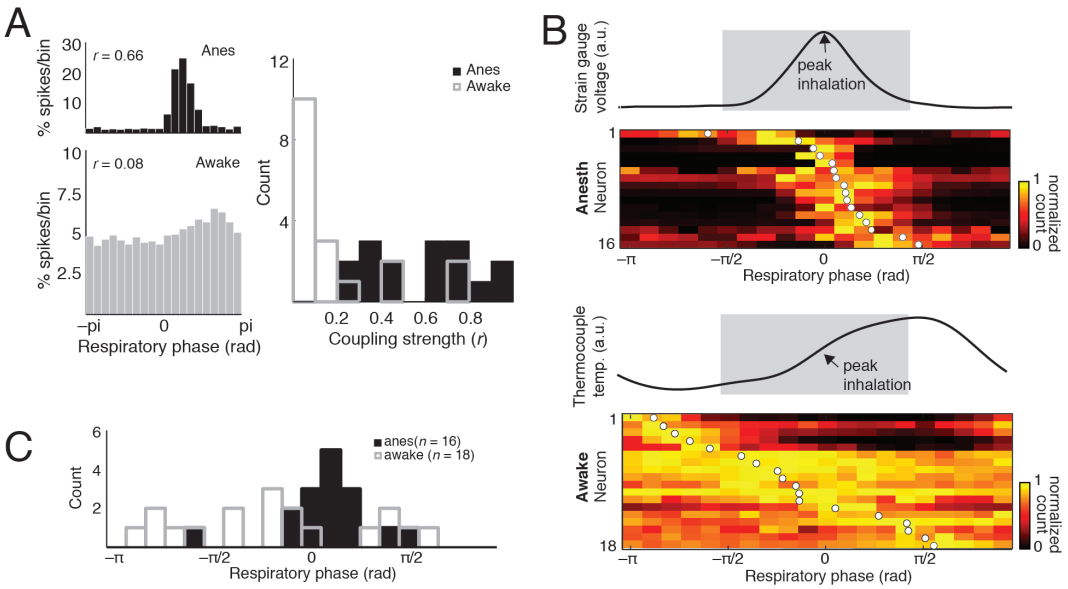

FIGURE 3.8: **Measures of GC firing rates show stronger and more dynamic odour responses during wakefulness.** (A) Respiratory phase coupling histograms for a representative (near mean coupling strength) anesthetized state GC (isoflurane; black) and an awake state GC (gray). Histograms show the probability of spikes occurring in each pi/10 bin of the respiratory cycle. Data are computed from 878 breaths for the anesthetized cell and 870 breaths for awake cell. Zero corresponds to the peak of inspiration. The right panel shows a histogram (bin size = 0.1) of respiratory coupling strength (r) for anesthetized state GCs (black) and awake state GCs (gray). GCs in the anesthetized state are significantly more coupled to breathing than cells in the awake state (p = 0.00021, Mann Whitney U test). (B) Heatmap depicting baseline respiratory phase spike histograms for all anesthetized state GCs (top panel) and all awake state GCs (lower panel) (bin size = pi/10). Each row is a cell, and for each cell, spike count is normalized to the maximal bin for that cell. White dots denote the mean phase angle of firing for each cell. A representative breath trace is shown in black (top). Grey box in trace represents the inhalation period. (C) Histogram of mean firing phase for all cells under anesthesia (black) and during wakefulness (gray). The two distributions were significantly different (p = 0.0021, Kolmogorov Smirnov test). Median phase angle for anesthetized GCs was 0.67 radians, which corresponded to a median lag of 57 ms behind zero phase.

GCs recorded during wakefulness were significantly more weakly coupled to the breathing rhythm than GCs recorded under anesthesia (Fig.3-8A, right) (anesthesia r: mean $\pm$ s.d. = 0.59 $\pm$ 0.2, n = 16 cells from 15 animals; awake r: 0.25 $\pm$ 0.24, n = 18 cells from 13 animals; $U(32) = 388$, $p = 0.00021$). This observation was unchanged by locking firing to sniff initiation as opposed to peak inspiration (Fig.3-9). Differences in respiratory coupling between states are also unrelated to the timing, amplitude or variability of respiratory features (Fig.3-10).

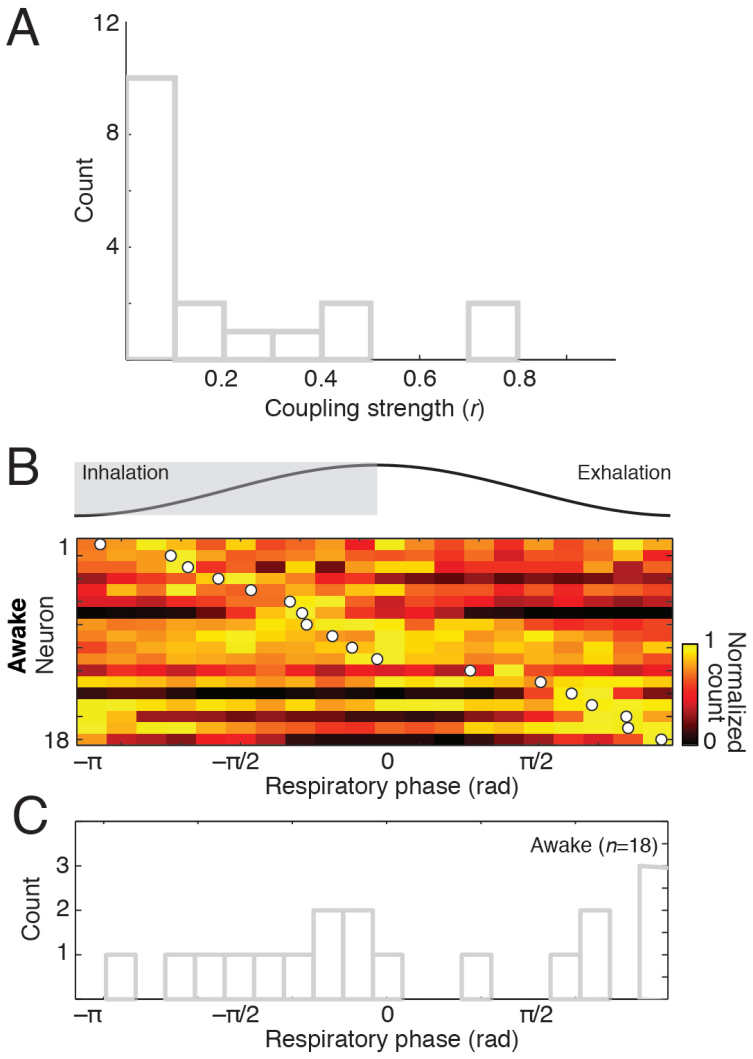

FIGURE 3.9: **Assessment of respiratory coupling when GC spiking is aligned to breathing onset.** (A) Histogram (bin size = 0.1) of respiratory coupling strength (r) for awake state GCs. As with alignment to peak inspiration, GCs still show weak respiratory coupling. (B) Heatmap depicting baseline respiratory phase spike histograms for all awake state GCs (bin size = pi/10). Each row is a cell, and for each cell, spike count is normalized to the maximal bin for that cell. White dots denote the mean phase angle of firing for each cell. A representative breath trace is shown in black (top). Grey box in trace represents the inhalation period. (C) Histogram of mean firing phase for all cells during wakefulness (gray).

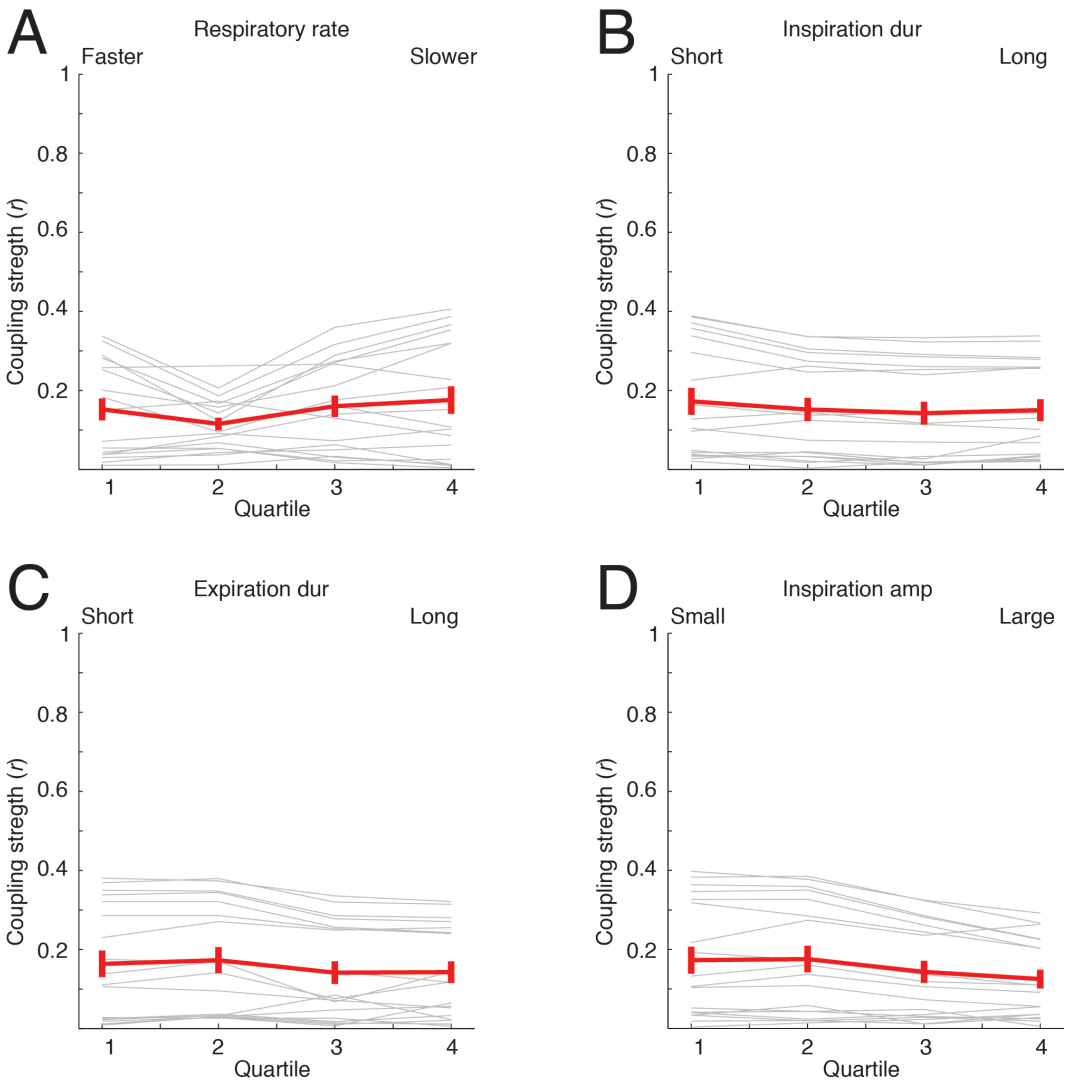

FIGURE 3.10: **Weak phase coupling in awake GCs is not a result of differences in breath parameters between wakefulness and anesthesia.** All breaths from 18 cells recorded in 13 awake animals were divided into quartiles for each cell according to one of four breath parameters. Respiratory coupling strength for spikes did not systematically vary with any of the breath parameters we measured: breathing rate (A), inspiratory duration (B), expiratory duration (C), and inspiratory amplitude (D). Comparing the distribution of coupling strength across quartiles for each parameter, we saw no significant differences (n = 18 cells; p = 0.79 (A), p = 0.66 (B), p = 0.70 (C), p = 0.66 (D), Kruskal-Wallis).

In addition to being strongly coupled to the breathing rhythm, GCs during anesthesia were as a population synchronized to a narrow window of the respiratory phase corresponding to the period just after the peak of inspiration (Fig.3-8B, top). Interestingly, this synchrony was not evident in the population of GCs recorded during wakefulness. Instead, in the awake state, GCs displayed divergence in their mean coupling phase angles, covering a much broader range of the respiratory cycle. The distributions of mean phase angles were significantly different for awake state GCs and anesthetized state GCs (Fig.3-8C; $D(32) = 0.6042$, $p = 0.0021$). Our observation that GCs show weaker and divergent respiratory coupling persisted during odour presentation (Fig.3-11A, B, and C). Awake GCs were more weakly coupled to breathing during odour presentation than anesthetized GCs (anesthesia r: mean $\pm$ s.d. $= 0.64 \pm 0.2$, n = 16 cells from 15 animals; awake r: 0.25 ± 0.25, n = 18 cells from 13 animals; $U(32) = 382$, $p = 0.00046$; Fig.3-11B) tending to fire at all phases of the breathing cycle (anesthesia mean firing phase: mean $\pm$ s.d. $= 0.57 \pm 1.0$, n = 16 cells from 15 animals; awake r: -0.90 ± 1.71, n = 18 cells from 13 animals; $D(32) = 0.6042$, $p = 0.0021$).

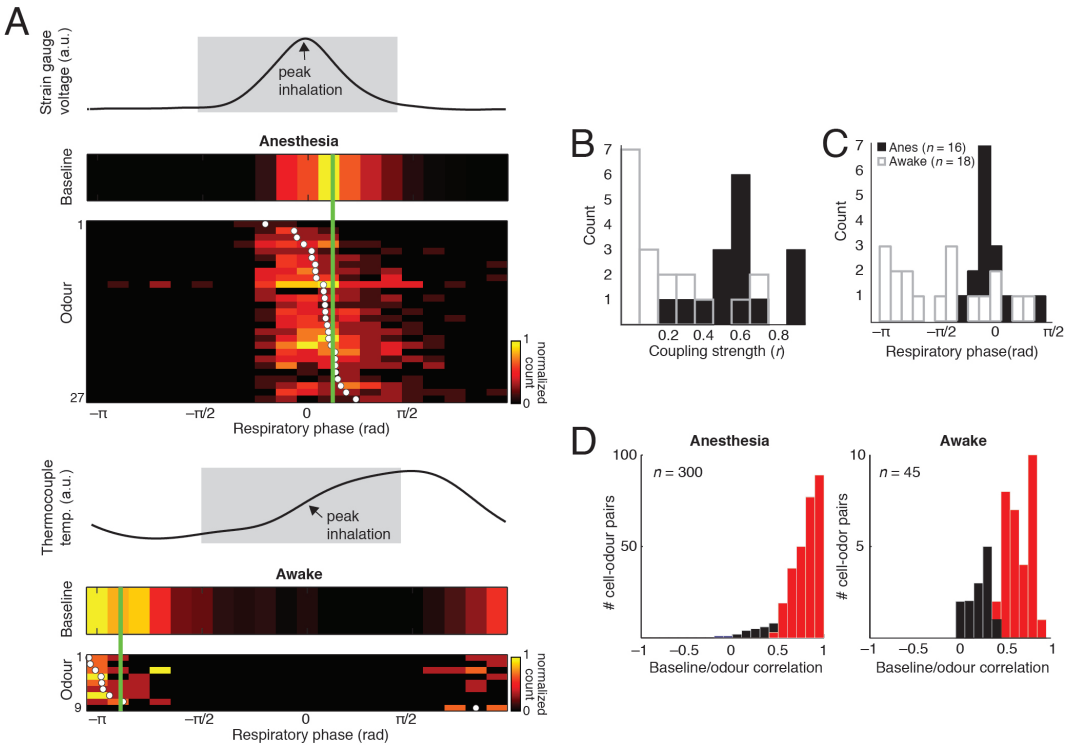

FIGURE 3.11: **Respiratory coupling phase of GC spiking is unaffected by odour stimuli.** (A) Heatmaps depicting baseline and odour-selective respiratory phase spike histograms for an example anesthetized state GC (isoflurane; top panels) and an example awake state GC (lower panels) (bin size = pi/10). Each row is an odour and for each odour, spike count is normalized to the maximal bin for that odour (or baseline). Data are computed from at least 8 breaths (2 trials per odour; average 4 breaths per odour). Only cell-odour pairs for which there was significant coupling in both the baseline and odour data are plotted. White dots denote the mean phase angle of firing for each odour and the green line denotes the mean baseline firing phase for each cell. (B) Histogram (bin size = 0.1) of respiratory coupling strength (r) during odour presentation for anesthetized state GCs (black) and awake state GCs (gray). All odours were considered regardless of whether they evoked significant responses. The two distributions were significantly different ($p = 0.00046$, Mann-Whitney U test). (C) Mean firing phase during odour presentation for all cells under anesthesia (black) and during wakefulness (gray). Anesthesia and wakefulness were significantly different ($p = 0.0021$; Kolmogorov Smirnov test). (D) Correlation of baseline and odour phase histograms for all cell-odour pairs revealed that the great majority of cell-odour pairs were highly and significantly correlated at baseline and during the odour (red = significantly correlated: multiple p's < 0.05, Pearson correlation). This was true in both anesthesia and wakefulness, and demonstrates that, unlike MTs, GCs do not encode odour identity as shifts in phase of respiratory coupling.

Mitral/tufted cells are phase coupled at baseline and frequently shift their coupling phase angle in the presence of an odour stimulus. The direction and magnitude of the phase angle shift depends on odour stimulus identity (Dhawale et al., 2010; Fantana, Soucy, & Meister, 2008; Khan, Thattai, & Bhalla, 2008). We therefore assessed whether phase coupling angle in GCs was stimulus-dependent in awake or anesthetized mice. We first selected neurons that showed significant respiratory coupling at baseline (16/16 anesthetized state GCs and 16/18 awake state GCs). For each baseline coupled cell, we identified all odours for which spiking during the trials of that odour was significantly coupled to respiration (Rayleigh test). This yielded 300 cell-odour pairs (from 15 cells) in anesthetized state GCs and 45 cell-odour pairs (from 10 cells) in awake state GCs. Figure 3-11A shows data from an example anesthetized state GC and an example awake state GC, comparing the baseline activity phase histogram with the stimulus-specific phase histograms for all odours that evoked significantly phase coupled activity from that cell. In each case, the stimulus-specific coupling phases for all odours clustered tightly around the mean baseline coupling phase. We quantified this close correspondence between baseline and stimulus-driven coupling by correlating the phase histograms of each cell-odour pair with the baseline phase histogram of its parent cell. A large majority of cell-odour pairs showed a significant positive correlation between their stimulus-driven histogram and baseline phase histogram (276/300 cell-odour pairs from anesthetized state GCs and 32/45 cell-odour pairs from awake state GCs), and the mean cell-odour pair correlation for both populations was high (anesthesia corr. coeff. r: 0.77 ± 0.2; awake corr. coeff. r: 0.57 ± 0.2). Finally, we compared coupling strength between baseline sniffs, the first sniff of odours, and all subsequent odour sniffs and saw no significant differences (Fig.3-12).

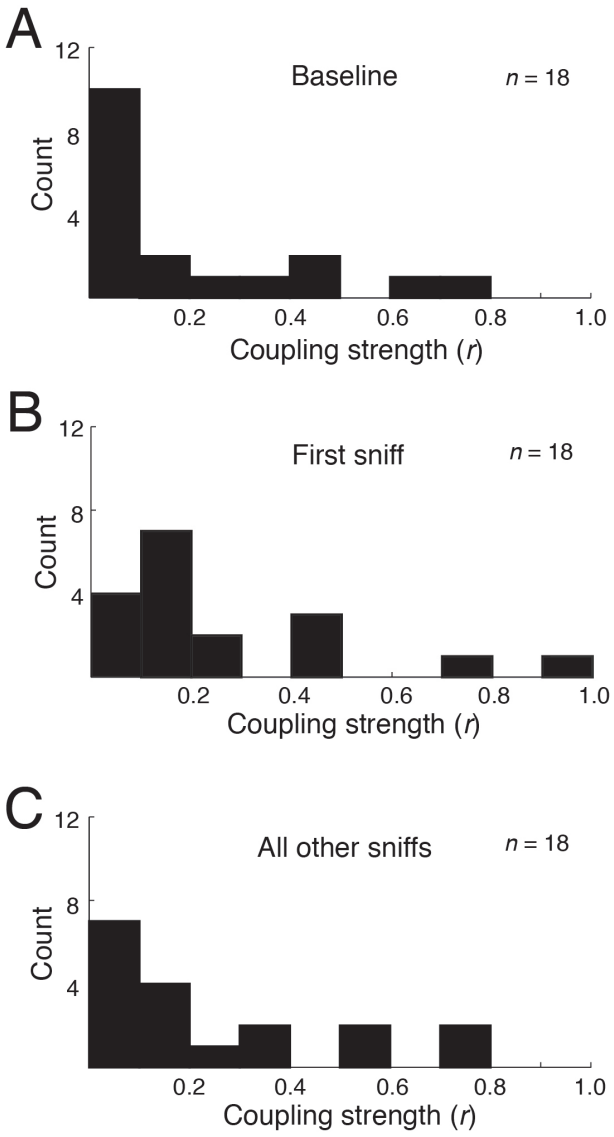

FIGURE 3.12: **Coupling strength in GCs recorded during wakefulness did not differ between baseline breaths, the first sniffs of the odour, and all subsequent odour sniffs.** (A-C) Histograms showing the distributions of coupling strength across n = 18 GCs recorded in 13 awake mice computed from data gathered between trials (baseline) (A), from the first sniff to odours (B), or from all subsequent odour sniffs. median coupling strength was 0.07 in (A), 0.18 in (B), and 0.13 in (C). Comparing the distributions of coupling strength across sniff type, we saw no significant differences (n = 18 cells; $H(2,51) = 2.54$, $p = 0.28$).

Thus contrary to our prediction, GCs are not strongly coupled to respiration during wakefulness. Taken together with our further observation that individual GCs have weak and diverse phase relationships with breathing and that this relationship is insensitive to odours, we conclude it is unlikely that GCs play a dominant role in influencing respiratory locking or odour-dependent phase shifts in MTs during wakefulness. Moreover, GCs do not appear to even merely follow the respiratory locking of MTs.

3.3.4 Odour Responses in Granule Cells are Independent of Respiration during Wakefulness

The analysis we describe above suggests that odour activity carried by GCs is independent of the breath cycle during wakefulness. If so, that argues against a role for GCs in patterning MT firing according to respiration. We therefore compared the dependence of odour coding in the two behaviour states on respiratory phase by syncing GC spiking data to breathing.

Figure 3-13A shows 2–D histograms of the response of the same anesthetized state GC analyzed with respect to time relative to stimulus onset or with respect to breath cycle number relative to the first inhalation after stimulus onset.

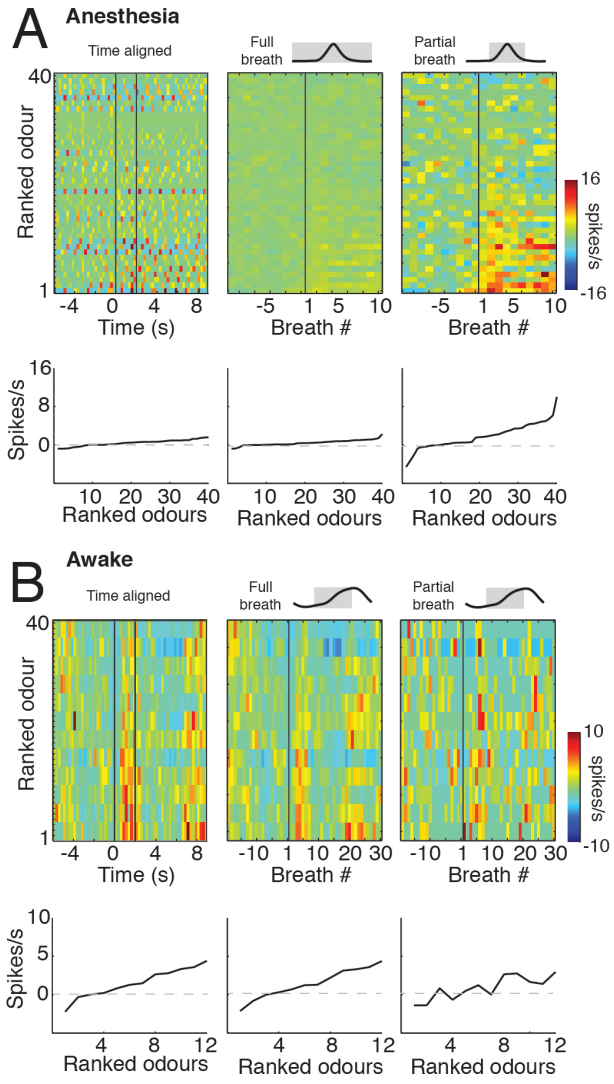

FIGURE 3.13: **Temporal structure of odour responses differs in anesthetized state and awake state GCs.** (A) PSTHs from a representative anesthetized state GC (isoflurane) computed with three different methods. Responses are mean responses across three trials of each odour. The left PSTH depicts mean firing in 250 ms time bins relative to the stimulus onset. The middle PSTH depicts mean firing over each entire breath relative to the first breath after stimulus onset. 'Full breath' refers to data calculated in this fashion. The right PSTH is similarly computed, but is restricted to firing in a discrete window of each breath (25 % of the respiratory cycle). 'Partial breath' refers to data calculated in this fashion. Structure in the cell's response to stimuli becomes more apparent after syncing to the breath cycle and especially after restricting analysis to part of the breath. Below each PSTH is plotted the corresponding ranked tuning curve computed with each method. Tuning curves and PSTHs are ranked according to strength of the response during the odour. (B) Corresponding data from a representative awake state GC.

Averaging firing rates in time bins relative to stimulus onset (Fig.3-13A, left histogram) revealed little structure in the response to odours, as in Fig.3.7A. The tuning curve computed from these data during the stimulus was very flat (Fig.3-13A, left tuning curve). Constructing the histogram such that each bin is a breath, with breath one corresponding to the first inhalation of the stimulus (see Methods), sufficiently aligned the data to reveal clearer and more widespread changes in spike rate per breath relative to the baseline per breath spiking rate (Fig.3-13A, middle histogram). However, the tuning curve computed from these data was still quite flat (Fig.3-13A, middle tuning curve).

Given our observation that most spiking in anesthetized state GCs occurs in a narrow window of the breath cycle, we assessed whether considering only part of the breath cycle improved tuning curve fidelity and whether the sensitivity of coding was a function of which part of the breath is considered. Restricting our firing rate computation to 25 % of the breath cycle revealed widespread and robust changes in firing rate per breath to many odours (Fig.3-13A, right histogram). This difference was reflected by a much steeper tuning curve (Fig.3-13A, right tuning curve). Visual inspection of the three histograms produced in the same manner from an example awake state GC suggested that the quality of stimulus discrimination was not affected by analysis of firing rate changes during a restricted respiratory phase (Fig.3-13B).

For anesthetized recordings, the degree of benefit from this analysis was a function of which 25 % of the breath cycle was analyzed. Sliding the 25 % window over the breath cycle revealed a peak in tuning curve correlation between the partial breath tuning curve and the time aligned tuning curve (Fig.3-14A). Additionally, high correlation between the partial breath tuning curve and the time-aligned tuning curve was maintained throughout most of the respiratory cycle (Fig.3-14A). These qualitative observations suggest that odour coding bandwidth in GCs is distributed throughout the respiratory cycle during wakefulness but is concentrated in a narrow window during anesthesia.

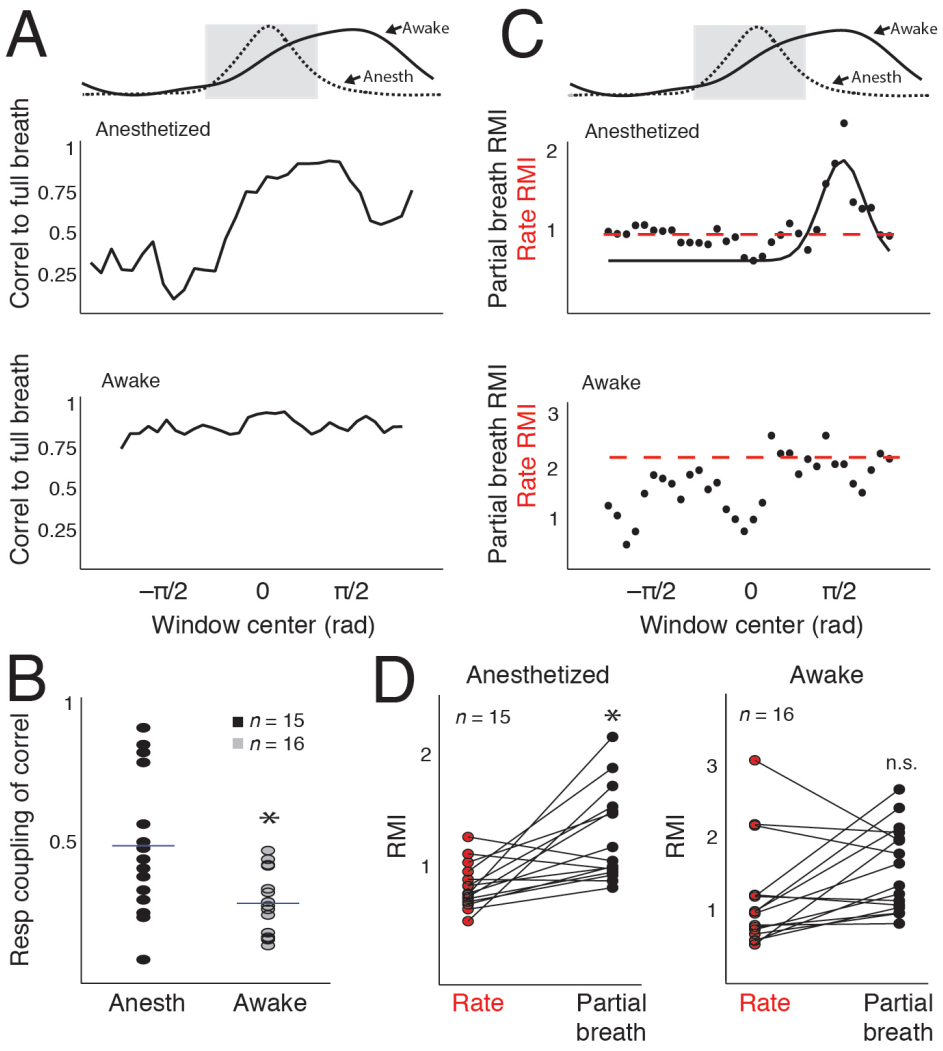

FIGURE 3.14: **Information about odours depends on the respiratory cycle in anesthetized state GCs but not in awake state GCs** (A) Partial breath correlation to the full breath tuning curve are plotted as a function of respiratory phase for a representative (near mean) anesthetized state GC (top panel) and an awake state GC (lower panel). For anesthetized state GCs, this measure of tuning curve robustness and accuracy were coupled to respiratory phase, while they were independent of the breath cycle in awake state GCs. (B) Plot comparing the strength of coupling in the correlation to the full breath tuning curve for anesthetized state GCs and awake state GCs. Awake state GCs showed significantly weaker coupling than anesthetized state GCs for both measures ($p = 0.0057$, t test). (C) RMI values for partial breath tuning curves are plotted as a function of respiratory phase for a representative (near mean) anesthetized state GC (top panel) and an awake state GC (lower panel). Where possible, the data were fit with a Gaussian (black curve) to identify the peak value as the maximal 'partial breath RMI'. If not possible, the mean value was used. The dashed red line indicates the RMI value computed from firing rate without respect to breathing (rate RMI). (D) Plots comparing the rate RMI values and the partial breath RMI values for anesthetized state GCs (left) and awake state GCs (right). Anesthetized state GCs showed significantly increased RMI values computed from partial breath tuning curves ($p = 0.011$, one way ANOVA comparing rate, full breath, and partial breath RMI values). Awake state GCs showed no significant difference ($p = 0.087$) in this comparison.

To quantify this difference for all cells, we measured the dependence of partial breath tuning curve correlation on respiratory phase angle by measuring the coupling of this variable to the breath cycle. Tuning curve correlation tended to show peaks at specific points in the breath cycle under anesthesia while during wakefulness, this correlation tended to be invariant with respiration (Fig.3-14B). As a population, compared to anesthetized GCs, awake state GCs exhibited significantly lower respiratory coupling of correlation to time aligned tuning curves (anesthesia coupling strength: mean $\pm$ s.d. = 0.49 $\pm$ 0.2, n=15 cells from 14 animals; awake coupling strength: 0.29 $\pm$ 0.1, n=16 cells from 11 animals; t(29) = 2.98, p = 0.005; Fig.3-14B).

We further quantified whether partial breath tuning curves improved coding fidelity by measuring response modulation index (RMI) as a function of respiratory phase angle. We computed RMI values for time aligned data as well as data in a sliding window restricted to 25 % of the breath cycle (Methods). Where possible, partial breath RMI values were fit with a Gaussian function, and the peak of the Gaussian was taken as the peak RMI for partial breath analysis (e.g. Fig-3.14C, top). For cells that could not be well fit with a Gaussian function (e.g. Fig.3-14C, bottom), the mean RMI value over the respiratory cycle was used. Considered as a population (Fig.3-14D), anesthetized state GCs exhibited significantly higher RMI values for partial breath as compared to time-aligned analysis (time-aligned firing rate RMI: mean $\pm$ s.d. = 0.83 $\pm$ 0.2; partial breath-aligned firing rate RMI: 1.27 $\pm$ 0.4; n = 15 cells from 14 animals, F(42) = 5.03, p = 0.011), whereas awake state GCs did not (time-aligned firing rate RMI: 1.56 $\pm$ 0.6; partial breath-aligned firing rate RMI: 1.27 $\pm$ 0.4; n = 16 cells from 11 animals, F(47) = 2.58, p = 0.087).

These data indicate that odour information is distributed over the entire respiratory cycle during wakefulness. Likewise, ongoing activity in awake state GCs has limited temporal structure. As a result, odour responses and ongoing activity exhibit slower and steadier dynamics that do not reflect a strong influence of respiration. We therefore find no evidence that GCs contribute to any temporal patterns in MTs related to breathing.

3.4 Discussion

Here we investigated state-dependent activity in GCs of the main olfactory bulb. Granule cells are the target of extensive central feedback projections and make reciprocal dendrodendritic synapses onto MTs. They are therefore well poised to be critical effectors of state modulation of MOB output. Indeed, we found dramatic differences in ongoing and stimulus-driven activity between GCs recorded in anesthetized and awake mice. These differences likely have important consequences for odour coding. Specifically, recordings during wakefulness suggest that GCs are likely to have more extensive lateral interactions with MTs, but are unlikely to strongly shape their temporal dynamics in accordance with breathing.

The activity of GCs under anesthesia was characterized by temporally sparse bursts that were synchronized across cells. As a result, spiking and therefore odourant information is concentrated in a narrow window aligned with respiration. Given the limited sampling rate of laser scanning microscopy, this temporal sparseness may explain why odour responses were not readily observed from GCs of anesthetized mice in a recent two photon imaging study (Kato et al., 2012). This is also relatively consistent with whole-cell recordings from GCs under anesthesia, which reveal a highly nonlinear spike threshold mechanism that enforces temporal sparseness despite strong subthreshold input (Cang & Isaacson, 2003). However, our data do stand in contrast with the large, sustained changes in firing rate reported for GCs in one recent study of anesthetized mice (Tan et al., 2010). Perhaps this is related to selection of an anesthetic, however we observed similar activity with two common anesthesia regimes (Fig.3-1).

The awake state was characterized by two major features. First, GCs exhibited higher firing rates and stronger, more widespread odour responses. Based on the fact that GCs define a circuit enabling mutual inhibition between neighboring MTs, it is widely held that they tune responses of individual MTs and sparsen population representations of odours (Abraham et al., 2010; Kato et al., 2012; Koulakov & Rinberg, 2011; Shepherd et al., 2007). The observation that GCs respond to more odours and more sensitively discriminate among them implies that under wakefulness they play a greater role in sculpting MT selectivity through

augmented lateral interactions. This conclusion is broadly consistent with experimental and theoretical observations regarding MT activity in awake animals and GC function (Davison & Katz, 2007; Kato et al., 2012; Koulakov & Rinberg, 2011; Rinberg, Koulakov, & Gelperin, 2006; Vucinić, Cohen, & Kosmidis, 2006; Yokoi, Mori, & Nakanishi, 1995).

Second, the awake state was characterized by reduced coupling to the breathing rhythm and divergence of respiratory coupling phase across cells. Consequently, unlike under anesthesia, information regarding odourant identity was distributed throughout the breathing cycle. The observation that GCs largely fire with little regard for the respiratory cycle leads us to conclude that it is unlikely they play a significant role in the enforcement of the respiratory locking exhibited by MTs in awake animals.

When compared with the temporal structure of activity observed in MTs in awake animals, our results are surprising in two respects. First, several studies have reported reliable stimulus-specific shifts in respiratory phase coupling of MTs (Cury & Uchida, 2010; Dhawale et al., 2010; Fantana, Soucy, & Meister, 2008; Khan, Thattai, & Bhalla, 2008). Granule cells have naturally been proposed as a likely contributor to this effect (Dhawale et al., 2010; Fantana, Soucy, & Meister, 2008). However, in our data, GCs have a characteristic coupling phase that is invariant to stimuli in both the awake and anesthetized states. Thus, if odour-specific phase shifts are accomplished via GC-mediated feedback inhibition, they are more likely to arise from modulation of the amplitude (as opposed to timing) of inhibitory pulses of specific GC ensembles to push and pull the phase of MT coupling. Second, the weak respiratory coupling and apparent slow rate coding we observed in GCs during wakefulness stands in contrast to the high temporal precision of MTs recorded under similar conditions (Cury & Uchida, 2010; Shusterman et al., 2011). Because of the strength of reciprocal coupling between GC and MTs, one might expect that GCs sculpt or at least reflect the precise MT bursts that tile the respiratory cycle in awake rodents (Shusterman et al., 2011). Nonetheless, we failed to find evidence that GCs participate substantially in this phase locking or even passively follow breathing. Although we cannot completely exclude highly cooperative population mechanisms for creating temporal structure GCs, our observations limit the potential influence of one or a small number of GCs on respiratory patterning in MTs. This

is surprising given respiration-dependent firing of the reciprocally connected MTs and some cortical neurons which may feed back onto the GCs. Future work will examine whether GCs may be targeted by respiration-independent cortical feedback and whether MT respiratory temporal patterning arises from other inhibitory networks (Pressler & Strowbridge, 2006; Kato et al., 2013; Miyamichi et al., 2011).

This work raises several questions concerning both the function of GCs and the influence of anesthetics on neural activity. One potential explanation of our results is that GCs in the awake state receive significantly more input from higher order and neuromodulatory centres. Several reports suggest these higher order olfactory areas may be quieted by anesthesia while axonal imaging of these structures suggests markedly increased and diverse activity of the processes in the GCL in awake animals (Boyd et al., 2012; Otazu et al., 2015). True tests of this hypothesis await further testing including careful manipulation of the feedback to the bulb while recording from GCs. Affirmative results would suggest that GCs in awake animals integrate information from sources beyond those originating in the sensory periphery and provide support for the idea that GCs shape MOB output according to top-down modulation and contextual cues.

Alternatively, anesthetics may also quiet GCs by altering their intrinsic properties. In our study, we measured GC activity under two different anesthetic regimes: ketamine/xylazine and isoflurane. Ketamine is thought to act through antagonism of the NMDA receptor (highly expressed on GCs) although it may have wider effects on neuromodulators (Sleigh et al., 2014). In contrast, isoflurane activates both GABAergic and glycine receptors and also may inhibit NMDA receptors (Garcia, Kolesky, & Jenkins, 2010). We saw similar effects with both anesthetics — a reduction in GC spontaneous and odour evoked activity — suggesting either that anesthetics alone are not responsible for our effects or that anesthetics, despite their different mechanisms of action, ultimately produce the same effect on GCs.

Granule cells receive synaptic input from several MTs. The increase in activity we observe here here could reflect only increased integration of activity from MTs. However, the responses of MTs make this case unlikely. MT activity tends to be sparse in awake animals

and broad in anesthetized animals (Rinberg & Gelperin, 2006). Often, odours that evoke responses in anesthetized animals fail to evoke responses in the same cells when the animal is awake. Thus, from the activity of MTs alone we might have instead expected GCs to show increased responses in anesthetized animals. Our results suggest something more complex is at work. Importantly, the observed increase in GC activity in the awake state widens the dynamic range for GC responses when GCs receive input from more than one MT. Such a range may become particularly important in the discrimination of perceptually similar odours or mixtures that activate overlapping sets of MTs. In support of this, disruption of GC activity disrupts an animal's ability to quickly discriminate among similar odours.

The olfactory cortex integrates population activity of MTs. Considerable evidence argues that the cortex spatially integrates input from multiple glomeruli (Apicella et al., 2010; Davison & Ehlers, 2011; Illig & Haberly, 2003; Miyamichi et al., 2011; Sosulski et al., 2011), but the temporal integration properties of the olfactory cortex are less clear and are under active investigation (Haddad et al., 2013; Miura, Mainen, & Uchida, 2012). Synchronous inhibition seems likely to entrain synchronous MT output which may be best extracted by coincidence detection, whereas the slower firing rate changes seen in our awake data may be best served by temporal integration upon readout. Potential support for regulated temporal integration comes from recent evidence revealing the existence of an intriguing mechanism for modulating MT synchrony to encode stimulus associations (Doucette et al., 2011).

Finally, while the state-dependent modulation we observed was between anesthesia and passive wakefulness, our results demonstrate remarkable lability of the MOB interneuron network. We speculate that this flexibility could reflect a capacity to adapt coding strategies for different conditions as described in Chapter 4.

Chapter 4

Granule Cells Track Odour Discrimination Performance

4.1 Introduction

The same sensory stimulus can drive vastly different behavioural choices depending on whether an organism associates that stimulus with a positive or negative outcome. Traditional models of the brain posit that representations of stimuli and valence reside in higher cortical and limbic structures while early sensory areas represent basic stimulus features. However, increasing evidence suggests that valence associations can also alter these sensory circuits (Poort et al., 2015; Kay & Laurent, 1999) such that their activity reflects not only a stimulus but also the particular outcome with which an animal associates that stimulus.

The olfactory bulb circuit is an excellent model in which to study flexibility in early sensory processing. Many animals rely on odours to navigate their environment, and the meaning associated with these odours can change, contingent on the environment in which the animal experiences the odour and the animal's previous history with that odour (Brennan & Keverne, 1997). This change in meaning often arises quickly (one trial learning or on the order of minutes) particularly when the odours are associated with salient stimuli or events. Neural activity in the olfactory processing circuit must change to reflect this new outcome and support a corresponding change in the animal's behaviour. Interestingly, MOB neurons show activity consistent with contextual representations of odours even on this fast

learning time scale. Mitral and tufted cells, the main excitatory output neurons of the MOB, display flexible activity depending on whether odours are paired with rewarding or punishing outcomes (Doucette & Restrepo, 2008; Kay & Laurent, 1999; Fletcher, 2012). These valence-dependent responses have been proposed to reflect cortical and neuromodulatory inputs to the MOB that reshape MOB circuits in accordance with non-sensory variables.

The majority of cortical and neuromodulatory inputs to the MOB target GCs. Both modeling studies and local field potential (LFP) recordings suggest GC responses change as stimuli acquire behavioural meaning. Association of odours with aversive stimuli increase *cfos* expression in GCs while beta oscillation power in the MOB, thought to rely in part on activity in GCs (David et al., 2015; Osinski & Kay, 2016), increases when animals associate odours with reward (Martin & Ravel, 2014; Martin et al., 2004). Recently, several groups showed that GCs exhibit significant differences in activity depending on the internal state of the animal (Cazakoff et al., 2014; Kato et al., 2012; Wienisch & Murthy, 2016), supporting the idea that GCs odour tuning is plastic and that GCs do not merely reflect the basic features of incoming odour information. However, GC activity in response to learned associations has never been assayed in real time.

We set out to explicitly test the hypothesis that GC activity reflects not only incoming odour information but also reflects the valence with which the animal associates an odour. To do so, we trained mice in a flexible go/no-go task in which mice learned to associate a previously rewarding odour with the punishing tastant quinine (QHCl). We could thus probe how the association of the same odour with a novel outcome changed activity in GCs. As animals performed the task, we conducted loose-patch recordings, a recording paradigm we have previously shown is amenable to assaying GC activity (see Chapters 2 and 3). Our results suggest that associative learning alters neural responses at the level of individual GCs, and that specifically, a subset of these GCs show profound activity changes contingent, not on valence per se, but rather the animal's engagement and overall performance in the task. This work highlights both the lability of sensory inhibitory circuits and suggests that GCs may alter odour representations in order to support recognition of odours in changing environments.

4.2 Methods

4.2.1 Animals

We performed experiments with adult, male CD-1 mice (age 4 weeks at start of training). We chose CD-1 mice for their large size at a young age (optimal for patch electrophysiology), but subsequent behavioural experiments with both GAD2-CRE mice (C57Bl/6 background) and Black Swiss mice suggest no difference between the learning capacity of these animals in our task. Animals were group housed (three to five mice per cage), maintained on a 12:12 h light/dark cycle (lights on at 07:00), and had access to food and water ad libitum. All experiments were conducted in accordance with the National Institutes of Health's Guide for the Care and Use of Laboratory Animals and approved by the Cold Spring Harbor Laboratory Institutional Animal Care and Use Committee.

4.2.2 Head-Bar Surgery

For head fixation, we secured custom head-bars to the skull of the animals in a manner previously described (Chapter 2 and Appendix A). Before we began any behavioural training, we permitted animals to recover for at least three days following surgery. Following the recovery period, we began water depriving animals to 85 % of their free-water weight, a practice that generally meant we provided the animals with 1–2 ml of water per day. We water-deprived animals for one week before we began behavioural training.

4.2.3 Odour Presentation

We presented odours using a custom-built odour machine (Eckmeier & Shea, 2014). We prepared 5 ml of 1 % odours diluted in mineral oil and then further diluted odours $10\times$ at the nose in an oxygen stream (200 ml/min odour in 2 L/min oxygen). All odour presentations were 1.5 s long with a random ISI between 7.5-9 s long. A continuous vacuum stream positioned behind the animal helped to clear odours during the interstimulus period. We

regularly measured the performance of our olfactometer using a PID. We could reliably detect odours 100-150 ms following odour onset and found that odours were rapidly cleared (within 50 ms) after odour offset. Table 4.1 shows the odour sets we used during both behavioural training and GC recording.

TABLE 4.1: Panels of Odourants Used for Training/Recording

Odour Panel A			
Anise oil	Methyl benzoate	Ethyl butyrate	Butenol
Acetophenone	Cineole	Isobutyl propionate	2-heptanone
Odour Panel B			
Ethyl tiglate	Valeraldehyde	Linalool	Heptanal
Pentyl acetate	Fenchone	R-carvone	Ethylbenzoyl acetate
Odour Panel C			
Pentanol	Octanal	Methyl benzoate	Heptanoic acid
Ethyl butyrate	Citral	2-butenol	Cyclohexylacetate
Odour Panel D			
Ethyl tiglate	Valeraldehyde	Limonene	Eugenol
Pentyl acetate	Fenchone	R-carvone	S-carvone

* We trained animals on Odour Panel A and recorded from GCs using Odour Panel B (vice versa), or we trained animals on Odour Panel C and recorded from GCs using Odour Panel D (vice versa).

4.2.4 Behaviour

We trained water-deprived mice to associate previously rewarding odours with a bitter-tasting QHCl outcome. In this way, we could track how the animal's association of an odour with a new valence altered activity in GCs. To track a mouse's association of odours with a particular outcome, we required that mice discriminate between the QHCl paired odour and an odour that was always rewarded with water. Mice learned to initiate licking during water reward odours in order to receive the reward and withhold licking to QHCl paired odours to avoid punishment. We found that, upon first ever exposure to QHCl, mice often ceased licking to both QHCl and water-paired odours. This was true for several different concentrations of QHCl (1 mM, 2.5 mM, 5 mM; mice licked even for punished odours at 0.5 mM) and precluded our efforts to examine the animal's discrimination and learning over time during the first session of QHCl exposure.

However, we found that on subsequent re-exposure to the odour paired with QHCl, mice displayed avoidance behaviour only to the QHCl-paired odour. As such, instead of recording from GCs in animals upon first exposure to QHCl, we instead trained animals to learn the overall idea of the task but remain flexible to which odours might be paired with which outcome (Fig.4-1).

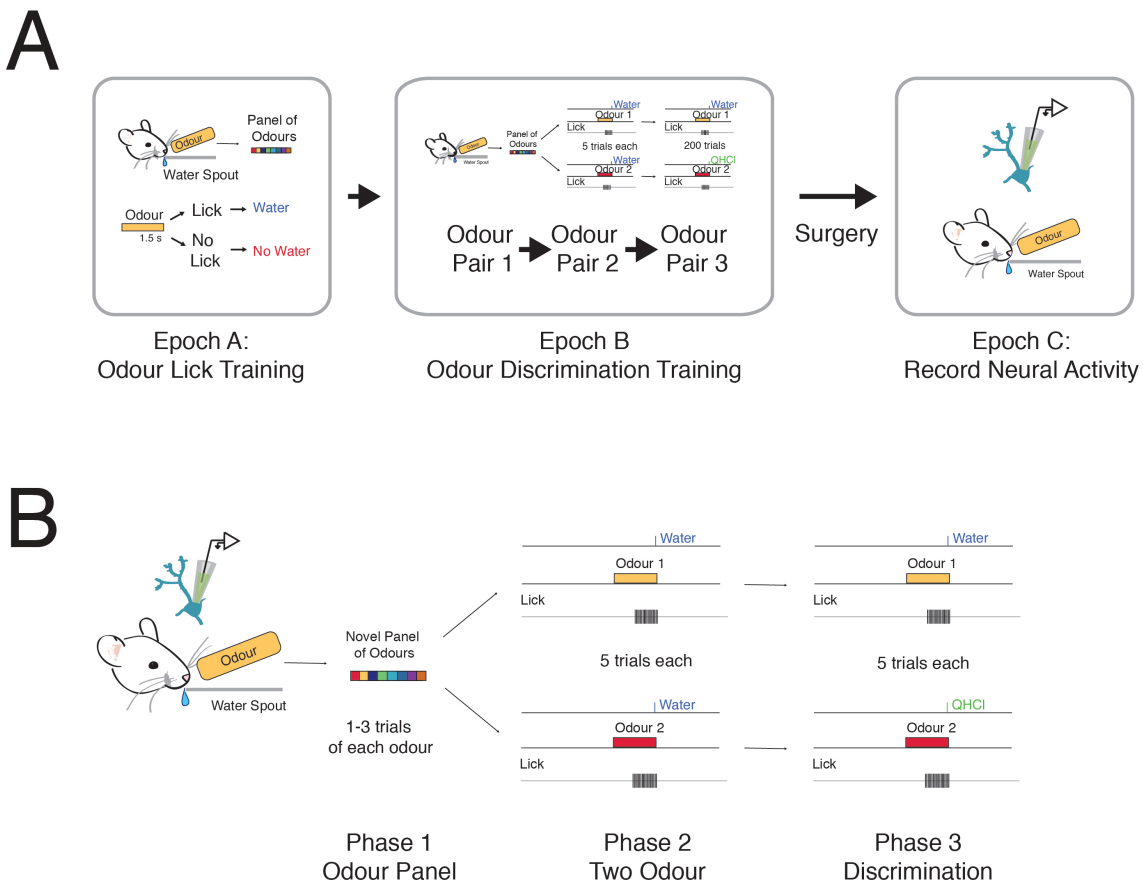

FIGURE 4.1: **Olfactory valence learning paradigm**. (A) Animals were trained to flexibly associate some odours with water and other odours with QHCl. Behavioural training progressed in three stages. After seven days of water deprivation, mice were trained to associate odours with water (Epoch A). We randomly presented several trials of 8 different odours (1.5 s long odour stimulus, 200 trials total). If the animal licked at any point during the 1.5 s odour, the animal received water reward. If it did not lick, it did not receive reward and had to wait until the next trial (7.5 - 9 s ISI) until another trial began. Once an animal reached a criterion of licking on 80 % of the trials in two sessions (200 trials per session), we advanced the animal to Epoch B. During Epoch B, we trained the animal to associate one odour with water reward and another odour with punishing QHCl. We first trained the animal on one odour pair (Pair 1), and once the animal reached criterion on this pair (two sessions with $d' > 2$), we trained the animal on Pair 2. If the animal showed criterion performance on this pair, we advanced the animal to Pair 3. Once the animal showed criterion performance on Pair 3, we implanted a nasal cannula and made a craniotomy over the MOB. Following this, we attempted to record from GCs while the animal performed the water/QHCl odour discrimination task (Epoch C). During Epoch C, we used a completely different panel of odours than that used during Epoch A or Epoch B. (B) For analysis of GC responses, we considered three different phases during Epoch C. Phase 1: Responses of GCs to a novel panel of odours (all odours were paired with water). Phase 2: Two odour. We chose two odours from the panel that elicited responses in GCs and then presented five trials of each of these odours to assay odour evoked respones in the GC prior to learning. Phase 3: QHCl/water paired odour discrimination. We paired one of the two odours from Phase 2 with QHCl. Thus, as the animal learned the new association, we could assay GC activity and compare this activity to the responses in the Phase 2 period.

We conducted all behaviour in head-fixed mice permitted to freely run on a rotating wheel (see Chapter 2 and Appendix A). For two days, we habituated mice to the head-fixed apparatus by fixing animals in the apparatus for 15–30 min each day. Next, we introduced the lick spout to the animal and gave the animal free access to water while it was positioned on the ball. If the animal licked for at least 0.85-1 ml of water, we next trained it to associate odours with water. To detect licks, we used an infra-red beam sensor (Island Motion). During this part of the paradigm, we presented a panel of eight different odours to the animal (Table 5.1), and we rewarded the animal with 4 μl of water if the animal licked during the 1.5 s odour period. We re-calibrated the water spout on a weekly basis. If the animal licked at least two times during the odour presentation period, it received water in the last 50 ms of the odour period. In general, mice learned to lick only during the odour period with rare spurious licks during the ISI. As such, we did not punish mice with timeouts for ISI licks. For some animals, we increased the amount of water provided during this training phase to 6 μl of water as 4 μl was not always sufficiently rewarding to encourage licking behaviour. Once a mouse performed at 80 % on two consecutive days of 200 trials per day, we advanced it to the avoidance stage of training (Fig.4-1 Epoch B). During this stage of training, we employed a flexible presentation of odours whereby we first paired both discrimination odours with water and then across the course of training, we paired a single odour with QHCl (2.5 mM QHCl, Sigma-Aldrich). We initially presented a panel of eight odours to the animal (random presentation of single odours; one–two trials of each odour). If the animal licked during any of these odours, it received water reward. Following this, we chose two odours to continuously present to the animal across the rest of the session. We first presented five trials of each of these two odours in which we paired both odours with water. Then, we chose one odour and instead paired it with QHCl for the rest of the session (200 trials of water/quinine trials per session). We pseudorandomly presented water and QHCl trials such that within a block of twenty trials, the animal experienced ten water trials and ten QHCl trials randomly interspersed within the block. Across a session, the animal received no more than six QHCl trials or six water trials in a row. We categorized trials as either hits (at least two licks during presentation of water-paired odour), misses (fail to lick two or

more times during water-paired odour), false alarms (FA, at least two licks for QHCl-paired odour) and correct rejections (CR, less than two licks on QHCl-paired odour). We computed the animal's ability to distinguish between the water and QHCl paired odour as a d' score where:

$$d' = zHits - zFA \tag{4.1}$$

where *zHits* is the z-score of all session hits and *zFA* is the z-score of all session FAs. If an animal performed two sessions at $d' > 2$, we then trained it on a new odour pair until it performed at $d' > 2$ on this new odour pair. Preliminary testing revealed that animals displayed savings for the overall idea of the task, and by the third new pair, they were performing at $d' > 2$ on the first session of a new odour pair (Fig.4-2B). For all animals, we varied which odour we paired with the water and which odour we paired with QHCl. Prior to recording, we tested animals on at least two different odour pairs.

To compare the activity of GCs in animals that learned the task versus those that did not, we used two different control groups. Control group one never experienced odours in the presence of QHCl but learned to associate odours with water. Control group two experienced QHCl but not in direct association with an odour. Instead, we presented the QHCl randomly during the ISI. Mice rarely licked when we presented QHCl during this period. We matched control to test groups in terms of the number of training sessions.

4.2.5 Electrophysiology and Breathing Measurements

Once animals displayed accurate behaviour on the task, we implanted a cannula in their left nasal cavity in which we could placed a thermocouple. As described in Chapter 3, this allowed us to record breathing in the animals. We permitted animals one day of recovery before we commenced with electrophysiology.

We recorded from GCs using loose-patch techniques as previously described (Cazakoff, 2014, Chapter 2). On the day of recording, we anesthetized animals with isoflurane (1 % in O_2), and we made a small craniotomy over the olfactory bulb. Generally, we anesthetized animals for 10-15 min, and we allowed animals at least 4 h of recovery before commencing

recording. We made multiple craniotomies in each mouse (at least one over each hemisphere of the MOB).

During recording, we presented a new panel of odours not used during the training phase. We rationalized that new odours might elicit stronger learning-related responses from GCs as the use of new odours would limit overtraining in the animals. Once we patched a GC, we first screened this GC for odours that elicited responses. We presented a panel of eight odours (one–three trials per odour). We quickly determined evoked responses using online generation of PSTHs (100 ms bins) and subsequently chose two odours that elicited responses from the cell defined by at least two bins that showed significant differences from baseline. In general, at least one odour elicited a response from the cells we recorded, and in the event we could not find two odours that elicited excitatory responses, we chose odours that suppressed GC firing. We subsequently presented these two odours to the animal for the rest of the session. First, we paired both odours with water, and animals received water reward if they licked to the odours. Then, we randomly chose one odour to pair with QHCl. We punished all subsequent licks to this odour with 4 μl of QHCl per trial while we continued to reward licks to the other odour.

In GC naive and control group animals, we also used a novel panel of odours during recording. However, in most animals, we did not choose two odours for repeated presentation during recording. Instead, we presented two–three trials of each odour in the odour panel, and then moved on to recording a new cell. In a subset of the animals, we chose two odours for repetitive presentation. Following multiple days of recording, we sacrificed animals and stained the olfactory bulbs with streptavidin:Alexa Fluor 488 in accordance with our previously described protocol (Chapter 2).

4.2.6 Data Analysis

Analysis of Breathing

To determine the number of breaths in a recording/behavioural session, we used methods as described in Chapter 3. Briefly, we determined the peaks (inspiration end) and troughs

(inspiration start) of data on the raw breath trace as well as the max inspiration period (peak on the differentiated breath signal). We then annotated breaths according to the baseline period (3 s duration immediately before odour onset), the odour period (1.5 s period), and reward period (3 s duration starting immediately after odour offset).

We calculated the instantaneous breathing frequency as the inverse of cycle time where cycle time is defined as the duration between one inspiration start time and the next. Our data revealed few periods where the animal either did not either inspire or expire indicating that the duration between inspiration start time was a good measure of cycle time. For population data, we constructed instantaneous breath histograms for each mouse across all breaths in the time period examined. For the hit, miss, FA, and CR analysis, we then constructed a mean histogram from all mice. To compare different trials within a session, we computed receiver operating characteristic (ROC) curves using the instantaneous breath rates on each trial and tested for significance among trials using Kruskal-Wallis (Bonferroni post hoc) or Mann-Whitney U (Bonferroni correction $p<0.05/n$ where n = number of independent tests completed) testing where appropriate. For correlation of histograms, we binned data in 100 ms bins and used a Pearson correlation ($p<0.05/n$, where n = number of independent sessions).

Analysis of Electrophysiology

We filtered data between 500 and 3000 kHz and spike-sorted using Spike2. We completed all other analysis in Matlab with custom built software. We determined odour responses and broadness of tuning as described in Chapter 3. We constructed PSTHs from no less than five trials (generally 5-6 trials during the water only epoch) and no more than ten trials of an odour (generally ten trials during the water/QHCl epochs). For z-score mean responses and 2–D histograms, we computed the mean and s.t.d in from the entire recording trace binned in 1.5 s bins (Fig.4-4) or 100 ms bins (histograms). For visualization purposes (Fig.4-8), we computed spike density plots from the PSTHs (1 ms bins) by convolving with a Gaussian kernel with a 50 ms width.

We computed learning related shifts in GC activity in several ways. First, we computed the change in mean response between water-only paired trials (Phase 2 epoch) and the ten consecutive water/QHCl paired trials in which the animal achieved its highest discrimination performance (Phase 3 best epoch). For each trial, we determined the mean spike rate across the entire stimulus period (1.5 s odour and 2 s contingency) and subtracted the spike rate during the 2 s baseline period immediately prior to odour onset. We then computed an overall mean baseline subtracted spike rate from these trials. To compare the Phase 2 and Phase 3 best period, we computed the Phase 3 normalized firing rate by setting the Phase 2 rate to one and shifting the Phase 3 period accordingly. Thus, changes less than one indicate response decreases while changes greater than one indicate response increases. We used a one-sample t-test to determine if the population of GC responses was significantly different from one ($p < 0.05$). We computed this response change independently for the odour that was always water paired and the odour that was eventually paired with QHCl. As a control, we examined data from animals to which we repeatedly presented two water paired odours (never QHCl paired). We denoted the first five trials of an odour in these controls as the Phase 2 period and the last five-ten trials of an odour in these controls as the Phase 3 best period.

To examine changes in GC activity across learning, we applied a sliding window analysis to trials whereby we computed the d' across 10 trials (starting at trial one of Phase 3) and then shifted the window by one trial to compute the next d' value. Within the same window, we computed the mean response for all water trials in the window and the mean response for all QHCl trials in the window. Due to the way we constructed our behaviour, there are no more than 6 trials of the same odour in a row. Thus, in each window there were at least 4 trials of each odour from which to compute the mean response. In these windows, we also computed normalized responses as described above. We correlated the sliding window d' values and the normalized values for each odour using a Spearman correlation ($p<0.05/13$, $n = 13$ cells). We further determined if these correlations were due to chance by shuffling the data 1000 times within a session, computing the correlations coefficients for each shuffled data set, and comparing the coefficient values computed on the shuffled data to the observed values. Due

to lack of data, we had to omit one cell from the analysis.

For K-means cluster analysis, we clustered PSTHs (100 ms bins) for each trial of an odour collapsed across Phase 2 and Phase 3 of the behaviour. We tested between two and 10 different clusters and confirmed cluster number using the Calinski-Harabasz criterion.

4.3 Results

4.3.1 Mice Can Perform a Flexible Go/No-go Task

Discrimination paradigms typically involve training mice to discriminate only two odours and/or mixtures of these odours. Across several hundred to thousands of sessions, the mice achieve stable levels of performance, and then, investigators interrogate neural circuits while again presenting the same two odours. However, in their natural environment, animals often form associations and make decisions on much faster time scales. We thus, instead, decided to employ a more flexible strategy – a version of which was first introduced in rats (Kay & Laurent, 1999) – whereby the animal learned to discriminate novel odour pairs upon their first exposure to these odours. We reasoned that such a strategy provided us with several advantages. First, because we did not limit the animal to discriminating between two set odours, we could first screen, with a panel of odours, any patched GCs for odours that evoked responses. GC patch recordings are generally difficult and low-throughput even at the best of times. In the event, we obtained a good recording, we wanted to be able to record this cell during our behavioural paradigm. We did not want to limit ourselves to searching for cells that responded to a limited set of two odours. Second, because we employed a flexible strategy, we better ensured that we did not over-train the animals on a given odour pair and that our paradigm better matched those paradigms in which investigators observed flexibile processing in MTs . We thus demanded that the animal actually learn the new stimulus association, and we interrogated GCs during this learning as opposed to interrogating the association once the animal had already learned it.

When first exposed to QHCl, mice often stopped licking to all odours regardless of their outcome, precluding recording from GCs in this first session. Thus, prior to any electrophysiological recordings, we first serially trained mice to discriminate between two odours across several sessions. During this behavioural training, we changed the identity of the odour discrimination pair across sessions. In the section below, we summarize this behavioural data.

Mice quickly learn to discriminate new odours

We trained mice on three different odour pairs. Once mice accurately discriminated between the Pair 1 odours, we exposed them to Pair 2 and then Pair 3. Figure 4-2A shows example Pair 3 discrimination data for one mouse upon its first exposure to Pair 3. Similar to all mice, this trained mouse showed a few mistakes at the beginning of a trial. However, it quickly learned to lick during presentation of only the water-rewarded odour (Fig.4-2A), and as a result, d' values computed over blocks of 20 trials steadily increased (Fig.4-2A right).

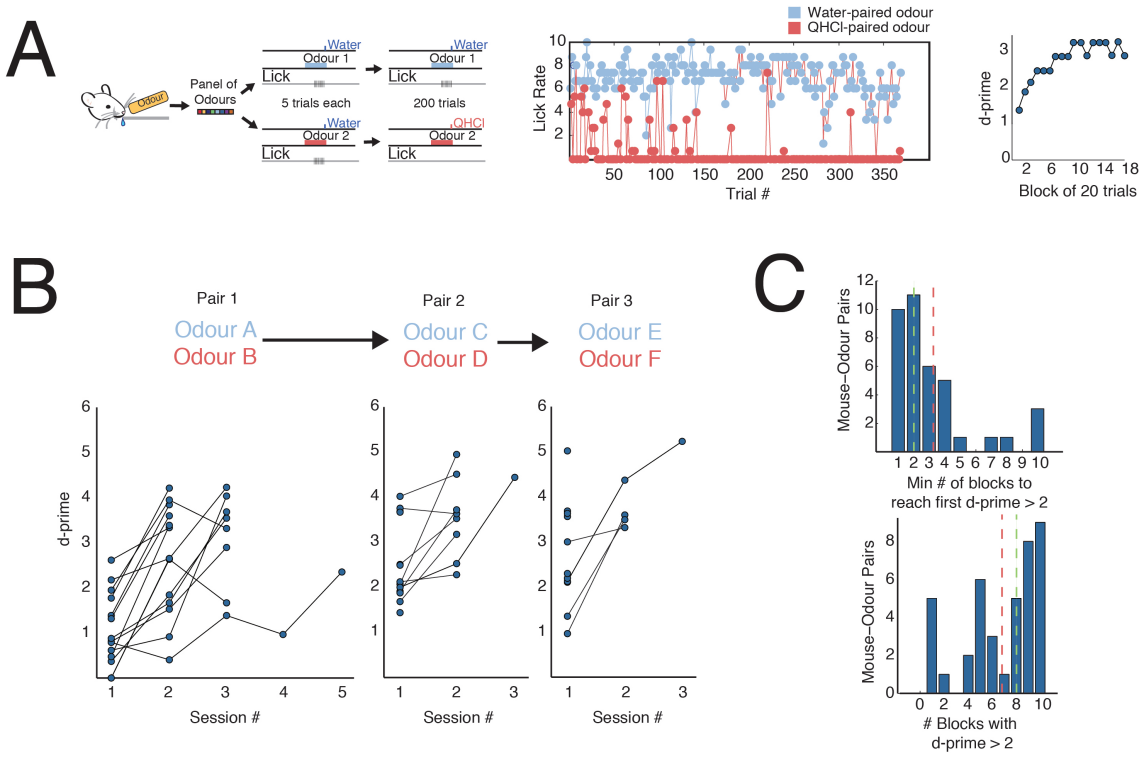

FIGURE 4.2: **Mice can learn a flexible association task.** (A) We trained mice on a flexible go/no-go task in which mice learned, in a single session, to discriminate two odours which were randomly chosen from a panel of odours. Middle: Lick plot for a trained mouse introduced to a novel odour pair. Each dot is a the lick rate on one trial. Right: d' for the mouse's lick data computed across every 20 trials in a single session. (B) Behavioural data for all mice across all odour pairs tested. d' computed across the entire session (200 trials) is plotted. Mice first learned to discriminate odour A and odour B (Pair 1). Once they had reached a stable performance ($d' > 2$ on 2.5 sessions), we trained them on Pair 2. Once the mice reached criterion on this pair ($d' > 2.5$ in one session), we trained them on Pair 3. Mice generally improved over time, taking fewer sessions to learn a new pair. Mean number of sessions of 200 trials to achieve a $d' > 2$ = 2.7 (Pair 1), 1.6 (Pair 2) and 1.1 (Pair 3). (C) Mice quickly learn new odour pairs. Top = Histograms of minimum number of blocks to display criterion performance and number of blocks in a session with criterion performance for all mouse odour pairs. Block = 20 trials. Mice require 3.3 $\pm$ 2.9 blocks (mean $\pm$ s.t.d) or 66 trials to first display criterion performance in a block and display criterion performance in 6.7 $\pm$ 3.1 blocks. Red and green dotted lines show the mean and median respectively.

The population of mice generally took two to four sessions (200 trials per session) to discriminate between Pair 1 odours (mean number of sessions to criterion = 2.7 $\pm$ 0.8; session = 200 trials; Fig.4-2B left). For Pair 2, most mice quickly learned to discriminate the odours within one to two sessions (mean number of sessions to criterion > 2 = 1.6 $\pm$ 1.0), demonstrating some savings for the overall idea of the task. Again, on Pair 3, they demonstrated even faster learning (mean number of sessions to criterion = 1.1 $\pm$ 1.2; Fig.4-2B). With the exception of three mice, we trained most animals on three pairs of odours.

Mouse performance improves quickly within a session

While the results above detail the performance of mice across sessions, it was equally important to us to examine how mice perform in a session. From the data we presented in Chapter 2, we know that the mean length of time for which we can record a GC is between 8 and 18 min. We were interested if, in our behaviour, mice presented with novel odours showed learning across such a time window.

For Pairs 2 and 3, we divided each session into blocks of 20 trials and calculated the d' in each block (Fig.4-2A right). In a session of 200 trials, we thus calculated d' values for 10 blocks. For all mice, we then determined in which block (1–10) the mouse first displayed behaviour with a d' value > 2 (Fig.4-2C). Most mice showed criterion performance within the first 40-70 trials (mean first block to criterion = 3.3 $\pm$ 2.9 and median first block to criterion = 2). With at most a 9 s ISI, mice thus showed some indication of learning within 6 to 10 min. Further, mice also performed at criterion for several blocks within a session, suggesting this learning is not transient (Fig.4-2C). On average, mice performed at criterion for 6.7 $\pm$ 3.1 blocks (roughly 130 trials). Overall, this indicated that mice could learn to accurately discriminate two novel odours within the time window of which we can record GC spiking activty.

4.3.2 Behaviour is Odour-dependent

To ensure learning in this task was dependent on odour identity and not some other variable that might fluctuate in the task (clicking of solenoid valves, odour pressure differences), we conducted several control experiments. First, when we use mineral oil as both the water paired and QHCl paired odour, behavioural performance collapses to chance in a trained mouse (Fig.4-3A). Second, if in a performing mouse, we switch the vials/solenoids from which we play the odours, there is no effect on performance (Fig.4-3B). This suggests the animals do not pay attention to audible differences in solenoid clicking. Finally, when we use the same odour as both the punished and rewarded odour, mice quickly stop licking to all odours in order to avoid QHCl (Fig.4-3C). This is true when we use the same odour with both contingencies across a session (Fig.4.3C top) or when we switch to the same two odours in a session where a mouse is already performing (Fig.4-3C bottom).

Taken together, these behavioural data suggest that mice can quickly discriminate between odours even when the odours are novel. Within only tens of trials, they learn to associate an odour with a new contingency and accordingly adjust their licking behaviour. We next recorded GC activity in these trained mice to explore how these novel associations updated activity in GCs. During recording, we presented a novel panel of odours to the animal.

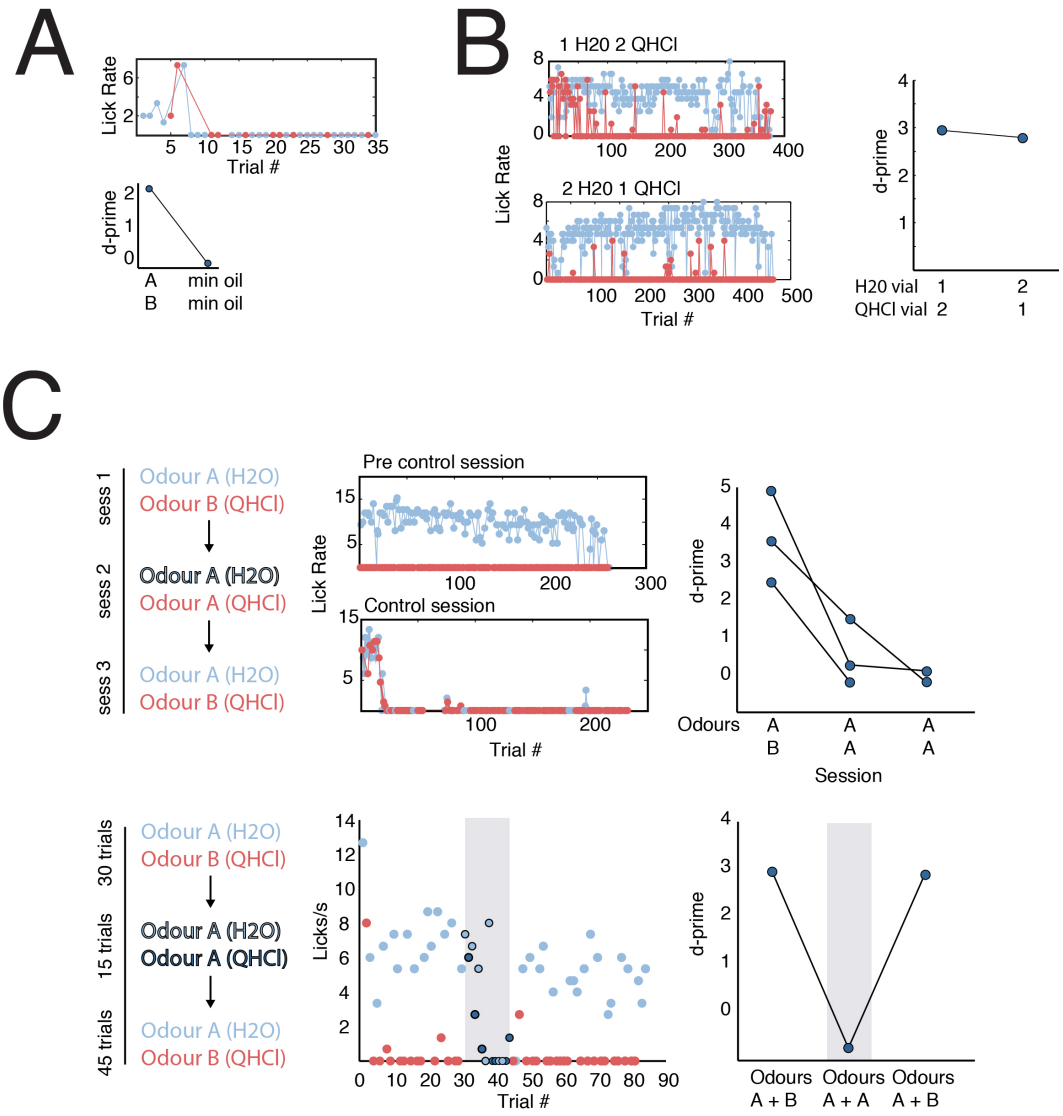

FIGURE 4.3: **Behaviour is odour dependent.** (A) Mouse does not perform when mineral oil is the stimulus. Top: example lick plot when we use mineral oil as both the water and QHCl paired stimulus. We ended the session early as the mouse would not lick. Bottom: d' values for single mouse in session preceding mineral oil session (d' = 2.4) and in the mineral oil session (d' = 0.0294). (B) Performance of a mouse does not change if we keep the water and QHCl odour identity the same but switch the vials from which they emanate. On left, lick rate across a session when vial one = water odour and vial two = QHCl odour (top) and vice versa (bottom). D-prime for each session is plotted on the left (d' session 1 = 2.9 and session 2 = 2.7). (C) Behaviour when the same odour is used as the water and QHCl paired odour. Top: Same odour used with both contingencies across an entire session. (Mean d' across sessions: 3.6 $\pm$ 1.2, 0.5 $\pm$ 0.9, -0.1 $\pm$ 0.2, n = 3 mice. Bottom: Data from a single mouse in which we switched odours during a session. For 30 trials, the mouse could discriminate between odours A and B. Then only odour A was played, paired with both water and QHCl. Following 15 trials of this, we resumed presentation of odour A and B. D-prime dropped to -0.4 during the 15 trial control period.

4.3.3 Odours Evoke Strong Responses in Trained Mice

We recorded from GCs across several phases of the recording/behavioural session (Fig.4-1). Because we conducted our experiments in a different species of mouse (CD-1), we first confirmed that we saw similar odour response profiles in these mice as in the animals used Chapter 3. To do so, we determined the tuning profiles of GCs to a panel of novel odours (Phase 1). Consistent with our previous results, GCs in these animals responsed to odours and generally showed significant responses to several odours out of the panel of 8 we presented (Fig4-4A). We noticed early on that in these mice, we often saw much stronger responses to odours than what we had seen in animals that passively experience odours like those examined in Chapter 3. (Fig.4-4A,B). Tuning curves were even steeper, with some cells responding at 60 spikes/s greater than baseline (compared to 10 spikes/s in passive animals; Chapter 3).

In our previous experiments, animals had access to a lick spout and water but were not explicitly trained to associate odours with punishment. We thus wondered whether the difference we saw might reflect punishment learning in our animals. To explore this, we recorded from a group of animals trained in Phase 1 of our task but then advanced passed this stage. We then compared the z-score responses of GCs recorded from animals that passively experienced odours (49 cells, 24 mice), animals that were trained in the QHCl task (15 cells, 10 mice) and this group of animals that were trained to expect water reward with odours but never trained with QHCl (12 cells, 6 mice; Fig.4-4B). We saw no differences among the three groups (Kruskal-Wallis test; $H(2,734) = 3.89$, $p=0.14$) suggesting that the three groups did not differ from each other by this measure.

We were still struck, however, by the wider shape of the histograms from both the water rewarded and QHCl punished groups. Both groups had cell-odour pairs that displayed stronger suppressive and excitatory responses than the passive group as evidenced by the histograms and the cumulative probability plots for these groups (Fig.4-4C). These stronger responses did not derive from any one mouse in particular but rather 6 out of the 16 mice, and 11 cell odour pairs (10 QHCl trained mice and 6 water trained mice) showed a response

3 s.t.d outside the passive mean. By comparison, two mice (three cells odour pairs) showed such a response in in the passive mice. This suggested that the association of odours with reward might alter GC responses. To examine this, we collapsed the data across the two trained groups (water only trained or QHCl trained) – collectively called the rewarded group– and plotted the cumulative distribution of z-scores against the passive group. A two-sample Kolmogorov-Smirnov comparison revealed a significant difference between the passive and rewarded groups ($D = 0.13$, $p = 0.011$). For comparison and because we lacked cell numbers in the rewarded group, we sub-sampled the passive group (Fig.4-4C right grey plots) to examine what we might expect if we had a similar number of cell-odour pairs in each group. Even with sub-sampling, we still observed a difference between the two groups (arrow in Fig.4-4C), suggesting the difference is real.

These results reveal that GCs in trained animals respond to odours and that the broadness of GC tuning holds across different strains of mice. Furthermore, consistent with reports from MTs (Doucette et al., 2011), an animal's association of odours with rewarding stimuli or the animal's general state of water deprivation may alter overall tuning of GCs. While we need to collect more data, we see a trend towards enhanced responsiveness to odours in animals trained to associate odour with any stimulus.

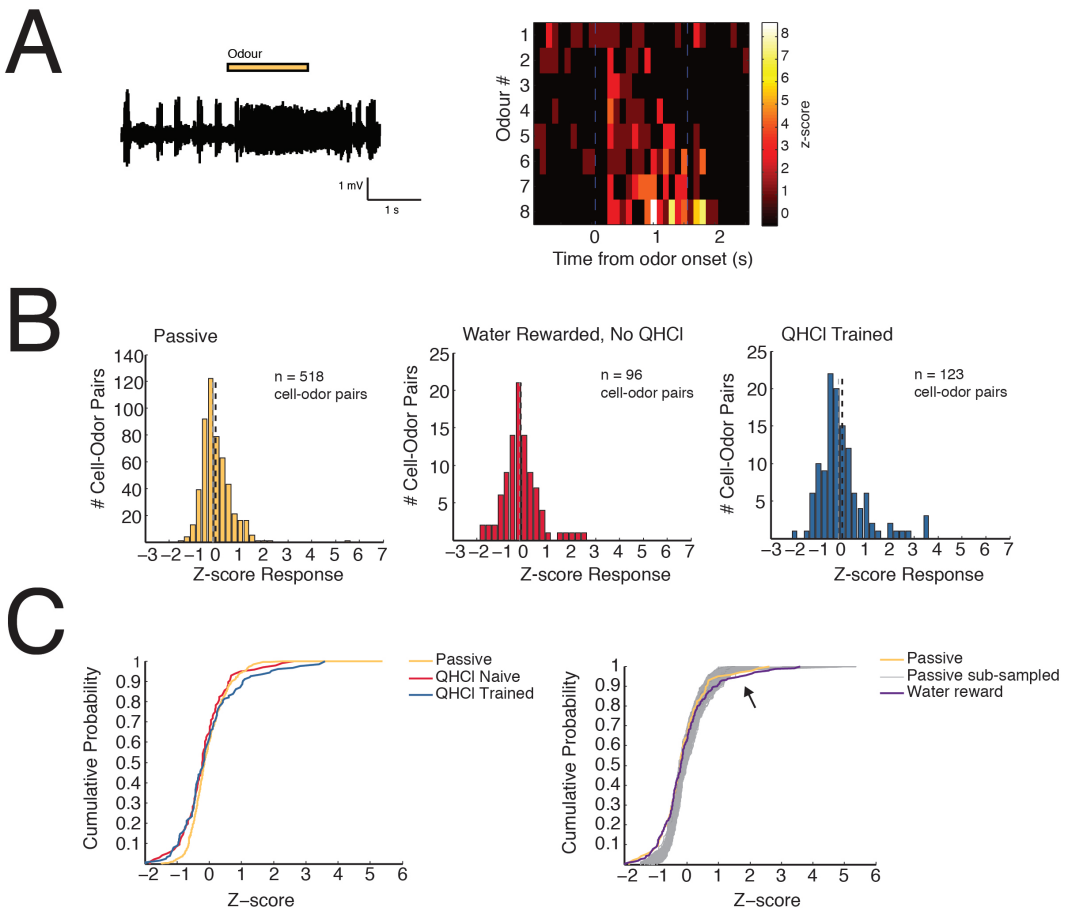

FIGURE 4.4: **Mice trained in an associative task display enhanced responses** (A) Example raw response and z-score odour response histogram of single GC. Histogram is binned in 100 ms bins. (B) Histograms of z-score responses to odours in animals not trained to associate odour with an outcome (passive, mean $\pm$ s.t.d = -0.03 $\pm$ 0.61, median = -0.14), animals trained to associate odour with water and QHCl (mean = -0.00 $\pm$ 0.98, median = -0.16), and animals trained to associate odour with water (mean = -0.14 $\pm$ 0.75, median = -0.21), Grey and black dotted lines denote the median and mean respectively. The three groups were were not significantly different (Kruskal-Wallis, p = 0.41) but note the number of cell odour pairs and the longer tails in the second two groups. (C) Cumulative probability plot for all three groups. On the left, we collapsed the data across the QHCl Naive and QHCl Trained groups. We sub-sampled the passive group 1000 times to compare to the rewarded group.

4.3.4 Responses of Granule Cells to Novel, Learned Contingencies

We next asked how GC responses change when animals associate an odour with a punishing stimulus, QHCl, instead of a rewarding water stimulus. We were able to record from 14 cells in 10 animals. On average, we recorded from these cells for 9.5 $\pm$ 5.2 min (66 $\pm$ 35 trials; mean $\pm$ s.t.d), and during recording the animals displayed varying levels of behavioural performance. Prior to the switch from water to QHCl, animals licked with similar rates to both odours (Fig.4-5A left). Consistent with our behaviour only results, after the switch, most mice initially displayed poor behaviour ($d' < 2$) and improved as the session progressed (Fig.4-5A right). This allowed us to track GC activity across the switch from water to QHCl and track GC activity as animals learned new odour contingencies and shifted their behaviour to match these contingencies.

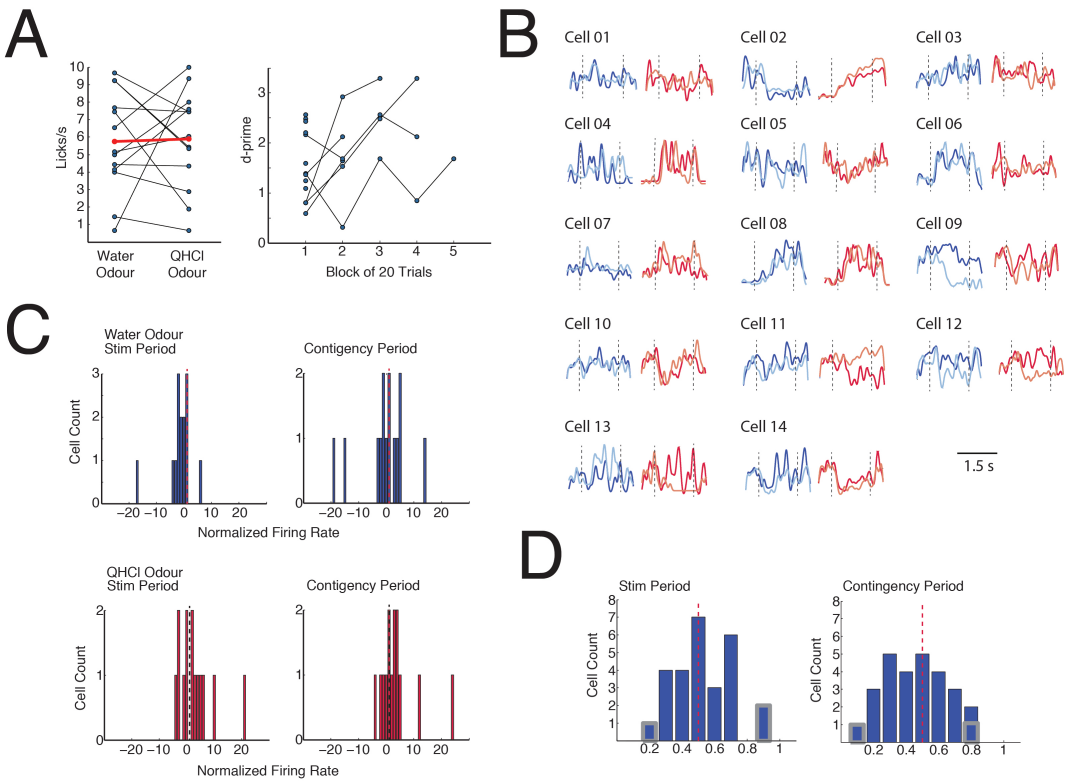

FIGURE 4.5: **GC responses shift when animals associate an odour with a new contingency.** (A) Behavioural performance of mice from which we recorded GCs. Prior to switching to the QHCl epoch, mice licked at an equal rate for both odours. Black dots are lick rates on individual sessions for either the water-paired odour or the eventual QHCl paired odour. Mean $\pm$ std water odour = 5.7 $\pm$ 2.9 and eventual QHCl odour = 5.9 $\pm$ 2.9. Right: Behavioural performance of mice during the epoch when one odour is paired with QHCl. Data are plotted as the d' in a block of 20 trials. For some mice, we were only able to obtain GC data for 20 or less trials. Each line is a single session from a mouse. n = 14 cells, 10 mice. (B) PSTHs for every cell we recorded. Blue lines show PSTH for the water-paired odour. Red lines show PSTHs for the QHCl paired odour. Dark lines display the PSTH prior to the QHCl switch while light lines display the PSTH after the switch during the block in which the animal reached its peak performance (highest d'). Dotted vertical lines display when the odour turned on and off. (C) Histogram of mean firing rate change. We compared the mean firing rate during the QHCl epoch during 10 consecutive trials during which the animal achieved its highest behavioural performance to the mean firing rate change for the same odour during the Phase 2 (water only) epoch. A value of zero indicates no change, negative values indicate a response decrease, and positive values indicate a response increase. Response changes for both odours are shown during both the odour stimulus period (1.5 s duration) and the reward period (2 s period following odour offset). Individual cells showed significant changes, but none of the populations showed significant differences from 0 (one sample t-test; water stim p = 0.2, water reward p = 0.3, QHCl stim p = 0.4, QHCl reward = 0.6). (B). For each cell, we determined the PSTH for an odour before the QHCl epoch and for the same odour during the 10 trials in which an animal reached peak performance during the QHCl epoch (performance computed over a block of 20 trials). Data were binned in 100 ms bins. We then correlated the two PSTHs. Red bars denote significant correlations (Pearson, $p < 0.05/14$).

We first examined how the responses of GCs changed from the water-only trials – a period of time we denote as the Phase 2 epoch – to the trials in which animals accurately discriminated among water paired and QHCl odours – a period of time we denote as the Phase 3 best period. This allowed us to examine how GC activity might be different when animals accurately associated an odour with two different contingencies (water or QHCl). In Figure 4-5B, we plot the mean odour evoked response for every cell during the epoch where both odours were paired with water (dark trace). We then overlay the mean response during the Phase 3 best period for each odour computed from the 10 trials where the animal performed the best (highest d' in a 20 trial block of water and QHCl paired odours, light trace). Many of the cells showed a divergence in responding following the switch to the QHCl epoch. Surprisingly, GCs showed divergence not only for the QHCl trials but also for the water trials suggesting GC activity does not explicitly track odour contingency.

To quantify this observed divergence, we normalized the mean Phase 3 best response by the mean Phase 2 response across either the 1.5 s odour stimulus period or the 2 s contingency period following the delivery of QHCl/water (see methods). The population of GCs we recorded did not show differences between the Phase 2 and Phase 3 best periods. For the water-paired odour, neither the histogram of the normalized response computed during the odour (mean $\pm$ s.t.d. response = -1.6 $\pm$ 5.0) nor the histogram of normalized responses computed during the contingency period differed significantly from 1 (Mann-Whitney U, p = 0.07, 0.5). Similarly the histograms for the QHCl odour did not differ from one (odour mean = -2.9 $\pm$ 6.4, p = 0.3; contingency mean = 3.7 $\pm$ 6.9, p = 0.2). However, many of the individual cells showed considerable changes. In particular, for some cells, GC responses to the odour tended to decrease in the Phase 3 best period while others showed increases (Fig.4-5C left and example Fig.4-5B Cell 8,9,11,12). To quantify this, we performed ROC analysis on the Phase 2 vs. Phase 3 best data. Many of the cells showed large AUC differences from 0.5, but out of 28 cell-odour pairs, only three of these pairs displayed significantly different mean responses during the odour period, and only two of these pairs showed significantly different mean responses during the contingency period.

As a control, we compared this Phase 2 and Phase 3 best data to data from mice that

received extended periods of water paired odours (no QHCl pairings during the session; n = 6 cells; 6 mice). This provided an appreciation for how much GC activity may naturally fluctuate as animals experience several presentations of the same odour. In the control group, we assigned the first five trials of an odour as the Phase 2 period (comparable to Phase 2 trials) and the last five-ten trials of an odour as the Phase 3 best period. We then computed the normalized firing rate for this control group and compared this data to the normalized firing rate data from the test group. Overall, we largely saw similar changes in the control group as we observed in the the test group (Fig.4-6A). The control group displayed an overall mean $\pm$ s.t.d response change of 1.9 ± 5.8 compared to 0.6 ± 6.1 across all cell odour pairs in the QHCl group. Only two of the cell-odour pairs in the QHCl group showed changes greater than that observed in the control group, and the distributions were not different from each other (Mann-Whitney U, $p = 0.7$). In the ROC analysis, none of individual control cells showed significant differences between the Phase 2 and the Phase 3 best period. Comparatively, five of the cell odour pairs in the trained group were significantly different between Phase 2 and Phase 3 best (Fig.4-5D).

This data suggests that, for most cells, GC firing rate does not change when animals learn a new odour contingency. Rather, if changes exist, only a subset of the GC population actually significantly changes. While we still need to collect more data, at present, only about 19 % of the cell odour pairs display response changes when animals learn to associate one odour with a new contingency. The observed changes do not always occur in response to the odour paired with QHCl, suggesting that GC activity reflects more than the learned association or the presence of QHCl. For example, GC activity may reflect a learning or attentive state in the animal that manifests when the animal must discriminate among odours.

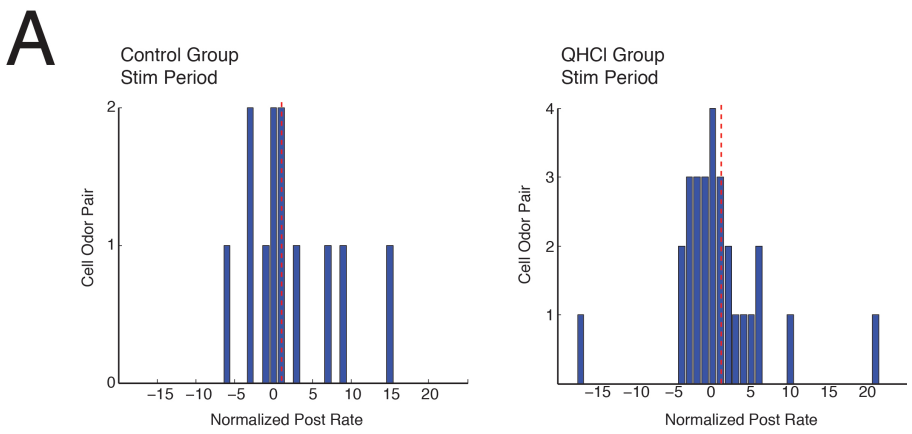

FIGURE 4.6: **Comparison of GC response shifts between control and QHCl trained group.** To determine whether any of the changes in GC activity we observed were meaningful, we compared mean GC activity responses in the group of animals that learned the odour association and a group of animals to which we repeatedly presented two different odours that were always paired with water. (A) Histograms of normalized firing rate for the control group (water only) and the learned association group (water and QHCl paired odours). Data less than one indicate a decrease in response during the Phase 3 period while data greater than one indicate an increase. For simplicity, only data during the odour stimulation period is shown, and data in each group are collapsed across both odours.

4.3.5 Granule Cell Activity Across Learning

In LFP recordings, changes in GC related oscillatory power often only arise when animals accurately perform discriminations (i.e. well trained animals) but MTs can show learning divergence even before animals show highly accurate performance (Beshel, Kopell, & Kay, 2007; Doucette & Restrepo, 2008). By extension, our observed changes in GCs may thus only arise when animals accurately discriminate among odours or could arise earlier to reflect an overall change in task demands. To examine this, we tracked the activity of individual GCs from the moment animals first experienced QHCl in a session to the end of the session (Fig.4-7A, Fig.4-8A example histograms).

State changes in granule cell activity

Interestingly, the first thing we noticed was that some of the GCs displayed profound changes in activity quickly after the switch from Phase 2 to Phase 3 (Fig.4-7A left). In this example, the mouse did not begin to accurately discriminate among the odours until 20-30 trials after the Phase 3 epoch began. However, the shift in GC activity emerged long before this. K-means clustering (not shown) and PCA analysis on the PSTHs further revealed that the odour evoked activity shifted dramatically from Phase 2 to Phase 3, long before the animal learned to accurately discriminate among the two different odours (Fig.4-7A,B). The baseline activity decreased and the odour response became more prominent at about four trials following the start of Phase 3 (Fig.4-7A, PCA coefficients). The animal, however, did not display highly accurate discrimination until later in the session (starts to improve between block 2 and 3; around 50 trials). While we have only thus far observed this sort of activity in one out of 14 cells (7 %), this one cell hints at the interesting possibility that GC responses change to reflect the overall demands of a task. The cells may exist in one state when odours are informative of reward and another state when the animal must discriminate between odours that are informative of both reward and punishment.

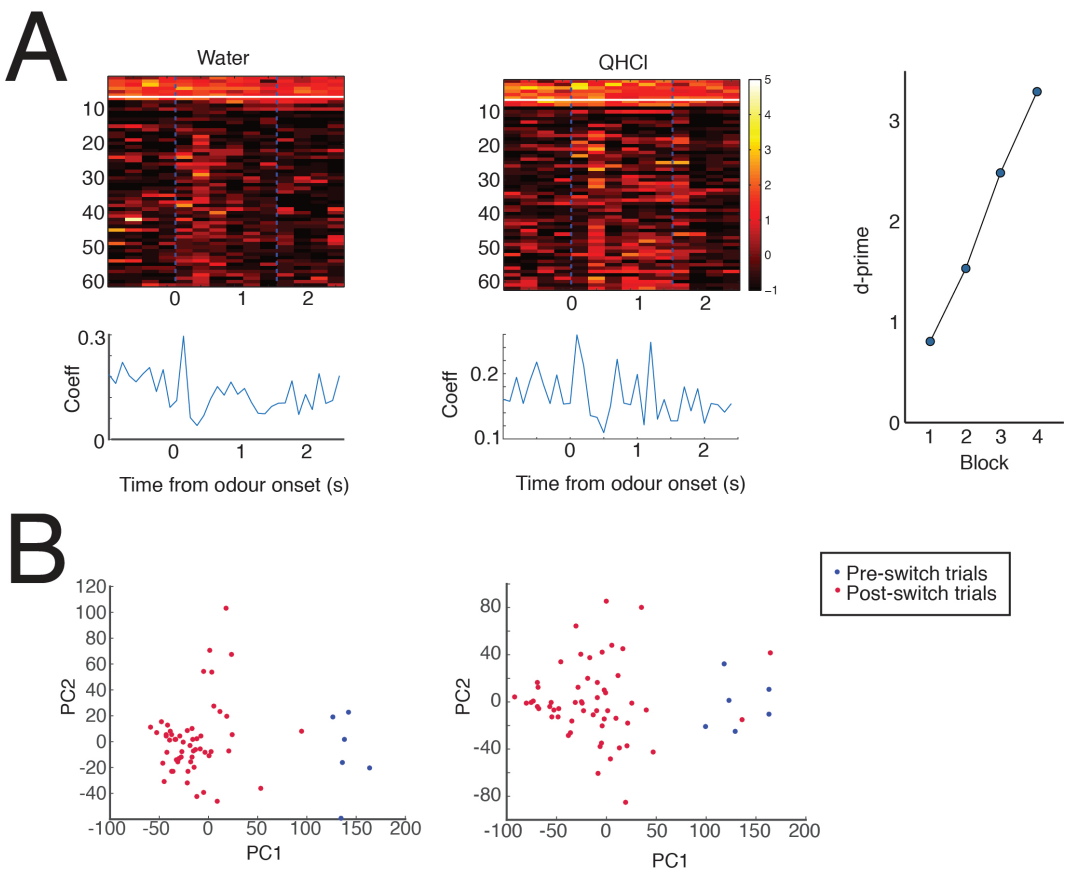

FIGURE 4.7: **State changes in GCs.** Large shifts in activity emerge before an animal performs well in the task. (A) GC response and behavioural data from one example cell that shows abrupt changes once animals begin Phase 3 of the session. On the left, trial histograms for both the water and QHCl odours. White line denotes the shift from Phase 2 to Phase 3. Blue dotted lines denote odour on and odour off. Below each histogram, the coefficient values for the first component derived with PCA (variance explained water odour = 33.8 %, QHCl odour = 34.0 %). On the right, behavioural performance of the same animal. d' computed for a block of 20 trials (10 water and 10 QHCl trials). (B) PCA plot for odour responses of neuron in (A). Each dot is a response on the trial of the odour. Data are colored according to session Phase (Phase 2 both odours paired with water (blue) or Phase 3 one odour paired with QHCl (red). Left plot shows data for the odour that was always water paired and Right plot shows data for the odour that was eventually QHCl paired.

Subsets of granule cells track behavioural performance

We further explored how GC activity evolved as animals improved or deteriorated in behavioural performance. In Fig.4-8A, we plot example trial z-score histograms for four cells: one cell that did not change across learning and three cells that significantly did. In many of the cells, changes in activity emerged gradually. To quantify whether these shifts tracked learning or simply fluctuated in time, we tracked the mean responses of GCs to odours across a sliding window of trials (10 trials, shifted by one trial each time) and compared these responses to d' values computed across the same time window (Examples Fig.4-8B). This gave us at least 4 trials of each odour (and no more than 6) over which to compute a mean response. Interestingly, many of these cells tracked behavioural performance. In some cases, performance and activity appeared positively correlated while in others they were negatively correlated. Consistent with our earlier analysis, these shifts generally meant that the cells became divergent from the Phase 2 activity as performance increased. In some sessions, the animal initially performed well on the task but then dropped in performance over time (Fig.4-8B 2nd and 5th example). GC activity shifts tracked this change (in one case it correlated and another it was anti-correlated), suggesting that GC activity does not just fluctuate in time but rather tracks task engagement/discrimination capacity over short time windows.

To quantify this behavioural performance correlation, we correlated the sliding d' values with the normalized responses for each odour (normalized to Phase 2 epoch) using a Spearman Rank correlation ($p<0.05/n$; n = 13 cells; Fig.4-8C). For GC responses to the QHCl odour, we saw both positive and negative correlations between d' and odour evoked activity (Fig.4-8B, Scatter plots in C). While the entire distribution of correlation coefficients (observed mean $\pm$ s.t.d. = -0.04 $\pm$ 0.41) was not significantly different from the overall shuffled data, several of the individual cells showed significant correlations between GC activity and behavioural performance (Fig.4-8C left). We also saw activity-performance correlations for the water paired odour (Fig.4-8B,C). Again, the distribution of correlation coefficients across the entire population ((mean $\pm$ s.t.d. = -0.09 $\pm$ 0.44) was not different from the shuffled data distribution; however, individual cells did show significant correlations. In particular, as

performance increased, the baseline subtracted activity of GCs tended to decrease or grow more negative in response to the water-paired odour.

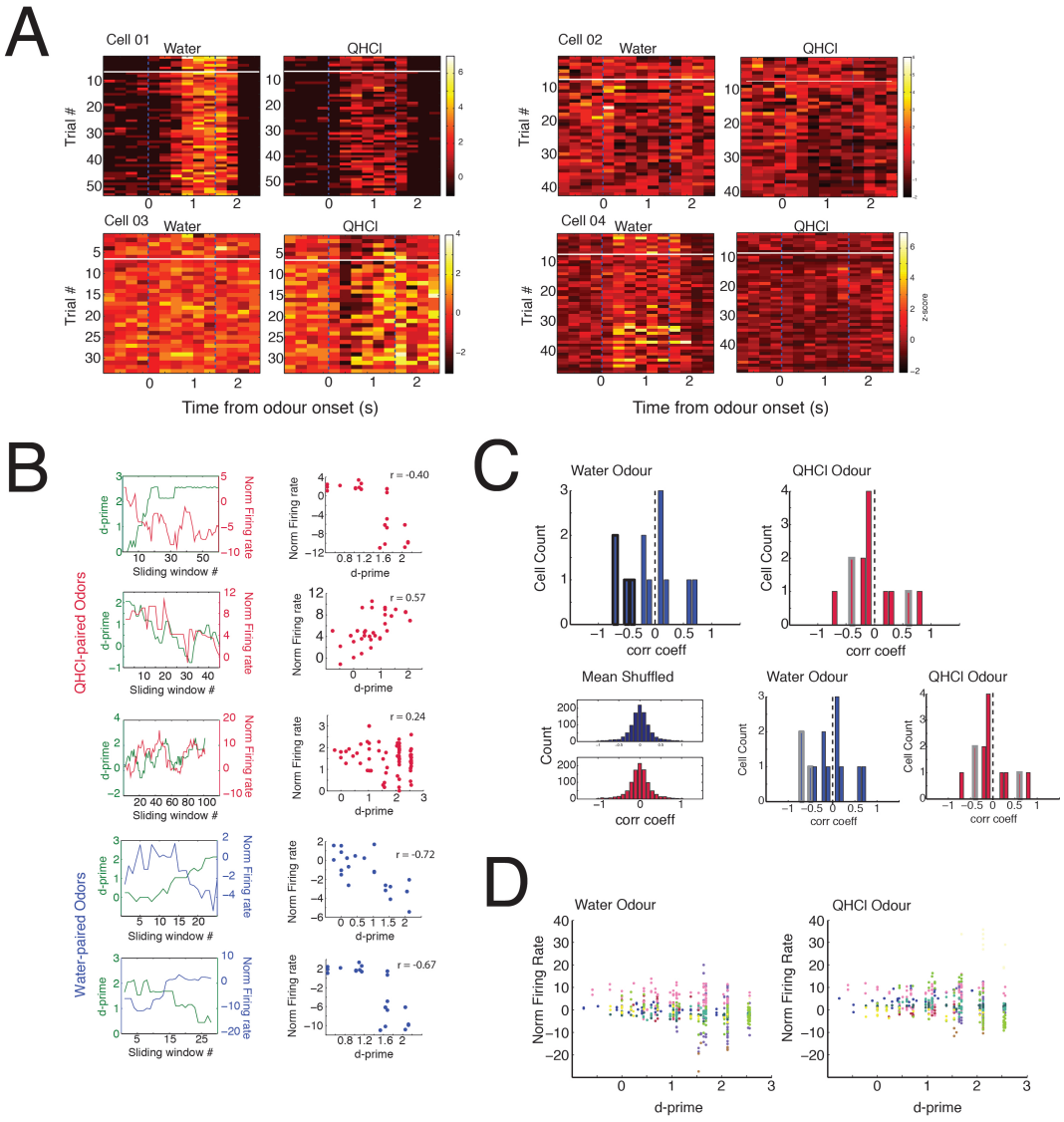

FIGURE 4.8: **GC responses track behavioural performance.** (A) Trial histograms of four different cells. White horizontal line indicates the switch from Phase 2 to Phase 3. Blue dotted lines indicate odour onset and odour offset. While the activity of many cells did not change across learning (top left), other cells showed dynamic activity. (B) Example data from five cell-odour pairs for the correlation of behavioural performance with normalized GC activity. Left: Sliding window d' data and normalized firing rate data plotted in time. Right: Scatter plot of d' data vs. normalized firing rate. Firing rate data was normalized to the Phase 2 period for each cell-odour pair (see methods). (C) Coefficients for correlations of d' activity vs. normalized firing rate activity. Top: Experimentally observed data. Darkened bars show significant correlations (Spearman Rank). Bottom: Shuffled data. For each cell, we shuffled the response data (1000 iterations). On the left, we show the mean histogram for shuffled data for all cells. We tested whether experimentally observed correlations fell within the lower or upper 2.5 % of the shuffled distribution. On left, we re-plot the observed correlation coefficients with darkened bars indicating significant correlations compared to shuffled data. Dotted line denotes correlation coefficient of zero. While individual cells showed differences from their respective shuffled data, the population of experimentally observed and the population of shuffled data were not significantly different for either the water or QHCl paired odours (KS test; H(1.14), p = 0.76; n = 13 cells). (D) Population scatter plot of d' vs. GC activity. We observed no trends in the population data for either the water or QHCl paired odours. Colors denote data for individual cell-odour pairs. n = 13 cells in 9 mice (26 cell-odour pairs).

Overall, we observed considerable heterogeneity in responses in time. Some responses were positively correlated with behaviour while others were negatively correlated. As a result, QHCl odour and water odour scatter plots of the population of GCs vs. d' revealed little correlation (Fig.4-8D). Furthermore, we could not predict the direction of the correlation based on the initial response (Phase 2 epoch response) of the cell to an odour. We saw performance modulation in 6 out of the 26 responses to odours (5 cells; Fig4-9A), and cells that were initially excited or suppressed by the odour displayed dynamic relationships with behavioural performance. Along with the state changes we observed in one cell (Fig.4-7), this indicates that individual GC activity may change to reflect task/trial demands or the attentional state of the animal. Further, at a circuit level, these changes interact in a complex manner to influence overall odour coding.

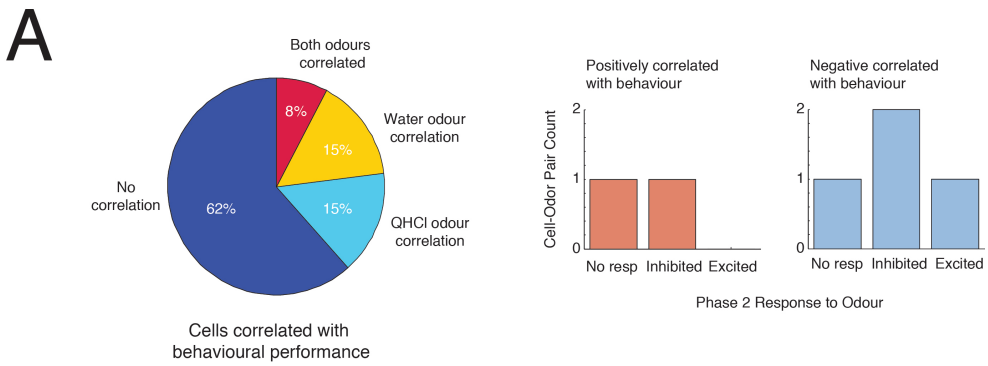

FIGURE 4.9: **Summary of GC performance correlations.** (A) Pie chart: Percentage of cells that showed response correlations with behavioural performance for at least one odour. n = 13 cells in 9 animals. Bar plots: The mean Phase 2 response of the odour (before shift to QHCl period in behaviour) does not predict the direction of the performance correlation.

4.3.6 Breath Rate Correlates with Behavioural Decision

One possibility is that GCs reflect behavioural dependent differences in the sampling behaviour of the mice. Mice sample their olfactory environment through sniffing and will modulate their breathing rates in accordance with expectation (Kepecs, Uchida, & Mainen, 2007; Zariwala et al., 2013). Considerable evidence suggests that patterns of MT activity and olfactory decisions correlate with breathing (Cury & Uchida, 2010; Smear et al., 2011; Shusterman et al., 2011). In our task, any changes we see in behaviour or neural activity could thus reflect changes in the breathing activity of the animal. We were thus interested if breath/sniff rates changed over the course of learning. To measure breathing, we implanted a cannula in the left nasal cavity of the mouse and placed a thermocouple in this cavity. Unfortunately, we were only able to record breathing in one animal while we simultaneously collected data from a GC (see Fig 4-11). We did, however, have breathing data from animals that performed the task in the absence of GC recording (n=3 mice, 5 sessions).

In Figure 4-10A, we plot example breath data for a single mouse in one behavioural session of the task (no GC recording). We noticed that breath rate was variable from trial to trial, and at times, increased during both the odour and/or the contingency period (1.5-3.5 s after odour offset, Fig.10-9A bottom). Consistent with previous reports in head-fixed animals, our mice did not show an appreciable amount of breathing in the sniff frequency range (6-9 Hz). Across all mice and all time points, the median instantaneous frequency of breathing was 2.5 breaths/s and ranged from 0.5 to 9.2 breaths/s (Fig.10-9B). Mice tended to breath at a median frequency of 2.8 breaths/s during the odour period while they breathed at a median frequency of 2.7 breaths/s during the contingency period (QHCl/water delivery + 2 s following odour offset).

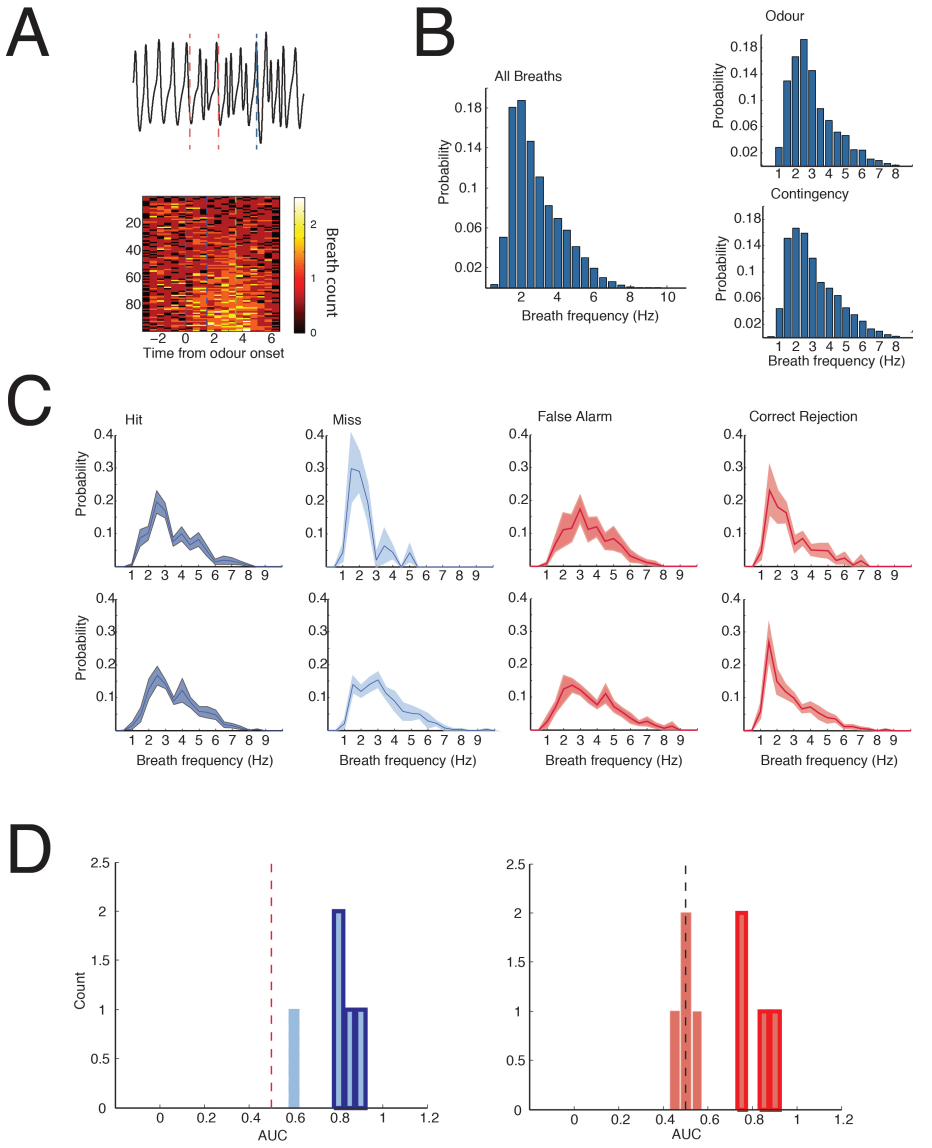

FIGURE 4.10: **Breath rate decreases on miss trials.** (A) Example breathing data from one mouse. Histogram is binned in 500 ms bins. We examined breathing across all trials and breathing split by behavioural decision (hit, miss, FA, CR). (B) Left. Histogram of all instantaneous breath rates across all sessions (median = 2.8 breaths/s). Data are binned in 0.5 breaths/s time bins. Right: Instantaneous breath rates for all mice across all session during only the odour period (top, median = 3.1 breaths/s) or contingency period (bottom, median = 3.1 breaths/s). The odour period is 1.5 s long while the contingency period is 2 s long and follows odour offset. (B) Breath data split by trial type for all mice. Top row = data during the odour period. Bottom row = data during the reward period. Data are plotted as the mean probability $\pm$ s.e.m (n = 8 sessions, 5 mice) (C) Area under the curve analysis for each session and each odour. Left: ROC comparison of hits and misses. Right: ROC comparison of false alarms and correct rejections. Highlighted bars denote those sessions for which the comparisons were significantly different (Mann-Whitney U, $p < [0.05/8]$.

While this crude measure of breathing gives an overall picture of animals' breath profiles, it fails to take into account the fact that not all trials are the same. Rather, some trials are informative for reward while others are informative for punishment. We split the breathing data for hits, misses, FAs, and CRs (Fig.4-10A,C). On hit, CR and FA trials, animals breathed faster during the odour period compared to miss trials (mean $\pm$ s.e.m breaths/s hit = 3.5 $\pm$ 1.0, miss = 2.5 $\pm$ 0.7, FA = 3.6 $\pm$ 1.1, CR = 2.8 $\pm$ 1.0). Similar results were obtained during the reward period (mean $\pm$ s.e.m breath/s hit = 3.5 $\pm$ 0.7, miss = 3.2 $\pm$ 0.5, FA = 3.7 $\pm$ 0.8, CR = 2.7 $\pm$ 0.6). Kruskal-Wallis testing revealed a significant difference among groups during the odour presentation ($p = 0.01$) while subsequent post-hoc analysis (Bonferroni method) revealed that, on miss trials, mice breathed at a significantly lower frequency than on hit and false alarm trials. ROC analysis of the two different odours revealed that, for most mice, breathing frequency was greater on hit trials than on miss trials (Fig.4-10D). Comparatively, only half of the mice showed increased breathing during the FA trials compared to the correct rejection trials (Fig.4-10D right). In principle, fewer sniffs may lead to a failure to recognize that an odour is present and thus may contribute to the lower frequency trend on miss trials during the odour. As performance improves in a task, animals commit fewer misses and thus may overall breathe faster. At least for the water paired odour, the correlation between behavioural performance and GC activity shifts could reflect this overall change in breathing.

4.3.7 Breathing and Behavioural Performance: Data from One Granule Cell

We had breathing data for one session in which we were able to record a GC and the animal performed the behavioural task (Fig.4-11). Unfortunately, we lost the recording quite early such that the mouse only performed 46 trials during which we were able to assess GC activity. In general, both odours initially suppressed spiking during some period of the odour on time, and this response gradually changed over the course of the session (Fig.4-11A Middle histograms). The cell showed significant anticorrelation between GC activity and behavioural performance on the water paired odour (correlation coefficient = -0.72, Spearman

rank correlation p = 0.00004) but no significant correlation on the QHCl paired odour (correlation coefficient = -0.11, p = 0.58; Fig.4-10A).

Across 34 trials, this mouse failed to commit any misses. Instead, we examined breathing on hits, FAs, and CRs. Across time, breathing rates tended to fluctuate slightly, but generally increased following odour onset and decreased thereafter (Fig.4-11B). Consistent with our behaviour only analysis, we found that the mean baseline subtracted breath rate on hit trials (mean $\pm$ s.t.d = -0.7 $\pm$ 1.0 breaths/s; median = -0.7 breath/s) was similar to that on FA trials (-0.8 $\pm$ 1.6 breaths/s; median = -1.4) and CR trials (-0.6 $\pm$ 1.5; median = -0.5) although the FA breath rate tended to be more variable (Fig.4-11B). Subsequent statistical comparison (Kruskal-Wallis) revealed no differences among the three trials (H(2,20) = 0.35, p = 0.84).

This analysis does not take into account that, even across hit trials alone (or FA/CR), the animal may change its breathing pattern over time. Because we only saw a significant correlation between GC activity shifts and the water (hit) odour, we next examined how breath-rate changed over the trial and compared this to the sliding window d' data (Fig.4-11C). The two were highly anti-correlated (Spearman rank correlation: rho = -0.64, p = 0.00064). This suggests that the shift we see in GC activity, at least in this cell, could be due to small changes in breathing. When we examined whether mean spike rate within each breath changed on every hit trial and whether this correlated with breath rate, we saw no correlation (Fig.4-10C left; Spearman Rank correlation, rho = -0.03, p = 0.9). This suggests that the activity shifts we see in GCs cannot be accounted for by spike changes within a breath. Rather because the animal breathes less, the cell likely spikes less across the entire odour period due to decreased input.

We conclude that, at least for this particular GC, breathing rate changes can influence GC spike activity. Overtime, the animal decreased its breath rate for the water paired odour and GC activity became even more suppressed by the odour. While we still need to collect more data to buttress or refute our result, we next postulated whether such a relationship might exist for all of the cells we observed.

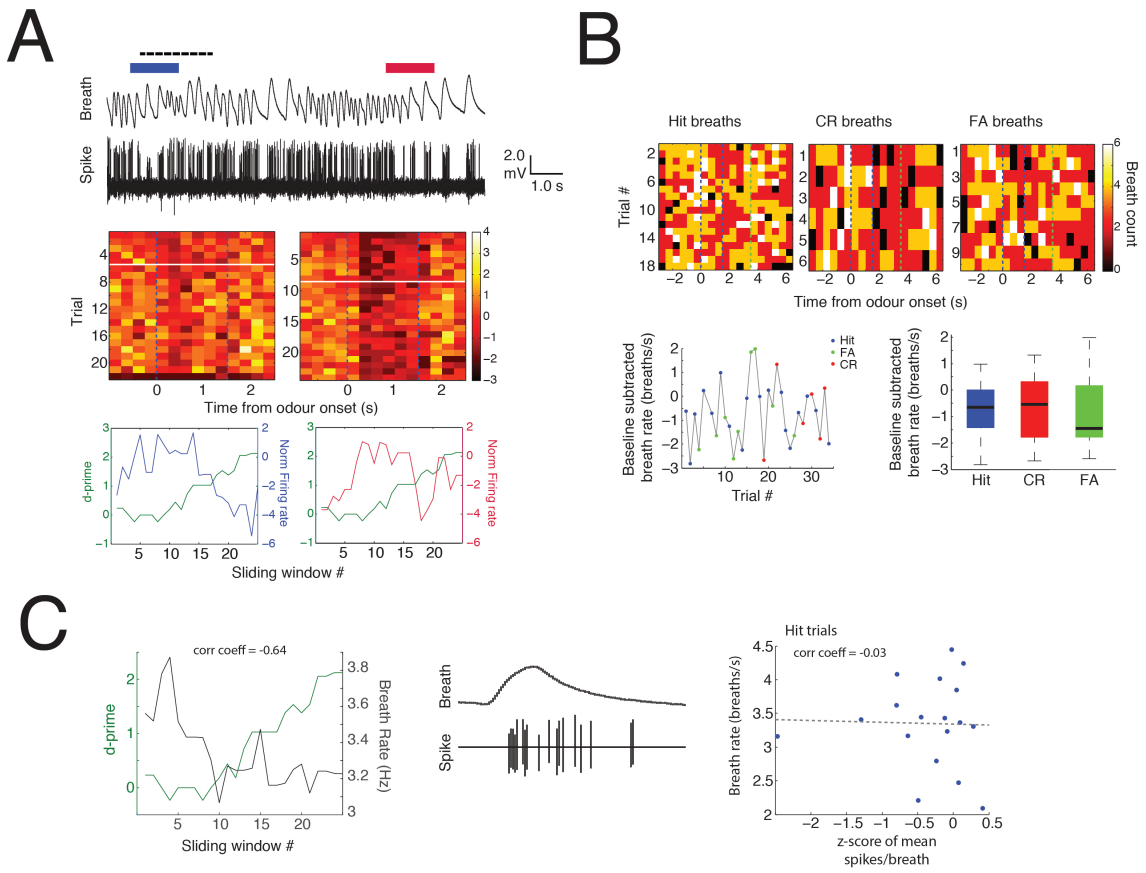

FIGURE 4.11: **Breathing and GC activity in one cell.** We recorded breathing and GC activity across learning in one cell. (A) Top: Raw breathing and spike trace for this cell. The colored bars denote the odour period (blue = water paired odour; red = QHCl paired odour). The dotted line denotes the licking period. Middle: Trial PSTHs for this cell. Water paired odour on left and QHCl paired odour on right. Blue lines denote odour on and off times. White line displays the shift from Phase 2 to Phase 3 in the session. (B) Top: Breath count PSTHs for each decision type. The animal did not commit any misses. PSTHs are binned in 0.5 s bins. Bottom: Baseline subtracted breath rates across the entire session. Boxplot medians: hit = -0.66, CR = -0.52, FA = -1.47. Medians were not significantly different (one-way ANOVA, $F(3,20) = 0.03$; $p = 0.97$). (C) Left: For the water paired odour, breath rate during the odour trial negatively correlates with behavioural performance. While the change in breathing is not large (around one less breath from beginning of session to end), the breath change did track the GC firing rate for the water odour in (A). Right: Spikes within a breath. We computed the mean firing rate of GCs within each breath during the odour period. Scatter plot: The number of spikes within each breath did not change if the animal breathed faster during the odour period or slower. Spearman rank: $p = 0.9$.

4.3.8 Granule Cell Activity Does not Correlate with Behavioural Decision

Because we lacked breathing data from most mice, we instead looked at how GC responses varied depending on the decisions of the animal. This allowed use to examine how behavioural decisions influence GC activity, and because breath rate changed with behavioural decision (Fig.4-9), we could postulate about how breathing may influence GC activity. Across all sessions, we had 276 hit trials, 66 miss trials, 227 CR trials, and 91 FA trials from which to examine GC activity in accordance with behavioural choice. Mice tended to commit more hits and CRs than FAs and misses, consistent with improvements in behavioural performance over time (Fig.4-12B). Furthermore, while mice tended to perform several hit and CR trials in a row, they often performed for long epochs without a miss or FA trial (Fig.4-12B left). On three out of 13 of the sessions, mice failed to commit any misses, and thus, for these sessions, we could not examine how activity differed between miss and hit trials.

To examine how GC activity may differ depending on the behaviour choice of the animal, we computed a mean z-score response during the odour period (computed across the entire 2 s odour period) or during the reward period (2 s following reward/punishment delivery) across the entire session. We computed these values separately for each different behavioural choice type. We then compared the z-score data for hit trials to miss trials as well as the z-score data for CR trials to FA trials. Analysis with a one-way ANOVA revealed no difference among groups ($F(7,82) = 0.55$, $p = 0.80$). We did not see large differences between activity on hits (z-score mean $\pm$ s.t.d = 0.03 ± 0.44 and misses 0.13 ± 0.45) or between activity on FAs (-0.06 ± 0.35) and CRs (0.11 ± 0.48) (Fig.4-12C). This was true when we computed responses during the odour period (Fig.4-12C top) and during the contingency period (Fig.4-12C bottom).

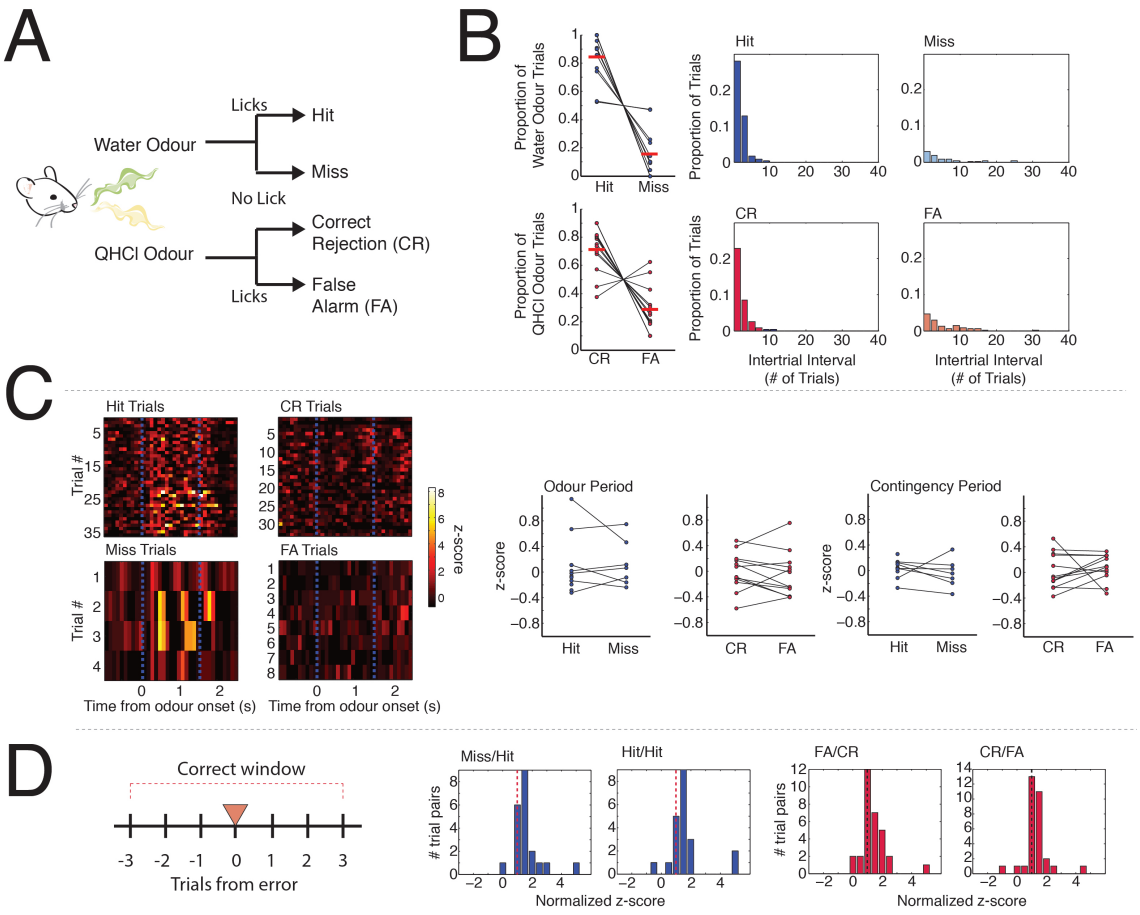

FIGURE 4.12: **GC activity does not vary with trial decision.** (A) We split up GC responses according to the animal's decision on each trial. Each trial could fall into one of four categories depending on the odour presented and the animal's subsequent choice to lick or not lick. (B) Histogram of activity for a single cell. Data are split according to the animal's choice. Animals tend towards correct choices (i.e. Hits or CRs). On the left, proportion of the trials that fall into each category. Data are split according to water paired odour trials or QHCl paired odour trials, and each black dot-line pair is one session (n = 13 sessions, 9 mice for all but miss trials; mice in 4 sessions did not commit a miss). Red bars denote the mean (Hit = 0.84 $\pm$ 0.16; Miss = 0.16 $\pm$ 0.16; CR = 0.71 $\pm$ 0.16; FA = 0.29 $\pm$ 0.16). Right: Number of trials between each consecutive choice type. Data are shown as a proportion of all 608 trials observed across 13 session. Mean inter-trial interval $\pm$ s.t.d: Hit = 2.3 $\pm$ 1.3, Miss = 6.7 $\pm$ 10.1, CR = 2.6 $\pm$ 1.8 , FA = 6.1 $\pm$ 6.6). (C) Example Z-score PSTH for the responses of one GC. 100 ms time bins. Blue lines = odour on and odour off. Left: Dot plots of Mean z-score response for each session. Plots depict the responses computed during the odour window and bottom plots depict the responses computed during the reward/punishment period. With the exception of one cell, responses tended to be similar regardless of the animal's choice. (D) Similarity of error trials to the preceding correct trial. We found error trials flanked (no more than trials away) by correct trials for the same odour. Histograms z-scores of error trials normalized by z-score on the preceding correct trial or z-scores of the correct trial normalized by the preceding correct trial. Error normalized histograms (either miss or FA) did not differ from the corresponding correct normalized histograms (paired t-test between Miss and hit, p = 0.92; paired t-test between FA and CR, p = 0.39). Dotted line represents no change.

In Figure 4-8, we demonstrated that GC activity correlated with behavioural performance on a sub-session time-scale. As such, computing the mean z-score for each trial type may hide finer structure. To examine this, we asked how similar single error trials were to the correct trials around it. We looked for error deserts: one or two error trials (either miss or FAs) flanked by correct trials (hits for miss errors or CRs for FA errors). To minimize the influence of time on activity, we only examined error deserts that had correct trials that were three or less trials away from the error (Fig.4-12D). We computed the mean response z-score for single trials and then normalized this value on single error trials to the single correct trial preceding it. Most of the miss/FA trials showed no difference from the hit/CR trials preceding them (Fig.4-12D). Similarly, the distributions of normalized error trials did not differ from distributions computed from comparisons of two correct trials.

Overall, this analysis indicates that the GCs do not track the behavioural decision of the animal on each trial. Rather, their activity may change over time to support learning and discrimination, but ultimately, the choice of the animal on a trial-to-trial basis cannot be read out from GC rate activity. Further, while not conclusive, the changes in breathing (and by extension odour sampling) during miss trials cannot explain all of the shifts in GC activity we observe. Taken together, all of this breathing data suggests that some, but not all, GC changes in activity correlate with behavioural performance. Plausibly, both breathing and GC activity may reflect a more basal variable — like attention or motivation. As a result, the two sometimes correlate while at other times they do not contingent on how attentional variables modulate GC activity.

4.4 Discussion

In the work described above, we trained mice to perform a flexible go/no-go association task in order to examine how GC activity changes across learning. After a brief period of training, mice could quickly discriminate (< 40-60 trials) between rewarded and punished odours, even when these odours were novel. We then tracked GC activity as animals learned to associate a previously rewarding odour with a punishing stimulus and noticed that GC

activity tended to diverge from pre-punishment levels when the animals accurately discriminated among odours. Our results from GC recordings suggest that, at least in a subset of GCs, the firing patterns of individual MOB inhibitory neurons can signal both whether an odour is rewarded or punished and whether an animal is in a rewarded phase of a task or a reward/punishment phase of a task. These shifts in firing may help to alter odour processing in the MOB such that animals can better recognize punishing odours and discriminate them from those that are rewarding.

4.4.1 State-dependent Changes in GC Activity

Consistent with our data from passive animals in Chapter 3, GCs displayed broad odour tuning in our trained animals. In our paradigm, we trained animals on the overall structure of the discrimination task before we attempted any GC recordings. This pre-exposure to QHCl did not significantly alter the responses of GCs as odour tuning between GCs in trained animals and those not exposed to QHCl did not differ. From this, we suggest that our animals were, indeed, not "over-trained" on our task. GCs were not tuned to expect punishment and any changes we saw were indeed due to learning within a session. Interestingly, compared to the odour responses were recorded in Chapter 3, the responses we observed in trained animals were noticeably larger (sometimes 40 spikes/s > baseline compared to 10 in the passive data set). This difference may reflect an overall difference in the genetic background of the animals (CD-1s vs. C57Bl/6s). However, subsequent tests we have run with both trained C57Bl/6 and trained Black Swiss mice agree with the data we see in CD-1s. One interesting possibility is that GC activity, instead, reflects the state of the animal. In our case, trained animals are water deprived and have learned to generally associate odours with water. By comparison, animals that passively experience odour lack this association or the motivation to work for water. In flies and mice, hunger state can profoundly influence olfactory processing at early stages of the olfactory circuit (Ko et al., 2015; Root et al., 2011; Soria-Gómez et al., 2014). Water deprivation might have a similar effect on olfactory neurons such that MOB neurons respond differently to odours, particularly when they are informative for water. In

support of this state hypothesis, we also saw profound state changes in a subset of GCs (1/14 cells) when the behavioural demands of the task changed within a session (Fig.4-7).

4.4.2 Discrimination Shifts GC Responses

Several lines of evidence from our study suggest that GCs do not track a learned contingency per se but rather the behavioural performance and possibly the engagement of an animal in a task. First, we did not see differences in GCs, on a trial to trial basis, when the animal made a correct vs. incorrect decision for the same odour. Hit trials and miss trials did not differ from each other when they were examined in a close window of time. Simiarly, FA and miss trials did not differ. Second, while we did see shifts in GC activity when an animal had formed an association of an odour with QHCl, we often saw a corresponding change in the water-paired odour. Instead, GC activity correlated with overall behavioural performance of a mouse across a session. When the animal performed better in a given time period (10 trials), GC activity diverged compared to the period of time when the animal had not associated an odour with QHCl (Phase 2 epoch) and diverged compared to the periods of time when the animal did not accurately discriminate among the water and QHCl paired odours.

Previous work in MTs suggest that at least some MTs show an acute dependence on odour contingency. Both MTs and cells in PC show stimulus value related activity (Doucette & Restrepo, 2008; Doucette et al., 2011; Gire et al., 2013; Kay & Laurent, 1999). In particular, MTs show both divergent responses in single neuron firing and temporal synchrony as animals learn to associate odours with reward or punishment. Similarly, APC neurons show enhanced responses to odours associated with reward vs. those unassociated with odours. Unlike these results, we observed a more complex pattern in GCs. GC activity did not track the learned contingency as we saw performance-related response shifts to both QHCl and water-paired odours when animals discriminated between them. How then, do we rectify the results in MTs with our results observed here? One possibility is that we have simply not sampled enough GCs to observe those cells that might drive odour contingency changes in MTs. Indeed, with this small data-set, it is too preliminary to make any sweeping conclusions. Another possibility is that heterogeneous shifts at the single cell level coordinate in a

structured manner at the GC population level. Future GCaMP imaging experiments should shed light on this possibility; our data suggest that these imaging experiments will prove fruitful as, with GCaMP, one will be able to detect the considerable performance related changes in GC spike rates like those we report here.

Thus far, we have not performed permanent or reversible lesions of the GCL in this task. Previous lesion experiments in tasks similar to ours suggested that GCs play a minimal role in simple odour discrimination (Gschwend et al., 2015; Abraham et al., 2010). This data contrasted with that collected from cfos and LFP studies which, in some cases, implicated GC activity in the discrimination of both perceptually different and similar odours. In our data set, we only saw changes in a small subset of GCs (at most 18-30 % depending on the metric examined). The lesion studies often only affected a small subset of the GC population (also on the order of 30 %). This leaves open the possibility that the lesions failed to influence the GCs required for discriminating between odors in these tasks. In our task, we also demanded that animals learn to discriminate between novel odours for which they did not, prior to our recording, know the contingency. Previous groups have especially implicated GC activity in the difficult discriminations (Nunes & Kuner, 2015). The novel odour component of our task may add a level of difficulty to the more simple go/no-go task, and thus may have aided our ability to observe shifts in GC activity.

Taken together, these results suggest GC activity may reflect an animal's behavioural performance and possibly its engagement in a discrimination task. In the future to further test this hypothesis, we could record from single GCs in an animal and vary the ability for animal to engage in the task (for example by removing the water port) within the session. True tests of GC influence on or reflection of attention will require a different task.

4.4.3 Do Sampling Differences Explain Our Results?

One major caveat of this work is that we do not have breathing information for all of the cells we recorded, particularly not those cells that showed divergence in GC activity contingent

on the choice of the animal. In our task, mice modulated their breathing patterns depending on their behavioural choice and often decreased their breathing during miss trials and CRs. Conceivably, then, breathing could produce the divergence in GC activity we see as behavioural performance is explicitly defined by the proportion of correct and incorrect decisions. In our one example (Fig.4-12), GC activity changes appeared to track breathing such that we could plausibly explain the activity through sampling related decreases in input to the GC.

However, we do not think cells will simply follow breath-sampling rate nor do we think that less odour input (as a result of decreased breathing) can explain all of the shifts in our activity. Interestingly, for the one cell odour in which we simultaneously recorded breathing and GC activity, odour evoked an inhibitory response in this cell. This response became even more suppressed when breathing decreased. This suggests that the mechanism at play is not simply a breath-sampling rate related decrease in the odour activity of the MT contacting this GC. Rather, the GC may be actively suppressed in accordance with breathing changes or the suppression may manifest through multi-synaptic action. Similarly, while, for all other cells, we failed to simultaneously record GC activity and breathing, the correlation patterns we see suggest that decreased input due to breath-sampling differences will not explain all shifts in GC activity. Some cells showed positive correlations between d' and GC activity. If these animals, like the example animal, similarly decreased their breath rate as performance increased, decreased sampling (and thus odour input to the bulb) will not explain the correlation. Furthermore, the divergent GC activity remains even when animals perform trials incorrectly even though breathing can vary from correct to incorrect trials.

Perspective

The data included in this Chapter, while preliminary, indicate the exciting possibility that interneurons in the MOB track the behavioural performance of an animal. GC neurons can have a profound influence on MT processing and the neural circuits that assist in the accurate identification of odours. The shifts in GCs activity, then, may work to improve this

identification when odours become particularly meaningful, such as when one odour signals punishment and when animals must meet variable task demands.

Chapter 5

Conclusions and Perspectives

With this work, I endeavoured to explore how contextual variables like state and learning alter firing patterns in olfactory GCs. Granule cells have long been proposed to act as modulators of MOB circuits, updating MT firing patterns in accordance with the context in which odours are experienced. However, all previous studies of GC activity had been conducted either *in vitro* or in anesthetized animals. As a result, we lacked an understanding of the GC activity dynamics. We, instead, chose to record from GCs in awake animals and developed methods to do so. Our results provide unprecedented insight into the activity of a crucial population of inhibitory neurons in the MOB and, in particular, add several key results to our understanding of GC activity *in vivo*:

- Using patch clamp and head-fixed techniques, we reliably recorded from GCs in awake animals. This allowed us to probe GCs, for the first time, in behaviourally relevant contexts. Our method provides as a straight forward way to record GCs on a ms time scale, and moving forward, other groups could easily employ this technique to further explore the dynamics of GC activity in awake mice (Chapter 2).
- Contrary to previous *in vivo*, anesthetized reports, GCs display considerable spike activity and broader odour tuning in awake animals. Unlike the behaviour observed in MTs in awake animals, GCs show little coupling to the breath rhythm indicating breath related activity may not be important for coding of passive odour experience in these cells (Chapter 3).

- Granule cells show enhanced responsiveness in animals trained in a discrimination task vs. those that are not. Furthermore, GCs appear to track the discrimination performance of a mouse. This suggests that as an animal discriminates between two odours, GC activity sculpts MOB output to support accurate identification of different odours (Chapter 4).

5.1 What All of This Means for the Olfactory System

Overall, these results support the idea that the olfactory system, even at early stages, is a flexible processor. Consistent with other reports concerning the excitatory cells of the MOB (Doucette & Restrepo, 2008; Doucette et al., 2011; Fletcher, 2012; Kato et al., 2012; Kay & Laurent, 1999), responses of MOB cells to odours are plastic and can reflect the current state of the animal as well as learned associations. This may assist an animal in the recognition of stimulu such that the animal can quickly and accurately make decisions based on its current environment.

5.1.1 The Influence of State on Olfactory Granule Cells

In Chapter 3, we demonstated for the first time that individual GCs in awake animals display profound differences in activity compared to GCs in anesthetized animals. Along with comparisons of MTs in anesthetized and awake mice (Doucette & Restrepo, 2008; Kato et al., 2012; Kay & Laurent, 1999), these results support the idea that the state of an animal can significantly influence MOB processing of odours.

We hypothesized that GCs in awake animals would display more dynamic responses to odours. In agreement with our hypothesis, GCs in awake animals showed much broader odour tuning than that observed in the anesthetized animals. This enhancement of inhibition could explain the overall sparser tuning of MTs in awake animals. In the future, manipulations of GC activity – for example brief suppression of GC activity with light activated opsins – accompanied by recordings from MTs could aid in exploration of this possibility. The enhancement of GC activity also suggests that GCs, during wakefulness, may receive enhanced

excitatory signals and/or suppressed inhibitory signals from centrifugal feedback fibres. For example, both cholinergic and noradrenergic nuclei show enhanced and more dynamic activity in awake animals (Watson, Baghdoyan, & Lydic, 2010). Suppression of the feedback fibres along with simultaneously recording from GCs should shed light on whether and how this feedback activity influences GC odour tuning in awake animals.

Interestingly, we did not see significant phase coupling of GCs with the breathing rhythm. This is consistent with recent reports exploring the generation of theta rhythms in the MOB. Fukunaga and colleagues (2014) reported no change in theta coupling of MTs following suppression of GC activity. They found that theta rhythms in the bulb were largely dictated by local glomerular interactions. Instead, GC activity influences faster rhythms in the MOB including those in the beta and gamma frequency range. The low phase coupling of GCs indicates two possibilities concerning GC inputs: (1) GC activity does not merely follow the activity of distinct MTs that fire during specific phases of the breathing rhythm. Instead, GCs may receive inputs from multiple MTs that fire at different periods during a breath, leading to the distributed phase firing of GCs. (2) GC activity may be influenced by top-down activity that fires independently of the breathing rhythm and thus leads to the distributed activity we observed in GCs.

Why might state dependent differences in processing be important? At a basic level, the differences may reflect the need to balance the animal's needs in its current environment with metabolic costs of neuronal activity. For example, while we did not explicitly examine the activity of mice while they were asleep, one could predict that GC activity decreases overall during sleep as, at this time, odour identification and discrimination is not performed or particularly needed. The differences we see across anesthesia and wakefulness may similarly reflect metabolic demands.

State-dependent flexibility in odour responses could also alter the animal's recognition of an odour and/or the meaning the animal ascribes to it. For example, in flies, odour responses in the AL are dynamic depending on the fed state of the animal. Food odours that usually elicit aversive responses fail to do so in starved flies, possibly helping to expand the animal's representation of what it would be willing to eat in desperate times (Ko et al., 2015;

Root et al., 2011). In Chapter 3, we showed that GC activity can similarly change across states and that odour tuning dramatically changes across these states. The broadness of GC tuning could have profound effects on the MT circuit, effectively acting to sparsen MT activity. This sparse activity may, in turn, aid odour recognition as MT patterns for different odours are rendered less overlapping. Further, the increased dynamics of GC activity in awake animals provide a rich substrate for further changes such as those induced by learning.

5.1.2 Learning and Discrimination Updates of Granule Cell Activity

For the first time, we presented direct evidence that the activity of single GCs changes in real-time as animals learn to associate odours with punishing stimuli and discriminate between odours with different meanings. Previous IEG and GC suppression studies suggested GCs might display such activity, but until now, we did not have a picture of how those changes might manifest. While we still need to confirm these results with more data, these preliminary results suggests interesting possibilities concerning the role GCs play in learning and in assisting animals in meeting task demands.

We observed that, in a subset of GCs, neuronal activity tracked an animal's behavioural performance. This tracking was not observed in control animals, and at least for some cells, could not be explained by breathing alone (although this result is not conclusive). Instead, GCs reflected how well an animal discriminated between odours on a minute to minute basis within a session. One hypothesis is that this activity in GCs corresponds with the overall motivational or attentional state of the animal. Shifts in GC activity that correlate with behavioural performance may thus reflect task engagement. Similar results have been observed in other sensory processing, including visual cortex and auditory cortex where the activity of pyramidal neurons fluctuates depending on whether an animal engages in a discrimination task or passively experiences stimuli (Poort et al., 2015; Otazu et al., 2009). However, to my knowledge, this is the first demonstration of this sort of activity in interneurons located in a early sensory processing centre.

Interestingly, neuromodulatory activity also shifts with task engagement and contextual processing (Picciotto, Higley, & Mineur, 2012; Sara, 2009). In particular, acetylcholine has been implicated in shifting activity in cortical neurons in order to assist animals in meeting task demands (Kuchibhotla et al., 2016). The MOB receives dense feedback from cholinergic centres, many of which target GCs. Furthermore, blockade of cholinergic signaling in the MOB can disrupt olfactory discrimination learning (Devore, Almeida, & Linster, 2014). If, upon further data collection, our result in GCs persists, it will be interesting to explore how acetylcholine release in the bulb influences this activity.

In at least one of our cells, we found that GC activity correlated with both behavioural performance and breathing. In the future, it will not only be important to explore in more detail how GCs reflect breathing in discrimination tasks but it will also be important to explore other temporal aspects of single GCs across learning. For example, GC activity is heavily implicated in the generation of fast rhythms in the MOB. These rhythms often arise or increase in power when animals engage in discrimination tasks (Kay et al., 2009). For the first time, using the methods I have described, the simultaneous collection of spike data from individual GCs and LFP activity in the MOB is possible. Doing so may reveal additional learning related structure in GCs. It will also be important to collect population data from GCs using larger scale imaging methods. While these methods cannot currently provide us with information concerning possible temporal coding of learned information, they can provide us with information about how several GC neurons may change in concert to support learning. In our own data, we saw behavioural performance related spike rate changes in GCs. Imaging could prove powerful in observing these rate changes over a wider spatial area.

5.2 Where Should We Go Next?

The results reported in this thesis shed significant insight on the activity of GCs in awake mice. However, as with most scientific studies, these results by no means leave us with a complete picture of the context-dependent activity of GCs or how these changes in activity

may arise. For my work, I indiscriminately recorded from GCs — I did not not restrict the recordings to specific depths of the MOB or to specific genetic subsets. However, there are over 5 million GCs in the mouse MOB, and these GCs span a region of several mm^3. Previous studies that examined the wiring patterns of GCs suggest that each GC may not be exactly alike in function (Woolf, Shepherd, & Greer, 1991b; Woolf, Shepherd, & Greer, 1991a). In our own studies, we observed considerable heterogeneity with respect to GC activity in response to odours. For example, in Chapter 4, we observed that some cells changed their activity over the course of learning while others remained constant. Furthermore, the direction of change was not consistent. This heterogeneity likely reflects a combination of different inputs, different outputs, and different gene expression profiles. Future studies that explore these sources of heterogeneity in conjunction with recordings from GCs should shed light not only on why GCs show differential responses but how the MOB itself represents odour stimuli. As outlined below, several advances in connectivity tracing could support this effort.

5.2.1 Mapping Inputs and Outputs to Granule Cells

GC connectivity could be mapped both anatomically with the use of anatomical tracers and functionally through manipulations/observations of known inputs. Already, several groups have examined GC inputs to MTs using viral-based tracers like retrograde pseudorabies and trans-synaptic rabies tracers (Miyamichi et al., 2013; Willhite et al., 2006). These studies revealed preferred targeting of GCs to distinct areas of the MCL. However, they lacked any correlation between this mapping and the odour evoked activity of GCs.

In principle, the methods I described in this thesis could be combined with these viral tracers to reveal meaningful structure/function relationships. For example, instead of filling GCs with NB, we could instead electroporate GCs with a plasmid or virus. Expression of a fluorescent protein from these constructs could improve the stability and longevity of markers for cell identification and improve the expression of markers throughout the GC dendritic tree. We could record the activity of GCs in response to odours, electroporate the GC with a tracer, and then examine the local connectivity of the GC in terms of where its

dendrites terminate in the EPL or, using transynaptic strategies, determine to which MTs a particular GC projects.

Combining patch recordings from GCs along with viral anatomical tracing methods could shed light on whether specific structure–function relationships exist at the level of individual GCs. Early anatomical studies suggest GCs show significant differences in their spatial identity, particularly concerning where one finds their cell bodies within the GCL and where, in the EPL, GC dendrites terminate. Using Golgi staining, Woolf et al (1991) suggest dividing the population of GCs into three distinct classes: type I, type II and type III. Type I neurons are found throughout the GCL and project throughout the EPL while Type II and III show more restricted spatial patterning. Specifically, Type II GC somata are found deeper in the GCL and project preferentially to the lower one third of the EPL. Based on this patterning, Woolf and colleagues suggested that Type II neurons may preferentially contact MCs. Conversely, Type III neurons are found in the superficial GCL and tend to project to the upper EPL where they may preferentially contact TCs (Woolf, Shepherd, & Greer, 1991a). In our data, we did not distinguish among these putative GC types; in many cases, we could not do so because, with NB staining alone, we often lacked accurate information concerning the GC dendritic projections.

Mitral cells and tufted cells have different odour response profiles whereby TCs are much more broadly tuned than MCs (Fukunaga et al., 2012; Igarashi et al., 2012). Further, TCs tend to fire during the exhalation phase of the breathing, and activity at the GC-TC synapse is thought to modulatae gamma activity in a higher frequency range. Conversely, MCs fire around inhalation, and the GC-MC ciricuit is thought to modulate low gamma. (Fukunaga et al., 2012). Whether these differences between MCs and TCs reflects differences in GC connectivity and activity is unknown. However, we might expect type III GCs to be more sparsely tuned than type II GCs such that TCs then receive less inhibition. We could test this hypothesis using combined loose patch methods and anatomical tracing techniques.

5.2.2 Possible Role of Centrifugal Inputs

Granule cells receive feedforward input from MTs as well as feedback input from cortical and neuromodulatory centres. The state and learning dependent effects we report here indicate that the context-dependent activity of GCs does not depend on differences in MTs alone. GC activity does not always follow that of MTs. Instead, a likely source for difference in GC activity is the extensive feedback to the MOB.

For example, both HDB (a cholinergic nucleus) and LC (a noradrenergic nucleus) project to the MOB and terminate in the GCL. The activity of these nuclei fluctuates with the state of the animal, and in many cases, dictates the overall attentiveness and motivation of the animal (Watson, Baghdoyan, & Lydic, 2010). Noradrenergic inputs to the MOB are known to affect odour memories on long time scales (Shea, Katz, & Mooney, 2008) and are known to affect the ability of mice to discriminate odours (Doucette, Milder, & Restrepo, 2007). However, how GC activity is influenced by NA has not been examined *in vivo* (but see Appendix B). Similarly, inhibition of the HDB or suppression of cholinergic signalling in the MOB disrupts olfactory learning suggesting acetylcholine may play a role in updating GC activity as animals form olfactory associations and discriminate among odours. While the influence of acetylcholine on GCs has been explored *in vitro* (Devore & Linster, 2012), we have little information concerning how these effects translate *in vivo* or how acetylcholine influences GCs when animals recognize odour meaning. Future studies that assay GC activity and simultaneously alter the activity of NA or HDB feedback will provide important insight concerning how neuromodulators influence the state and learning related responses of GCs to odours.

5.3 What We Could not See: Activity at Dendrodendritic Synapses

Our data exclusively concerned spiking in GCs. We were thus blind to the subthreshold activity in GCs as well as any local processing at GC-MT synapses. Granule cells express several different types of activity dependent ion channels including NMDA channels, voltage-gated sodium channels, and voltage gated Ca^{2+} channels. These different channels confer GCs with different types of electrophysiological activity including Ca^{2+} dependent subthreshold activity, low threshold Ca^{2+} spikes, and somatic APs, and many groups have suggested that GCs may thus possess several information processing states. For example, local subthreshold Ca^{2+} activity exclusively at the dendritic spine is enough to mediate reciprocal inhibition of MTs (Egger, Svoboda, & Mainen, 2003; Egger, Svoboda, & Mainen, 2005). In principle, olfactory association learning and discrimination could influence synaptic weights and boost local Ca^{2+} signaling in a manner that never augments GC spiking. We would thus not see these changes in our current regime. Instead, we would need to conduct whole cell patch recordings or imaging studies *in vivo*. To my knowledge, only one group thus far has reported whole cell recordings from GCs in awake mice (Youngstrom & Strowbridge, 2015). Contrary to our spike results, spontaneous GC subthreshold activity is modulated by the breathing rhythm and often locks with preferred phase of the breathing cycle. This suggests that recordings of GC subthreshold activity in tasks like ours may reveal even richer data with respect to how GC activity changes across state and learning.

5.4 General Conclusions and Perspectives

5.4.1 Inhibition as a Modulator of Sensory Context

Granule cells occupy a key position in the MOB as one of the primary integrators of both sensory and centrifugal input. Through dendrodendritic synapses, they can profoundly modulate the activity of excitatory neurons of the bulb and update olfactory information in response to contextual cues. This role of inhibition need not be exclusive to GCs, but instead likely reflects a general role for inhibition in sensory circuits.

Across sensory systems, local interneurons play a fundamental role in refining the responses of excitatory neurons to sensory stimuli. These interneurons often show context and state dependent activity (McGinley et al., 2015; Pakan et al., 2016; Petersen & Crochet, 2013; Poort et al., 2015; Vinck et al., 2015). Studies of GCs may not only inform how the MOB solves olfactory coding problems in the face of changing stimuli but also globally inform how inhibitory neurons update circuits in light of contextual information. The ease of access to GCs as well as a mouse's acute dependence on its olfactory sense thus make the MOB and its inhibitory circuits a great model for understanding the role of inhibition in sensory processing.

5.4.2 Learning and Context: Where and How Should We Look

Traditional hierarchical models of the brain view sensory areas as information filters that reliably encode the basic features of a stimulus. Results like ours, however, reinforce the idea that these simple hierarchal models are incomplete. Instead, an organism's state and history can have a profound influence on neuronal activity even at early stages of sensory processing, and higher cortical areas may thus receive more dynamic information than previously assumed. This has important implications for how we study learning, design experiments, and analyze data.

First, while these studies do not obviate the need to explore learning in higher cortical structures, they require us to embrace the idea that these higher order structures receive complex information that can change. We should not assume that the information that a higher order centre receives from lower sensory processors is constant. Even with the same external stimulus (i.e. an odour), the information these higher order centres receive can fluctuate.

Second, in the area of sensory neuroscience, results like ours emphasize the need for careful control in experiments that marry functional interrogations of neuronal activity and behaviour. Observed results may reflect variables the researchers anticipates but may also

reflect variables, such as an animal's level of arousal, that the researcher does not measure. We should thus use a judicious hand in the design and interpretation of our research.

Finally, our results suggest that the responses of even early sensory structures fluctuate with both external variables related to the stimulus and internal variables like the animal's state. Thus, the responses of neurons to each trial of the stimulus may be vastly different, and these differences may be obscured by the typical analysis method of averaging across several trials. Single trial or trial-by-trial analysis of data in addition to careful control of task parameters may reveal new insight into how neurons respond to stimuli.

Fin

Appendix A

Awake, In vivo Recording Protocol

This protocol was originally published in Neural Tracing Methods : Tracing Neurons and Their Connections (2015) under the title "Simultaneous Collection of In Vivo Functional and Anatomical Data from Individual Neurons in Awake Mice."

Chapter 4

Simultaneous Collection of In Vivo Functional and Anatomical Data from Individual Neurons in Awake Mice

Brittany N. Cazakoff and Stephen D. Shea

Abstract

Ideally, to trace neural circuits, one often desires access to functional data that may be linked to anatomical attributes such as neuron type or projection target. Here we describe methods used for this purpose in our laboratory. We aim for this chapter to serve as a practical guide to applying "loose patch" or "cell-attached patch" electrophysiology techniques in vivo to simultaneously obtain information about neuronal firing (e.g., responses to sensory stimuli) and detailed anatomical information including dendritic morphology and axonal targeting. Since data on neuronal circuit function are often most useful when gathered during wakeful behavior, we pay special attention here to the use of these techniques in awake, head-fixed mice. However, the same methods may easily be applied to anesthetized animals.

Key words Electrophysiology, In vivo, Awake, Loose patch, Extracellular, Neuroanatomy

1 Introduction

Ultimately, to better understand neural circuits, neuroscientists must be able to associate the detailed wiring diagrams obtained via anatomical tracing methods with data characterizing the activity of circuits in terms of neuronal firing [1]. The most direct approach to making this connection is to simultaneously obtain electrophysiological and anatomical data from the same neurons. Moreover, assuming a major objective of modern neuroscience is to understand how neural circuitry gives rise to behavior, it is perhaps optimal to obtain functional data on neural firing patterns from animals that are consciously perceiving stimuli and behaviorally responding [4]. These electrophysiology data, when corresponded with anatomical morphology and connectivity, are invaluable for revealing what information is carried in the "wires" traced using anatomical methods.

A number of existing techniques allow measurement of electrical activity of isolated neurons in vivo. Here we focus on a

Benjamin R. Arenkiel (ed.), *Neural Tracing Methods: Tracing Neurons and Their Connections*, Neuromethods, vol. 92, DOI 10.1007/978-1-4939-1963-5_4,

technique ("loose patch" recording) that is compatible with acquisition of anatomical information about the recorded cell. We find the loose patch method is a particularly mechanically stable recording configuration, so we also describe procedures specifically for making recordings in awake animals. In our laboratory, we use these techniques in mice, although in principle they could be used in rats or other small animals. As a sample application, here we demonstrate the fidelity and stability of these methods by describing their use to record from granule cells of the mouse main olfactory bulb, a class of small cells that are otherwise difficult to electrophysiologically target.

We have included general protocols and notes for performing the following procedures:

1. Construction of a head-fixed recording rig.
2. Implantation of a head fixation bar.
3. Loose patch recording/cell-labeling techniques.

2 Materials

2.1 Construction of a Head-Fixed Recording Rig

In this section, we describe each of the major components of our head-fixed recording rig and explain some of our design choices. The reader may make different choices or assemble them differently depending on the demands of a particular experiment.

2.1.1 Head Fixation System

In our laboratory, we use a custom-machined head bar and clamp system (Fig. 1). The head bar (20 mm × 3 mm) is laser cut from a 1.27 mm-thick titanium sheet and is tapered on the ends where it is grasped on each side by a clamp. The clamps are held in place by custom rails and optical hardware (Thorlabs). The tapered ends of the bar fit into the mouths of the clamps, and custom thumbscrews allow quick fixation and release of the head bar. In Sect. 2.2, we describe procedures for stably affixing these head bars to the skull of a mouse.

In choosing this design, we had a number of considerations. First, we wanted to achieve maximal stability of the preparation; thus, we chose to grasp the bar in two locations on either side of the head. Second, we wanted the implant to be as lightweight as possible so that it minimally interferes with the animal's behavior. Third, we wanted the implant to be as low profile as possible so that it could be placed very close to the craniotomy. As we will describe in Sect. 2.2, secure placement close to the target brain region is critical for achieving stable recordings. We have used these head bars effectively in recordings from the main olfactory bulb, the auditory cortex, and the somatosensory cortex. It is important to consider optimal placement of the head bar for different target regions.

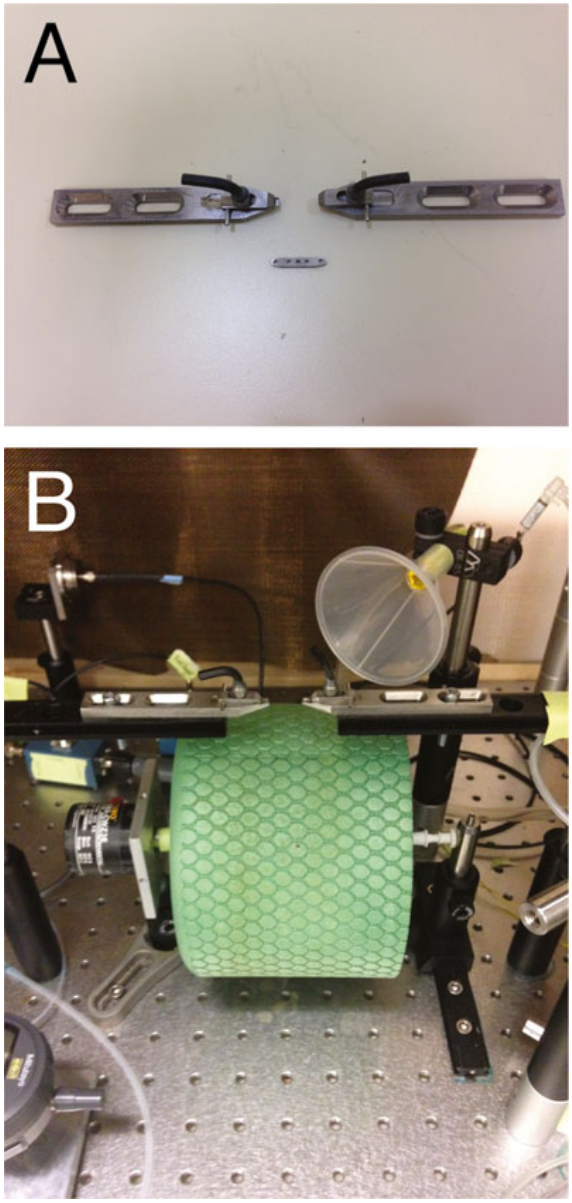

Fig. 1 Photos of the head fixation system. (**a**) Head fixation clamps and a head bar. (**b**) Clamping system positioned over the wheel

2.1.2 Animal Support Structure

In our laboratory, the head clamps are positioned so that the mouse rests on a freely rotating cylindrical wheel, cut from a foam pillow (Exervo TeraNova EVA foam roller) (Fig. 1). This particular product has the dual advantages of (1) having a textured surface that facilitates running and (2) being easy to clean. The wheel has a rod through the center that is held on either side by optical posts. The design of our wheel is simple and also somewhat arbitrary. Any wheel or ball can suffice as long as it rotates easily with minimal drag. Optional enhancements can include spring mounts for the axle or a ball that moves in two dimensions as opposed to axially [3].

Unless the experiment explicitly requires or uses a ball that rotates with more than one degree of freedom, we recommend avoiding this as the animal may slide laterally. Another feature we have included in our set up is the microcontroller-based velocity sensor that computes and outputs an analog signal proportional to linear velocity of the wheel surface (see below).

As alternatives to a running wheel or ball, one may use a static platform or tube. Many laboratories have reported success using these structures to hold the animal; however, in our experience, when the animal is unable to run, there is a tendency for it to grab an edge of the structure and apply force. This could lead to movement that will be inhibitory to stable recordings or, in the worst case, detachment of the head bar. Therefore, the choice of a wheel has two benefits. First, it keeps the animal alert, active, and relatively comfortable. Second, when the animal does move, the wheel diffuses the kinetic energy, and the animal cannot push or pull on the head bar.

2.1.3 Amplifier

This choice is mostly up to personal preference, as essentially any current clamp or "bridge" amplifier will work. Features that are important include (1) an ability to gate and/or command current pulses flexibly, (2) a head stage capable of making positive and negative current pulses of up to 1 nA through a micropipette of up to 50 M**Ω** resistance, (3) a "buzz capacitance" button with adjustable duration for transiently overcompensating the electrode capacitance, and (4) an adjustable high-pass filter ranging from DC to at least 100 Hz. Virtually all amplifiers are compatible with a wide range of pipette holders. Select a pipette holder that fits 1.5 mm OD glass pipettes, includes a silver wire that reaches down close to the pipette tip, and also features a side pressure port for applying positive and negative pressure.

2.1.4 Wheel Velocity Sensor

Depending on your experimental needs, you may optionally equip the running wheel with a rotary encoder that outputs a signal that can be used to calculate running velocity. Here we provide a simple inexpensive method for building this component and use a microcontroller to produce an analog signal proportional to velocity.

2.1.5 Micromanipulator

To stably and flexibly position your recording pipette above and into the brain, you will first need a coarse manipulator with three or, ideally, four axes. As an example, we recommend the MX110 from Siskiyou Design. Second, you will need one axis of fine manipulation used to advance the pipette once it is in the brain. The full array of choices for this task is beyond the scope of this paper; however, in our laboratory we use either a hydraulic microdrive from Soma Scientific or a Luigs and Neumann piezoelectric drive. Each one has a different user feel, so the choice is somewhat a matter of personal preference. You should also of course consider the range in the depth axis to be sure it is appropriate for your target.

Parts List

Amplifier (we use NPI ELC-03 or BA-0X).

Desktop computer with data acquisition system (we use Spike2 equipped with a Power1401 ADC/DAC board).

Oscilloscope.

Appropriate BNC cables to connect devices to the computer.

Head bar clamp and frame (constructed from custom-machined hardware and optical posts and rails from Thorlabs).

Coarse four-axis micromanipulator and mounting post.

Foam wheel cylinder (Exervo TeraNova EVA foam roller; cut into 6″ cylinder).

Axial mount for wheel (constructed from optical posts and rails from Thorlabs).

Rotary encoder (model COM-11102 available from SparkFun).

Arduino Uno microcontroller.

MAX500 DAC integrated circuit chip.

12 V DC power supply.

Miscellaneous wire, connectors, and a power source for assembling the velocity sensor.

2.2 Implantation of a Head Fixation Bar

Parts List

Absorbent points (Henry Schein, part no. 9004703).

Air hose.

Anesthetic for recovery surgery (e.g., ketamine and xylazine).

C&B-Metabond Quick! cement system (Parkell Inc., part no. S380).

Cotton swabs.

Dental cement powder (A-M Systems, part no. 525000).

Dental cement solvent (A-M Systems, part no. 526000).

Gelfoam absorbable gelatin dental sponge (Pfizer).

Head bar (2 cm × 0.3 cm × 0.1 cm) with tapered ends.

Microdrill or dental drill.

Stainless steel, flat-head machine screws (Amazon Supply, part no. B002SG89OI).

Surgical tools (fine forceps, scalpel or spring-loaded scissors, needle driver).

Sutures.

2.3 Making Loose Patch Recordings in Awake Mice

Parts List

Borosilicate glass with filament (O.D. 1.5 mm, I.D. 0.86 mm; BF150-86-10, Sutter Instrument).

Micropipette puller with box filament.

1.5 % Neurobiotin dissolved in patch solution.

Patch solution.

10 mM HEPES.

2 mM magnesium chloride.

10 mM potassium chloride.

125 mM potassium gluconate.

Filter and freeze in 10–20 μl aliquots.

Pipette holder for patch pipettes.

Silver chloride pellet for ground electrode.

Silver wire.

Surgical tools (blade breaker, fine forceps).

Wire to connect ground to head stage.

3 Methods

3.1 Construction of a Head-Fixed Recording Rig

There is no fixed protocol or set procedure for constructing an electrophysiology rig because the needs of every experiment are different. However, careful thought should be given to the placement of all components so that there is easy access to the animal, plenty of room to see the preparation under a surgical microscope, and clearance to easily and quickly withdraw and replace your pipette. We strongly recommend that you perform your experiments inside a Faraday cage and carefully ground all the components of your rig to a common point that has a secure and heavy gauge path to AC ground. It is also important to keep AC-powered devices outside of the Faraday cage. Finally, you may wish to perform the experiments on an air table to dampen vibrations, although this is obviously less important when the animal will be awake and moving on its own.

One special feature we describe here is the attachment of a rotary encoder to the wheel in order to measure the direction and speed of running. Figure 2 is a schematic of how to wire together such a device. The axle of the encoder is placed in the center of the running wheel, and its output wires connect to an Arduino Uno microcontroller. In Appendix, we include software code that can be loaded onto the microcontroller so that it counts clicks from the encoder to integrate position change per unit time. At every time step, the microcontroller serially communicates with a DAC chip

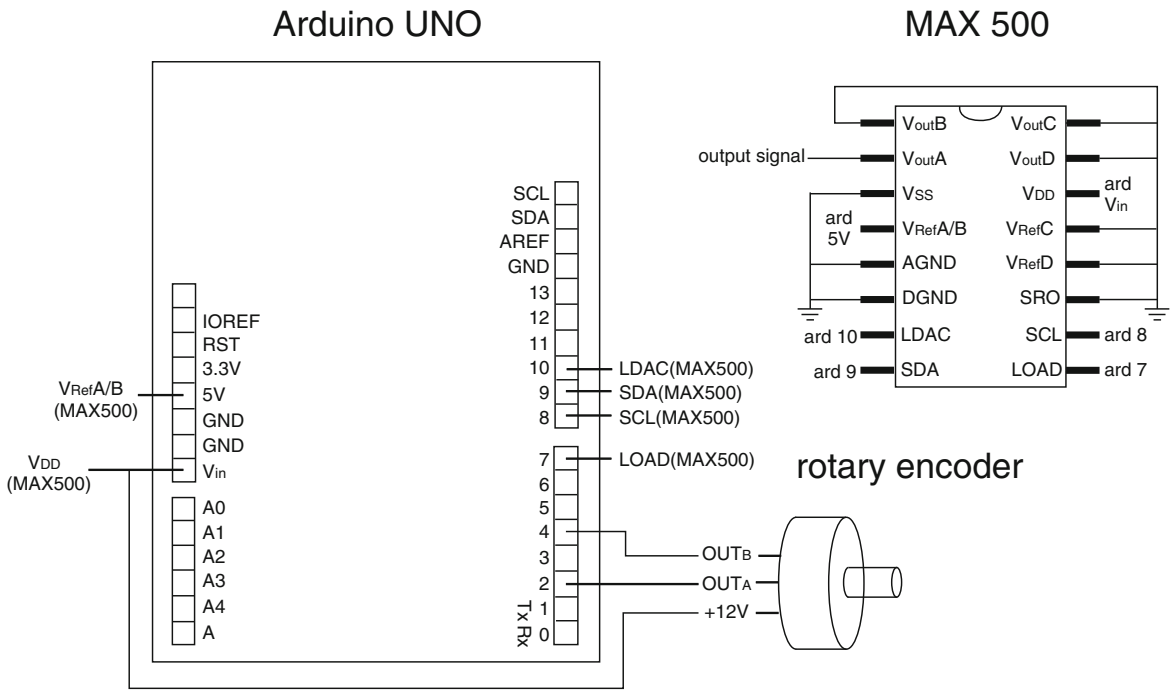

Fig. 2 Schematic for building a running wheel velocity sensor

to update the velocity reading, which the DAC chip outputs as an analog voltage that can be acquired along with your neural data and other physiological measures.

3.2 Implantation of a Head Fixation Bar

The procedure described here is for implantation of a head bar on an adult (approx. 6–10 weeks old) mouse but may be adapted for use in other animals. We secure head bars to the animal's skull using a combination of small machine screws and dental cement. This increases both the stability and longevity of the implant with minimal disruption to the animal's behavior. Surgery should be completed at least 3 days in advance of recording to allow the animal sufficient time to recover.

3.2.1 Surgery

The animal is first anesthetized, positioned in the stereotaxic frame, and the skull is exposed using a scalpel or spring-loaded scissors. You should completely clear the membranous tissue on the surface of the skull using fine forceps or by rubbing the skull surface with a cotton swab.

Using the microdrill, we make burr holes in which to position machine screws. Using a screwdriver and a pair of fine forceps, we then fasten these screws to the skull. Screws should be secured only halfway into the skull, taking care not to damage the underlying brain. While positioning of the screws will depend on the recording area of interest, we typically position 3–4 screws in a square pattern with two screws positioned far from the intended recording site and 1–2 screws positioned just next to the recording site.

Where possible, we position the caudal and rostral screws far enough apart from each other so the head bar may be positioned between them. Any bleeding from the burr holes should be cleaned using the absorbent tips or Gelfoam.

The head bar is secured to the skull using dental cement. While this cement is adequate for stabilizing the head bar, it does not itself adhere well to the skull. Instead, we first coat the skull surface in a thin layer of Metabond (prepared according to the manufacturer's instructions). We find that Metabond adheres tightly to the skull and provides a better surface on which the dental cement can be applied. Both the Metabond and the dental cement should only be applied to dry surfaces as fluid prevents adherence and thus compromises the stability of the head cap. The skull surface can be dried using a combination of cotton swabs, Gelfoam, or absorbent tips placed under the skin and pressurized air blown onto the skull surface. Once the Metabond is dry, the head bar can be placed on top of the Metabond and secured with ample dental cement, ensuring that the cement does not stick to the tapered ends of the head bar. Dental cement should completely cover the screws and the middle section of the head bar. Using this method, we find the head caps are stable across multiple recording sessions and continue to stick to the skull surface weeks after the initial surgery.

3.3 Making Loose Patch Recordings in Awake Mice

For awake recordings, we first anesthetize the mouse with isoflurane anesthesia (1 %) and make a craniotomy. Individual mice are used for multiple recordings, and a new craniotomy is made each day. This better ensures that Neurobiotin fills can be resolved postmortem. Mice tolerate well the brief period of anesthesia, and recordings are not made until at least one half hour after the animal wakes up. Local lidocaine anesthetic (4 % Topicaine) is used on the skin surrounding the area of interest to minimize discomfort to the animal during recording.

3.3.1 Craniotomy

Small (200 μm × 200 μm) clean craniotomies are essential for achieving stable loose patch recordings in awake animals. Large burr holes or cranial windows provide less support to the patch pipette and tend to bleed more often, inhibiting recording success. To achieve small craniotomies, we first shave down several layers of skull without breaking through skull to brain. When the skull is sufficiently thinned (pliable), we use a blade breaker to cut a small opening in the skull and expose brain. We keep the craniotomy moist and devoid of blood by covering it with Gelfoam soaked in 0.9 % saline until we are ready to record. For most of our recordings, we do not find it necessary to clear the dura mater as the patch pipettes are sharp and strong enough to pierce through this tissue.

3.3.2 Ground Electrode

We use a silver pellet ground wire positioned under the skin near the recording area of interest. Throughout the recording, we find it necessary to keep the tip of the ground wire wet using

saline-soaked dental foam. This increases the surface area in contact with the preparation and reduces noise.

Placement of the ground wire is critical for loose patch recordings. One should not position the ground wire near muscles that may displace the ground when the animal moves or breaths. This results in additional noise and/or breathing artifact in the recording. We find positioning the ground underneath the skin on one side of the top of the skull adequate and superior to positioning the ground underneath the skin near the neck muscles at the back of the head.

3.3.3 Loose Patch Recording Pipettes

Patch pipettes are pulled from standard wall borosilicate tubing using a Flaming/Brown type micropipette puller. While pulling parameters may differ with puller as well as ambient temperature and humidity, pipettes should be 15–25 MΩ resistance and have a relatively long taper. Depending on the depth of the target region, you will want the first few millimeter of the tip to flare minimally to prevent damage superficial to the recording site. We find that heating the glass capillary over three steps and pulling on the last step give us better resistance than pulling slowly over more steps or pulling in one step.

Using a 10 μl Hamilton Syringe, we fill loose patch pipettes with 1.5 % Neurobiotin in loose patch solution (3–4 μl). In some cases, Neurobiotin can spill out into the brain area of interest and label more cells than intended. It may then be necessary to backfill the pipette tip with label-free loose patch solution (~0.5 μl) and then fill the rest of the pipette with Neurobiotin patch solution. Patch solution should be aliquoted and kept frozen until ready for daily use.

3.3.4 Cell Search

Here we describe procedures similar to those pioneered by Pinault [5]. In a blind loose patch recording, you can determine whether you have encountered a cell by observing changes in voltage while applying fixed current (current clamp mode). Therefore, you should begin by using the computer or timing device such as a Master-8 (AMPI) to command repetitive negative current pulses from the amplifier. We use -200 pA square current pulses of 0.2 s duration delivered at ~2.5 Hz.

To begin searching for cells, first load the pipette onto the pipette holder and apply positive pressure to the pipette through the tubing attached to a 10 ml syringe. Generally, depressing the syringe plunger about 2–3 ml provides enough pressure to keep the pipette tip clear of debris as the pipette is advanced in the tissue. The positive pressure can be maintained by closing a three-way valve attached to the syringe on one end and the tubing on the other. While applying positive pressure, lower the pipette until it touches the surface of the brain. This can be observed through the microscope, or it may also be heard if the voltage output of the

amplifier is connected to an audio monitor. Once the pipette touches the surface, zero the fine manipulator reading and the amplifier potential, and then check the resistance of the patch pipette. Many amplifiers will have a test button for checking the resistance, but it can also be calculated using Ohm's law ($V = IR$). While applying 200 pA negative current steps, the voltage drop on the oscilloscope or recording software should be 3–5 mV for a 15–25 MΩ resistance.

You will be looking for abrupt transient increases in the size of this voltage step that result from increased resistance when approaching a cell. Therefore, you can make them easier to detect by compensating for most of the pipette resistance. Advance the pipette quickly (25–50 μm per s) to ~100 μm above the region of interest. While lowering the pipette, one should periodically "buzz" the capacitance to keep the pipette free of debris. Once you reach the area of interest, you should advance the pipette more slowly (2–3 μm per s) while checking for increases in voltage indicating the presence of a cell.

With experience, it will become evident that contact with a cell is marked by an abrupt and dramatic increase in the size of the voltage response to the current pulses. Slower drifting changes are almost always due to clogging of the pipette with debris. If such an abrupt increase is observed and maintained over several 2–3 μm steps, immediately vent away the positive pressure. Frequently, at this point, the pipette will increase further the tightness of its seal to the cell by two or more fold. Exactly how far you should advance the pipette before removing positive pressure, and whether you should advance pipette further after that, depends on the type of cell you are trying to record. You should experiment with different approaches. You may also find that applying a small amount of negative pressure accelerates the sealing process, but this is often not necessary. During good recordings, the series resistance measured through the pipette is usually one hundred to several hundred MOhm, but there is no specific target as long as there is adequate signal-to-noise ratio to allow good single unit isolation. Figure 3 depicts some raw traces obtained during the sealing process of a recording from a granule cell in the mouse main olfactory bulb.

3.3.5 Labeling Cells

Cells are filled with Neurobiotin using steps of positive current injection (+700–1,000 pA; 500 ms square pulse, 1 Hz). You should continue applying current injections for at least 20 min although, depending on the cell of interest, more or less time may be required. The cell may continue to spike during dye labeling, an indication that the seal is still present; however, loss of spiking is not always an indication that one has lost the seal. Instead, cell

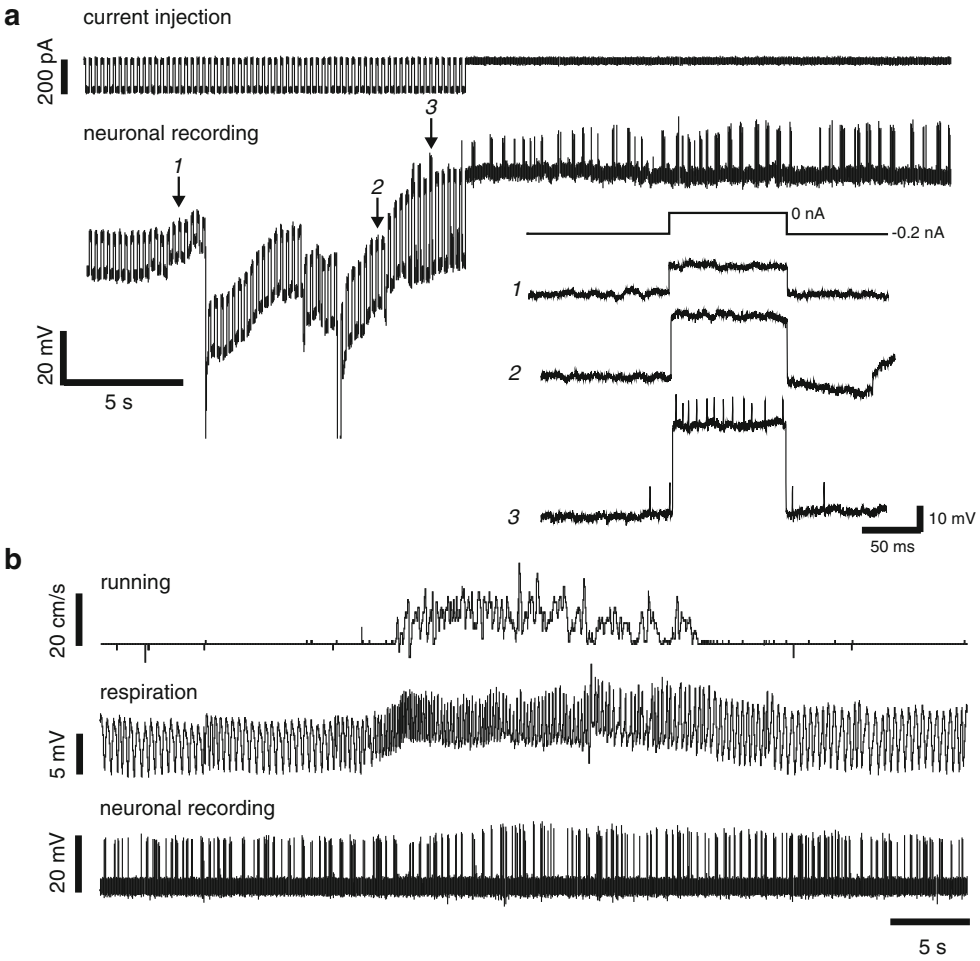

Fig. 3 Example data gathered during isolation and recording of a mouse main olfactory bulb granule cell in an awake, running mouse. (**a**) Raw physiology traces of current (*top*) and voltage (*bottom*) during acquisition and isolation of a granule cell. For the first half of this recording, 200 pA negative current pulses were used to monitor pipette resistance while searching for a cell. The numbered traces show the voltage response at the labeled time points. Note the increase in the voltage deflection. Near the halfway point, the pulses are turned off, and an isolated single unit emerges. (**b**) In our setup, unit recordings are stable during free running. The *top trace* shows the signal output of our wheel velocity sensor, reflecting a 20–25 s episode of running. The *middle trace* depicts the signal from a nasally implanted thermistor to sense respiration. The *bottom trace* is the voltage trace from the same neuron depicted in (**a**)

resistance can be checked periodically throughout the fill, and in cases where the seal is lost, filling should be terminated. The animal can then be anesthetized, and the skin over the recording area can be sutured, or the animal can be perfused with PBS followed by 4 % paraformaldehyde. Tissue is then sectioned and treated with a streptavidin-conjugated fluorophore to identify labeled cells as described [2].

4 Notes

Helpful Tips for Stable Head Caps

1. The skull surface should be kept as dry as possible throughout the surgery and especially before the application of dental cement. Both careful drilling of burr holes so as to minimize bleeding as well as drying the skull with pressurized air assist in this goal.
2. Screws should not be inserted so deep that the head of the screw is flush with the skull. In such a case, screws may spin in the burr holes and fail to provide a secure hold for the dental cement. Further, deep screws have the potential to damage the underlying brain.
3. Dental cement should extend adjacent to the recording area of interest. Securing the head bar and dental cement as close as possible to the recording site better ensures the target region will have little movement during recording.
4. Dental cement should not stick to nearby skin or muscle tissue. These surfaces are generally not stable or dry enough for the cement adherence. Further, glue on the skin is irritating to the animal.
5. Apply a final layer of superglue on the head cap to harden the cap and provide additional stability.

Helpful Tips for Loose Patch Recording

1. While recordings are generally attainable in mice of any age, young adult mice (5–7 weeks) are best.
2. Habituating the animal to the recording apparatus for at least 2 days (1 h each day) ensures the animal is calm and minimizes the loss of seals due to excessive running or struggling by the animal. Where the experiment allows, it is also helpful to water deprive the animal 24 h prior to the recording and provide water to the animal on the ball through a lick port.
3. Brain pulsation disrupts the stability of recording over long periods. Pulsation can arise with a messy or bloody craniotomy for several hours into an experiment. Covering the craniotomy with saline-soaked dental foam for several minutes may help, but we find it best to abandon the craniotomy and make a new one in the other hemisphere.
4. On occasion, one may encounter breathing artifact in the voltage recording. This can often be remedied by repositioning the ground wire.
5. Upon finding a cell, one can often advanced the electrode several more steps (10 μm) in order to improve the quality of the recording and achieve better seals.

Acknowledgments

The authors wish to thank R. Eifert for custom machining and J. Sanders for technical advice on design and construction of the velocity sensor.

Appendix: Arduino Code

```
#include<digitalWriteFast.h>   //include   this
library available from   //https://code.google.
com/p/digitalwritefast/
   // Define Arduino inputs
   #define c_EncoderInterrupt 0
   #define c_EncoderPinA 2
   #define c_EncoderPinB 4
   //Define Arduino serial outputs
   #define LOAD 7
   #define CLOCK 8
   #define DATA 9
   #define LDAC 10
   //Define variables
   volatile bool _EncoderBSet;
   volatile long _EncoderTicks=0;
   volatile long tmpdata=0;
   volatile long velocity=0;
   //set clock timing
   #define HALF_CLOCK_PERIOD 10
   //initialization routine
   void setup()
    {
   //Assign functions to inputs
   pinMode(c_EncoderPinA, INPUT);
   digitalWrite(c_EncoderPinA, LOW);
   pinMode(c_EncoderPinB, INPUT);
   digitalWrite(c_EncoderPinB, LOW);
   attachInterrupt(c_EncoderInterrupt,
HandleMotorInterruptA, RISING);
   //Assign functions to outputs
   pinMode(DATA, OUTPUT);
   pinMode(CLOCK,OUTPUT);
   pinMode(LOAD,OUTPUT);
   pinMode(LDAC,OUTPUT);
   //initialize serial outputs
   digitalWriteFast(DATA,LOW);
   digitalWriteFast(CLOCK,HIGH);
   digitalWriteFast(LOAD,HIGH);
```

```
   digitalWriteFast(LDAC,HIGH);
   Serial.begin (9600);
    }
   //Running loop function
   void loop()
    {
   tmpdata=_EncoderTicks;
   delay(40);//bin size in ms. if changed you
need to change denominator in    //next line
   velocity = (((_EncoderTicks-
tmpdata))/0.04)*0.047)+128;    //0.047    scal-
ing    //term assumes a 6" diameter wheel
   writeValue(velocity);
   Serial.print(velocity-128);
   Serial.print("\n");
    }
   // Interrupt function triggered by a click on
encoder OutA
   void HandleMotorInterruptA()
    {
   // Reading the state of encoder OutB deter-
mines the direction of rotation
   if (digitalReadFast(c_EncoderPinB) == LOW) {
   _EncoderTicks=_EncoderTicks-1;
   } else {
   _EncoderTicks=_EncoderTicks+1;
    }
    }
   //write value to serial connection to MAX500
   void writeValue(uint8_t value)
    {
   //start of sequence
   digitalWriteFast(DATA,LOW);
   delayMicroseconds(HALF_CLOCK_PERIOD);
   digitalWriteFast(CLOCK,LOW);
   delayMicroseconds(HALF_CLOCK_PERIOD);
   digitalWriteFast(CLOCK,HIGH);
   digitalWriteFast(DATA,LOW);
   delayMicroseconds(HALF_CLOCK_PERIOD);
   digitalWriteFast(CLOCK,LOW);
   delayMicroseconds(HALF_CLOCK_PERIOD);
   digitalWriteFast(CLOCK,HIGH);
   //send the 8 bit sample data
   for(int i=7;i>=0;i--){
   digitalWriteFast(DATA,((value&(1<<i)))>>i);
   delayMicroseconds(HALF_CLOCK_PERIOD);
   digitalWriteFast(CLOCK,LOW);
   delayMicroseconds(HALF_CLOCK_PERIOD);
```

```
digitalWriteFast(CLOCK,HIGH);
 }
//latch enable, DAC output is set
digitalWriteFast(DATA,LOW);
delayMicroseconds(HALF_CLOCK_PERIOD);
digitalWriteFast(LOAD,LOW);
delayMicroseconds(HALF_CLOCK_PERIOD);
delayMicroseconds(HALF_CLOCK_PERIOD);
digitalWriteFast(LOAD,HIGH);
delayMicroseconds(HALF_CLOCK_PERIOD);
digitalWriteFast(LDAC,LOW);
delayMicroseconds(HALF_CLOCK_PERIOD);
delayMicroseconds(HALF_CLOCK_PERIOD);
digitalWriteFast(LDAC,HIGH);
}
```

References

1. Bock DD, Lee WC, Kerlin AM, Andermann ML, Hood G, Wetzel AW, Yurgenson S, Soucy ER, Kim HS, Reid RC (2011) Network anatomy and in vivo physiology of visual cortical neurons. Nature 471:177–182
2. Cazakoff BN, Lau BY, Crump KL, Demmer HS, Shea SD (2014) Broadly tuned and respiration-independent inhibition in the olfactory bulb of awake mice. Nat Neurosci 17:569–576
3. Dombeck DA, Khabbaz AN, Collman F, Adelman TL, Tank DW (2007) Imaging large-scale neural activity with cellular resolution in awake, mobile mice. Neuron 56:43–57
4. Petersen CC (2009) Genetic manipulation, whole-cell recordings and functional imaging of the sensorimotor cortex of behaving mice. Acta Physiol (Oxf) 195:91–99
5. Pinault D (1996) A novel single-cell staining procedure performed in vivo under electrophysiological control: morpho-functional features of juxtacellularly labeled thalamic cells and other central neurons with biocytin or Neurobiotin. J Neurosci Methods 65:113–136

Appendix B

A Noradrenaline Experiment Re-examined

I collected this data in collaboration with Heike Demmer

As part of my PhD, I began to examine how noradrenaline (NA), an neuromodulator implicated in learning and memory, influences GC activity. This research grew out of the observation that NA modulates MT activity in the bulb in such a way that is consistent with a role in odour habituation. We hypothesized that GCs might mediate this effect of NA on MTs as the majority of NA feedback to the bulb terminates in the GCL. Unfortunately, the results were less than convincing for a number of reasons — most technological but some also biological. Here, for the sake of completeness, I review our findings and, in light of our findings concerning GCs in the awake animal, I suggest alternative ways to do this experiment that may reveal more insightful results.

B.1 Noradrenaline and Adult Olfactory-dependent Learning

Noradrenaline plays an important role in many processes including sleep-wake regulation, exploration, and memory; processes inherently dependent on arousal. Fundamentally, the involvement of NA in all of these behaviours seems to reflect its role in behavioural adaptation whereby NA release helps to coordinate changes in neural activity towards states that help animals meet shifting environment demands (Bouret & Sara, 2005).

The main source of NA in brain is the brainstem nucleus locus coeruleus (LC) although several smaller noradrenergic nuclei including subcoeruleus also have noradrenergic projections (Robertson et al., 2013). Locus coeruleus projects widely throughout the central nervous system including to the olfactory bulb, neocortex, hippocampus, cerebellum, thalamus, hypothalamus and spinal cord. Such widespread projections suggest NA could play a role in simultaneously activating and coordinating multiple brain areas, a function further suggested by the preferential projection pattern of single LC neurons to functionally related brain areas. However, deducing the precise roles of LC and brain NA in behaviour requires careful analysis of the action of NA on neural circuits in behaviourally relevant systems. Many forms of olfactory learning rely on NA release in the MOB. This, combined with the years of knowledge concerning the cells and circuits of the MOB, makes the MOB an excellent region in which to rigorously study how NA alters circuits to produce changes in perception and behaviour.

In rodents, NA modulates olfactory perception and learning across the lifespan of the organism. During a critical period of development, NA supports the imprinting of odours in pups, leading to a long-lasting preference for odours experienced during this critical period (Sullivan & Wilson, 1994). Pups exposed to an odour in association with either tactile stimulation or some aspect of their nest environment show a preference for this odour later in life. These effects are constrained to exposure during the first week of life and can be mimicked by replacing the associative/rewarding signal with release of NA in brain (Sullivan et al., 2000). Inhibiting the release of NA during this sensitive period abolishes the odour preference (Sullivan et al., 1994). In adults, NA produces complex effects on behaviour and seems to be important for olfactory memory and odour discrimination (Shea, Katz, & Mooney, 2008; Mandairon et al., 2008; Devore & Linster, 2012; Doucette, Milder, & Restrepo, 2007). In particular, NA release in the MOB is important for an animal's recognition of familiar individuals (mates and kin) and may suppress inappropriate aggressive/avoidance behaviours to these familiar individuals (Brennan & Keverne, 1997). Further, depending on the concentration, NA release in the bulb can dynamically regulate an animal's recognition and discrimination of previously experienced non-social odours (Guérin et al., 2008; Manella,

Alperin, & Linster, 2013).

While pup and adult NA-dependent learning exploit much of the same machinery in olfactory sensory systems, NA effects on olfactory circuit at these different time points can be widely divergent. For parsimony and brevity, I focus here only on the role of NA in modulating adult circuits, but it is important to keep in mind that many of the in vitro studies examining the influence of NA on olfactory circuits are completed in young mice. Correlating these results of these studies with the effects of NA on behaviour in adult mice, while regularly done in the literature, is complicated as both LC and its targets undergo profound changes during the development of the organism.

B.1.1 Noradrenaline and the Olfactory Bulb

B.1.2 Basic Anatomy

Locus coeruleus projects densely to the bulb with roughly 30 % of LC neurons sending axons to the MOB in rat (McLean et al., 1989; McLean & Shipley, 1991). Projection mapping using viruses suggests a similar pattern exists in the mouse (Kebschull et al., 2016; Schwarz et al., 2015) whereby the mouse olfactory bulb also receives dense projections from LC. These axons largely terminate in the GCL with fewer axons terminating on neurons in the MCL and EPL. Thus, NA action in the bulb is heavily biased towards modulation of GCs, and subsequent changes in olfactory behaviour likely reflect changes in GC activity and its actions on the MOB circuit. Several different adrenergic receptor subtypes have been identified. Granule cells, in particular, express both $\alpha 1$ and $\alpha 2$ receptors while MTs express $\alpha 1$, $\alpha 2$B, and β receptors as measured by both in-situ hybridization and antibody staining (Day et al., 1997; Domyancic & Morilak, 1997; Nai et al., 2009) or indirectly through electrophysiological measurements following receptor antagonism (Trombley & Shepherd, 1992; Trombley, 1992; Smith, Weitz, & Araneda, 2009). As described below, activation of the different receptor subtypes differentially alters the activity of both GCs and MTs, and activity can differ depending on the concentration of NA present.

B.1.3 Cell and Circuit Level Influence of Noradrenaline

Most knowledge concerning the influence of NA on olfactory neural activity derives from in vitro experiments. Early reports suggested that NA acts to decrease the release of GABA from GCs and thus acutely disinhibit MTs (Jahr & Nicoll, 1982b). However, further experiments suggested NA has complex effects depending on concentration of NA and receptor of activation. For example, in addition to its effect on inhibition of GABA release, NA acts on presynaptic MT α2 receptors to decrease excitatory glutamate release from these cells (Trombley & Shepherd, 1992; Trombley, 1992). This results in net disinhibition of MTs as GCs are both excited less and further release less GABA. At low levels of NA, α2 receptors are activated, and as concentration of NA increases, α1 receptors are activated. Activation of α1 receptors on GCs depolarizes GCs and increases the rate of spontaneous IPSCs (Nai et al., 2010; Mouly, Elaagouby, & Ravel, 1995) while activation of α2 receptors on GCs decreases IPSCs (Nai et al., 2010). Further, NA directly activates α1 receptors on MTs leading to depolarization (Nai et al., 2010; Hayar et al., 2001). As a result, the action of NA on MTs is heterogeneous such that MTs are first disinhibited by NA, but as NA concentration increases, MTs are rendered more excitable but also become increasingly inhibited by surrounding cells. Such activity may serve to increase the signal to noise ratio in the MOB and increase the synchronization between similar MTs (Escanilla et al., 2012; Devore & Linster, 2012). Indeed, NA release in MOB increases the responses of MTs to weak OSN input (Ciombor, Ennis, & Shipley, 1999; Jiang et al., 1996).

In vivo, repeated stimulation of LC suppresses the responses of MTs to odours specifically paired with LC stimulation (Shea, Katz, & Mooney, 2008). This effect is blocked by MOB application of NA receptor antagonists, suggesting the suppression is, at least in part, intrinsic to the bulb. Subsequent studies demonstrated that NA also suppresses OSN inputs to the MT cells; however, these effects are not specific to the paired odour (Eckmeier & Shea, 2014). As such, how the specificity in MT responses arises is still unclear. In one scenario, NA activity through GL interneurons, suppresses overall input to MTs but through additional actions on GCs, certain MTs are disinhibited while others are not. From this, we might expect that, if we record from GCs, we will see that NA suppresses some GCs but excites

others. This may occur in a odour-NA coincident activity dependent manner: GCs will only be suppressed to odours when those odours evoke a response in the GC at the same time there is an increase in concentration of NA in the bulb but not when NA release does not occur at the same time as the odour response.

B.1.4 Outstanding Questions

From the decades of research concerning action of NA in the MOB, we now know that NA has complex effects on olfactory circuits. Interestingly, we have little information in vivo concerning how NA affects its main olfactory target: GCs. Thus, several outstanding questions remain:

1. How does noradrenaline influence olfactory GCs in vivo and where effects exists, how specific are they?
2. If noradrenaline alters GC activity in vivo, how is this reflected in the MOB circuit?

These unanswered questions reflect a bigger question of how circuit level changes induced by NA reflect or implement changes in the animal's behaviour. To begin to address these questions, we employed a similar strategy to that used in Shea et al. (2008) in which we record from MOB neurons, in this case GCs, in anesthetized animals while electrically stimulating LC. Unfortunately, compared to controls, we failed to see any robust effect of LC stimulation on GC activity.

B.2 Methods

B.2.1 Animals

Experiments were performed on male and female C57Bl/6 mice (aged 6-10 weeks). Mice were group housed with up to five mice per cage. Animals were maintained on a 12:12 h light/dark cycle (lights on at 07:00) and had access to food and water ad libitum. All experiments were completed in accordance with the National Institutes of Health's Guide for the

Care and Use of Laboratory Animals and approved by the Cold Spring Harbor Laboratory Institutional Animal Care and Use Committee.

B.2.2 Anesthesia and Surgery

All electrophysiology experiments were conducted in anesthetized animals. Mice were anesthetized with ketamine:xylazine (80:20; 1.25 ml/kg) and furthered maintained on isoflurane (1 %) as necessary. Mice were then positioned in a stereotaxic frame, and the skull over the MOB and cerebellum was exposed for recordings from the MOB and LC respectively. Respiration was measured using a foil strain gauge (Omega Engineering) positioned on one side of the animal's abdomen, and anesthesia was adjusted to maintain a steady breathing rate of 1-2 breaths/s.

B.2.3 Locus Coeruleus Stimulation

To determine the influence of LC stimulation on MOB activity, we stimulated LC with a metal electrode while simultaneously recording from cells in MOB (Fig.B-1A). We shortened tungsten electrodes (MicroProbes, 1MΩ) to 8 mm from the tip and soldered the electrodes to a gold pin. We then secured the tungsten wire inside a borosilicate glass micropipette (Sutter Instruments). The position of LC was determined electrophysiologically whereby LC neurons display a distinct shape and firing rate (Fig.B-1). We further verified this position through tail pinches as, upon tail pinch, LC neurons respond with a burst of action potentials (Shea, Katz, & Mooney, 2008). In some animals, we chronically implanted stimulating electrodes 2-5 days before MOB recordings. We secured these chronic electrodes using dental cement. In other animals, we acutely positioned stimulating electrodes on the day of MOB recording. Comparison of these two groups revealed no differences in the effect of LC stimulation on GC firing rate, response to odour, or effect of LC stimulation.

For stimulation, we connected the stimulating electrode to an isolated pulse stimulator (A-M Systems Model 2100) and positioned a ground electrode under the mouse's skin

behind its ear. We triggered a pulse generator 1 s prior to odour presentation onset and continued this stimulation for 5 s. The stimulation consisted of 40 μA biphasic pulses of 100 μs duration generated at 5 Hz. We delivered twenty stimulation trials with an inter-trial interval of 30 s. At the end of an experiment, we then lesioned the area surrounding the stimulating electrode (10 s duration, 10 μA, 3X) for the purpose of identifying where we had placed the stimulating electrode. We lesioned tissue using a continuous pulse of

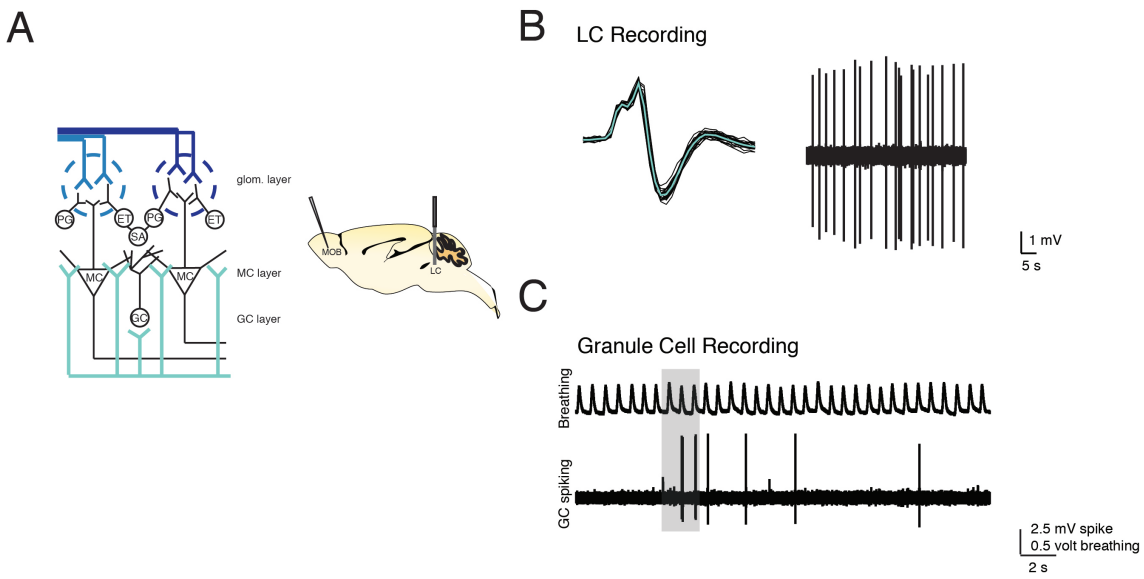

FIGURE B.1: **LC and olfactory bulb recordings** (A) To examine how noradrenergic feedback to the main olfactory bulb influences GCs, we positioned a tungsten electrode in LC and assayed MOB cell activity using loose patch recordings. (B) LC was identified based on its characteristic spike shape and increase in activity upon tail pinch of the animal. For the spike trace on the left, individual traces are shown in black and the mean trace is shown in teal. On the right, typical firing pattern of LC neurons in vivo. (C) Example breathing trace from anima (top) and loose patch recording trace from GC (bottom). The grey bar denotes the odour on period (2 s duration). GCs were recorded in response to odours and odours paired with LC stimulation.

B.2.4 Odour Stimuli

Stimuli included 40 different monomolecular and natural food odours diluted 1 % in mineral oil (5 ml). We delivered odours using a fluid dispensing robot (Fishnar Inc) customized for odour presentation (2 s long sitmulus), and we controlled delivery to the nose using a three way pinch valve (Cole Parmer). To achieve a final concentration of 0.1 % at the mouse's nose, we further diluted odours 1:10 in a steady stream of oxygen. For all odour experiments, once we achieved a reliable recording from a GC, we then presented the 40 odour stimuli until we found an odour that elicited a significant excitatory response from the GC. We then presented this odour 20X (30 s inter-trial interval) to establish the pre-LC stimulation response of the GC, 20X while stimulating LC (during period), and 20X following LC stimulation (post-LC stimulation period). In experiments where we assessed the specificity of LC stimulation, we used a blank odour (mineral oil) or a different excitatory odour (different from the odour used during the pre and post period) during LC stimulation.

B.2.5 MOB Electrophysiology

Loose patch recordings. To record MTs and GCs, we made a small craniotomy in the skull over the bulb ipsilateral to the LC stimulating electrode, and we positioned a silver pellet ground electrode on one side of the skull under the mouse's skin. As previously described in Chapters 2 and Chapter3, we conductediIn vivo, blind loose-patch recordings were conducted using borosilicate micropipettes. We lowered pipettes into the GCL (400 – 1200 μm). We acquired data using a BA-03X bridge amplifier (npi Electronic Instruments) and Spike2 software, low pass filtered the data at 3 kHz, and digitized it at 10 kHz.

B.2.6 Histology

At the end of the experiment, we filled recorded cells with 1.5 % NB and made electrolytic lesions with the LC stimulating electrode. Then, we sacrificed the animals using an overdose of sodium pentobarbital (Euthasol), and we transcardially perfused with PBS followed by 4 % paraformaldehyde. We stored the skull for 16-24 h in 4 % PFA, and then extracted and

stored the brain in 30 % sucrose in PBS for 24 h. Following this, we sectioned the brainstem and MOB (60 μm), mounted the tissue on gelatin coated slides, and stained the sections either with cresyl violet (brainstem) or streptavidin Alexafluor-488 (MOB) according to our standard procedures. The position of the LC stimulating electrode and identity of the recorded MOB cell were then verified under light microscopy (Olympus BX43). In this study, we only include experiments where the stimulating electrode was positioned in LC and where the recorded MOB cell was verified to be in the GCL.

B.2.7 Data Analysis

We manually spike-sorted recordings using a threshold in Spike2 (CED). We then performed all subsequent analyses in Matlab (Mathworks).

We only examined data that showed significant responses to the odour during either the pre-LC stimulation period or during the post-LC stimulation period. Even though the odour stimulus was 2 s long, many of the GCs only spiked during a narrow time window during odour presentation. As such, instead of considering spiking across the entire 2 s trial to determine significant responses, we examined responses in narrower bins. To determine these bins, we examined the data in a 250 ms sliding window (slid every 50 ms across the entire 2 s stimulus). Using an ROC analysis, we compared the data in every bin to a similar window in the 2 s baseline period prior to odour onset. Any cells that had two or more consecutive bins with an AUROC > 0.65 were considered significantly excitatory while cells with two or more bins with AUROC < 0.35 were considered inhibitory. Across all cells, the mean number of responsive bins was 21.5 (corresponding to a 1.1 s time window). All of these cells showed significant excitatory responses. This is likely due to the fact that spontaneous activity was so low, precluding observations of suppression. For all other analysis, we only included cells that showed significant responses, and we only considered the time window defined by the significant bins.

To determine the effect of LC stimulation on spontaneous activity, we computed spike rates during the 6 s period prior to odour onset. We computed a mean baseline rate across all

trials of the stimulus during the pre-LC stimulation period and during the post-LC stimulation period. We used a one-way anova to compare the two control groups (Sham stimulation and Blank odour stimulation) with the test group.

To determine the effect of LC stimulation, the 20 responses immediately prior to the start of LC stimulation were compared to the 20 responses immediately following LC stimulation. For some cells, the recording was lost before we could record responses to 20 stimulations during the post-stimulation period. In these cells, at least 10 responses were included in the analysis. To determine the overall effect of LC stimulation in the population of cells, mean pre-stimulation responses across all 20 stimulations for each cell were normalized to one using the following formula:

$$(pre - post) + 1; \tag{B.1}$$

.

where pre is the mean baseline subtracted response across all trials of the odour prior to LC stimulation and post is the mean baseline subtracted response across all trials of the odour following LC stimulation. Thus, numbers greater than one indicate that LC stimulation increased the response of the cell to the odour while numbers less than one indicate a decrease. In all groups, we tested for significant difference from one using a Wilcoxon ranked test.

B.3 Results

B.3.1 Noradrenaline Evoked Changes in GC Spontaneous Rate

While we did not find it difficult to patch GCs in vivo, we did find it difficult to find GCs that significantly responded to odour even with a panel of 40 different odours. Thus, our dataset is quite small. In the sections below, we present data from three different groups (Fig.B-2A):

- (1) the GC-LC group (8 cells). For these cells, we stimulated LC while presenting an odour that evoked a significant response from the cell.
- (2) the GC-Sham group (7 cells). For these cells, we presented an odour that evoked a significant response from the cell but did not stimulate LC.
- (3) the GC-Blank group (8 cells). For these cells, we stimulated LC while we presented a blank mineral oil odour to the animal.

We first assessed spontaneous activity in all of the groups. Across all groups, spontaneous activity prior to LC stimulation was low (GC-LC = 0.60 $\pm$ 0.51, GC-Sham = 0.45 $\pm$ 0.54, and GC-Blank = 0.44 $\pm$ 0.45) and did not differ amongst the groups in the pre-LC stimulation period (one-way anova $F(1,2) = 0.26$, $p = 0.77$). To determine whether the spontaneous rate changed following the LC stimulation period compared to the pre-stim period, we examined both the raw firing rates as well as normalized data where we normalized the pre-stimulation data to one and compared the post stimulation data accordingly. Our results suggest that neither the GC-LC group nor the GC-Sham group showed a significant change in spontaneous firing as a result of LC stimulation (Mann-Whitney U, $p = 1$ and $p = 0.69$ respectively, Fig.B-2B,C). However, the spontaneous rate did change in the GC-Blank group (Mann-Whitney U, $p = 0.0057$). In this group, spontaneous rate increased as a result of LC stimulation (Fig.B-2B,C). This effect was largely driven by increased activity in three cells (38 % of the cells).

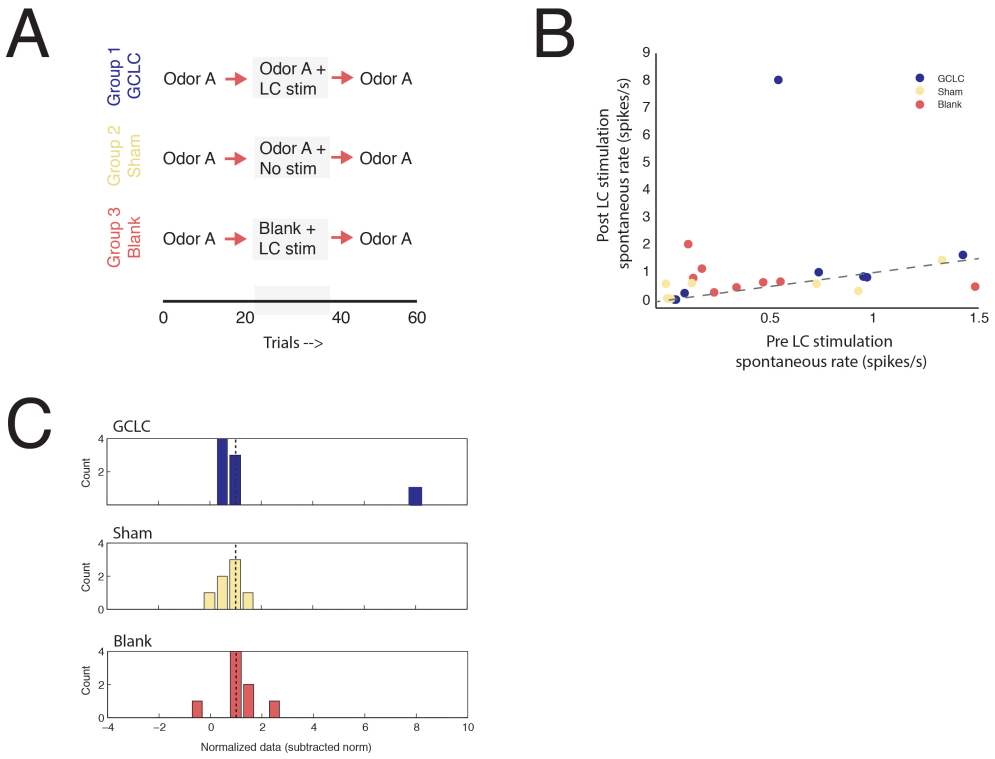

FIGURE B.2: **LC stimulation changes in the spontaneous rate for off-target odour LC pairings** (A) We compared data in three different groups: GC-LC, GC-Sham, and GC-Blank (see text). For all groups, we first screen the activity of the cell in a prestimulation period consisting of 20 trials, followed by a stim period of 20 trials, and then by a post-stimulation period of 20 trials. All comparisons are between the pre and post stimulation periods. (B) Scatter plot of mean spontaneous activity prior to LC stimulation vs. mean spontaneous activity following LC stimulation. Mean spontaneous activity did not change between the pre and post stimulation periods for the GC-LC and GC-Sham groups but showed a slight increase for the GC-Blank group (mean pre = 0.44 $\pm$ 0.45 and mean post = 0.78 $\pm$ 0.56, Mann-Whitney U p = 0.0057) . Each dot is a cell while the colors represent the different groups. (C) Mean post stimulation data compared to pre stimulation data (normalized to 1). Most cells showed normalized data around one indicating no change from the prestimulation spontaneous rates while the Blank group showed three data points higher than 1. GC-LC, GC-Sham, GC-Blank n = 8,7,8 cells.

Given our data in Chapter 3 as well as the known effects of LC stimulation on breathing, we wondered if this increase in spontaneous activity reflected the overall wakefulness state of the animal. To quantify this, we examined breathing changes in a session, using breathing rate as an overall measure of wakefulness. Similar to the spontaneous spike rate analysis, we quantified breathing in the 6 s window prior to odour stimulation. Due to lack of breathing data in one of the Sham stimulation cells, we could only analyze 6 cells in this group. Again, overall breathing rates did not differ amongst groups in the pre-LC stimulation period.

Compared to the pre-stimulation period, breathing rate in the post-stimulation period did not change in either the GC-LC (1.3 ± 0.5 breaths/s pre vs. 1.3 ± 0.6 post) or the GC-Blank group (1.1 ± 0.26 breaths/s pre vs. 1.2 ± 0.4). However, it did significantly decrease in the GC-Sham group (1.1 ± 0.3 breaths/s pre vs. 1.0 ± 0.4 , Mann-Whitney U compared to 1, $p = 0.48$). This may explain, to some degree, why GC-Sham spontaneous activity seems to decrease in the post-stimulation period (data not significant). While this change was significant statistically, whether such a change is relevant biologically is unknown, and indeed, this result lacks power.

While the overall breathing rate within the GC-Blank group did not change (and thus could not explain our observed effect on spontaneous spiking), animals showed both increases and decreases in breathing (Fig.B-3A). We thus wondered whether breathing rate in individual animals might relate in any way to the spontaneous firing rates. In Fig.B-3B, we plot the normalized post spontaneous spike rate vs. the normalized breathing rate. This revealed no systematic relationship between spike rate and breathing rate. In particular, there was no clear relationship between spontaneous spiking rate and breath rate in the cells that showed an increase in spontaneous activity in the Blank stimulation group (arrows). This indicates that breathing changes do not account for the increase in spontaneous activity in the GC-Blank group.

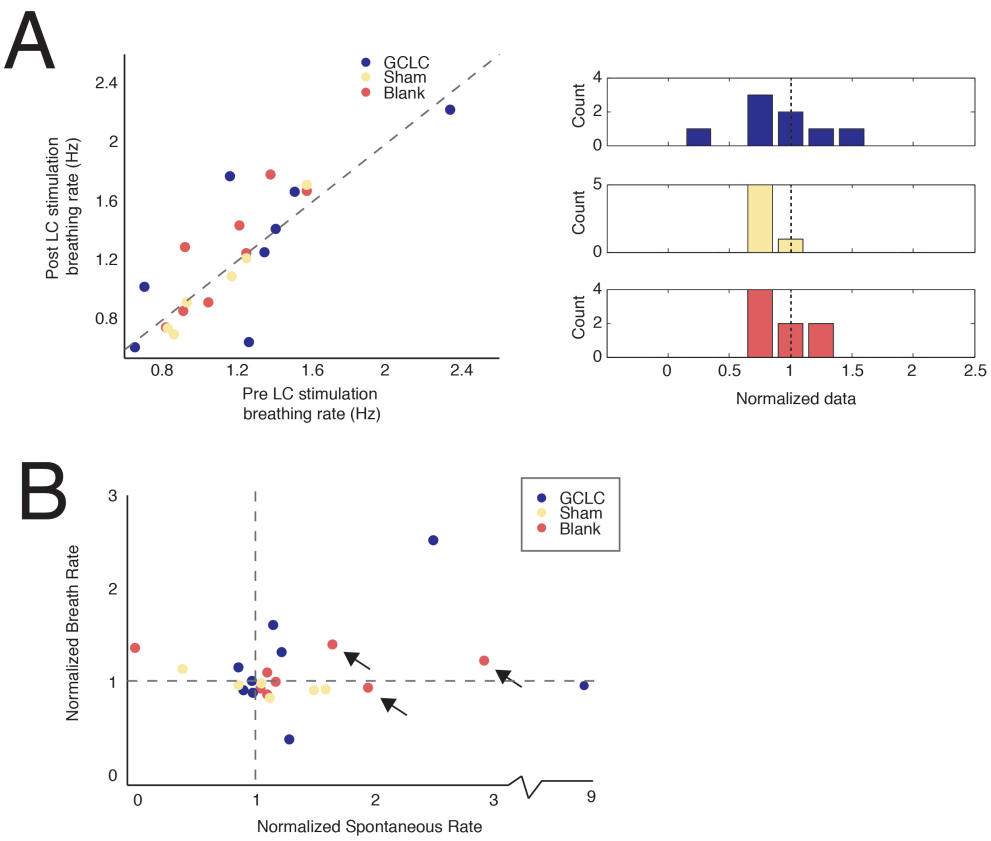

FIGURE B.3: **Breathing changes do not explain changes in spontaneous spike data** (A) Scatter plot (left) and normalized histogram data (right) show that mean breathing rates did not profoundly change between pre and post stimulation periods. Most cells fall close to the unity line or close to 1. (B) Changes in spontaneous spike rate did not correlate with changes in breathing rate. Arrows highlight the GC-Blank cells in which we saw increases in spontaneous firing rate. Note the cells show little differences in breathing changes despite large increases in spontaneous spike rate. Cells/mice for GCLC, Sham, and Blank Groups n = 8,6,8 cells.

B.3.2 Noradrenaline Evoked Changes in GC Odour Responses

We further examined how NA changes the responses of GCs to odours. For each cell, we determined the mean response to an odour on each trial (see methods). From this data, we computed an overall mean response to the odour during both the pre-LC stimulation period and the post-LC stimulation period (Fig.B-4A). When we paired LC stimulation with an odour that evoked a significant response in a GC, we observed both increases and decreases in the odour evoked firing rate (Fig.B-3B). For the most part, responsiveness decreased although the effect was not significant (mean pre response = 1.5 $\pm$ 1.1 spikes/s to mean post response = 1.2 $\pm$ 1.0 spikes/s, p_norm = 0.40). In contrast, we never observed any enhancement in responsiveness in the GC-Sham data. Rather, without LC stimulation, cells showed a significant decrease in their responsiveness to odours (mean pre response = 2.0 $\pm$ 1.3 to mean post reponse = 0.6 $\pm$ 0.8, p_norm = 0.02) suggesting LC stimulation may enhance the responsiveness of a subset of odours. To truly determine this, we need more data.

Contrary to our hypothesis, the GC-LC data differed little from the GC-Blank stimulation data (Fig.B-4B). In fact, some of the largest increases in responses to odours were observed in the blank stimulation data, and driven by these cells, the overall responsiveness of the population non-significantly increased (mean pre blank = 1.4 $\pm$ 1.3 to mean post blank = 2.6 $\pm$ 2.4, p = 1). This suggests any effect of LC stimulation is not specific, but rather, the simple act of NA release in the MOB results in enhanced responsiveness of a subset of cells to odours. Again, given the heterogeneity of the response changes, we would need more data to make any definitive statements about this.

In support of the idea that NA nonspecifically enhances the spiking of a subset of cells, in GC-Blank cells, enhanced responsiveness accompanied enhanced spontaneous rate (Fig.B-4C). There may also be a trend towards a significant correlation (r = 0.67, p = 0.09).

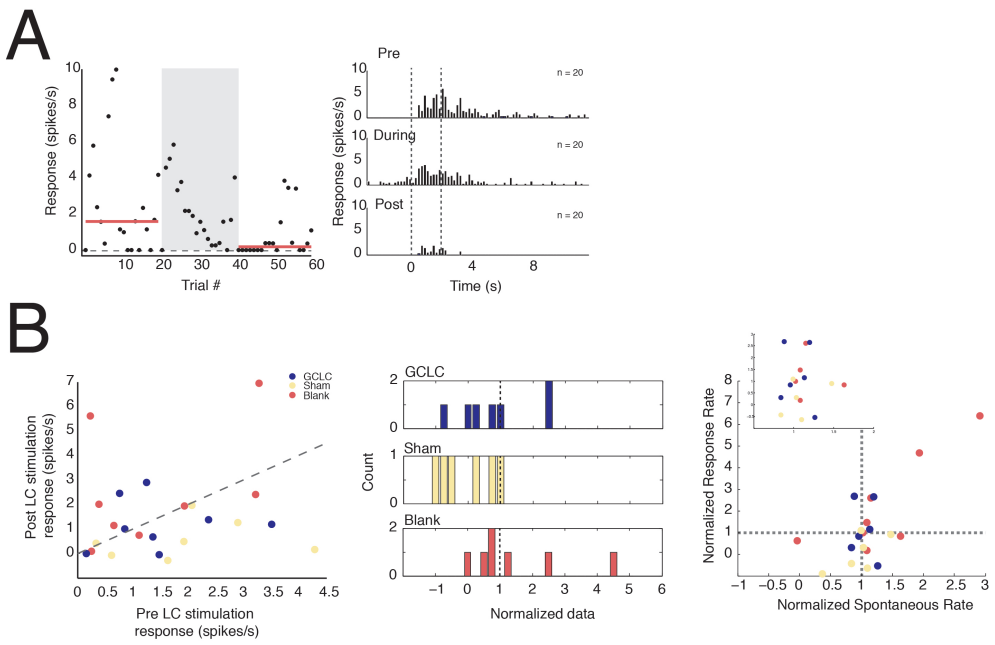

FIGURE B.4: **LC stimulation has complex effects on GC odour evoked responses** (A) Example trial plot and histogram for one cell. On the left, we plot the mean response to odour on each trial (black dots = mean on a trial, red line = mean across an epoch). The grey box denotes the period of LC stimulation. On the right we plot PSTHs for a single cell during each epoch (pre, during, and post LC stimulation). Data are binned in 100 ms bins and computed from 20 trials in each epoch. (B) Summary data for all cells across all three groups. On the left, we plot a scatter plot displaying the mean response during the pre stimulation period against the mean response during the post stimulation period. On the right, we plot the post stimulation data normalized to 1. GC-Sham data showed a significant decrease following LC stimulation (Mann-Whitney, p=0.02) while we observed no significant effects in the GC-Blank or GC-LC groups. (C) Normalized spontaneous rate plotted against the normalized odour evoked response. Inset shows zoomed in data that clusters around x=1 and y=1 on the larger graph. Although not significant, there appears to be some correlation between spontaneous rate changes and odour evoked changes (r = 0.67). n = 8, 7, 8 cells/mice for GCLC, GCSham, and GCBlank respectively.

B.3.3 Noradrenaline Induced Changes in Breath Coupling

Our own data (Chapter 3) suggests that, in anesthetized animals, GCs are breath coupled. However, this coupling breaks down in awake animals. We wondered whether centrifigal inputs, like those from LC, might contribute to this change. If observed, such changes could signal that NA alters the temporal patterns of GCs, an action that could ultimately alter temporal patterns of MTs and phase dependent readouts of activity in higher cortical areas.

We examined both the mean phase and the strength of spike coupling to the breathing cycle (see Methods and Chapter 3). In agreement with our previous results, GC spiking in all groups was significantly coupled to breathing in all groups during the pre stimulation period (baseline coupling r = 0.63 GCLC, 0.75 Sham, 0.68 Blank). Cells tended to fire during a period following the end of inspiration (Fig.B-5A), and there was no difference between baseline and odour evoked mean firing phase in any group (ANOVA, p = 0.2, example Fig.B-5A).

We then examined whether NA significantly altered breath coupled firing or the phase of firing in relation to the breathing cycle. We did not observe any dramatic shifts in phase coupling between the pre-LC stimulation period and the post-LC stimulation period. This was true for all groups examined (Fig.B-5C).

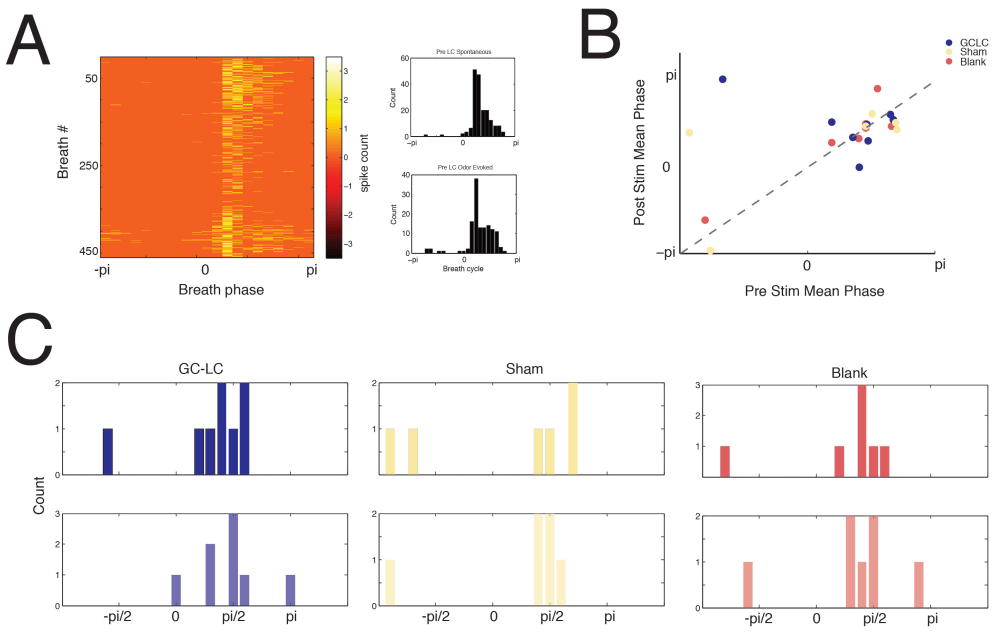

FIGURE B.5: **LC stimulation effects on breath phase coupling** (A) Example 2D breath plot and histogram for one cell. On the left, the histogram shows spike count during a single breath for each breath in a session (452 breaths). Breaths are plotted from -pi to pi with 0 denoting end inspiration. On the right, histogram shows mean breath phase for spikes in a session during both the pre (top) and post (bottom) LC stimulation period. GCs tended to fire in a period immediately following the end of inspiration. (B) Population data for mean phase of firing. Scatter plot depicts the mean firing phase of cells during the breathing cycle prior to LC stimulation vs. the mean firing phase following LC stimulation. Cells tended to cluster around the unity line, and we saw no significant changes in mean phase between the pre and post stimulation period nor did we observe any differences between the groups (ANOVA, p = 0.4) (C) Normalized histograms for three different groups (blue = GC-LC, yellow = GC-Sham, red = GC-Blank). Top panels show the phase coupling prior to LC stimulation and bottom panels show the phase coupling following LC stimulation. Except for a possible shifts to a later phase in the GC-LC (mean phase pre = 0.82 and mean phase post = 1.01, not significant) and GC-Blank groups (mean pre = 0.96 and mean post = 1.45, not significant), groups were similar before and after stimulation. GC-LC, GC-Sham, GC-Blank n = 8, 6, 7 cells.

B.4 Discussion

Although the data set is small, the results above suggest two main effects of NA on GCs in vivo:

- NA activity enhances spontaneous activity in a small subset of GCs.
- NA activity largely reduces the responsiveness of GCs to odours, but it enhances activity in a small subset of GCs. This is true whether or not there is an odour present during the acute release of NA.

None of these effects were particularly strong. This may be for a number of reasons highlighted below.

In our paradigm, the study of noradrenergic influence on GC activity was rate-limited by the experimenter's ability to find GCs with appreciable odour responses. Even with a stimulus set of 40 odours, presentation of odours often failed to evoke responses from identified GCs. This is consistent with the results outlined in Chapter 3 of this thesis in which we showed a profound influence of state on GC activity. In awake animals, GCs display much more dynamic activity. Compared to anesthetized animals, spontaneous spike rates increase and GCs are much more broadly tuned. This increase in activity may provide a more interesting substrate on which to study the effects of a modulator like NA. Given this, it may behoove us to abandon the current NA/GC experiment in favor of studying the influence of NA on MOB in awake mice. While this may be interesting and important, it will not necessarily be straightforward. Locus coeruleus activity is much more dynamic in awake animals, and, depending on the animal's behaviour, it can fire phasic bursts. Thus, the baseline level of NA release in the bulb may vary wildly across one recording session. We may thus have to consider a regime where we record both from LC and GCs at the same time and then correlate GC firing with LC activity. From there, we could consider blocking NA in the bulb while recording from GCs to examine how GC activity changes upon this manipulation.

While it is tempting to speculate that our results may look very different if we conducted our experiments in awake animals, it is also possible that the results described above are real. What then might be happening? With the low number of cells in the dataset in mind,

the most salient effect of NA was that of the NA induced enhancement in responsiveness of some cells in the GC-LC and GC-Blank groups. This effect was never observed when LC was not stimulated as in the GC-Sham group (Fig.B-4B,C). This suggests that in a subset of cells, NA increased the spiking of GCs. Such an effect might work to enhance inhibition of MTs, an effect consistent with our previous data suggesting NA decreases the responsiveness of MTs (Shea, Katz, & Mooney, 2008). Increases in a small subset of cells may provide some specificity to this inhibition whereby the firing in some MTs will be suppressed while others will not. Such incomplete inhibition has been proposed as a mechanism by which to sparsen MT population activity and decorrelate representations amongst similar odours (Koulakov & Rinberg, 2011).

With some caveats, the effect of NA was not specific. We saw suppressed and enhanced activity both when we paired an odour with LC stimulation and when we paired a mineral oil odour with LC stimulation. If real, this non-specificity is puzzling if we think about the effects of NA on the rest of the MOB circuit. At the level of the glomeruli, NA effects tend to be non-specific (Eckmeier & Shea, 2014) while at the level of the MTs, the effects are specific to stimulated odours (Shea, Katz, & Mooney, 2008). In light of the results reported here, these studies may suggest that the specificity arises at the level of the MTs themselves, directly at the local dendrodendritic synapse (with no effect on spiking), or possibly in interneuron populations in the glomerular layer. Future studies await this confirmation. Alternatively, in many of our "Blank" cells, we saw responses to the mineral oil. This could suggest that our blank was not as neutral as we thought, and that in the future, we might have to run a fourth control —- that of no mineral oil or odour — to better tease out the effects of NA.

Overall, the effects reported above suggest an intriguing and dynamic role for NA in the GC circuit. In particular, they suggest complex effects of NA whereby some cells suppress firing to odours following LC stimulation and others enhance firing. What dictates the direction of the change is unknown, but the concentration of NA that a particular GC experiences or the connectivity of a GC in a circuit may play a role. For example, perhaps GCs that receive input a particular pattern of input (timing or strength) from MTs will show enhancements such that GCs preferentially inhibit this specific activity. The effect could be

to suppress a particular subset of MTs that all share the same activity while leaving others MT responses intact.

The larger role GCs and NA play in olfactory learning and memory are still the subject of much study. In particular, few studies have examined how manipulating the activity of GCs in vivo effects habituation memories. Our results suggest that either broad inhibition or broad excitation of GCs could achieve the same effect — disruption of habituation memories — as both manipulations would disrupt some aspect of NA's actions on GCs.

Appendix C

Don't try this at home

C.1 Alternative Tasks on the Ball

In order to study the influence of contextual cues on olfactory bulb GC activity, I ultimately designed a task in which mice learn to associate certain odours with rewarding stimuli (water) and other odours with punishing stimuli (QHCl). While this task has proven fruitful, it was not the first task I tried. Initially, I attempted to examine odour habituation on the ball using sniff frequency as a measure of the animal's interest and memory for an odour. Ultimately, I found such a readout to be inadequate as a measure of habituation. Next, I attempted to condition the mice to associate odours with aversive stimuli in a matter akin to olfactory fear conditioning. While I observed mild effects in freely moving animals, I ultimately did not get this behaviour to work in a mouse running on the ball. Nevertheless, for completeness and in the hopes that others may think twice before attempting such experiments, the results are described below.

C.2 Olfactory Habituation on the Ball

Olfactory habituation describes a form of non-associative olfactory learning whereby an animal's response to an odour decreases with prolonged or repetitive exposure. Tasks designed to test habituation memories involve repeatedly exposing an animal to an odour and testing the animal's exploration/sniffing time upon each re-exposure to the odour. Over time, as the

animal habituates to the odour, it explores the odour for a shorter period. Using a similar task, researchers can also examine the non-associative discrimination capability of an animal. If an animal, upon habituation to one odour, is exposed to another odour, the animal will explore the novel odour for a longer period of time than it will explore the familiar, habituated odour. Similar exploration times are taken as an indication that the animal cannot adequately discriminate between the two odours. Compared to most associative paradigms, olfactory habituation paradigms are easy to implement as learning is fast (interstimulus intervals vary from a few minutes to one day), and the animals do not require any training.

Habituation and non-associative discrimination of odours depends on activity in the MOB. Mitral cells display decreased activity with repetitive odour exposure (Chaudhury et al., 2010). Importantly, this is not a simple densitization of receptor proteins on MTs as, upon exposure to novel odours, MT responding resumes. Performance in these tasks also depends on centrifugal input to the MOB, particularly noradrenergic inputs from locus coeruleus and cholinergic inputs from the nucleus of the horizontal limb of the diagonal band (HDB). Blockade of cholinergic or noradrenergic receptors in the MOB blocks an organism's ability to discriminate amongst odours (Shea, Katz, & Mooney, 2008; Mandairon et al., 2006; Mandairon et al., 2008).

Given the major action of centrifugal inputs on GC activity, I was interested in examining GC activity in non-associative learning tasks. However, I needed to adapt these tasks to a head-fixed preparation as a head-fixed paradigm best permitted us to study GCs using loose-patch techniques. Non-associative tasks use sniffing as a primary measure of habituation/novelty detection, so I decided to examine whether breathing in a head-fixed animal changes in a reliable way upon repetitive exposure to the same odour. Previous experiments in head-fixed mice suggest they do not show classic sniff rates (6-10 Hz) associated with free exploration of the environment. Head-fixed mice instead typically breath at around 2-6 Hz (our own data). Nonetheless, it is possible that the mice modulate their breathing within this range in response to novel and familiar odours.

C.2.1 Methods

I affixed a head-bar to the head of the animal and implanted a cannula in the nasal cavity of an animal as previously described in Chapters 2 and 3. All procedures were conducted in accordance with the National Institutes of Health's Guide for the Care and Use of Laboratory Animals and approved by the Cold Spring Harbor Laboratory Institutional Animal Care and Use Committee. I head-fixed animals in our standard setup (wheel), and I measured breathing using a thermocouple. I presented ten trials of two s long odour stimuli to the animal with inter-stimulus intervals of one min. These timescales were chosen to reflect times used in freely moving tasks in which appreciable habituation memories were reported. I tested animals with three different odours. For sake of clarity, I display data for only one odour in the results. All other odours followed the same trend although overall breathing rate to an odour did differ depending on the odour presented.

C.2.2 Results

I tested breathing habituation in four mice. I examined two features of breathing that I hypothesized might vary with odour habituation: breathing frequency and latency to first breath. I expected breathing frequency might decrease with repeated presentations of the stimulus and that simultaneously, latency to breath might become slower as animals modulated their breathing less.

Mean breathing frequency across all four animals followed a trend whereby breathing to the first odour increased in comparison to subsequent presentations of the same odour. Unfortunately, in single mice, the data were much noisier. While most mice displayed increased rates on the first trial (Fig.C-1A), they did not all decrease their breathing on subsequent trials (Fig.C-1B). Similarly, latency to breath did not follow any clear trend (Fig.C-1C).

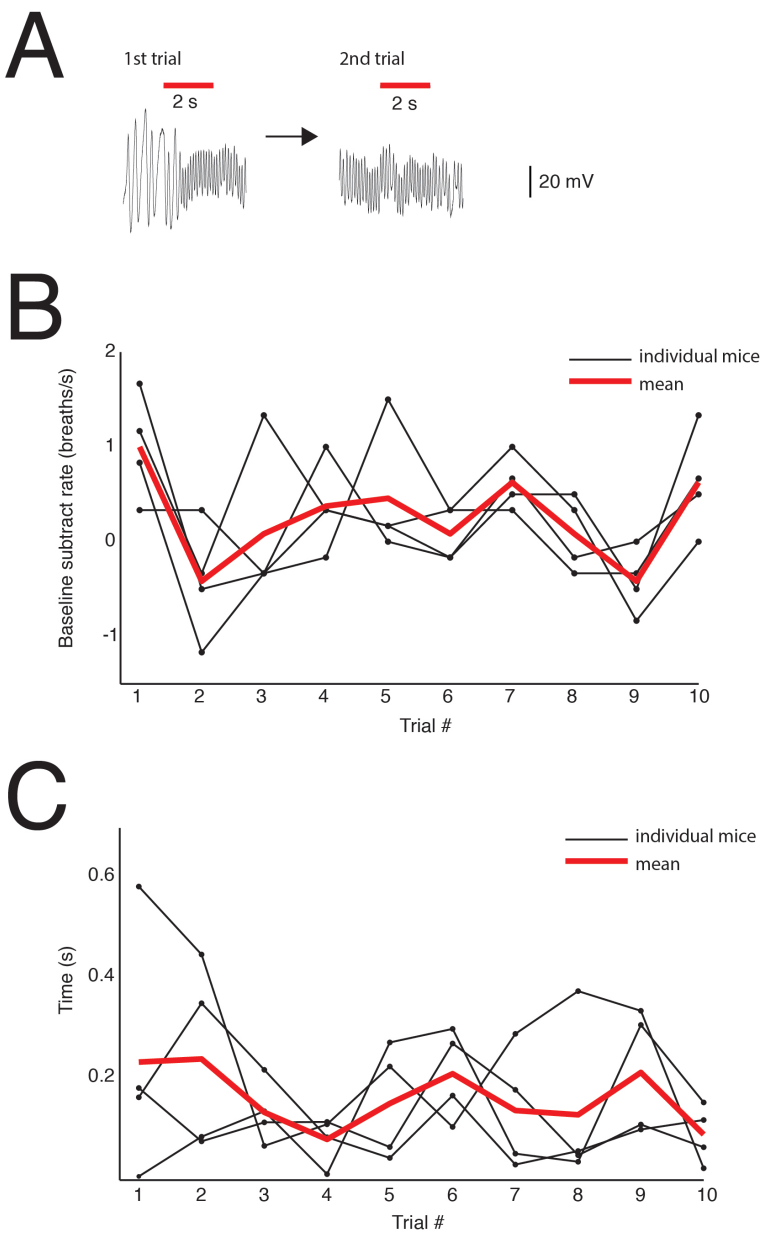

FIGURE C.1: **Breathing rhythms do not indicate olfactory habituation in head-fixed mice.** (A) Example breath traces from one animal during the first and second presentation of an odour. 2 s long odour stimulus denoted by red bar. (B) Mean substracted breath rates across 10 trials of an odour for 4 mice. Mean breath rate across all mice on each trial is plotted in red. (C) Latency to first breath on each trial of an odour. Black lines show individual mice and red lines show mean across all 4 mice.

C.2.3 Discussion

I decided not to use this habituation task. While mice often showed increased breath rates for the first presentation of an odour, sniff frequencies did not change in a reliable way for subsequent odour presentations. This presented us with two problems:

- Given the lack of discernible sniff patterns with repetitive odour stimulation, I would not be able to easily correlate GC activity with a specific pattern of sniffing over time.
- The fast habituation following the first presentation of the odour, while intriguing, ultimately did not provide us with enough power with which to make strong conclusions about GC activity. Odour responses in MTs and GCs are inherently noisy - the same pattern of activity is not evoked by every trial of the same stimulus. Even if I saw strong activity with the first trial of an odour, untangling GC responses to this odour from just the overall noisiness of odour evoked responses would be difficult and require a massive amount of data.

Our failure to observe systematic changes in breathing may relate to the nature of the head-fixation task. In our task, the mouse's nose is always directed at the odour port. As a result, the mouse does not have to work hard or explore to locate an odour — the odour is readily available when triggered. In our hands, spontaneous breathing also varied wildly (Fig.C-1A). In some cases, the spontaneous rate was already at the maximum for breathing rate in head-fixed animals (around 8-10 Hz) while at other times, it was at a minimum (1-2 Hz). Modulations by the mouse thus would have been difficult. In the future, other groups might consider only triggering odour presentation following specific spontaneous breathing frequencies.

Ultimately, I decided to forego any further studies of olfactory habituation in head-fixed mice. However, the results here in no way capture the rich complexity of olfactory habituation tasks. Other groups might conduct more exhaustive explorations of sniffing while varying odour duration and inter-stimulus interval times. Such explorations might prove

more fruitful. For example, evidence from patterns of MT and GC activation in olfactory habituation over several days suggest sniff patterns might be altered at longer timescales (Kato et al., 2012).

C.3 Olfactory Looming Conditioning Task

Several reports suggest the olfactory bulb plays a role in fear conditioning beyond its role in sensation of the odour. Both OSNs and MTs in the bulb respond differentially to conditioned versus unconditioned odours (Kass et al., 2013; Fletcher, 2012). Changes in GC activity likely underlie some of these changes, but GC electrical activity has never been measured during these tasks.

I attempted to create a fear memory in mice running on the wheel in our head-fixed preparation. In freely moving animals, fear conditioning paradigms typically involve foot or tail shocks. These stimuli produce significant behavioural changes in the animal: typically, mice jump violently and then freeze. The violence of the behaviour induced by shock precluded its use in our head-fixed preparation as such stimuli evoked too much movement in the animal and subsequent loss of loose patch seals. As a result, I attempted to use other aversive stimuli in order to induce freezing.

In open field arenas, looming stimuli over the head of the animal evoke long periods of freezing or fleeing to a safe location when such a location is provided (Yilmaz & Meister, 2013). This looming stimulus is thought to mimic overhead predators that mice might experience in the wild, and the observed freezing can often last for tens of seconds — a time period longer than what is often seen with footshock. I reasoned that this looming stimulus might be used for associative conditioning, and that it might be optimal in our case, as if it worked, I could create association memories without having to touch the animal.

To measure changes in in behaviour of the animal in response to looming stimuli, I used a lick suppression task. In these tasks, water deprived animals are continuously provided with small amounts of water. Animals that lick continuously maximize the amount of water they receive. Aversive stimuli like startling tones suppress this continuous licking (Yu et al.,

2016). In our task, I paired looming stimuli with odours and then quantified the amount of lick suppression an animal displayed in response to both the looming stimulus and the odour after pairing with the looming stimulus. I also tested the effectiveness of the looming stimulus for use in fear conditioning in freely moving animals. Unfortunately, while I observed mild effects in the freely moving mice, I failed to see any effect in the head-fixed animals.

C.3.1 Methods

I tested whether I could use a looming stimulus for olfactory conditioning in two different paradigms: a a freely moving mouse paradigm and head-fixed paradigm (Fig.C-2A,B).

Looming stimulus: I presented the looming stimulus on a LED computer screen placed over the animal's head in a manner described previously (Yilmaz & Meister, 2013). The screen was grey while the looming stimulus was a black expanding disc.

Behaviour. In the freely moving paradigm, I tested four mice in an open field arena. The arena was constructed from black plexiglass (30 cm by 30 cm arena) that was open at the top. On top of this arena, I placed the LED computer screen on which to present the looming stimulus. I videotaped the mouse using two cameras — one placed overhead next to the LED screen and another placed at the level of the mouse in one side of the arena. In the habituation phase, I first exposed mice to the odour of interest (1 % odour). The odour was presented from an opening in one side of the arena. During this phase, mouse spent ten min in an open field arena and received ten trials of the odour (20 s long) separated by about one min each. During the conditioning phase, I again presented the odour but this time in the presence of the looming stimulus. For this phase of the paradigm, I only presented odours when the animal entered the centre of the arena as this spot had been shown to be optimal for inducing freezing in loom alone tasks. Odour presentations were again 20 s long, and the looming stimulus coterminated with the odour off time. Mice received five trials of odour+loom. Twenty-four hours later, I tested the animal's memory for the odour loom association. During this testing phase, I presented ten trials of the odour alone to the

animal and manually scored freezing during the odour on periods. For the test phase, I changed the floor of the arena (green stripes on floor) to minimize the effect of context in any freezing I might see. For controls, I tested freezing in animals that were exposed to the looming stimulus alone and to the odour alone during the conditioning phase.

I also examined the discrimination capacity of some mice in the freely moving task. In these mice, all procedures were identical to those described above expect that during the habituation and testing phase, I presented two odours (odour A and odour B). During the conditioning phase, only one of these odours was presented and paired with the looming stimulus. Then, during the testing phase, instead of presented multiple trials of an odour, I instead placed two cotton swabs on opposite ends of the arena. One cotton swab was soaked in a 1 % solution of odour A while the other was soaked in a 1 % solution of odour B. In this way, I could test the discrimination and generalization of freezing behaviour in the event it existed. I expected mice would explore B more and explore A less if they had formed an aversion to odour A.

In the head-fixed paradigm, I examined the lick suppression behaviour of three mice in response to odours paired with looming stimuli. I first water deprived animals to 85 % of their free-water weight and then habituated them to the head-fixed set-up (30 min). Following habituation, I introduced animals to the water spout and trained animals to lick freely and continuously to receive water. To do so, I delivered 1 ms pulses of water (separated by 10 ms) using a solenoid (Lee Company) attached to a 50 ml syringe full of water. This pulse schedule meant that, if a mouse licked continuously for 5 min, they would receive 1 ml of water. Licking was measured as breaks of an infrared beam as described in Chapter 4. Once mice showed continuous licking (at least 2 min of uninterrupted licking), I trained them in the odour loom task. Much like the freely moving paradigm, this task also had a habituation, conditioning, and testing phase. However, I decreased the length of the odour as, in a head-fixed set-up, the mouse sits directly adjacent to the odour tube. Twenty s of odour could thus quickly become aversive on its own. Instead, I presented 6 s stimuli (0.1 % odour concentration) that again co-terminated with the looming stimulus. I also decreased the interstimulus interval time to 1 min. During the habituation trials, I presented two odours. Then, during

the looming period, I presented 10 trials of only one of the habituation odours along with the looming stimulus. During the testing phase, I again presented the two odours from the habituation period and measured the amount of lick suppression to both odours.

To quantify the amount of lick suppression during testing, I only considered the time during the odour period and only considered trials in which the animal was continuously licking prior to odour onset. I had eight trials across all three mice that met the latter criteria because, after eight trials, some of the mice stopped licking completely. This is presumably because they were no longer thirsty. As such, only eight trials are shown in the results. I quantified the amount of freezing as the amount of time not spent licking during the 6 s odour period. To do so, I binned licks in 1 s intervals and then compared the mean number of licks in each bin to mean number of licks in each bin prior to the odour onset. Complete suppression of licking would be quantified as 100 % freezing while no difference in licking in any of the bins would be quantified as 0 % licking compared to the baseline period.

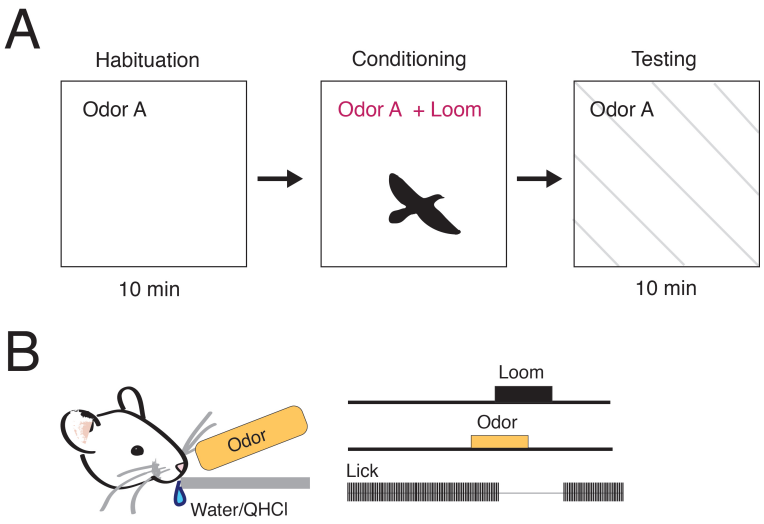

FIGURE C.2: **odour loom behavioural paradigms.** (A) Freely moving paradigm. (B) Head-fixed paradigm.

C.3.2 Results

In the freely moving paradigm, mice that experienced an odour with a looming stimulus displayed increased freezing (Fig.C-3A) compared to controls that experienced either the odour without the looming stimulus or only the looming stimulus during the training period. This indicates that the looming stimulus may work as an aversive stimulus in fear conditioning. However, it is important to keep in mind that, in traditional fear conditioning protocols, the percentage of time mice spend freezing is much larger than I see in the current task. In traditional tasks, freezing is on the order of 60-70 % while I only observed 30 % time spent freezing. In the freely moving discrimination paradigm, I failed to see a difference in exploration time between the conditioned and unconditioned odour (Fig.C-3B). This may be because the animals generalized their aversion of the looming stimulus to all odours or because the mice simply habituated to all of the odours. In the future, tests of this should include a third, never experienced odour during the discrimination test phase.

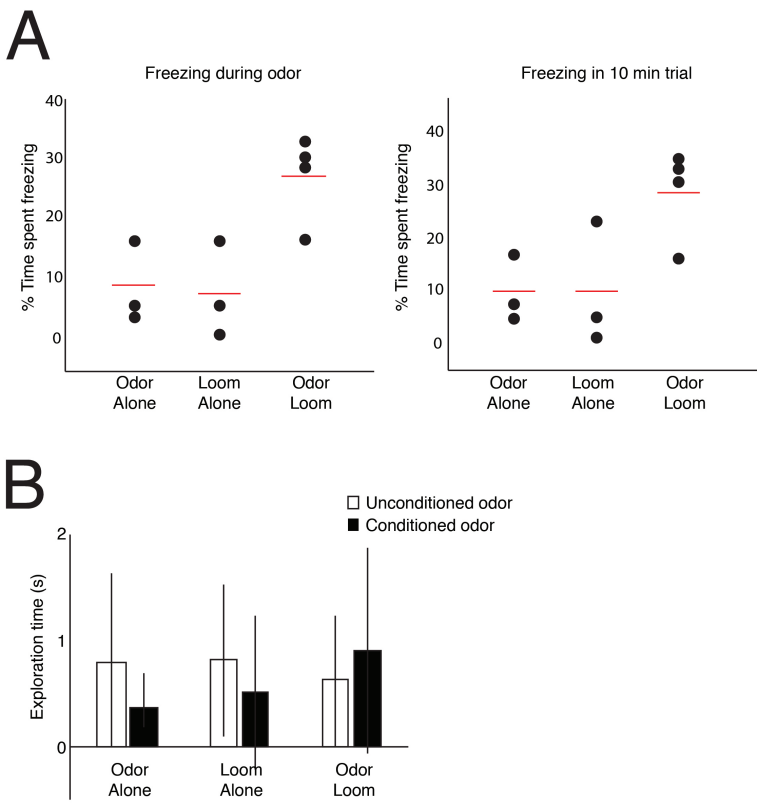

FIGURE C.3: **Mice show some associative memory in an odour loom paradigm but not odour-loom discrimination paradigm.** (A) Freezing to a single odour paired with a looming stimulus. Freely moving mice show increased freezing to an odour paired with a looming stimulus compared to control animals that only experienced either an odour or a looming stimulus during the conditioning phase. This was true if we quantified freezing during only the odour on period and freezing across the entire 10 min trial. Mean freezing times across all mice in a group are shown in red while individual mice freezing times are plotted in black. Animals that experience an odour and loom together explore the loom conditioned odour and the unconditioned odour for equal amounts of time and for similar amounts of time as control mice. n = 3 mice.

While I saw a mild effect of the odour-loom paradigm in freely moving mice, I could not replicate this effect in head-fixed mice. I expected mice would suppress their licking during the loom-associated odour, but they did not. Mice did not even suppress licking during the conditioning phase (Fig.C-4A). During these trials, while the mice stopped licking on the first trial of a stimulus, they resumed licking for all other trials. I further did not see lick suppression when I tested the mice to the odour alone following the odour-loom conditioning phase (Fig.C-4B). Subsequent sessions with 10 s odours and 20 s odours along with multiple presentations of the looming stimulus during a single odour stimulus did improve our results (data not shown).

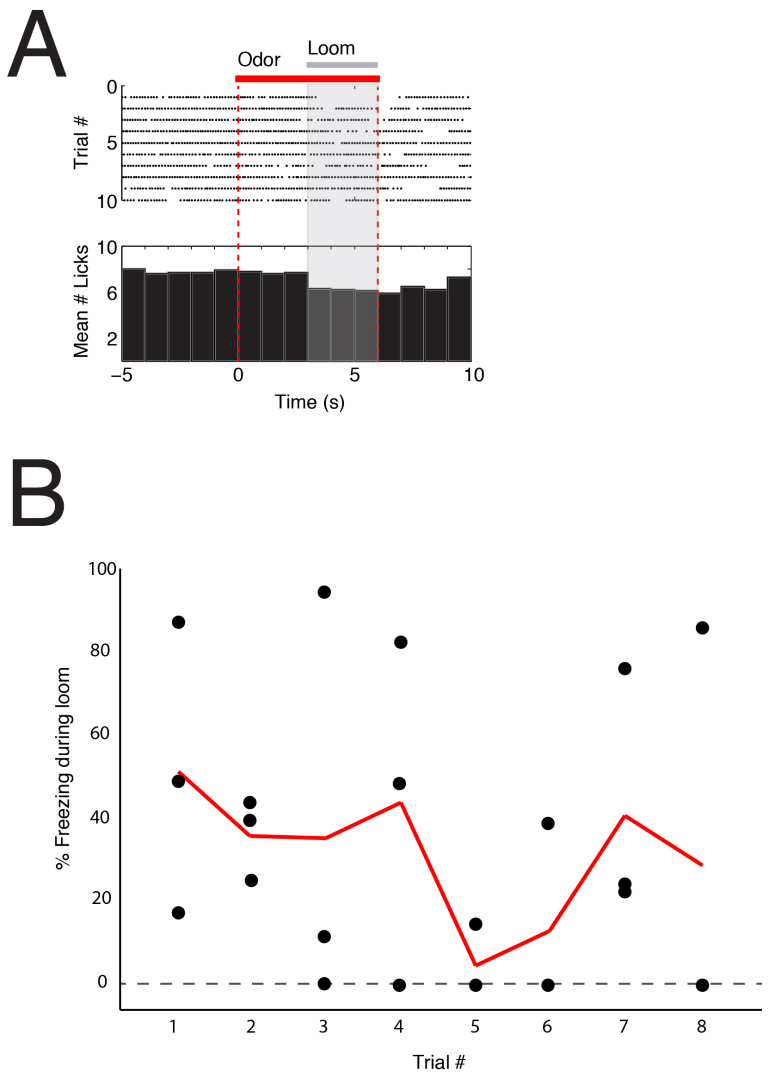

FIGURE C.4: **Mice do not suppress licking in response to an odour paired with a looming stimulus.** (A) Raster and mean lick histogram for a single mouse during looming phase of a trial. On the top, each row is a trial and ta single black dot represents a single lick. Red and grey lines show the odour and loom on periods respectively. Histogram is binned in 1 s bins and shows the mean number of licks in a bin. (B) Freezing percentage across 8 trials of 3 mice. Mean freezing percentage is shown in red while data for single mice are shown as black circles. While some mice froze to the loom, this was not true for all mice and not consistent across trials.

C.3.3 Discussion

For the most part, the odour-loom paradigms were a failure in my hands. I saw only a weak effect in the freely moving animals and failed to see any effect in the head-fixed animals.

The weak effect in the freely moving animals may reflect several variables. First, while I tried to present the odour and loom when the animal was in the centre of the arena, I could not always do so. Often, while the animal was in the centre of the arena when the the odour stimulus started, the animal had already left the centre when the subsequent looming stimulus began. Future iterations of the stimulus loom pairing might shorten the odour time to better catch the animal when it is in the arena centre. The weak affect may also reflect the fact that the looming stimulus is simply a weaker aversive stimulus than a footshock. A footshock is both unexpected and potentially painful while a looming stimulus lacks the painful component.

My failure to observe an effect in the head-fixed paradigm likely reflects a blurring of motivational states. While the mice might have been motivated to suppress licking, they were more motivated to receive water. Thus, they habituated quickly to the loom.

C.4 Overall Discussion

Ultimately, I did not end up using the habituation paradigm or the odour-loom paradigm for explorations of GC activity during learning. Neither paradigm produced robust enough results to merit its use. Instead, I switched to an olfactory conditioning/discrimination paradigm in which I paired some odours with a rewarding water stimulus and other odours with a punishing QHCl stimulus. While this stimulus ultimately involved more training than I would have liked, it did produce more reliable results across mice.

The paradigms described above serve as a lesson that not everything one tries during a PhD can be used for further gains. However, I would like to stress that while I did not continue with these paradigms, this should not mean that future iterations of these paradigms

will not work. I did not exhaust the possibilities for odours nor the possibilities for odour-loom pairings, so other investigators who invest more time and effort, might see different results. The only information that can be gleaned from this data is that the paradigms did not work in my hands in the manner that I used them.

Bibliography

Abraham, Nixon M et al. (2010). Synaptic inhibition in the olfactory bulb accelerates odor discrimination in mice. *Neuron* **65**: 399–411.

Apicella, Alfonso et al. (2010). Pyramidal cells in piriform cortex receive convergent input from distinct olfactory bulb glomeruli. *J Neurosci* **30**: 14255–60.

Arevian, Armen C, Vikrant Kapoor, & Nathaniel N Urban (2008). Activity-dependent gating of lateral inhibition in the mouse olfactory bulb. *Nat Neurosci* **11**: 80–7.

Bathellier, Brice et al. (2008). Dynamic ensemble odor coding in the mammalian olfactory bulb: sensory information at different timescales. *Neuron* **57**: 586–98.

Belluscio, L & L C Katz (2001). Symmetry, stereotypy, and topography of odorant representations in mouse olfactory bulbs. *J Neurosci* **21**: 2113–22.

Belluscio, Leonardo et al. (2002). Odorant receptors instruct functional circuitry in the mouse olfactory bulb. *Nature* **419**: 296–300.

Berens, P. (2009). CircStat: A MATLAB Toolbox for Circular Statistics. *Journal of Statistical Software* **31**: 1–21.

Beshel, Jennifer, Nancy Kopell, & Leslie M Kay (2007). Olfactory bulb gamma oscillations are enhanced with task demands. *J Neurosci* **27**: 8358–65.

Bouret, Sebastien & Susan J Sara (2005). Network reset: a simplified overarching theory of locus coeruleus noradrenaline function. *Trends Neurosci* **28**: 574–82.

Boyd, Alison M et al. (2012). Cortical feedback control of olfactory bulb circuits. *Neuron* **76**: 1161–74.

Bozza, Thomas et al. (2004). In vivo imaging of neuronal activity by targeted expression of a genetically encoded probe in the mouse. *Neuron* **42**: 9–21.

Brea, Jorge N, Leslie M Kay, & Nancy J Kopell (2009). Biophysical model for gamma rhythms in the olfactory bulb via subthreshold oscillations. *Proc Natl Acad Sci U S A* **106**: 21954–9.

Brennan, P A & E B Keverne (1997). Neural mechanisms of mammalian olfactory learning. *Prog Neurobiol* **51**: 457–81.

Brennan, P A et al. (1998). Changes in neurotransmitter release in the main olfactory bulb following an olfactory conditioning procedure in mice. *Neuroscience* **87**: 583–90.

Buck, L & R Axel (1991). A novel multigene family may encode odorant receptors: a molecular basis for odor recognition. *Cell* **65**: 175–87.

Cameron, Jameason D, Gary S Goldfield, & Éric Doucet (2012). Fasting for 24 h improves nasal chemosensory performance and food palatability in a related manner. *Appetite* **58**: 978–81.

Cang, Jianhua & Jeffry S Isaacson (2003). In vivo whole-cell recording of odor-evoked synaptic transmission in the rat olfactory bulb. *J Neurosci* **23**: 4108–16.

Cardin, Jessica A et al. (2009). Driving fast-spiking cells induces gamma rhythm and controls sensory responses. *Nature* **459**: 663–7.

Cazakoff, Brittany N et al. (2014). Broadly tuned and respiration-independent inhibition in the olfactory bulb of awake mice. *Nat Neurosci* **17**: 569–76.

Chaput, M & A Holley (1980). Single unit responses of olfactory bulb neurones to odour presentation in awake rabbits. *J Physiol (Paris)* **76**: 551–8.

Chaudhury, Dipesh et al. (2010). Olfactory bulb habituation to odor stimuli. *Behav Neurosci* **124**: 490–9.

Chen, W R, W Xiong, & G M Shepherd (2000). Analysis of relations between NMDA receptors and GABA release at olfactory bulb reciprocal synapses. *Neuron* **25**: 625–33.

Ciombor, K J, M Ennis, & M T Shipley (1999). Norepinephrine increases rat mitral cell excitatory responses to weak olfactory nerve input via alpha-1 receptors in vitro. *Neuroscience* **90**: 595–606.

Cury, Kevin M & Naoshige Uchida (2010). Robust odor coding via inhalation-coupled transient activity in the mammalian olfactory bulb. *Neuron* **68**: 570–85.

David, François et al. (2015). Competing Mechanisms of Gamma and Beta Oscillations in the Olfactory Bulb Based on Multimodal Inhibition of Mitral Cells Over a Respiratory Cycle. *eNeuro* **2**.

Davison, Ian G & Michael D Ehlers (2011). Neural circuit mechanisms for pattern detection and feature combination in olfactory cortex. *Neuron* **70**: 82–94.

Davison, Ian G & Lawrence C Katz (2007). Sparse and selective odor coding by mitral/tufted neurons in the main olfactory bulb. *J Neurosci* **27**: 2091–101.

Day, H E et al. (1997). Distribution of alpha 1a-, alpha 1b- and alpha 1d-adrenergic receptor mRNA in the rat brain and spinal cord. *J Chem Neuroanat* **13**: 115–39.

Devore, Sasha, Licurgo de Almeida, & Christiane Linster (2014). Distinct roles of bulbar muscarinic and nicotinic receptors in olfactory discrimination learning. *J Neurosci* **34**: 11244–60.

Devore, Sasha & Christiane Linster (2012). Noradrenergic and cholinergic modulation of olfactory bulb sensory processing. *Front Behav Neurosci* **6**: 52.

DeWeese, Michael R (2007). Whole-cell recording in vivo. *Curr Protoc Neurosci* **Chapter 6**: Unit 6.22.

Dhawale, Ashesh K et al. (2010). Non-redundant odor coding by sister mitral cells revealed by light addressable glomeruli in the mouse. *Nat Neurosci* **13**: 1404–12.

Domyancic, A V & D A Morilak (1997). Distribution of alpha1A adrenergic receptor mRNA in the rat brain visualized by in situ hybridization. *J Comp Neurol* **386**: 358–78.

Doucette, Wilder, Julie Milder, & Diego Restrepo (2007). Adrenergic modulation of olfactory bulb circuitry affects odor discrimination. *Learn Mem* **14**: 539–47.

Doucette, Wilder & Diego Restrepo (2008). Profound context-dependent plasticity of mitral cell responses in olfactory bulb. *PLoS Biol* **6**: e258.

Doucette, Wilder et al. (2011). Associative cortex features in the first olfactory brain relay station. *Neuron* **69**: 1176–87.

Eckmeier, Dennis & Stephen D Shea (2014). Noradrenergic plasticity of olfactory sensory neuron inputs to the main olfactory bulb. *J Neurosci* **34**: 15234–43.

Egger, Veronica (2008). Synaptic sodium spikes trigger long-lasting depolarizations and slow calcium entry in rat olfactory bulb granule cells. *Eur J Neurosci* **27**: 2066–75.

Egger, Veronica, Karel Svoboda, & Zachary F Mainen (2003). Mechanisms of lateral inhibition in the olfactory bulb: efficiency and modulation of spike-evoked calcium influx into granule cells. *J Neurosci* **23**: 7551–8.

— (2005). Dendrodendritic synaptic signals in olfactory bulb granule cells: local spine boost and global low-threshold spike. *J Neurosci* **25**: 3521–30.

Escanilla, Olga et al. (2012). Noradrenergic but not cholinergic modulation of olfactory bulb during processing of near threshold concentration stimuli. *Behav Neurosci* **126**: 720–8.

Fantana, Antoniu L, Edward R Soucy, & Markus Meister (2008). Rat olfactory bulb mitral cells receive sparse glomerular inputs. *Neuron* **59**: 802–14.

Fee, Michale S & Michael A Long (2011). New methods for localizing and manipulating neuronal dynamics in behaving animals. *Curr Opin Neurobiol* **21**: 693–700.

Fletcher, Max L (2012). Olfactory aversive conditioning alters olfactory bulb mitral/tufted cell glomerular odor responses. *Front Syst Neurosci* **6**: 16.

Fletcher, Max L & Wei R Chen (2010). Neural correlates of olfactory learning: Critical role of centrifugal neuromodulation. *Learn Mem* **17**: 561–70.

Frederick, Donald E et al. (2016). Gamma and Beta Oscillations Define a Sequence of Neurocognitive Modes Present in Odor Processing. *J Neurosci* **36**: 7750–67.

Friedrich, R W & G Laurent (2001). Dynamic optimization of odor representations by slow temporal patterning of mitral cell activity. *Science* **291**: 889–94.

Fuentes, Romulo A et al. (2008). Neuronal activity of mitral-tufted cells in awake rats during passive and active odorant stimulation. *J Neurophysiol* **100**: 422–30.

Fukunaga, Izumi et al. (2012). Two distinct channels of olfactory bulb output. *Neuron* **75**: 320–9.

Fukunaga, Izumi et al. (2014). Independent control of gamma and theta activity by distinct interneuron networks in the olfactory bulb. *Nat Neurosci* **17**: 1208–16.

Funk, D & S Amir (2000). Enhanced fos expression within the primary olfactory and limbic pathways induced by an aversive conditioned odor stimulus. *Neuroscience* **98**: 403–6.

Gao, Yuan & Ben W Strowbridge (2009). Long-term plasticity of excitatory inputs to granule cells in the rat olfactory bulb. *Nat Neurosci* **12**: 731–3.

Garcia, Paul S, Scott E Kolesky, & Andrew Jenkins (2010). General anesthetic actions on GABA(A) receptors. *Curr Neuropharmacol* **8**: 2–9.

Gentet, Luc J et al. (2012). Unique functional properties of somatostatin-expressing GABAergic neurons in mouse barrel cortex. *Nat Neurosci* **15**: 607–12.

Gilbert, Charles D & Mariano Sigman (2007). Brain states: top-down influences in sensory processing. *Neuron* **54**: 677–96.

Gire, David H et al. (2013). Information for decision-making and stimulus identification is multiplexed in sensory cortex. *Nat Neurosci* **16**: 991–3.

Giridhar, Sonya & Nathaniel N Urban (2012). Mechanisms and benefits of granule cell latency coding in the mouse olfactory bulb. *Front Neural Circuits* **6**: 40.

Gschwend, Olivier et al. (2015). Neuronal pattern separation in the olfactory bulb improves odor discrimination learning. *Nat Neurosci* **18**: 1474–82.

Guérin, Delphine et al. (2008). Noradrenergic neuromodulation in the olfactory bulb modulates odor habituation and spontaneous discrimination. *Behav Neurosci* **122**: 816–26.

Haddad, Rafi et al. (2013). Olfactory cortical neurons read out a relative time code in the olfactory bulb. *Nat Neurosci* **16**: 949–57.

Haider, Bilal, Michael Häusser, & Matteo Carandini (2013). Inhibition dominates sensory responses in the awake cortex. *Nature* **493**: 97–100.

Halabisky, B et al. (2000). Calcium influx through NMDA receptors directly evokes GABA release in olfactory bulb granule cells. *J Neurosci* **20**: 5124–34.

Hayar, A et al. (2001). Direct excitation of mitral cells via activation of alpha1-noradrenergic receptors in rat olfactory bulb slices. *J Neurophysiol* **86**: 2173–82.

Hegdé, Jay & David C Van Essen (2005). Role of primate visual area V4 in the processing of 3-D shape characteristics defined by disparity. *J Neurophysiol* **94**: 2856–66.

Heinbockel, Thomas & Ze-Jun Wang (2016). Cellular Mechanisms of Action of Drug Abuse on Olfactory Neurons. *Int J Environ Res Public Health* **13**: ijerph13010005.

Igarashi, Kei M et al. (2012). Parallel mitral and tufted cell pathways route distinct odor information to different targets in the olfactory cortex. *J Neurosci* **32**: 7970–85.

Illig, Kurt R & Lewis B Haberly (2003). Odor-evoked activity is spatially distributed in piriform cortex. *J Comp Neurol* **457**: 361–73.

Isaacson, J S & B W Strowbridge (1998). Olfactory reciprocal synapses: dendritic signaling in the CNS. *Neuron* **20**: 749–61.

Jahr, C E & R A Nicoll (1980). Dendrodendritic inhibition: demonstration with intracellular recording. *Science* **207**: 1473–5.

— (1982a). An intracellular analysis of dendrodendritic inhibition in the turtle in vitro olfactory bulb. *J Physiol* **326**: 213–34.

— (1982b). Noradrenergic modulation of dendrodendritic inhibition in the olfactory bulb. *Nature* **297**: 227–9.

Jiang, M et al. (1996). Activation of locus coeruleus enhances the responses of olfactory bulb mitral cells to weak olfactory nerve input. *J Neurosci* **16**: 6319–29.

Kass, Marley D et al. (2013). Fear learning enhances neural responses to threat-predictive sensory stimuli. *Science* **342**: 1389–92.

Kato, Hiroyuki K et al. (2012). Dynamic sensory representations in the olfactory bulb: modulation by wakefulness and experience. *Neuron* **76**: 962–75.

Kato, Hiroyuki K et al. (2013). Parvalbumin-expressing interneurons linearly control olfactory bulb output. *Neuron* **80**: 1218–31.

Kay, L M & G Laurent (1999). Odor- and context-dependent modulation of mitral cell activity in behaving rats. *Nat Neurosci* **2**: 1003–9.

Kay, Leslie M & Jennifer Beshel (2010). A beta oscillation network in the rat olfactory system during a 2-alternative choice odor discrimination task. *J Neurophysiol* **104**: 829–39.

Kay, Leslie M et al. (2009). Olfactory oscillations: the what, how and what for. *Trends Neurosci* **32**: 207–14.

Kebschull, Justus M et al. (2016). High-Throughput Mapping of Single-Neuron Projections by Sequencing of Barcoded RNA. *Neuron* **91**: 975–87.

Kepecs, Adam & Gordon Fishell (2014). Interneuron cell types are fit to function. *Nature* **505**: 318–26.

Kepecs, Adam, Naoshige Uchida, & Zachary F Mainen (2007). Rapid and precise control of sniffing during olfactory discrimination in rats. *J Neurophysiol* **98**: 205–13.

Kermen, Florence et al. (2016). Topographical representation of odor hedonics in the olfactory bulb. *Nat Neurosci* **19**: 876–8.

Khan, Adil G, Mukund Thattai, & Upinder S Bhalla (2008). Odor representations in the rat olfactory bulb change smoothly with morphing stimuli. *Neuron* **57**: 571–85.

Knudsen, E I, S du Lac, & S D Esterly (1987). Computational maps in the brain. *Annu Rev Neurosci* **10**: 41–65.

Ko, Kang I et al. (2015). Starvation promotes concerted modulation of appetitive olfactory behavior via parallel neuromodulatory circuits. *Elife* **4**.

Koulakov, Alexei, Alan Gelperin, & Dmitry Rinberg (2007). Olfactory coding with all-or-nothing glomeruli. *J Neurophysiol* **98**: 3134–42.

Koulakov, Alexei A & Dmitry Rinberg (2011). Sparse incomplete representations: a potential role of olfactory granule cells. *Neuron* **72**: 124–36.

Kuchibhotla, Kishore V et al. (2016). Parallel processing by cortical inhibition enables context-dependent behavior. *Nat Neurosci*.

Lagier, Samuel, Alan Carleton, & Pierre-Marie Lledo (2004). Interplay between local GABAergic interneurons and relay neurons generates gamma oscillations in the rat olfactory bulb. *J Neurosci* **24**: 4382–92.

Lepousez, Gabriel & Pierre-Marie Lledo (2013). Odor discrimination requires proper olfactory fast oscillations in awake mice. *Neuron* **80**: 1010–24.

Lima, Susana Q et al. (2009). PINP: a new method of tagging neuronal populations for identification during in vivo electrophysiological recording. *PLoS One* **4**: e6099.

Macrides, F & S L Chorover (1972). Olfactory bulb units: activity correlated with inhalation cycles and odor quality. *Science* **175**: 84–7.

Mandairon, Nathalie et al. (2006). Cholinergic modulation in the olfactory bulb influences spontaneous olfactory discrimination in adult rats. *Eur J Neurosci* **24**: 3234–44.

Mandairon, Nathalie et al. (2008). Noradrenergic modulation in the olfactory bulb influences spontaneous and reward-motivated discrimination, but not the formation of habituation memory. *Eur J Neurosci* **27**: 1210–9.

Manella, Laura C, Samuel Alperin, & Christiane Linster (2013). Stressors impair odor recognition memory via an olfactory bulb-dependent noradrenergic mechanism. *Front Integr Neurosci* **7**: 97.

Markopoulos, Foivos et al. (2012). Functional properties of cortical feedback projections to the olfactory bulb. *Neuron* **76**: 1175–88.

Martin, Claire & Nadine Ravel (2014). Beta and gamma oscillatory activities associated with olfactory memory tasks: different rhythms for different functional networks? *Front Behav Neurosci* **8**: 218.

Martin, Claire et al. (2004). Learning modulation of odor-induced oscillatory responses in the rat olfactory bulb: a correlate of odor recognition? *J Neurosci* **24**: 389–97.

Martin, Claire et al. (2006). Learning-induced oscillatory activities correlated to odour recognition: a network activity. *Eur J Neurosci* **23**: 1801–10.

McGinley, Matthew J et al. (2015). Waking State: Rapid Variations Modulate Neural and Behavioral Responses. *Neuron* **87**: 1143–61.

McLean, J H & M T Shipley (1991). Postnatal development of the noradrenergic projection from locus coeruleus to the olfactory bulb in the rat. *J Comp Neurol* **304**: 467–77.

McLean, J H et al. (1989). Chemoanatomical organization of the noradrenergic input from locus coeruleus to the olfactory bulb of the adult rat. *J Comp Neurol* **285**: 339–49.

Meredith, M (1986). Patterned response to odor in mammalian olfactory bulb: the influence of intensity. *J Neurophysiol* **56**: 572–97.

Miura, Keiji, Zachary F Mainen, & Naoshige Uchida (2012). Odor representations in olfactory cortex: distributed rate coding and decorrelated population activity. *Neuron* **74**: 1087–98.

Miyamichi, Kazunari et al. (2005). Continuous and overlapping expression domains of odorant receptor genes in the olfactory epithelium determine the dorsal/ventral positioning of glomeruli in the olfactory bulb. *J Neurosci* **25**: 3586–92.

Miyamichi, Kazunari et al. (2011). Cortical representations of olfactory input by trans-synaptic tracing. *Nature* **472**: 191–6.

Miyamichi, Kazunari et al. (2013). Dissecting local circuits: parvalbumin interneurons underlie broad feedback control of olfactory bulb output. *Neuron* **80**: 1232–45.

Mombaerts, Peter (2004). Odorant receptor gene choice in olfactory sensory neurons: the one receptor-one neuron hypothesis revisited. *Curr Opin Neurobiol* **14**: 31–6.

Mouly, A M, A Elaagouby, & N Ravel (1995). A study of the effects of noradrenaline in the rat olfactory bulb using evoked field potential response. *Brain Res* **681**: 47–57.

Mouret, Aurélie, Kerren Murray, & Pierre-Marie Lledo (2009). Centrifugal drive onto local inhibitory interneurons of the olfactory bulb. *Ann N Y Acad Sci* **1170**: 239–54.

Murthy, Venkatesh N (2011). Olfactory maps in the brain. *Annu Rev Neurosci* **34**: 233–58.

Nabavi, Sadegh et al. (2014). Engineering a memory with LTD and LTP. *Nature* **511**: 348–52.

Nai, Q et al. (2010). Activation of alpha1 and alpha2 noradrenergic receptors exert opposing effects on excitability of main olfactory bulb granule cells. *Neuroscience* **169**: 882–92.

Nai, Qiang et al. (2009). Noradrenergic regulation of GABAergic inhibition of main olfactory bulb mitral cells varies as a function of concentration and receptor subtype. *J Neurophysiol* **101**: 2472–84.

Niell, Cristopher M & Michael P Stryker (2008). Highly selective receptive fields in mouse visual cortex. *J Neurosci* **28**: 7520–36.

— (2010). Modulation of visual responses by behavioral state in mouse visual cortex. *Neuron* **65**: 472–9.

Nunes, Daniel & Thomas Kuner (2015). Disinhibition of olfactory bulb granule cells accelerates odour discrimination in mice. *Nat Commun* **6**: 8950–.

Nunez-Parra, Alexia, Anan Li, & Diego Restrepo (2014). Coding odor identity and odor value in awake rodents. *Prog Brain Res* **208**: 205–22.

Osinski, Bolesław L & Leslie M Kay (2016). Granule cell excitability regulates gamma and beta oscillations in a model of the olfactory bulb dendrodendritic microcircuit. *J Neurophysiol* **116**: 522–39.

Otazu, Gonzalo H et al. (2009). Engaging in an auditory task suppresses responses in auditory cortex. *Nat Neurosci* **12**: 646–54.

Otazu, Gonzalo H et al. (2015). Cortical Feedback Decorrelates Olfactory Bulb Output in Awake Mice. *Neuron* **86**: 1461–77.

Pager, J et al. (1972). A selective control of olfactory bulb electrical activity in relation to food deprivation and satiety in rats. *Physiol Behav* **9**: 573–9.

Pakan, Janelle Mp et al. (2016). Behavioral-state modulation of inhibition is context-dependent and cell type specific in mouse visual cortex. *Elife* **5**.

Petersen, Carl C H & Sylvain Crochet (2013). Synaptic computation and sensory processing in neocortical layer 2/3. *Neuron* **78**: 28–48.

Picciotto, Marina R, Michael J Higley, & Yann S Mineur (2012). Acetylcholine as a neuromodulator: cholinergic signaling shapes nervous system function and behavior. *Neuron* **76**: 116–29.

Polack, Pierre-Olivier, Jonathan Friedman, & Peyman Golshani (2013). Cellular mechanisms of brain state-dependent gain modulation in visual cortex. *Nat Neurosci* **16**: 1331–9.

Poort, Jasper et al. (2015). Learning Enhances Sensory and Multiple Non-sensory Representations in Primary Visual Cortex. *Neuron* **86**: 1478–90.

Pressler, R Todd & Ben W Strowbridge (2006). Blanes cells mediate persistent feedforward inhibition onto granule cells in the olfactory bulb. *Neuron* **49**: 889–904.

Price, J L & T P Powell (1970). The synaptology of the granule cells of the olfactory bulb. *J Cell Sci* **7**: 125–55.

Rall, W et al. (1966). Dendrodendritic synaptic pathway for inhibition in the olfactory bulb. *Exp Neurol* **14**: 44–56.

Ravel, Nadine et al. (2003). Olfactory learning modifies the expression of odour-induced oscillatory responses in the gamma (60-90 Hz) and beta (15-40 Hz) bands in the rat olfactory bulb. *Eur J Neurosci* **17**: 350–8.

Rinberg, Dmitry & Alan Gelperin (2006). Olfactory neuronal dynamics in behaving animals. *Semin Cell Dev Biol* **17**: 454–61.

Rinberg, Dmitry, Alex Koulakov, & Alan Gelperin (2006). Sparse odor coding in awake behaving mice. *J Neurosci* **26**: 8857–65.

Robertson, Sabrina D et al. (2013). Developmental origins of central norepinephrine neuron diversity. *Nat Neurosci* **16**: 1016–23.

Rokni, Dan et al. (2014). An olfactory cocktail party: figure-ground segregation of odorants in rodents. *Nat Neurosci* **17**: 1225–32.

Root, Cory M et al. (2011). Presynaptic facilitation by neuropeptide signaling mediates odor-driven food search. *Cell* **145**: 133–44.

Royet, J P et al. (1987). Specificity of spatial patterns of glomerular activation in the mouse olfactory bulb: computer-assisted image analysis of 2-deoxyglucose autoradiograms. *Brain Res* **417**: 1–11.

Rubin, B D & L C Katz (1999). Optical imaging of odorant representations in the mammalian olfactory bulb. *Neuron* **23**: 499–511.

Sara, Susan J (2009). The locus coeruleus and noradrenergic modulation of cognition. *Nat Rev Neurosci* **10**: 211–23.

Schneider, David M, Anders Nelson, & Richard Mooney (2014). A synaptic and circuit basis for corollary discharge in the auditory cortex. *Nature* **513**: 189–94.

Schneider, S P & F Macrides (1978). Laminar distributions of internuerons in the main olfactory bulb of the adult hamster. *Brain Res Bull* **3**: 73–82.

Schoenfeld, Thomas A & Thomas A Cleland (2005). The anatomical logic of smell. *Trends Neurosci* **28**: 620–7.

Schoppa, N E (2006). A novel local circuit in the olfactory bulb involving an old short-axon cell. *Neuron* **49**: 783–4.

Schoppa, N E et al. (1998). Dendrodendritic inhibition in the olfactory bulb is driven by NMDA receptors. *J Neurosci* **18**: 6790–802.

Schwarz, Lindsay A et al. (2015). Viral-genetic tracing of the input-output organization of a central noradrenaline circuit. *Nature* **524**: 88–92.

Scott, J W, J K McDonald, & J L Pemberton (1987). Short axon cells of the rat olfactory bulb display NADPH-diaphorase activity, neuropeptide Y-like immunoreactivity, and somatostatin-like immunoreactivity. *J Comp Neurol* **260**: 378–91.

Shea, Stephen D, Lawrence C Katz, & Richard Mooney (2008). Noradrenergic induction of odor-specific neural habituation and olfactory memories. *J Neurosci* **28**: 10711–9.

Shepherd, Gordon M et al. (2007). The olfactory granule cell: from classical enigma to central role in olfactory processing. *Brain Res Rev* **55**: 373–82.

Shusterman, Roman et al. (2011). Precise olfactory responses tile the sniff cycle. *Nat Neurosci* **14**: 1039–44.

Sleigh, Jamie et al. (2014). Ketamine–More mechanisms of action than just NMDA blockade. *Trends in Anaesthesia and Critical Care* **4**: 76–81.

Smear, Matthew et al. (2011). Perception of sniff phase in mouse olfaction. *Nature* **479**: 397–400.

Smith, Richard S, Christopher J Weitz, & Ricardo C Araneda (2009). Excitatory actions of noradrenaline and metabotropic glutamate receptor activation in granule cells of the accessory olfactory bulb. *J Neurophysiol* **102**: 1103–14.

Sohal, Vikaas S et al. (2009). Parvalbumin neurons and gamma rhythms enhance cortical circuit performance. *Nature* **459**: 698–702.

Soria-Gómez, Edgar et al. (2014). The endocannabinoid system controls food intake via olfactory processes. *Nat Neurosci* **17**: 407–15.

Sosulski, Dara L et al. (2011). Distinct representations of olfactory information in different cortical centres. *Nature* **472**: 213–6.

Soucy, Edward R et al. (2009). Precision and diversity in an odor map on the olfactory bulb. *Nat Neurosci* **12**: 210–20.

Spors, Hartwig & Amiram Grinvald (2002). Spatio-temporal dynamics of odor representations in the mammalian olfactory bulb. *Neuron* **34**: 301–15.

Stopfer, M et al. (1997). Impaired odour discrimination on desynchronization of odour-encoding neural assemblies. *Nature* **390**: 70–4.

Sullivan, R M & D A Wilson (1994). The locus coeruleus, norepinephrine, and memory in newborns. *Brain Res Bull* **35**: 467–72.

Sullivan, R M et al. (1994). Bilateral 6-OHDA lesions of the locus coeruleus impair associative olfactory learning in newborn rats. *Brain Res* **643**: 306–9.

Sullivan, R M et al. (2000). Association of an odor with activation of olfactory bulb noradrenergic beta-receptors or locus coeruleus stimulation is sufficient to produce learned approach responses to that odor in neonatal rats. *Behav Neurosci* **114**: 957–62.

Sweatt, J David (2016). Neural Plasticity & Behavior - Sixty Years of Conceptual Advances. *J Neurochem*.

Tan, Jie et al. (2010). Odor information processing by the olfactory bulb analyzed in gene-targeted mice. *Neuron* **65**: 912–26.

Trombley, P Q (1992). Norepinephrine inhibits calcium currents and EPSPs via a G-protein-coupled mechanism in olfactory bulb neurons. *J Neurosci* **12**: 3992–8.

Trombley, P Q & G M Shepherd (1992). Noradrenergic inhibition of synaptic transmission between mitral and granule cells in mammalian olfactory bulb cultures. *J Neurosci* **12**: 3985–91.

Tsuno, Yusuke, Hideki Kashiwadani, & Kensaku Mori (2008). Behavioral state regulation of dendrodendritic synaptic inhibition in the olfactory bulb. *J Neurosci* **28**: 9227–38.

Tsuno, Yusuke & Kensaku Mori (2009). Behavioral state-dependent changes in the information processing mode in the olfactory system. *Commun Integr Biol* **2**: 362–4.

Vallentin, Daniela & Michael A Long (2015). Motor origin of precise synaptic inputs onto forebrain neurons driving a skilled behavior. *J Neurosci* **35**: 299–307.

Vinck, Martin et al. (2015). Arousal and locomotion make distinct contributions to cortical activity patterns and visual encoding. *Neuron* **86**: 740–54.

Vucinić, Dejan, Lawrence B Cohen, & Efstratios K Kosmidis (2006). Interglomerular center-surround inhibition shapes odorant-evoked input to the mouse olfactory bulb in vivo. *J Neurophysiol* **95**: 1881–7.

Wachowiak, M & L B Cohen (2001). Representation of odorants by receptor neuron input to the mouse olfactory bulb. *Neuron* **32**: 723–35.

Wang, F et al. (1998). Odorant receptors govern the formation of a precise topographic map. *Cell* **93**: 47–60.

Watson, Christopher J, Helen A Baghdoyan, & Ralph Lydic (2010). Neuropharmacology of Sleep and Wakefulness. *Sleep Med Clin* **5**: 513–528.

Wellis, D P & J S Kauer (1993). GABAA and glutamate receptor involvement in dendrodendritic synaptic interactions from salamander olfactory bulb. *J Physiol* **469**: 315–39.

Wellis, D P & J W Scott (1990). Intracellular responses of identified rat olfactory bulb interneurons to electrical and odor stimulation. *J Neurophysiol* **64**: 932–47.

Wienisch, Martin & Venkatesh N Murthy (2016). Population imaging at subcellular resolution supports specific and local inhibition by granule cells in the olfactory bulb. *Sci Rep* **6**: 29308.

Willhite, David C et al. (2006). Viral tracing identifies distributed columnar organization in the olfactory bulb. *Proceedings of the National Academy of Sciences* **103**: 12592–12597.

Wilson, Rachel I & Zachary F Mainen (2006). Early events in olfactory processing. *Annu Rev Neurosci* **29**: 163–201.

Woolf, T B, G M Shepherd, & C A Greer (1991a). Local information processing in dendritic trees: subsets of spines in granule cells of the mammalian olfactory bulb. *J Neurosci* **11**: 1837–54.

— (1991b). Serial reconstructions of granule cell spines in the mammalian olfactory bulb. *Synapse* **7**: 181–92.

Yilmaz, Melis & Markus Meister (2013). Rapid innate defensive responses of mice to looming visual stimuli. *Curr Biol* **23**: 2011–5.

Yokoi, M, K Mori, & S Nakanishi (1995). Refinement of odor molecule tuning by dendrodendritic synaptic inhibition in the olfactory bulb. *Proc Natl Acad Sci U S A* **92**: 3371–5.

Youngstrom, Isaac A & Ben W Strowbridge (2015). Respiratory modulation of spontaneous subthreshold synaptic activity in olfactory bulb granule cells recorded in awake, head-fixed mice. *The Journal of Neuroscience* **35**: 8758–8767.

Yu, Kai et al. (2016). Central Amygdala Somatostatin Neurons Gate Passive and Active Defensive Behaviors. *J Neurosci* **36**: 6488–96.

Zariwala, Hatim A et al. (2013). The limits of deliberation in a perceptual decision task. *Neuron* **78**: 339–351.